MAGNETIC, METALLOMESOGENIC AND THERMOELECTRIC STUDIES OF Cu(II), Ni(II), Co(II), Fe(II) AND Mn(II) COMPLEXES WITH BENZOATES, CYCLAM AND 4-ALKYLOXYPYRIDINES AS LIGANDS

SITI AMIRA BINTI MAT HUSSIN

FACULTY OF SCIENCE
UNIVERSITY OF MALAYA
KUALA LUMPUR

2016

MAGNETIC, METALLOMESOGENIC AND THERMOELECTRIC STUDIES OF Cu(II), Ni(II), Co(II), Fe(II) AND Mn(II) COMPLEXES WITH BENZOATES, CYCLAM AND 4-ALKYLOXYPYRIDINES AS LIGANDS

SITI AMIRA BINTI MAT HUSSIN

DISSERTATION SUBMITTED IN FULFILMENT OF THE REQUIREMENTS FOR THE DEGREE OF MASTER OF SCIENCE

FACULTY OF SCIENCE
UNIVERSITY OF MALAYA
KUALA LUMPUR

2016

UNIVERSITY OF MALAYA
ORIGINAL LITERARY WORK DECLARATION

Name of Candidate: **SITI AMIRA BINTI MAT HUSSIN**

Matric No: **SGR140061**

Name of Degree: **MASTER OF SCIENCE**

Title of Project Paper/Research Report/Dissertation/Thesis (“this Work”):

MAGNETIC, METALLOMESOGENIC AND THERMOELECTRIC STUDIES OF Cu(II), Ni(II), Co(II), Fe(II) AND Mn(II) COMPLEXES WITH BENZOATES, CYCLAM AND 4-ALKYLOXYPYRIDINES AS LIGANDS

Field of Study: **INORGANIC CHEMISTRY**

I do solemnly and sincerely declare that:

(1) I am the sole author/writer of this Work;
(2) This Work is original;
(3) Any use of any work in which copyright exists was done by way of fair dealing and for permitted purposes and any excerpt or extract from, or reference to or reproduction of any copyright work has been disclosed expressly and sufficiently and the title of the Work and its authorship have been acknowledged in this Work;
(4) I do not have any actual knowledge nor do I ought reasonably to know that the making of this work constitutes an infringement of any copyright work;
(5) I hereby assign all and every rights in the copyright to this Work to the University of Malaya (“UM”), who henceforth shall be owner of the copyright in this Work and that any reproduction or use in any form or by any means whatsoever is prohibited without the written consent of UM having been first had and obtained;
(6) I am fully aware that if in the course of making this Work I have infringed any copyright whether intentionally or otherwise, I may be subject to legal action or any other action as may be determined by UM.

Candidate’s Signature Date:

Subscribed and solemnly declared before,

Witness’s Signature Date:

Name:

Designation:

ABSTRACT

The main objective of the research was to synthesise and characterise thermally stable complexes, designed to be metallomesogenic with spin-crossover (SCO) and thermoelectric properties. 4-Hexadecyloxypyridine and complexes of general formula $[\text{M(cyclam)(L)}_2](\text{4-XC}_6\text{H}_4\text{COO})_{2/3}]$, where M = Cu(II), Ni(II), Co(II), Co(III), Fe(II), Fe(III), Mn(II) and Mn(III), L = 4-tetradecyloxypyridine or 4-hexadecyloxypyridine, X = H, CH_3, CH_3O and OH were successfully synthesized in good yields, and their structural formulae deduced from combined analytical data (elemental analyses and IR and UV-vis spectroscopies). The magnetic, thermoelectric, thermal, and mesomorphic properties of these complexes were then studied. The μ_{eff} values at room temperature were in the range of 1.47 BM to 1.77 BM for all Cu(II) complexes (**1**-**3**), and 1.83 BM for $[\text{Ni(cyclam)(L2)}_2](\text{C}_6\text{H}_5\text{COO})_2\cdot\text{H}_2\text{O}$ (**4**). Based on ^{1}H-NMR spectroscopy, $[\text{Co(cyclam)(L1)}_2](\text{R})_2\cdot3\text{H}_2\text{O}$ (**6**), $[\text{Fe(cyclam)(L2)}_2](\text{R})_3\cdot4\text{H}_2\text{O}\cdot2\text{CH}_3\text{CH}_2\text{OH}$ (**9**), $[\text{Mn(cyclam)(L1)}_2](\text{R})_2\cdot4\text{H}_2\text{O}$ **(10)** and $[\text{Mn(cyclam)(L2)(H}_2\text{O)}](\text{R})_3\cdot3\text{H}_2\text{O}$ (**11**) were paramagnetic, while $[\text{Ni(cyclam)(L1)(H}_2\text{O)}](\text{R})_2\cdot\text{H}_2\text{O}$ (**4**), $[\text{Co(cyclam)(L2)}_2](\text{R})_3\cdot4\text{H}_2\text{O}$ (**7**) and $[\text{Fe(cyclam)(L1)}_2](\text{R})_2\cdot2\text{H}_2\text{O}$ (**8**), where R = C_6H_5COO, were diamagnetic. The decomposition temperatures for all complexes were in the range of 130 ºC to 206 ºC. Complexes **3**, **9**, **11** were mesogenic, while the other complexes were non-mesogenic. The Seebeck coefficients (in mV K^{-1}) were in the range of -0.42 to -0.51 for all Cu(II) complexes in chloroform, +0.23 to +0.27 for Ni(II) complexes in ethanol, +0.24 to +0.33 for Co(II/III) complexes in DMSO, +0.33 and -0.8 for Fe(II)/III) complexes in MPN, and +0.22 and +0.24 for Mn(II/III) complexes in DMSO and ethanol.

ABSTRAK

Objektif utama penyelidikan ini adalah untuk mensintesis dan mencirikan kompleks stabil secara terma, yang direka bentuk menjadi metallomesogenik dengan sifat beralih spin dan termoelektrik. Ligan 4-tetradesiloksipiridina dan kompleks dengan formula umum $[\mathrm{M(cyclam)(L)_2](4\text{-}XC_6H_4COO)_{2/3}}]$, di mana M = Cu, Ni, Co, Fe, or Mn, L = 4-tetradesiloksipiridina atau 4-heksadesiloksipiridina, X = H, CH_3, CH_3O, dan OH berjaya disintesiskan dengan hasilan yang baik, dan formula struktur kompleks dideduksikan dari gabungan data analisis. Sifat magnet, termoelektrik, terma, dan mesomorfik kompleks-kompleks ini kemudiannya dikaji. Nilai μ_{eff} pada suhu bilik adalah dalam julat 1.47 BM hingga 1.77 BM untuk semua kompleks Cu(II) (**1**-**3**), dan 1.83 BM untuk $[\mathrm{Ni(siklam)(L2)_2](C_6H_5COO)_2.H_2O}$ (**5**). Berdasarkan spektroskopi ^{1}H-NMR, $[\mathrm{Co(siklam)(L1)_2](R)_2\cdot 3H_2O}$ (**6**), $[\mathrm{Fe(siklam)(L2)_2](R)_3\cdot 4H_2O\cdot 2CH_3CH_2OH}$ (**9**), $[\mathrm{Mn(siklam)(L1)_2](R)_2\cdot 4H_2O}$ **(10)** dan $[\mathrm{Mn(siklam)(L2)(H_2O)](R)_3\cdot 3H_2O}$ (**11**) adalah paramagnetik, manakala $[\mathrm{Ni(siklam)(L1)(H_2O)](R)_2\cdot H_2O}$ (**4**), $[\mathrm{Co(siklat)(L2)_2](R)_3\cdot 4H_2O}$ (**7**) dan $[\mathrm{Fe(siklam)(L1)_2](R)_2\cdot 2H_2O}$ (**8**), dengan R = C_6H_5COO, adalah diamagnetik. Suhu penguraian kompleks adalah dalam julat 130 ºC – 206 ºC. Kompleks **3**, **9**, **11** adalah mesogenik, manakala kompleks-kompleks yang lain adalah tidak mesogenik. Pekali Seebeck (mV K^{-1}) adalah dalam julat -0.42 hingga -0.51 untuk semua kompleks Cu(II) dalam kloroform, +0.23 hingga +0.27 untuk kompleks Ni(II) dalam etanol, +0.24 hingga +0.33 untuk kompleks Co(II/III) dalam DMSO, +0.33 dan -0.8 untuk kompleks Fe(II/III) dalam MPN, dan +0.22 dan +0.24 untuk kompleks Mn(II/III) dalam DMSO dan etanol.

ACKNOWLEDGEMENTS

Alhamdulillah, all praise to Allah S.W.T for His greatness and for giving me the strength and motivation to complete this research.

Firstly, I would like to thank my supervisor, Assoc. Prof. Dr. Norbani Abdullah for her guidance, patience and support throughout this project. This report would not be completed without her help. Her kindness in helping me in my project makes my research a very interesting experience.

Next, I would like to extend my appreciations to all researchers from Inorganic Chemistry Research Laboratory who have been very helpful and supportive in providing technical support, and to all staff in the Chemistry Department, Science Faculty, University of Malaya, for their cooperation and kindness.

Last but not least, I would like to thank my family and friends for their support and encouragement throughout this project. Thank you so much for all support and sacrifices.

This project was financially supported by the scholarship from Ministry of Higher Education Malaysia (MyMaster), High Impact Research Grant (UM.C/625/1/HIR/MOHE/05) and Postgraduate Research Grant (PG069 – 2015A).

TABLE OF CONTENTS

APPENDICES

LIST OF FIGURES

LIST OF TABLES

LIST OF SCHEMES

CHAPTER 1: INTRODUCTION

The main objectives of this research were synthesis and characterization of magnetic complexes designed to have mesomorphic and thermoelectric properties, and for Co(II), Co(III), Fe(II), Fe(III), Mn(II) and Mn(III) complexes to have spin-crossover (SCO) properties. The structural formulae of these complexes are shown in **Scheme 1.1** and **Scheme 1.2**.

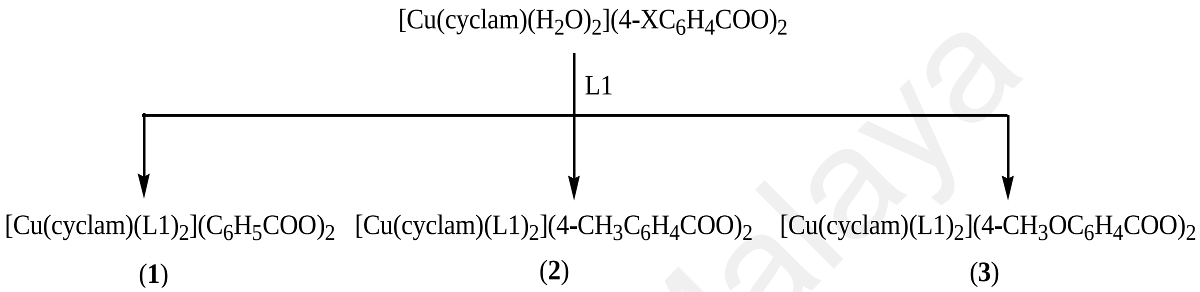

Scheme 1.1. Complexes of Cu(II) with cyclam, 4-tetradecyloxypyridine (L1) as ligand and 4-$XC_6H_4COO^-$ ($X = H, CH_3, CH_3O$) as counterion.

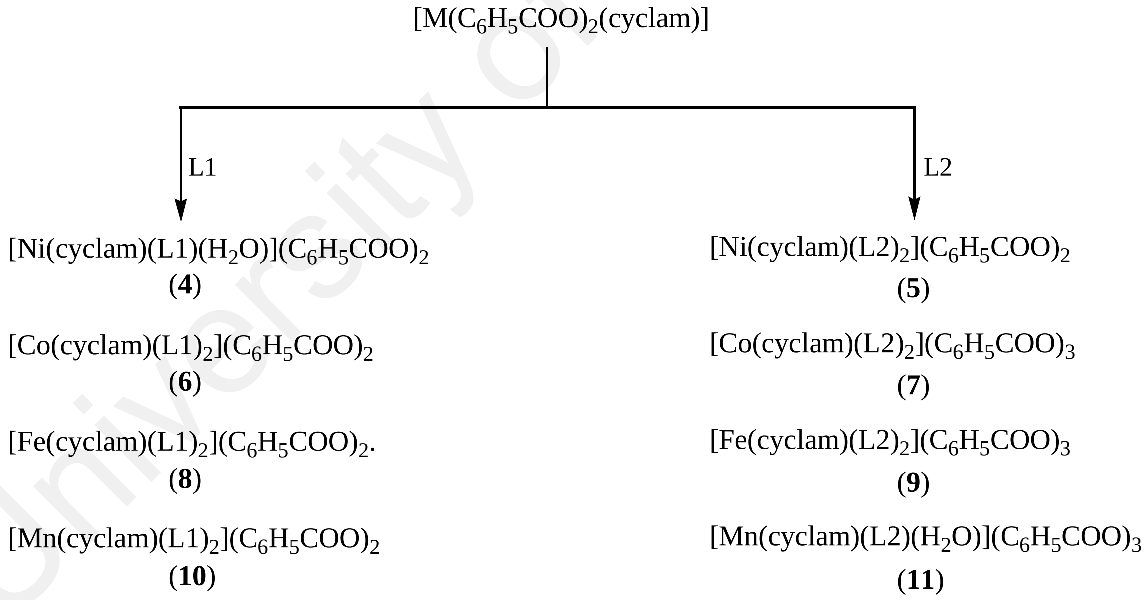

Scheme 1.2. Complexes of Ni(II), Co(II), Co(III), Fe(II), Fe(III), Mn(II) and Mn(III) with cyclam, 4-tetradecyloxypyridine (L1) or 4-hexadecyloxypyridine (L2) as ligands, and $C_6H_5COO^-$ as counterion

Metallomesogens are complexes exhibiting liquid-crystalline properties [1]. Liquid crystal is a state of matter between a solid phase and a liquid phase, and therefore exhibits the properties of both crystals and liquids, such as ordered structures and fluidity [2]. In addition, metallomesogens constructed from transition metal ions have combined properties of liquid crystal, such as anisotropy and fluidity, with those derived from the metal ions, such as variety of colours, geometries, oxidation states, magnetisms and electronic conductivities [3].

SCO is a phenomenon involving interconversion of electronic configurations between high spin (HS) and low spin (LS) states [4]. This phenomenon occurs in octahedral complexes of first-row transition metal ions with valence electronic configurations d^4-d^7 with ligands of intermediate strength, such as N- and O- donors. SCO can be reversibly induced by external stimuli, such as temperature, pressure, magnetic field, electric field and light, leading to changes in dielectric constant, colour, structure, magnetism and optical properties [5,6].

Thermoelectricity involves the conversion of heat directly to electricity. Thermoelectric materials are useful for power generation devices in order to convert waste heat into electrical energy, and are important in solid-state refrigeration devices [7]. An important thermoelectrical parameter is the Seebeck coefficient (S_e), which can be determined from the gradient of the linear graph of potential difference (ΔV) *versus* temperature difference (ΔT). The factors that determine the magnitude and sign of S_e are the entropy change and charge of the carrier, respectively [8].

For this research, a total of eleven (11) complexes were successfully synthesized and characterized. The structures of all complexes were deduced from CHN elemental analyses, FTIR spectroscopy, and UV-vis spectroscopy. Their magnetic properties were determined by the Gouy method at room temperature or inferred from ^{1}H-NMR spectroscopy, while their SCO properties were determined by variable temperature UV-vis spectroscopy. Their S_e values were determined in solutions of suitable solvents. Finally, their thermal properties were determined by thermogravimetry (TG), and their mesogenic properties by differential scanning calorimetry (DSC) and polarizing optical microscopy (POM). Some of the findings from this research were published in ISI journals (**Appendices 1 and 2**) and presented in an international conference (**Appendix 3**).

This thesis contains five chapters. **Chapter 1** introduces the objectives of the research, and the ligands and complexes synthesized and characterized. **Chapter 2** presents the relevant theories and literature reviews, namely complexes of cyclam, SCO behaviour, mesomorphisms, and thermoelectricity. **Chapter 3** presents the syntheses and instrumental techniques used in the characterization of 4-hexadecyloxypyridine (L2) and complexes of 4-tetradecyloxypyridine (L1) and L2. **Chapter 4** presents the results and discussions, and finally **Chapter 5** presents the conclusions and suggestions for future works. A list of references and appendices are included at the end of the thesis.

CHAPTER 2: THEORY AND LITERATURE REVIEW

2.1 Introduction

The main objectives of this research were to synthesise and study the magnetic, thermal, mesogenic, and thermoelectric properties of complexes formed from the reaction of arylcarboxylates of copper(II), nickel(II), cobalt(II), iron(II) and manganese(II) with cyclam and 4-tetradecyloxypyridine (L1) and 4-hexadecyloxypyridine (L2) as ligands.

2.2 Complexes of Copper(II), Arylcarboxylate Ions and Cyclam

Copper is a first-row transition metal with atomic number 29 (valence electron configuration $4s^1 3d^{10}$). Its most stable oxidation state is Cu^{2+} (valence electron configuration $3d^9$). In most complexes, the geometry of Cu^{2+} ion is easily altered (geometrically flexible), thus forming labile coordination complexes due to facile change in the numbers of ligand. Hence, its complexes have variable molecular geometries, such as octahedral, square pyramidal, trigonal bipyramidal, square planar and tetrahedral [9].

A large family of Cu^{2+} complexes are copper(II) arylcarboxylates. Most copper(II) arylcarboxylates are dinuclear complexes with the general formula $[Cu_2(RCOO)_4]$ and dimeric structure known as paddle-wheel (**Figure 2.1**) [1]. The dimer experienced a strong antiferromagnetic interaction ($-2J \sim 300$ cm^{-1}) [10], postulated to occur through the bridging carboxylate ligands (the super-exchange pathway) [11].

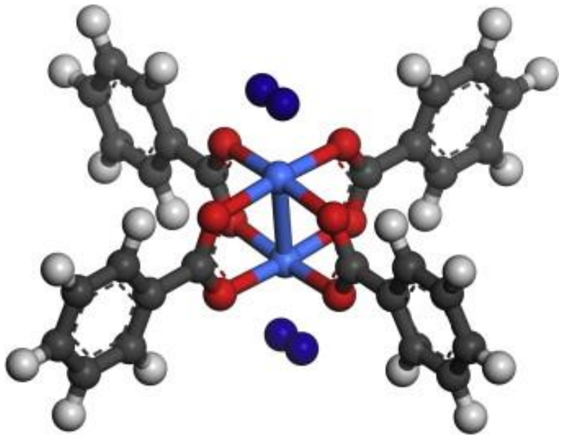

Figure 2.1 The dimeric paddle-wheel structure of $[Cu_2(C_6H_5COO)_4(H_2O)_2$ [1]

An arylcarboxylate anion ($ArCOO^-$) is a flexible ligand that can bind to a metal ion in different modes, such as monodentate, bidentate, bridging and chelating (**Figure 2.2**).

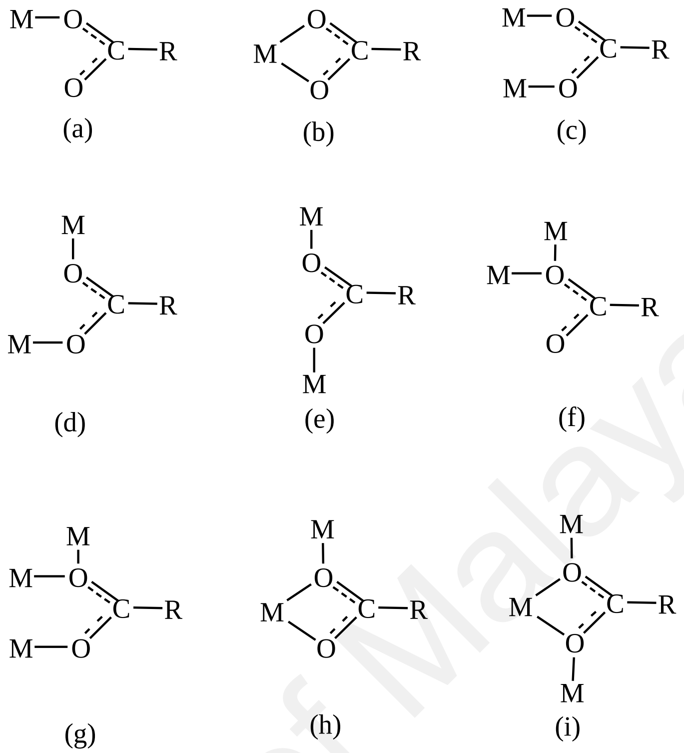

Figure 2.2 Different binding modes of a carboxylate ion: (a) monodentate; (b) chelating; (c) bridging bidentate (*syn–syn*); (d) bridging bidentate (*syn–anti*); (e) bridging bidentate (*anti–anti*); (f) monatomic bridging; (g) monatomic bridging additional bridging; and (h) and (i) chelating and bridging [12]

The actual binding modes of a $RCOO^-$ ion may be inferred from FTIR spectroscopy, based on the difference (Δ) in the values of the asymmetric vibration of COO group (v_{asym}) and the symmetric vibration of COO group (v_{sym}) (**Table 2.1**) [13].

Table 2.1 The value of **Δ** for the different binding mode of RCOO ligands obtained from FTIR spectrum

Binding mode	**$\Delta = v_{asym} - v_{sym}$ /cm^{-1}**
Monodentate	>200
Chelating	<156
Bridging monodentate	~200
Bridging bidentate	~ 160
Chelating bidentate	~100

For example, Iqbal *et al.* [14] reported green crystals of tetrakis(4-methoxyphenylacetato-μ-O,O')bis(pyridine-N)dicopper(II), synthesized from the reaction of an aqueous solution of sodium bicarbonate with 4-methoxyphenylacetic acid, copper(II) sulfate and pyridine at 60 ºC. Its structure (**Figure 2.3**) showed a paddlewheel dimeric complex, in which the two Cu(II) atoms were bonded to four identical carboxylate groups in a bridging bidentate mode. The coordination environment at copper was {$CuCuNO_4$} octahedron. Its FTIR spectrum give the Δ value of 182 cm^{-1} (υ_{asym} = 1580 cm^{-1} and υ_{sym} = 1398 cm^{-1}), in agreement with the bridging bidentate mode of the carboxylate group. Other peaks found were at 1613 cm^{-1}, 1435 cm^{-1} and 608 cm^{-1} for υ(C=C), υ(C=N-C=C), and υ(Cu-O), respectively.

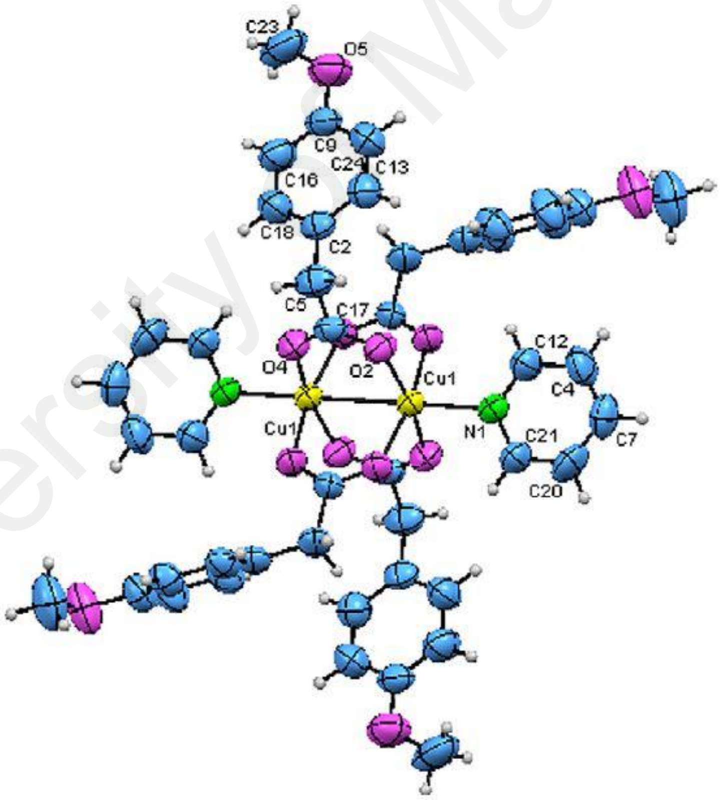

Figure 2.3 Crystal structure of [tetrakis(4-methoxyphenylacetato-μ-O,O')bis(pyridine-N)dicopper(II)] [14].

A large number of synthetic, as well as naturally occurring macrocycles have been known from several decades, and their complexation chemistry with a large variety of metal ion has undergone a thorough study [14,15,16]. An example of a macrocyclic ligand with nitrogen atoms as the electron pair donor is cyclam (1,4,8,11-tetraazacyclotetradecane) (**Figure 2.4**). Cyclam can form kinetically and thermodynamically stable complexes which bind strongly to transition metal ions (the metal ion is firmly held in the cavity of the macrocycle) [17,18,19]. Recently, cyclam complexes are of interest as sensors [21], catalysts [22] and pharmaceutical materials [23].

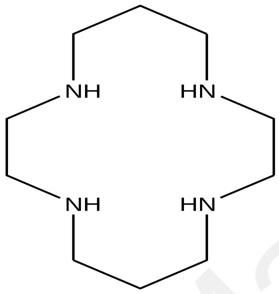

Figure 2.4 Structure of cyclam

Cu(II)-cyclam complexes are potential materials in molecular electronic, photonics and spintronics research because their properties may be tuned by steric and electronic effects [24]. Most copper(II)-cyclam complexes are ionic, and generally have weakly coordinated H_2O molecules at the axial positions of Cu(II) centre. An example is $[Cu(cyclam)(H_2O)_2](4\text{-}CH_3C_6H_4COO)_2\cdot H_2O$, reported by Tajidi *et al*. [25]. The complex was synthesized by reacting cyclam with $[Cu_2(4\text{-}CH_3C_6H_4COO)_4(H_2O)_2]$ in ethanol. It was obtained as purple prismatic crystals. Its crystal structure (**Figure 2.5**) showed copper(II) ion coordinated to cyclam through four nitrogen atoms at the basal plane of the cyclic ligand and by water molecules at the axial positions in a Jahn-Teller type of tetragonally distorted octahedral geometry. The carboxylate group interacts indirectly with the metal atom through the coordinated water molecules. The cation, anions and lattice water molecules are linked by N–H•••O and O–H•••O hydrogen bonds to form a layer structure.

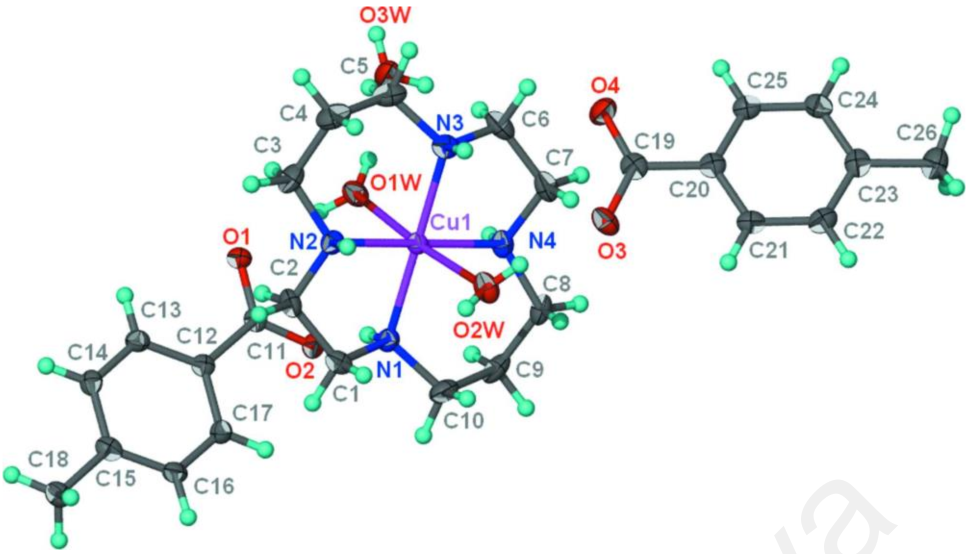

Figure 2.5 Crystal structure of $[Cu(cyclam)(H_2O)_2](4\text{-}CH_3C_6H_4COO)_2 \cdot H_2O$ [25]

Tajidi *et al* [26] also reported prismatic crystals of $[Cu(cyclam)(H_2O)_2](C_6F_5COO)_2 \cdot 2H_2O$ (**Figure 2.6**), obtained from the reaction of cyclam with a suspension of copper pentafluorobenzoate in ethanol. This complex has similar structure as $[Cu(cyclam)(H_2O)_2](4\text{-}CH_3C_6H_4COO)_2 \cdot H_2O$ [25].

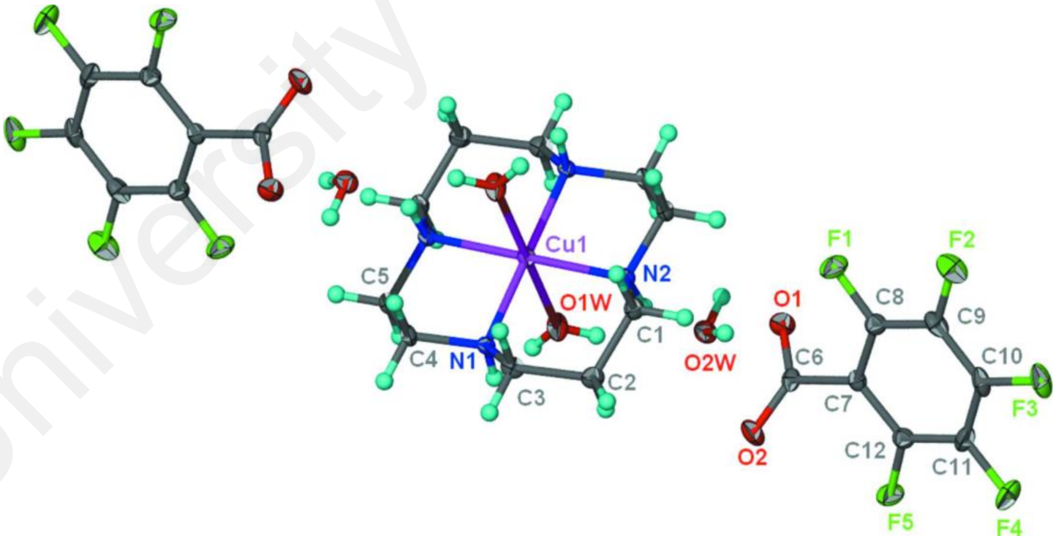

Figure 2.6 Crystal structure of $[Cu(cyclam)(H_2O)_2](C_6F_5CO_2)_2 \cdot 2H_2O$ [26].

The geometry of a transition metal ion of a complex can be deduced by UV-vis spectroscopy. This spectroscopy involves absorption of light in the visible region (380-750 nm) and UV region (190-380 nm). The UV and visible radiations absorbed by a sample causes the valence electrons to be excited from the ground state to the higher states. The light with exact amount of energy induced the transitions to a higher level. It may be used for quantitative and qualitative analyses of complexes. For quantitative analyses, the absorbance is directly proportional to the path length (l) and the concentration (c) of the absorbing species. This is known as the Beer's law, $A = \varepsilon cl$, where ε is a constant known as the molar absorptivity.

For qualitative analyses, the geometry of a metal ion in a complex is determined from the value of λ_{max} of the *d-d* band. For example, copper(II) has the λ_{max} value of about 600 nm for square planar geometry [27], about 700 nm for square pyramidal [28], and about 800 nm for tetrahedral [29] and octahedral geometries [30].

For example, Abdullah *et al.* [31] reported their work on crystals of $[Cu_2(CH_3(CH_2)_5COO)_4]$ (**Figure 2.7**), synthesized from reaction of $CH_3(CH_2)_5COONa$ with $CuCl_2{\cdot}2H_2O$ in hot ethanol. Its UV-vis spectrum in solution showed a broad *d-d* band at 671 nm (ε_{max} = 375 M^{-1} cm^{-1}), assigned to $^2B_2$ to $^2B_1$ electronic transition based on the C_{4v} point group at each Cu(II) [32], suggesting a square pyramidal binuclear Cu(II) complex [28].

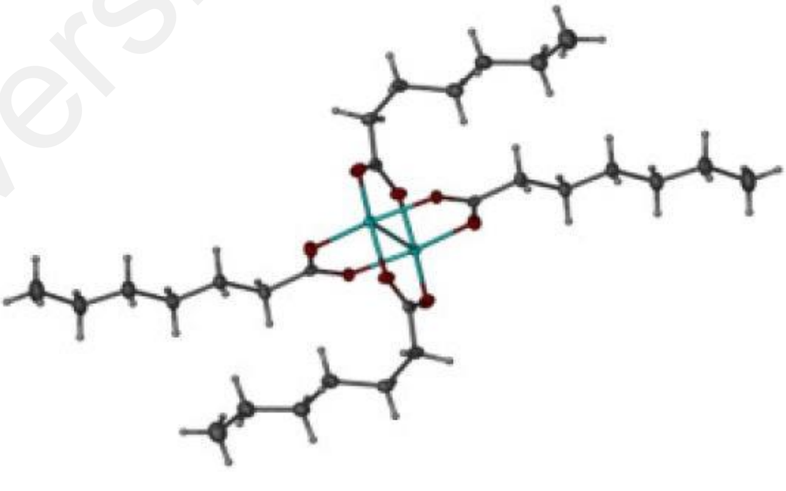

Figure 2.7 Crystal structure of $[Cu_2(CH_3(CH_2)_5COO)_4]$ [31].

For transition metal complexes, the electronic transitions were mostly focused on electrons in the *d* orbitals as explanation for their colours. These *d-d* transitions are adequately explained by the crystal field theory (CFT). This theory is a model of electronic orbitals that describes the breaking of degeneracy due the presence of ligands to the central transition metal ion. The energy levels of the *d* orbital in octahedral, tetrahedral and square-planar fields are shown in **Figure 2.8**.

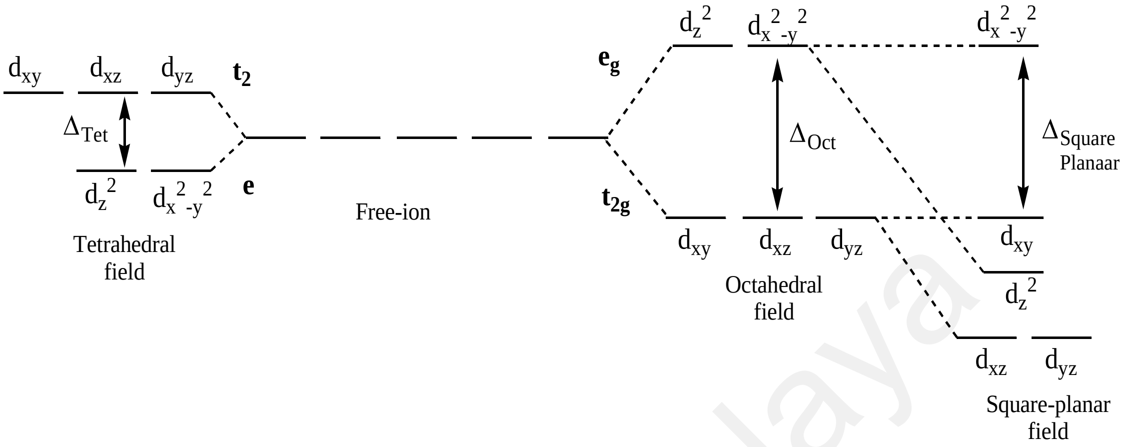

Figure 2.8 Splitting of *d*-orbitals energy levels in octahedral, tetrahedral and square planar geometries

Magnetism is an important characteristic for many first-row transition metal complexes. There are two main types: diamagnetism and paramagnetism. The magnetic properties of materials can be observed and measured in the presence of an external magnetic field. Diamagnetic substances have no unpaired electron(s), and are repelled by an external magnetic field. In contrast, paramagnetic substances have unpaired electron(s), and are attracted by an external magnetic field. Most transition metal complexes are paramagnetic due to the presence of unpaired *d* electron(s).

The interaction between permanent magnetic dipoles in paramagnetic materials can be further classified to three groups: ferromagnetic, antiferromagnetic, and ferrimagnetic (**Figure 2.9**). Ferromagnetism arises when the unpaired electron spins are held in parallel alignment. Antiferromagnetism arises when the unpaired electron spins are held in antiparallel alignment, and may lead to zero net magnetic moments when there are equal numbers of magnetic moments in opposite direction. Ferrimagnetism is enhanced magnetism due to unequal number of magnetic moments in opposite direction, and result in some net magnetic moments.

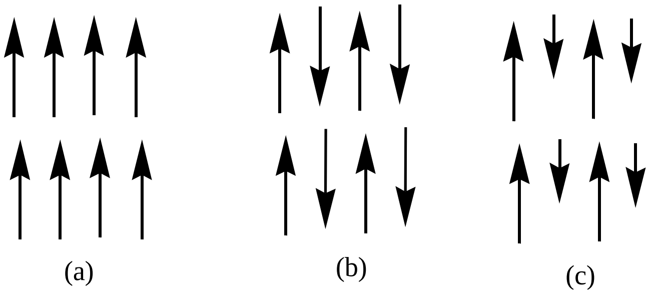

Figure 2.9 Magnetic alignments in: (a) ferromagnetic; (b) antiferromagnetic; and (c) ferromagnetic materials

The strength of paramagnetism or diamagnetism depends on the types of atom or molecules, the amount, and matrix present. The degree of magnetization in an external magnetic field can be measured by magnetic susceptibility. Materials are paramagnetic when the magnetic susceptibility is positive, and diamagnetic when the magnetic susceptibility is negative. Magnetic susceptibility for a solid sample at room temperature may be determined by the Gouy method [33]. This method measures the gram magnetic susceptibility (χ_g). From this value, the molar magnetic susceptibily (χ_m) is obtained from the relationship $\chi_m = \chi_g$ x formula mass. The value of χ_m has to be corrected for the inherent diamagnetic susceptibility contribution (χ_{dia}) from the ligands and metal ions using the equation $\chi_m^{corr} = \chi_m - \chi_{dia}$. The χ_{dia} value can be calculated by Pascal's constant [34]. From the value of χ_m^{corr}, the value of the effective magnetic moment (μ_{eff}) is calculated from the formula: $\mu_{eff} = 2.828\sqrt{\chi_m^{corr}T}$. From the value of μ_{eff}, the number of unpaired electrons (n) ay be calculated from the formula $\mu_{eff} = \sqrt{n(n+2)}$. Hence, the distinction between a high-spin (HS) and low-spin (LS) complex, spectral behavior and structure may be inferred from μ_{eff} values.

For example, Creaven *et al*. [35] reported crystals of $[Cu(L)_2]$, where L = 7-(2,4-dihydroxybenzylideneamino)-4-methylquinolin-2(1H)-one (**Figure 2.10**), synthesized from the reaction of copper(II) acetate with H_2L in methanol. Its μ_{eff} value was 1.69 BM, consistent with the presence of one unpaired electron (d^9), and was within the expected range for mononuclear copper(II) complexes (1.73 BM).

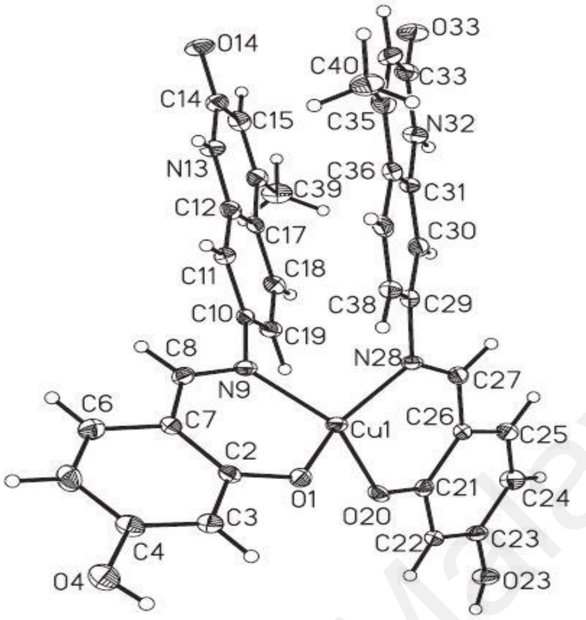

Figure 2.10 Crystal structure of $[Cu(L)_2]$ [35]

Magnetic properties of complexes can be inferred by ^{1}H-NMR spectroscopy. Diamagnetic complexes are NMR active, and therefore produce well resolved ^{1}H-NMR signals. Paramagnetic complexes are partially NMR active, and therefore do not produce well resolved ^{1}H-NMR signals (the broadening peak) [35,36] or some peaks were missing) due to the unfavorable electronic relaxation time [37,38,39].

For example, Subramanian *et al.* [9] reported violet-blue crystals of $[Cu(dien)(2\text{-}MeBzim)](ClO_4)_2$ (2-MeBzim = 2-methylbenzimidazole) (**Figure 2.11**), synthesized by reacting an aqueous solution of $CuSO_4{\cdot}5H_2O$ with dien, 2-methylbenzimidazole and $NaClO_4{\cdot}H_2O$. The complex was paramagnetic and its μ_{eff} value was 1.72 BM (at room temperature by the Evans method). Hence, it was partially NMR active and did not show signals for all of its protons. Its ^{1}H-NMR spectrum showed 6 to 10 non-equivalent protons with line broadening. Although it was impossible to get well-resolved signals for every proton signals, the peaks for CH_3, NH_2 and CH_2 protons were recorded in different solvents (**Table 2.2**).

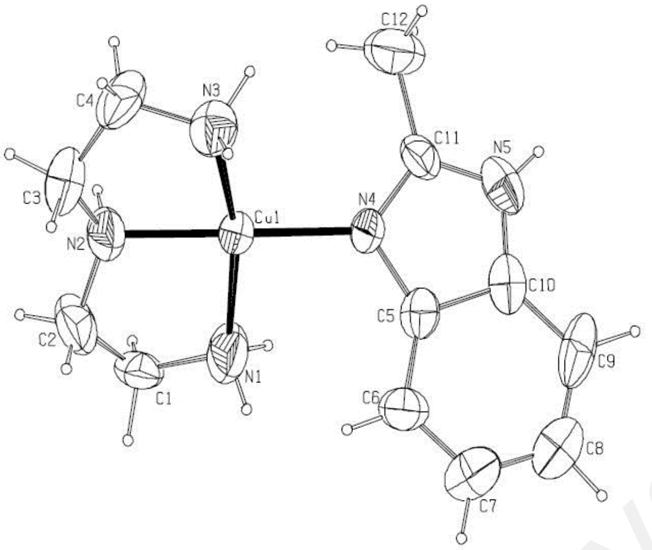

Figure 2.11 Crystal structure $[Cu(dien)(2\text{-}MeBzim)](ClO_4)_2$ [9]

Table 2.2 ^{1}H NMR chemical shift (δ) values for $[Cu(dien)(2\text{-}MeBzim)](ClO_4)_2$ [9]

Solvent	δ (ppm)		
	$-CH_3$	$-NH_2$	$-CH_2$
Acetone-D_6	-3.67	3.18	20.12
CD_3CN	-3.95	2.59	19.70
MeOD	-1.57	absent	15.20-
D_2O	-1.06	absent	14.09
DMSO	-0.37	3.44	14.09

Thermal stabilities of complexes can be determined by thermogravimetry (TG). This technique measures mass loss as a function of temperature (from ambient to 1000 ºC) or time, and under an inert atmosphere (normally N_2). For example, Caglar *et al.* [41] reported the thermal data for $[Cu(bba)_2(pypr)_2]$, where bba = 2-benzoylbenzoate and pypr = 2-pyridilpropanoxy (**Figure 2.12**). This complex was synthesized by reacting $CuSO_4.5H_2O$ with 2-benzoylbenzoic acid and 2-pyridilpropanol in ethanol. It showed two decomposition stages. The first stage was between 126 ºC and 314 ºC, assigned to the removal of two pypr and bba ligands with release of CO_2 (exp. = 77.70%; calc. = 77.55%). The next stage in the 314–546 ºC range was assigned to pyrolysis of the organic residue (exp. = 13.6%; calc. = 14.3%). The residue was CuO.

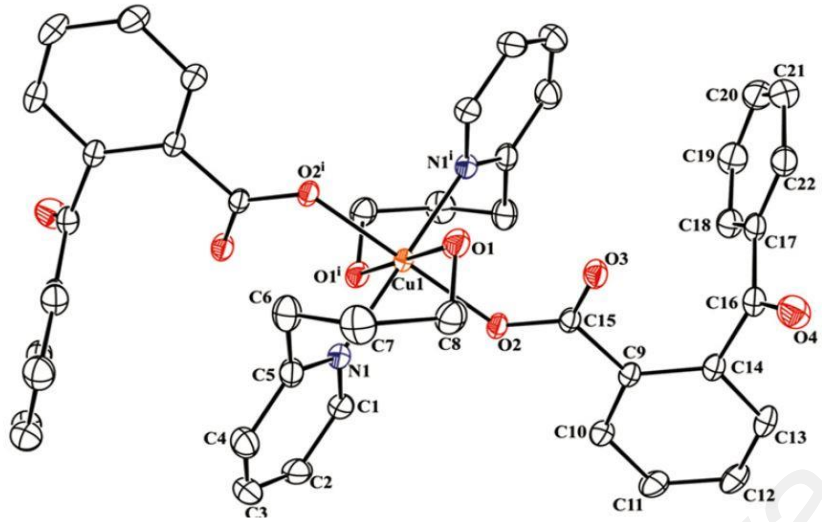

Figure 2.12 Crystal structure of [Cu(bba)$_2$(pypr)$_2$] [41]

Mesomorphisms (liquid crystalline properties) of complexes usually are commonly determined by optical polarizing microscopy (OPM) and differential scanning calorimetry (DSC). Metal complexes exhibiting liquid crystal properties are known as metallomesogens. These materials combine the properties of liquid crystals (fluidity, easy processability, order, self-healing) with properties of the metal ions (magnetism, optical properties, conductivity, colour) [4].

The liquid crystal (mesophase) is a state of matter between the crystal phase and liquid phase that combines order and mobility. The different order of solid, liquid and liquid crystal is shown in **Figure 2.13**.

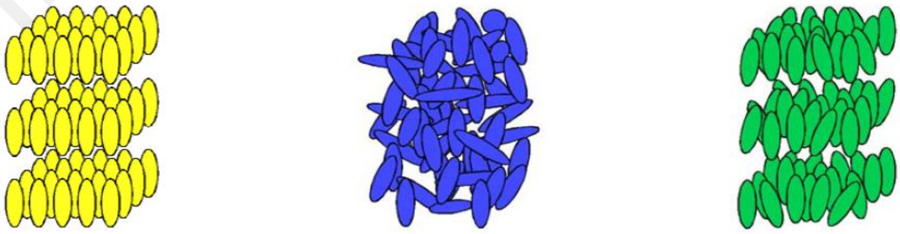

Figure 2.13 The arrangement of molecules in different states: (a) solid; (b) liquid; and (c) liquid crystal

Molecules in the liquid crystal phases need to have sufficient disorder to generate softness and fluidity. They have anisotropic shapes: calamitic, discotic or catenar. There are three main types of liquid crystal phases: nematic, smectic and columnar. These phases occur at distinct temperature range between crystalline solid state (Cr) and isotropic liquid state (I), and are held together by intermolecular forces (Van der Waals). They are birefringent as a result of anisotropy (variation of physical properties with crystallographic directions) in their structures. [42].

For example, Bhattacharjee *et al*. [43] reported the mesomorphic properties of [Cu((4-$C_{18}H_{37}O)_2$salen)], where salen = N,N'-cyclohexane-*bis*(salicylideneiminato). This complex was synthesized by mixing $Cu(OAc)_2 \cdot H_2O$ in methanol with N,N'-bis(4-(4-n-octadecyloxy)salicylidene)-*trans*-1,2-diaminocyclohexane in absolute ethanol. Its structure was optimized by DFT calculation (**Figure 2.14**). The complex showed an enantiotropic mesomorphism at 111-212 °C. Under OPM, it showed leaf-like textures (**Figure 2.15**) at 206 °C upon cooling from the isotropic phase, suggesting a columnar mesophase [44]. Its DSC scans showed two transitions on heating and cooling, and the enthalpy change (ΔH_{iso}) was about 30 kJ mol^{-1} for the mesophase-to-isotropic liquid transition.

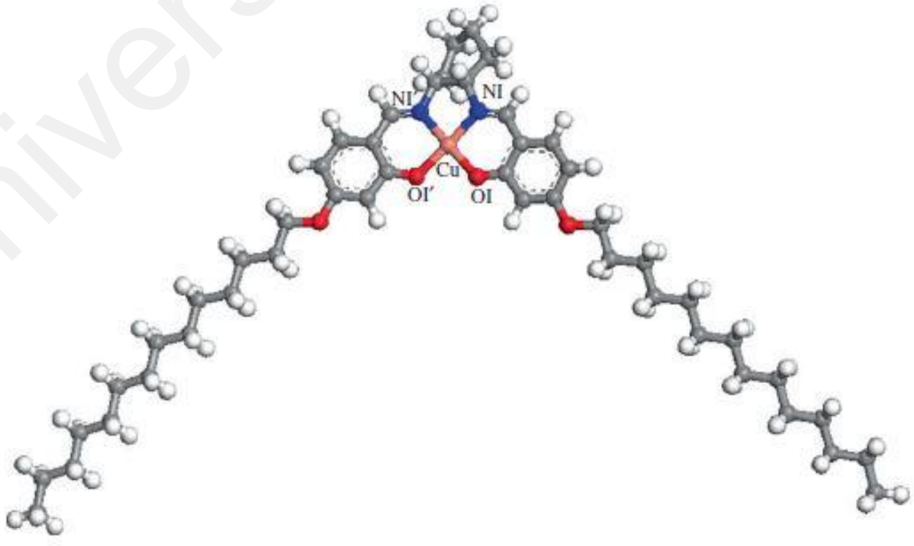

Figure 2.14 DFT optimized structure of [Cu((4-$C_{18}H_{37}O)_2$salen)] [43]

Figure 2.15 Leaf-like texture of [Cu((4-$C_{18}H_{37}O)_2$salen)] at 206 ºC [43]

Another example is [Cu(cyclam)($H_2O)_2$](4-$ClC_6H_4COO)_2$, reported by Abdullah *et al*. [45]. This complex was synthesized from the reaction of [Cu_2(4-$ClC_6H_4COO)_4(EtOH)_2$] with cyclam in ethanol. The proposed structure of the complex was deduced based on the results of elemental analyses and spectral data comparison with crystal of similar complexes. The calculated percentages of C, H, and N from the proposed formula were 47.2% C, 5.9% H and 9.2% N, while the results from elemental analyses were 47.0% C, 6.0% H and 9.0% N. Its FTIR spectrum gave Δ = 176 cm^{-1}, suggesting free 4-$ClC_6H_4COO^-$ ion. Its UV-vis spectrum showed a broad *d-d* band at 541 nm (ε_{max} = 87 M^{-1} cm^{-1}), consistent with a mononuclear ionic complex in solution. To form magnetic mesomorphic complex, it was reacted with 4-hexadecyloxypyridine (L) to form [Cu(cyclam)$(L)_2$](4-$ClC_6H_4COO)_2$. The complex melted at 70 ºC, and showed an optical texture at 100 ºC (**Figure 2.16**) on cooling from the isotropic liquid, suggesting discotic mesomorphism.

Figure 2.16 Photomicrograph of [Cu(cyclam)(L)$_2$](4-ClC$_6$H$_4$COO)$_2$ at 100 °C on cooling from isotropic liquid [45]

Thermoelectricity involves the conversion of heat directly to electricity [46]. Thermoelectrical materials are useful for power generation devices to convert waste heat into electrical energy and important in solid-state refrigeration devices [47]. An important thermolectrical parameter is the Seebeck coefficient (S_e), which can be determined from the gradient of the linear graph of potential difference (ΔV) *versus* temperature difference (ΔT). The aspects that determine the magnitude and sign of S_e are entropy change (ΔS) and charge of the carrier, respectively [49]. Currently, the thermoelectrical properties for complexes were reported in solutions. This is because redox couple-based thermo-electrochemical systems gave higher S_e values than semiconductor thermocells [48]. A simple experimental set-up for the thermoelectrical measurements in solutions is shown in **Figure 2.17**. It consists of a solution made up of the complex, an electrolyte such as tetrabutylammonium tetrafluoroborate (TBATFB), and a redox couple such as KI/KI$_3$. The solution is filled into a cell made up of two compartments, each containing a platinum wire electrode. The compartments are placed in two separate water baths and connected by a bridge containing the same solution. One water bath is heated with a hot plate (hot side) and the other is at room temperature [49].

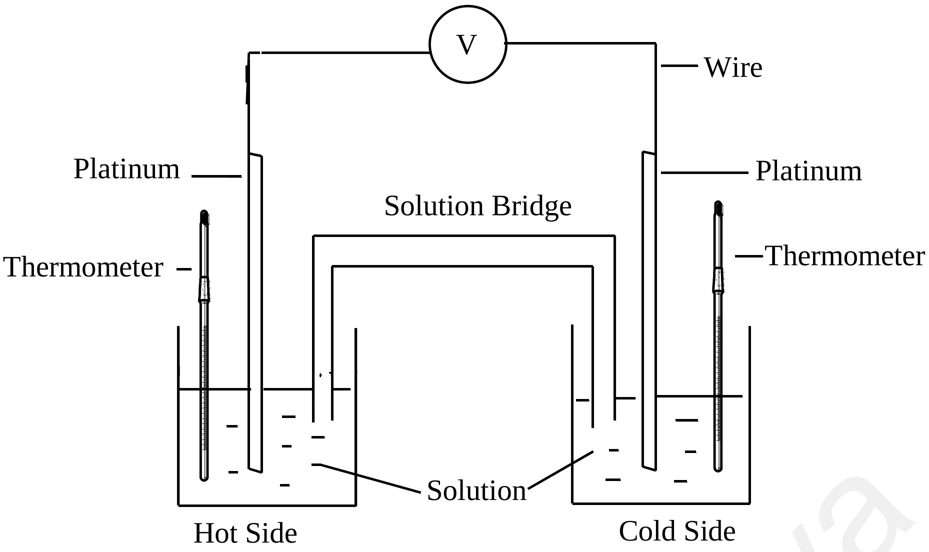

Figure 2.17 An experimental set-up for the thermoelectrical measurement in solutions

Recently, SCO was found to affect the thermoelectric properties of several complexes [78]. This was ascribed to entropy change (ΔS), since the bond lengths for an octahedral complex in the HS state are longer (weaker) compared to those of the LS state. A larger ΔS results in a higher S_e value.

Previous thermoelectrical study was done on a polymeric Cu(II) complex $[Cu_2(R)_4(bpy)]_x$ where R = 2-hexyldecanoato and bpy = 4,4'-bipyridine (**Figure 2.18**), formed from the reaction of $[Cu_2(R)_4(RH)_2]$ with bpy in hot ethanol [49]. Its S_e value in the presence of $KI–KI_3$ and TBATFB was -0.47 mV K^{-1}, and was postulated to arise from a one-electron reduction of $[Cu^{II}Cu^{II}(R)_4(bpy)]_x$ to $[Cu^{II}Cu^{I}(R)_4(bpy)]_x^-$ by I^- ion, followed by dissociation of R^- from the mixed-valence anionic polymer.

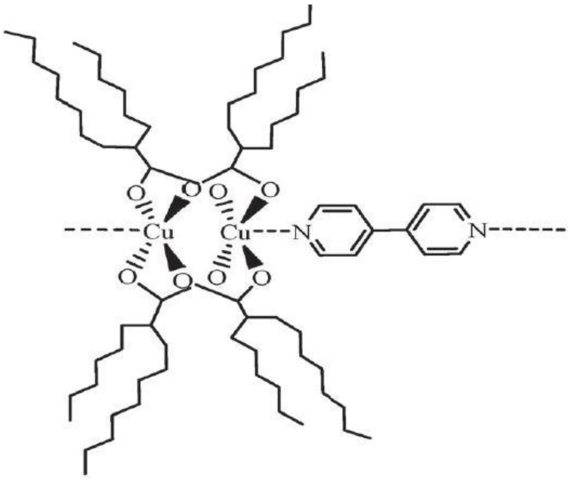

Figure 2.18 The proposed structure of [$Cu_2(R)_4(bpy)]_x$ [49]

2.3 Complexes of Nickel(II), Arylcarboxylate Ions and Cyclam

Nickel is a first-row transition metal with atomic number 28 (valence electron configuration $4s^2 3d^8$). Its most stable ion is Ni(II) ($3d^8$), and complexes of Ni(II) may either be octahedral, tetrahedral or square planar. Octahedral and tetrahedral Ni(II) complexes are paramagnetic with two unpaired electrons, while square planar complexes are diamagnetic (no unpaired electron). Complexes with weak field ligands tend to be tetrahedral, while those with strong field ligands tend to be square planar. The strength of field ligands are in the following order:

$Br^- < Cl^-$, $-SCN^-$, F^-, $OH^- < H_2O < -NCS^- < NH_3 < NO_2^- < CN^-$, CO
Weak-field ligands Strong-field ligands

The type of ligands influenced the geometry of Ni(II) complexes. Most Ni(II) arylcarboxylates were dimeric with octahedral geometry, while Ni(II)-cyclam complexes were octahedral with arylcarboxylato ligands at the axial positions. Most complexes gave μ_{eff} value of about 3 BM at room temperature.

An example is $[(Ni_2(\mu\text{-}H_2O)(\mu\text{-}R)_2(C_5H_5N)_4(R)_2].C_7H_8.RH$ (R = C_6H_5COO; C_7H_8 = toluene; C_5H_5N = pyridine) reported by Karmakar *et al.* [50]. The complex was obtained as blue monoclinic crystals from a solid state reaction between RH, KOH, and $NiCl_2$, followed by C_5H_5N. Its molecular structure (**Figure 2.19**) shows Ni(II) centers bridged by $C_6H_5COO^-$ and H_2O ligands and two nitrogen donor of pyridine each attached to Ni(II). Its IR spectrum showed peaks (in cm^{-1}) at 3062, 1711, 1613, 1567, 1537, 1398, 1224, 1160, 1070, and 824. Its UV-vis spectrum showed a *d-d* transition at 653 nm (ε = 14.1 M^{-1} cm^{-1}).

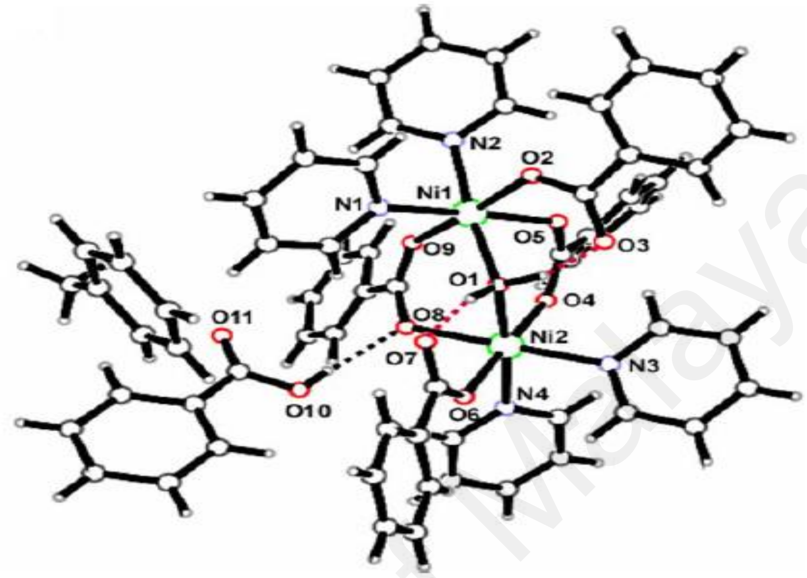

Figure 2.19 Crystal structure of $[(Ni_2(\mu\text{-}H_2O)(\mu\text{-}R)_2(C_5H_5N)_4(R)_2]{\cdot}C_7H_8.RH$ (R = C_6H_5COO) [50]

Kuppusamy *et al.*[51] reported an octahedral complex, $[Ni(N_2H_5)_2(C_6H_5COO)_4]$ (**Figure 2.20**), isolated as a light blue powder from the reaction involving an aqueous solution of nickel(II) nitrate hexahydrate and hydrazinium benzoate. Its X-ray powder pattern showed that the complex was non-isomorphous. Its IR spectrum showed peaks (in cm^{-1}) at 3360, 2660, 1685 and 1400 for NH_2, NH_3^+, υ_{asym}COO and υ_{sym}COO, respectively. The Δ value was 285 cm^{-1} (υ_{asym} = 1685 cm^{-1}; υ_{sym} = 1400 cm^{-1}), suggesting a monodentate coordination mode for $C_6H_5COO^-$ ion [13]. Its UV-vis spectrum showed two bands at 1030 nm and 351 nm, assigned to $^3A_{2g}$(F) to $^3T_{2g}$(F) and $^3A_{2g}$(F) to $^3T_{1g}$(P) electronic transitions of an octahedral Ni(II) complex (**Figure 2.21**), respectively. Its μ_{eff} value was 3.52 BM at room temperature. There were four decomposition stages from its TGA trace. The first stage in the temperature range of 130 – 240 ºC was for the formation of $Ni(C_6H_5COO)_2C_6H_5COOH$ (found = 30.00%; calculated = 30.56%), the second stage in the temperature range of 240 - 325 ºC was for the formation of $Ni(C_6H_5COO)_2$ (found = 50.50%; calculated = 50.61%), the third stage in the temperature range of 325 - 380 ºC was for the formation of NiC_2O_4 (found = 50.50%; calculated = 50.61%), and the last stage in the temperature range of 380 - 450 ºC was for the formation of NiO (found = 88.00%; calculated = 87.74%).

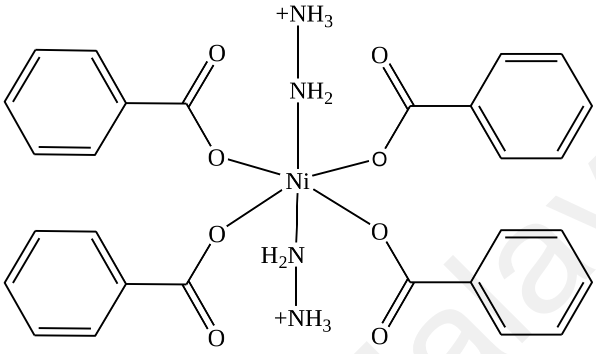

Figure 2.20 Proposed structure of $[Ni(N_2H_5)_2(C_6H_5COO)_4]$ [51]

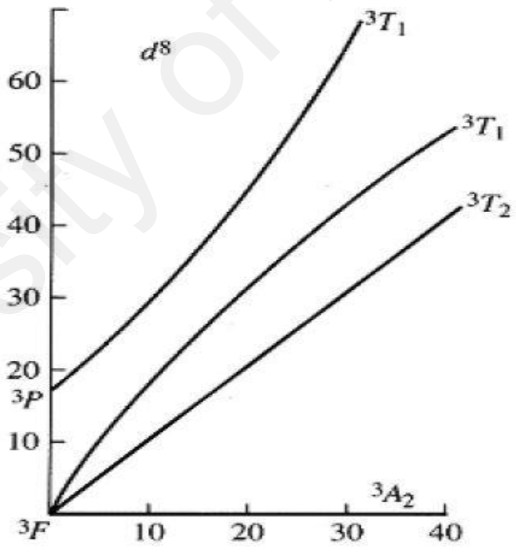

Figure 2.21 Tanabe-Sugano diagram showing for octahedral Ni(II) complexes (d^8)

Karmakar *et al.* [52] reported another dinuclear Ni(II) carboxylate, $[Ni_2(H_2O)(OOCC_6H_5)_4(py)_4]\cdot H_2O$ (**Figure 2.22**), synthesized by adding pyridine (py) to a heterogeneous solid mixture of nickel(II) chloride hexahydrate and potassium hydroxide, followed by benzoic acid. The complex was obtained as blue crystals. Its crystal structure shows that each of its Ni(II) center has an octahedral geometry with two bridging benzoato ligands, two coordinated pyridine molecules and a monodentate benzoato ligand, and separated by a bridging aqua group. Its UV-vis shows an absorption maximum at 648 nm (ε_{max} = 18.91 $M^{-1}cm^{-1}$), assigned to $^3A_2$ to $^3T_1$ transition, suggesting a distorted octahedral geometry at both Ni(II) centres.

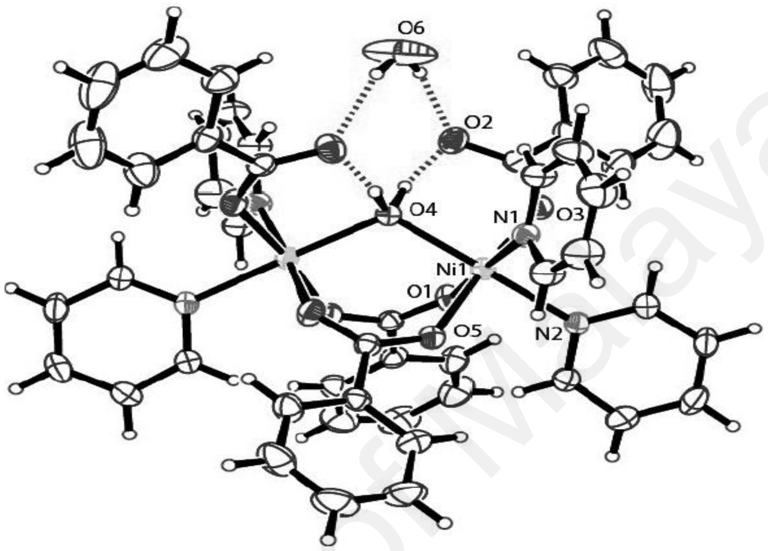

Figure 2.22 Crystal structure of $[Ni_2(H_2O)(OOCC_6H_5)_4(py)_4].H_2O$ [52]

Deka *et al*. reported on $[Ni(L_2)(py)_3(H_2O)_2]L_2$, where L = 2-carbomethoxybenzoate and py = pyridine (**Figure 2.23**) [53], synthesized from the reaction of nickel(II) chloride hexahydrate with phthalic anhydride and pyridine. The calculated percentages of C, H, and N from the proposed formula were 57.4% C, 4.7% H and 6.1% N, while the results from the elemental analyses were 58.0% C, 4.9% H and 5.9% N. Its IR spectrum showed peaks (in cm^{-1}) at 3086, 1639, and 1603 for υ(OH), υ(COO) for coordinated and υ(COO) for free carboxylic acid, respectively. Its UV-vis spectrum showed a *d-d* band at 648 nm, assigned $^3A_2$ to $^3T_1$ transition. The μ_{eff} value was 3.04 BM from the presence of two unpaired electrons of Ni(II) atom (d^8).

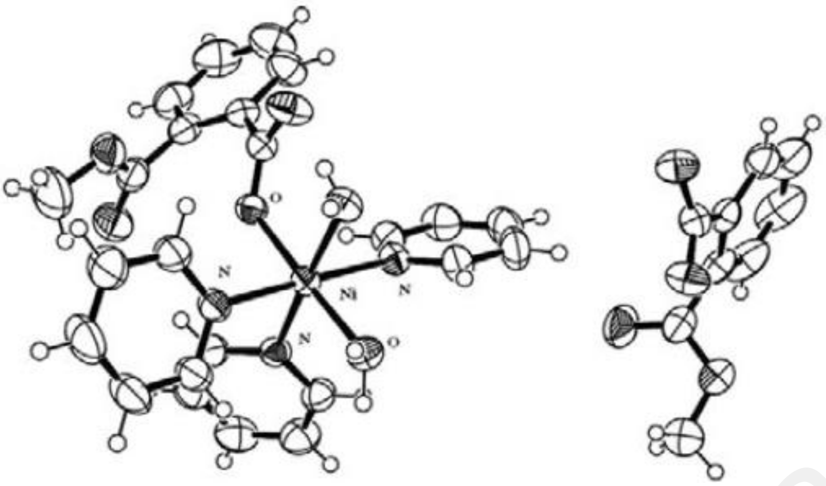

Figure 2.23 Crystal structure of [Ni(L_2)$(py)_3$$(H_2O)_2$]$L_2$ [53]

Lindoy *et al*. reported on crystals of [Ni(cyclam)$(C_6H_5COO)_2$] (**Figure 2.24**) [54], synthesized by adding nickel(II) carbonate tetrahydrate to a hot methanolic solution of benzoic acid. The calculated percentages for C, H, and N from the proposed formula were 57.5% C, 6.8% H and 11.2% N, while the results from the elemental analyses were 57.6% C, 6.7% H and 11.5% N. The complex has a tetragonally distorted octahedral Ni(II) atom with benzoate ions coordinated to the metal(II) atom at the axial positions. Its UV-vis spectrum showed a *d-d* band at 522, 635, 721, 873 and 975 nm, suggesting a tetragonally distorted octahedral Ni(II) atom.

Glidewell *et al.* [55] reported on a mononuclear [Ni(cyclam)$(4\text{-}HOC_6H_4COO)_2$] (**Figure 2.25**), synthesized by mixing an aqueous solution of [Ni(cyclam)]$(ClO_4)_2$ with 4-HOC_6H_4COONa. The complex was isolated as orange-brown crystals. Its crystal structure showed a Ni(II) atom adopting a *trans*-octahedral geometry with 4-$HOC_6H_4COO^-$ ligands at the axial positions, similar to that of [Ni(cyclam)$(C_6H_5COO)_2$]. The 4-$HOC_6H_4COO^-$ ligands were attached to the metal in a monodentate fashion and connected to cyclam by N–H•••O hydrogen bonds.

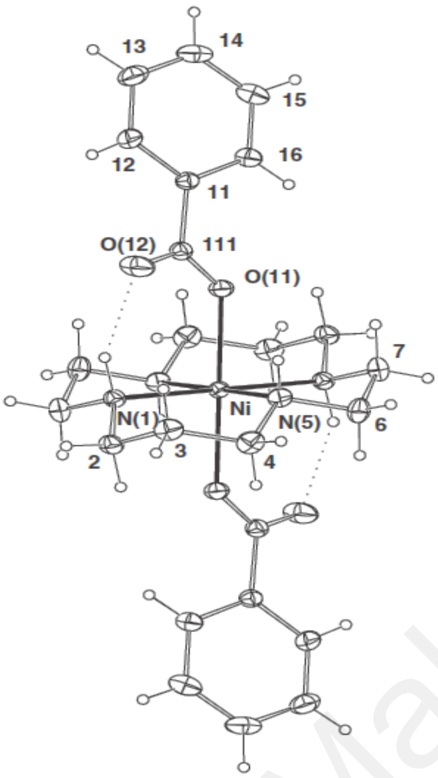

Figure 2.24 Crystal structure of [Ni(cyclam)($C_6H_5COO)_2$] [54]

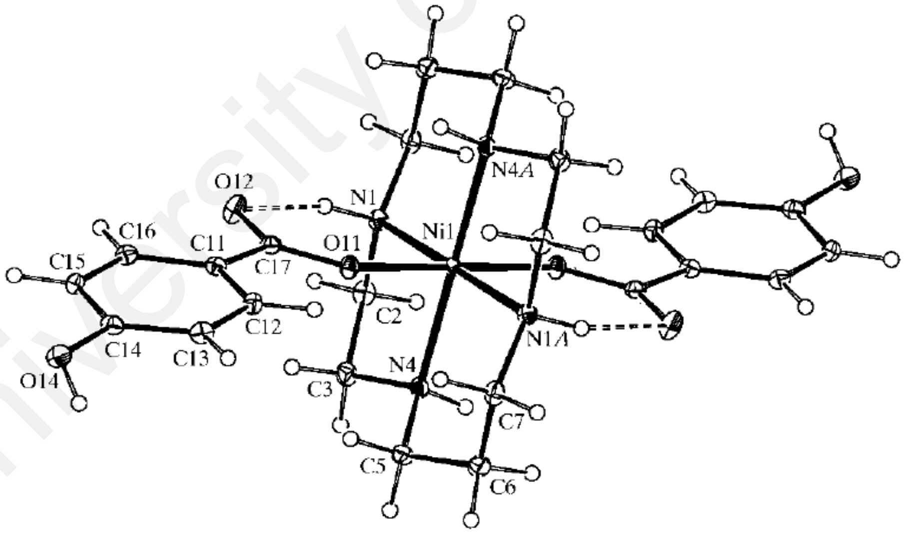

Figure 2.25 Crystal structure of [Ni(cyclam)(4-$HOC_6H_4COO)_2$] [55]

Trávníček *et al*. reported a mononuclear complex, [Ni($Bz_2dtc)_2$(cyclam)], where Bz_2dtc = N,N-dibenzyldithiocarbamate(1-) anion (**Figure 2.26**) [56], synthesized by reacting [Ni($Bz_2dtc)_2$] with cyclam in chloroform. The calculated percentages for C, H, and N from the proposed formula were 59.8% C, 6.5% H and 10.4% N, while the results from the elemental analyses were 59.3% C, 6.9% H and 10.5% N. Its IR spectrum showed peaks (in cm^{-1}) at 1493 and 983 for υ(C-N) and υ(C-S), respectively. Its UV-vis spectrum showed *d-d* bands at 800 nm (ε = 17 M^{-1} cm^{-1}), 555 nm (ε = 28 M^{-1} cm^{-1}) and 401 nm (ε = 72 M^{-1} cm^{-1}), assigned to $^3A_{2g}$ to $^3T_{2g}$, $^3A_{2g}$ to $^3T_{1g}$ and $^3A_{2g}$ to $^3T_{1g}$(P) electronic transitions, respectively, suggesting an octahedral geometry of Ni(II) atom [57]. The complex was paramagnetic and the μ_{eff} value was 3.12 BM at room temperature [58]. Its TGA and DTA results indicated that its decomposition temperature was in the range of 134-193 ºC, and the decay continued without forming thermally stable intermediates in some steps, but did not complete even at 1050 ºC. The major *exo*-effects were detected at *ca*. 480 ºC, suggesting the decomposition of the organic part of the complex.

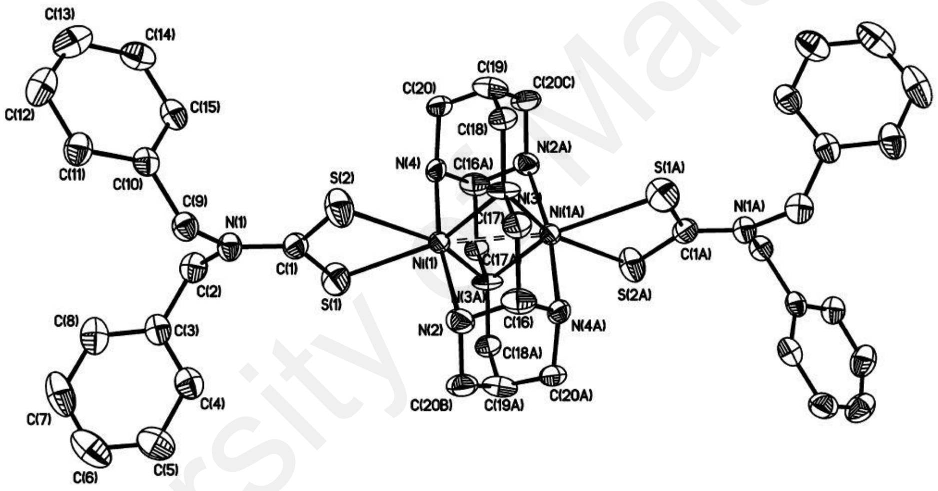

Figure 2.26 Crystal structure of [Ni(Bz_2dtc)$_2$(cyclam)] [56]

2.4 Complexes of Cobalt(II), Arylcarboxylate Ions and Cyclam

Cobalt is a first-row transition metal with atomic number 27 (valence electron configuration $4s^23d^7$). Its two most stable ions are Co(II) ($3d^7$) and Co(III) ($3d^6$). Co(II) octahedral complexes are paramagnetic, and depending on the ligands, may either be high spin (HS; $t_{2g}^5e_g^2$) with three unpaired electrons, or low spin (LS, $t_{2g}^6e_g^1$) with one unpaired electron. Co(II) complexes are also found in tetrahedral geometry, while square planar complexes are quite uncommon. Co(III) octahedral complexes are paramagnetic for HS ($t_{2g}^4e_g^2$; 4 unpaired electrons), but diamagnetic for LS ($t_{2g}^6e_g^0$).

Cobalt(II) arylcarboxylates have various structural motifs, but most of them are dinuclear with bridging aqua ligand [59]. Examples are $[(\mu_2\text{-}H_2O)(\mu_2\text{-bz})_2\{Co(bz)(L)_2\}_2]$ (L = pyridine, 4-methylpyridine, isoquinoline, furo[3,2-c]pyridine, 2-methylfuro[3,2-c]pyridine and 2,3-dimethylfuro-[3,2-c]pyridinedinuclear), bz = benzoato reported by Hudák *et al.* [60]. These complexes have two benzoato bridging and one aqua ligands, and showed weak antiferromagnetic interactions between the metal ions.

Another example is $[(\mu_2\text{-}H_2O)(\mu_2\text{-}R)_2\{Co(R\text{-}\kappa^1\text{-}O)(py)_2\}_2]\cdot 0.5RH\cdot 1.5MePh$, where R = PhCOO, py = pyridine (**Figure 2.27**), isolated as pink crystals [60]. The complex was synthesized by adding toluene to a solid mixture of sodium benzoate and cobalt(II) chloride, followed by addition of pyridine. Its crystal structure showed Co(II) centers linked by one aqua and two benzoato bridges, while each of its Co(II) atom was coordinated by one terminal monodentate benzoate ligand and two pyridine ligands. Its UV-vis spectrum showed *d-d* transitions at 833 nm, 556 nm, 526 nm and 444 nm, assigned to $^4T_{1g}(F)$ to $^4T_{2g}$, $^4A_{2g}$, $^4A_{2g}$, and $^4T_{1g}(P)$ electronic transitions, respectively, indicating an octahedral HS Co(II) complex, based on d^7 Tanabe-Sugano diagram (**Figure 2.28**).

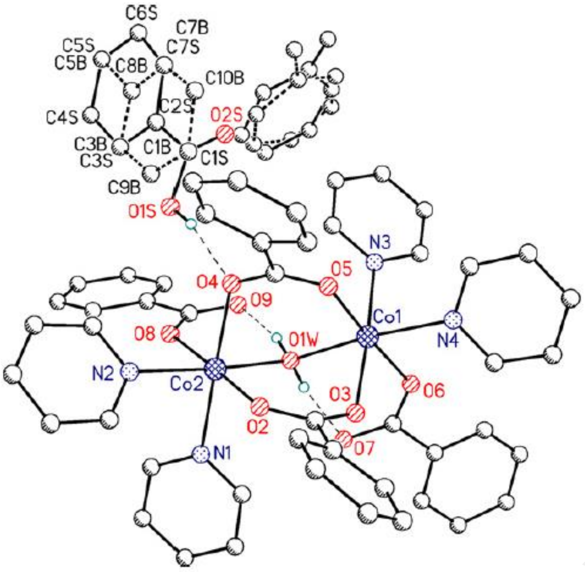

Figure 2.27 Crystal structure of $[(\mu_2\text{-}H_2O)(\mu_2\text{-}R)_2\{Co(R\text{-}\kappa^1\text{-}O)(py)_2\}_2]\cdot 0.5RH\cdot 1.5MePh$ (R = PhCOO [60]

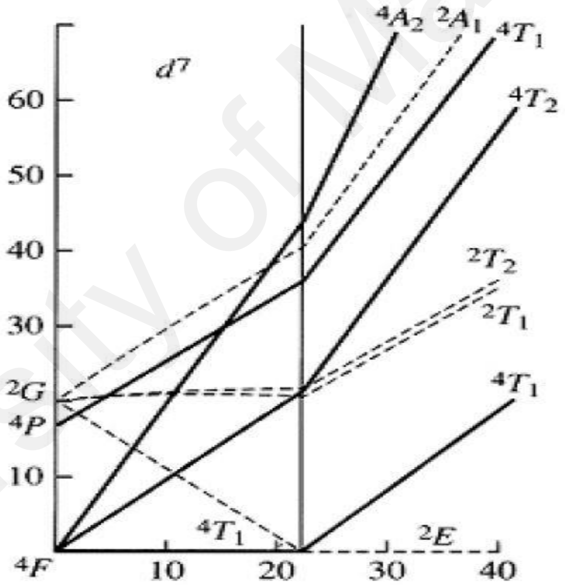

Figure 2.28 Tanabe-Sugano diagram for *d^7*

Cobalt(II) benzoates may be found as mononuclear, dinuclear, trinuclear, and polynuclear complexes [61]. Mononuclear complexes were mostly made up of hexacoordinated central atom and monodentate benzoato ligand. [61]. Dinuclear complexes can be divided to two groups. The first group has pentacoordinated Co(II) and benzoato bridge. Examples are $[Co_2(quin)_2(C_6H_5CO_2)_4]$ where quin = quinolone [62] (**Figure 2.29**).

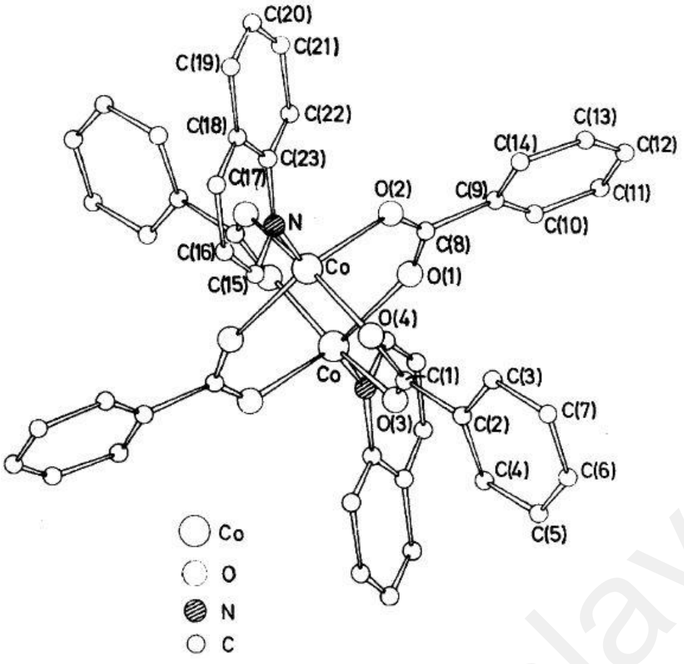

Figure 2.29 Crystal structure of [$Co_2(quin)_2(C_6H_5CO_2)_4$] [62]

The second group has hexacoordinated Co(II) and one aqua bridging ligand. An example is [$Co_2(\mu\text{-}H_2O)(\mu\text{-}OBz)_2(OBz)_2(Py)_4$]$\cdot$1.5$C_6H_6$ (**Figure 2.30**) [63].

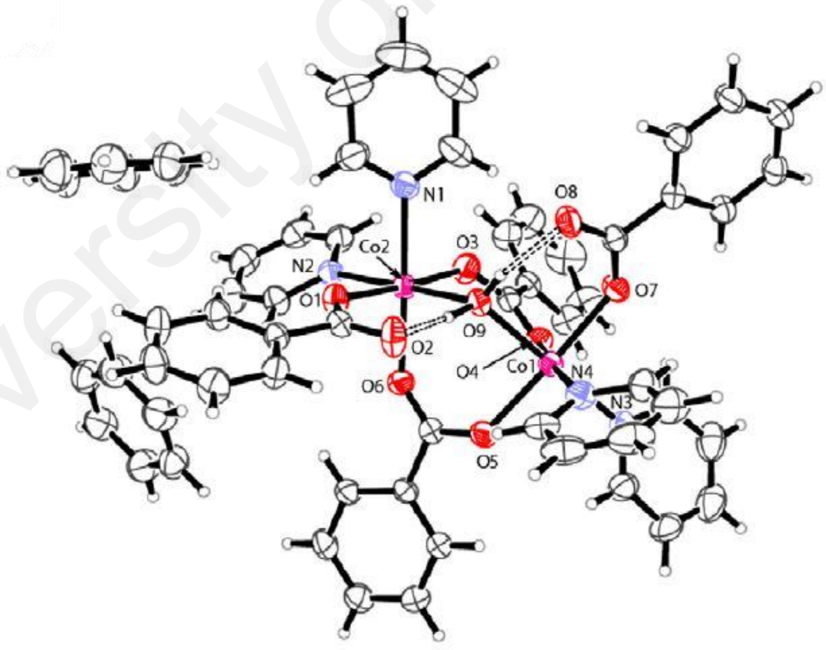

Figure 2.30 Crystal structure of [$Co_2(\mu\text{-}H_2O)(\mu\text{-}OBz)_2(OBz)_2(Py)_4$]$\cdot$1.5$C_6H_6$ [63]

The trinuclear complexes have the composition [(μ_2-bz-O,O,O')$_2$(μ_2-bz-O,O')$_4$$Co_3(py)_2$], in which the central unit was hexacoordinated and the peripheral units were pentacoordinated. An example is $[Co_3(PhCOO)_6(L)_2]\cdot 2CH_3CN$, where L = 4-[2-(tetrathiafulvalenyl)ethenyl]pyridine (**Figure 2.31**) [64].

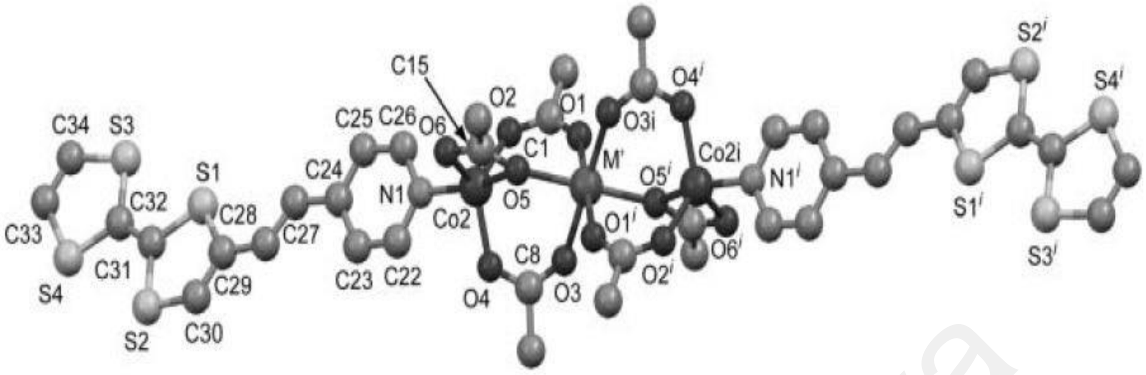

Figure 2.31 Crystal structure of $[Co_3(PhCOO)_6(L)_2]\cdot 2CH_3CN$ [64]

Caneschi *et al.* [65] reported $[Co(Me_4\text{-cyclam})(PhenSQ)]PF_6$, where PhenSQ = 9,10-dioxyphenanthrene (**Figure 2.32**), synthesized by mixing a methanolic solution of 9,10-dihydroxyphenanthrene to a methanolic solution of $[Co(Me_4\text{-cyclam})(CH_3CO_2)]PF_6$, followed by NaOH, a solution of ferrocenium hexafluorophosphate in acetone, and an aqueous solution of KPF_6. The complex was obtained as blue microcrystals. Its crystal structure showed that the cobalt(II) ion was hexacoordinated, the macrocyclic cyclam was bound in a folded configuration and PhenSQ was bound as a bidentate ligand. The calculated percentages were 50.0% C, 6.6% H and 8.3% N, while the results from the elemental analyses were 49.8% C, 6.2% H and 8.1% N. Its UV-vis spectrum showed a peak at 657 nm and 585 nm that assigned to MLCT transitions, and its χT value at 300 K was 3.6 $cm^3\ K\ mol^{-1}$, indicating a HS Co(II) complex.

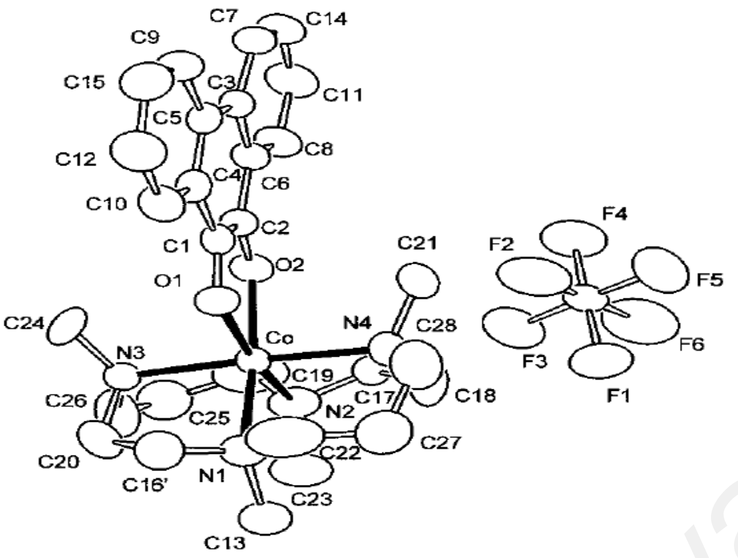

Figure 2.32 Crystal structure of [Co(Me$_4$-cyclam)(PhenSQ)]PF$_6$ [65].

Ivanikova´ *et al*. [66] reported bright-green crystals of [CoCl$_2$(cyclam)]Cl (**Figure 2.33**), synthesized from the reaction of CoCl$_2$.6H$_2$O with cyclam in refluxing methanol. Accordingly, Co(II) was oxidised to Co(III) in air during synthesis. Its structure showed Co(III) atom in a distorted octahedral geometry involving cyclam and two chloride anions. The Co(III) atom was placed on a centre of inversion, and the free Cl$^-$ ion formed N-H•••Cl hydrogen bonds.

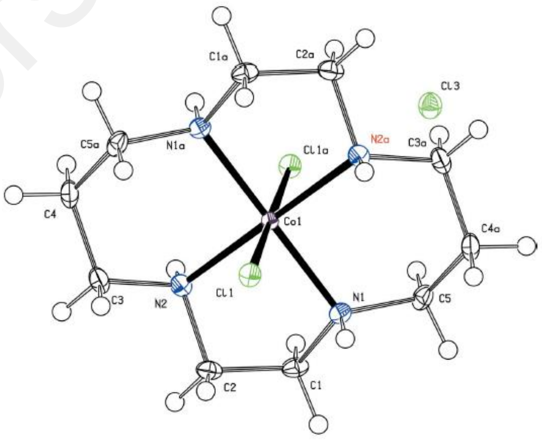

Figure 2.33 Crystal structure of [CoCl$_2$(cyclam)]Cl [66].

Simon *et al.* [67] reported [Co(cyclam)(acac)](BF$_4$)$_2$, (**Figure 2.34**) synthesized by adding an aqueous solution of tetrafluoroboric acid to a methanolic solution of [Co(cyclam)(acac)](acac)$_2$, where acac = acetylacetonate. Its IR spectrum showed peaks (in cm^{-1}) at 1613, 1568, 1525 for υ(C-O$_{\text{non-chelated}}$), υC=O and υC=C, respectively. Its structure showed that cobalt(III) atom was hexacoordinated by four nitrogen atoms and two oxygen atoms in a slightly distorted octahedron. Its UV-vis spectrum showed two *d-d* transitions at 516 nm (ε_{max} = 224) and 330 nm, assigned to $^1A_{1g}$ to $^1T_{1g}$ and $^1A_{1g}$ to $^1T_{2g}$, respectively [68].

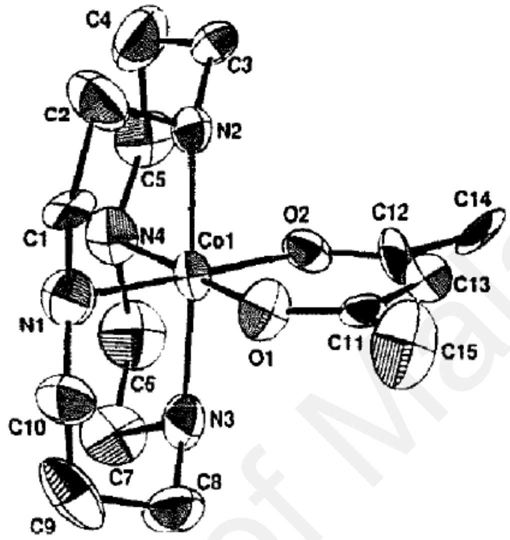

Figure 2.34 Crystal structure of [Co(cyclam)(acac)](acac)$_2$ [67]

Another example of a Co(III)-cyclam complex is [Co(AQ2C)$_2$(cyclam)]Cl, where AQ2CH = anthraquinone-2-carboxylic acid (**Figure 2.35**) [69], obtained as a pale pink powder. The calculated percentages for C, H, and N were 59.6% C, 4.9% H and 7.0% N, while the results from the elemental analyses were 59.7% C, 5.8% H and 6.4% N. Its IR spectrum showed peaks (in cm^{-1}) at 1674, 1604, 1556, 1484, 1400, and 1334. Its mass spectrum (ESI positive ion) gave the *m/z* of 761 for [Co(AQ2C)$_2$(cyclam)]$^+$ ion.

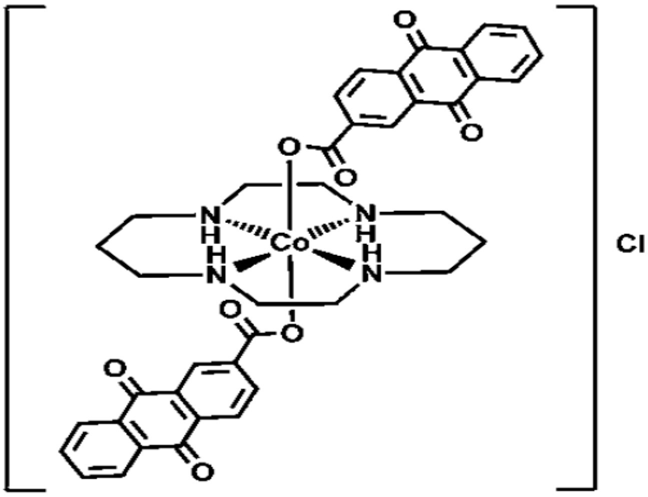

Figure 2.35 Proposed structure of $[Co(AQ2C)_2(cyclam)]Cl$ [69]

Co(II) and Co(III) complexes are examples of spin crossover (SCO) materials. This is a phenomenon involving electronic transition between LS and HS states, and vice versa, and is exhibited by octahedral complexes of first-row transition-metal ions with labile electronic configurations (d^4-d^7) (**Figure 2.36**) and ligands of intermediate field strengths, such as N- and O- donors. Weak field ligands stabilize HS (maximum spin multiplicity) ground state, while strong field ligands stabilize LS (minimum multiplicity) ground state. The coordinate bonds in HS complexes are longer (weaker) than in LS complexes. The SCO transition may be induced by external stimuli, such as temperature, pressure and light [4], which leads to distinctive changes in magnetism, colour and structure, and presents interesting fundamental aspects and potential applications, such as in memories storage, switching devices and sensors [4].

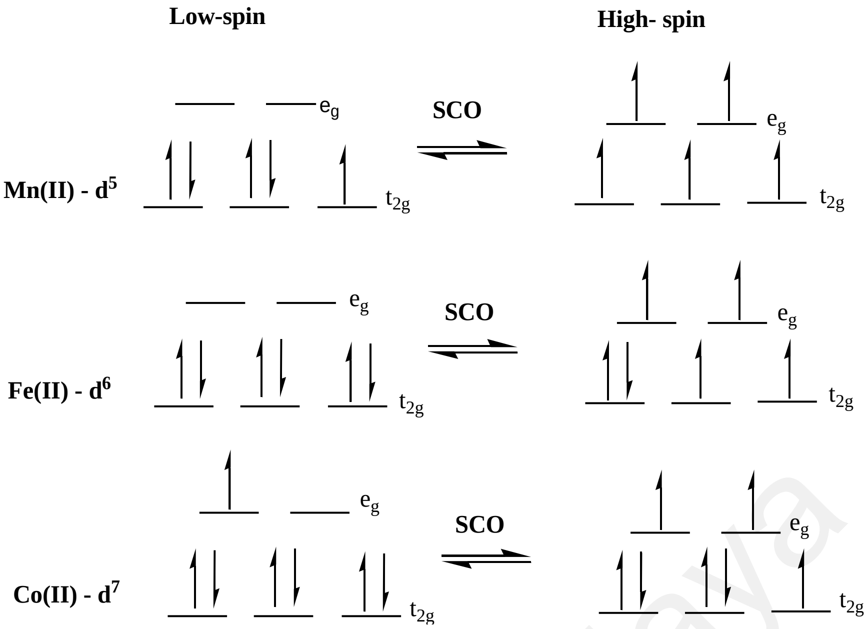

Figure 2.36 Valence electronic configurations for low spin and high spin metal(II) complexes that show SCO behaviour

The SCO phenomenon was first reported by Cambi *et. al.* [70], and currently there are hundreds of SCO complexes synthesized and characterized, either as bulk or diluted materials. An ideal SCO behaviour shows: (a) abrupt transition (need strong intermolecular interaction); (b) $T_{1/2}$ (temperature where there is 50% LS and 50% HS complexes) at room temperature; and (c) wide hysteresis ($\Delta T_{1/2}$) loop (**Figure 2.37**).

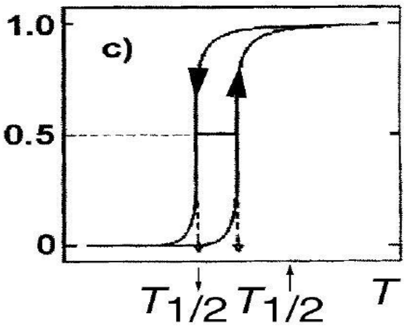

Figure 2.37 An ideal SCO behaviour

For example, Enachescu *et al.* [71] reported the SCO behavior of $[Co(terpy)_2](ClO_4)_2$ (terpy = 2,2':6',2''-terpyridine) by optical spectroscopy and magnetic susceptibility measurements. The temperature dependence of the solution UV-vis spectrum of the complex at room temperature showed peaks at 667 nm

(ε = 86 M^{-1} cm^{-1}), 549 nm (ε = 405 M^{-1} cm^{-1}), 505 nm (ε = 1100 M^{-1} cm^{-1}) and 442 nm (ε = 1285 M^{-1} cm^{-1}). The broad band at 667 nm was assigned to transitions from $^2A_1$ in a compressed D_{2d} symmetry to low-symmetry and spin orbit levels arising from $^2T_{1g}$ and $^2T_{2g}$ ligand-field states of octahedral parentage [72]. The peaks at 549 nm, 505 nm and 442 nm were assigned to MLCT transitions (low-spin species), which decreased in intensity as the temperature was increased, in agreement with normal thermal spin transition. An increase in temperature had caused the *d–d* band of the low-spin species between 741 nm and 645 nm to decrease. Earlier studies using magnetic measurements and the Evans technique [73] have shown that in solutions at room temperature, about 30% of the complex was LS [74]. The magnetic susceptibility measurements show typical behaviour for a cobalt(II) SCO complex, with χ_T close to 0.4 cm^3 mol^{-1} K at lower temperature (spin-only value for LS) and around 2.4 cm^3 mol^{-1} K at room temperature (suggesting around 80% HS) [69,72].

Hayami *et al*. [76] reported magnetic properties and structural characteristics of several SCO cobalt(II) complexes with terpy (terpy = terpyridine (**Figure 2.38**) derivatives attached with various substituents at the 4-position. Substitution at the 4-position of terpy ligand gives various magnetic behavior of cobalt(II) complexes by improving intermolecular interactions. The interaction between other molecules from the outside and terpy-appended cobalt(II) complexes also affects their magnetic property. For example, $[Co(terpy)_2](ClO_4)_2{\cdot}nH_2O$ (n = 0, 0.5) and $[Co(OH\text{-}terpy)_2](ClO_4)_2{\cdot}nH_2O$ (n = 3, 4) showed gradual SCO behaviour, while $[Co(pyterpy)Cl_2]S$ (5·S) showed SCO depending on the guest solvent molecules involved. Meanwhile, [Co(4’-5’’’-decyl-1’’’-heptadecyloxy-2,2’:6’,2’’-terpy)$_2$](BF$_4$)$_2$ with branched alkyl chains exhibited SCO with liquid crystal behaviour, and $[Co(C_nterpy)_2](BF_4)_2$ (n = 12, 14, 16) with long alkyl chains showed unique SCO behaviour, namely “reverse spin transition” or “re-entrant SCO”.

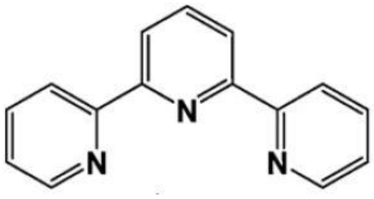

Figure 2.38 The chemical structure of terpyridine

Hayami *et al.* [77] reported that cobalt(II) complexes of 4′-methoxy-2,2′:6′,2″-terpyridine, $[Co(MeO\text{-}terpy)_2](BF_4)_2\cdot H_2O$ (**1**·H_2O) and $[Co(MeO\text{-}terpy)_2](BF_4)_2\cdot$acetone (**1**·acetone) showed different magnetic properties. **1**·H_2O showed gradual SCO, whereas **1**·acetone was HS at all temperatures. These complexes were then annealed to form two desolvated **1** and **1′**. The solvated **1**·H_2O showed a two-step SCO behaviour while the non-solvated **1** showed a gradual SCO behaviour, whereas **1′** shows a "reverse spin transition" that can be associated to a structural phase transition.

Abdullah *et al* [78] reported three Co(II) complexes, $[Co(L^{12})_2](BF_4)_2$ (**1**), $[Co(L^{14})_2](BF_4)_2\cdot H_2O$ (**2**) and $[Co(L^{16})_2](BF_4)_2\cdot H_2O$ (**3**), produced by facile one-pot reactions involving $Co(BF_4)_2\cdot 6H_2O$, 2,6-pyridinedicarboxaldehyde, and $C_nH_{2n+1}NH_2$ (n = 12, 14, 16), respectively. The complexes were brick-red solids. Complex **1** **(Figure 2.39)** showed a tetragonally compressed CoN_6 coordination geometry based on single crystal X-ray crystallography. All complexes were thermally stable with low melting temperatures and displayed a columnar rectangular mesophase. At room temperature, these complexes were HS. Complexes **1** and **3** exhibited normal thermal SCO behaviour with weak hysteresis loops at temperatures below their melting temperatures. Hence, these complexes showed uncoupled phase transitions (class iiia) [4]. In addition, thermoelectrical measurements gave similar Seebeck values for $\mathbf{1}^{2+,3+}$ (S_e = 1.89 ± 0.02 mV K^{-1} and $\mathbf{2}^{2+,3+}$ (1.92 ± 0.08 mV K^{-1}).

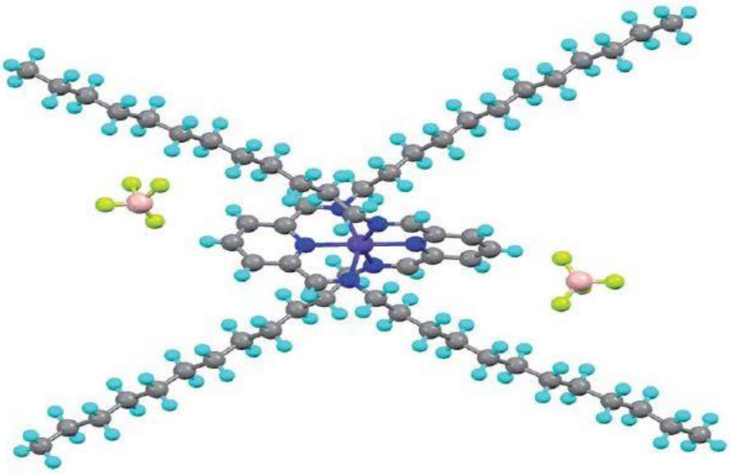

Figure 2.39 The structure of $[Co(L^{12})_2](BF_4)_2$ [78]

To summarise, most cobalt(II) and cobalt(III) arylcarboxylates are octahedral and dinuclear with bridging aqua, while cobalt-cyclam complexes are octahedral. Depending on the ligands, these complexes may either be HS or LS, or may exhibit normal or reverse SCO behaviour. In addition, complexes with long alkyl chain ligands exhibit SCO with liquid crystal behavior or re-entrant SCO. Currently, the thermoelectrical studies were reported for mixed valence cobalt(II/III) complexes.

2.5 Complexes of Iron(II), Arylcarboxylate Ions and Cyclam

Iron is a first-row transition metal with atomic number 26 (valence electron configuration $4s^2d^6$). The valence electronic configuration for Fe(II) ion is $3d^6$ and for Fe(III) ion is $3d^5$. HS octahedral complexes of Fe(II) are paramagnetic ($t_{2g}^4e_g^2$; 4 unpaired electrons), while LS complexes are diamagnetic (t_{2g}^6; 0 unpaired electron). In contrast, both HS ($t_{2g}^3e_g^2$) and LS ($t_{2g}^5e_g^0$) octahedral Fe(III) are paramagnetic, with five and one unpaired electrons, respectively. Fe(II) complexes are easily oxidized to Fe(III) complexes in the presence of oxygen and in alkaline medium.

Iron(II) carboxylates are normally octahedral. An example is dimeric Fe(II) carboxylate, $[Fe(H_4L)_2]$ (**Figure 2.40**) [79]. The complex was isolated as single crystals from the reaction of $FeCl_2·4H_2O$ with H_5L ($4-(HOOCC_6H_4CH_2N(CH_2PO_3H_2)_2)$) and 4,4'-

bipy in water. Its crystal structure showed that Fe(II) was hexacoordinated with six phosphonate oxygen from four H_4L^- anions. H_4L^- ion acted as a tridentate ligand and its oxygen atoms were monodentate, while the carbonyl oxygen atom of the COOH group was coordinated to the metal ion. The calculated percentages of C, H, and N were 32.8% C, 3.9% H and 3.8% N, while the results found from the elemental analyses were 32.9% C, 3.8% H and 3.8% N.

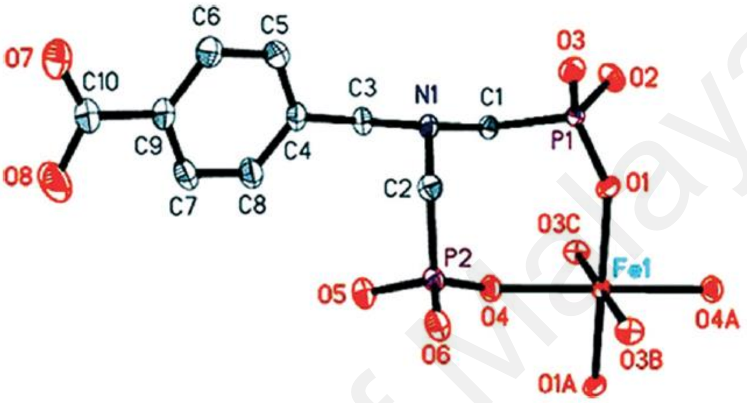

Figure 2.40 Crystal structure of $[Fe(H_4L)_2]$ [79].

Another example is *trans*-$[Fe_2(CH_3COO)_4(L1)_2]$ [80] (**Figure 2.41(a)**), formed as a dark purple powder from the reaction of 4,4'-bis[3,4-bis(tetradecyloxy)styryl]-2,2'-bipyridine (L1) in chloroform with a methanolic solution of $Fe(CH_3COO)_2$ and ascorbic acid. Its proposed structure as geometry optimized, and IR spectral simulation modeled on *trans*-$[Fe_2(CH_3COO)_4(L3])$ (L3 = 4,4'-bis(tetramethoxy)styryl-2,2'-bipyridine) (**Figure 2.41(b)**) was performed within the domain of DFT. Its IR spectrum showed peak at 1672 cm^{-1}, 1596 cm^{-1} for υ_{asym}COO and 1466 cm^{-1} for υ_{sym}COO. Hence, the Δ values were 130 cm^{-1} and 206 cm^{-1}, suggesting bidentate chelating and monodentate bridging modes, respectively for CH_3COO ligand [81]. Its UV-vis spectrum showed a strong peak at 544 nm (ε_{max} = 2194 M^{-1} cm^{-1}) for MLCT (t_{2g} to π^*) [82] and two *d-d* peaks at 1412 nm (ε_{max} = 26 M^{-1} cm^{-1}) and 1755 nm (ε_{max} = 26 M^{-1} cm^{-1}), assigned to the electronic transitions, $^5T_{2g}$ to ^5E_g and $^5T_{2g}$ to $^5T_{2g}$ for a distorted octahedral HS Fe(II) complex (**Figure 2.42**). There was another *d-d* peak assigned to $^1A_{1g}$ to $^1T_{1g}$ for LS Fe(II). Hence, the complex consisted of a mixture of HS and LS Fe(II) atoms, which was supported by its magnetic data indicating 56.8% HS and 43.2% LS Fe(II) atoms 294 K [83].

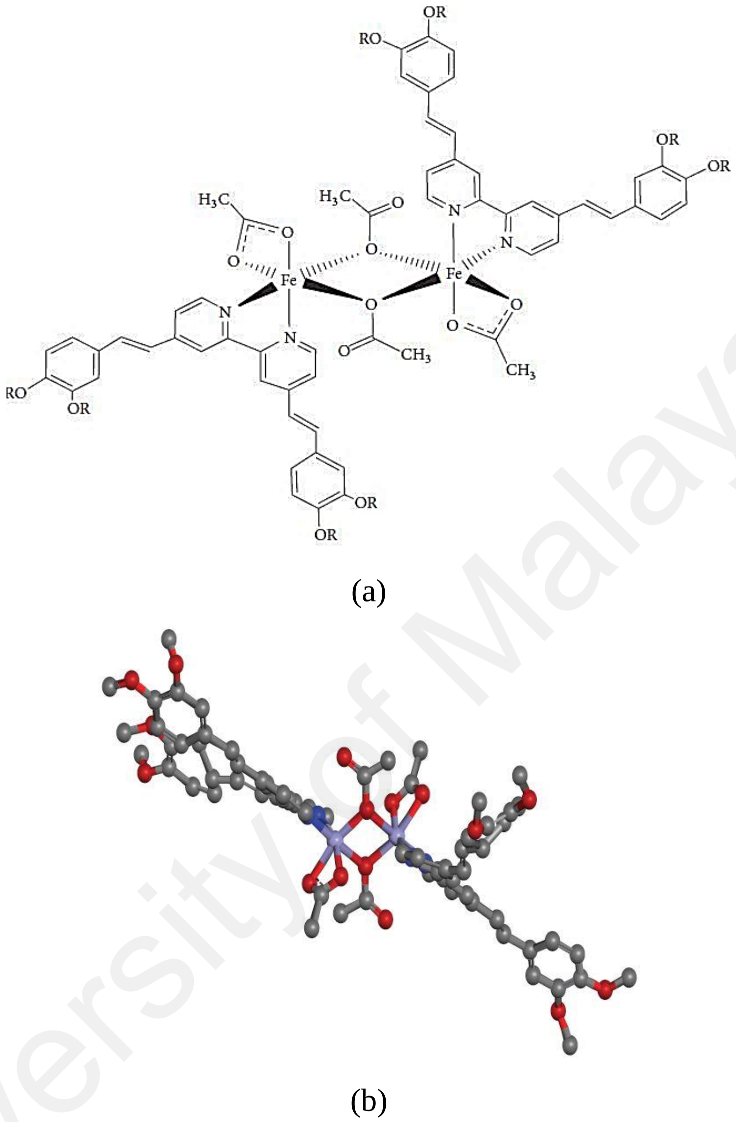

Figure 2.41(a) Proposed structure of *trans*-$[Fe_2(CH_3COO)_4(L1)_2]$ (R = $CH_3(CH_2)_{13}$); and (b) molecular model for *trans*-$[Fe_2(CH_3COO)_4(L3])$ [80]

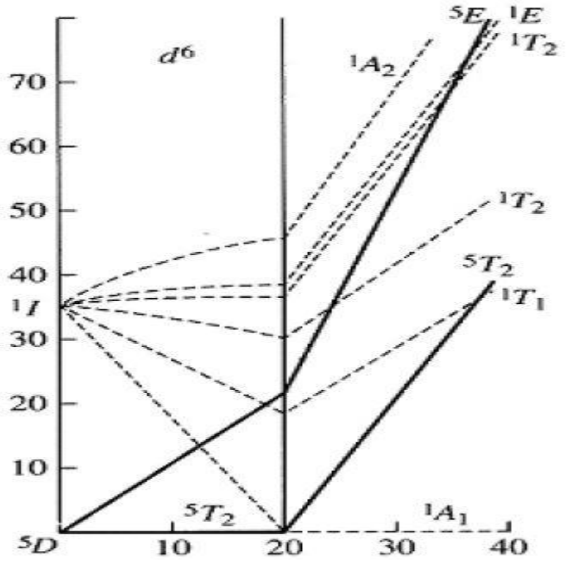

Figure 2.42 Tanabe-Sugano diagram for d^6 complexes

Lee *et al.* [84] reported $[Fe(L3)_2](BF_4)_2$ (**Figure 2.43**), obtained as a sticky dark-purple solid from the reaction $FeCl_2.4H_2O$ with $NaBF_4$, ascorbic acid and 2,2'-(4-(5-decylheptadecyloxy)pyridine-2,6-diyl)bis(1-(5-decylheptadecyl)1Hbenzo[d]imidazole (L3). The $\chi_M T$ value of the complex was 1.44 cm^3 K mol^{-1} at 33 K, indicating 43% HS iron(II) atom. On heating, the $\chi_M T$ values did not change up to 123 K, then gradually increased from 1.35 cm^3 K mol^{-1} at 124 K to 1.86 cm^3 K mol^{-1} at 233 K, and then abruptly decreased at around $T_{½}$ = 236 K due to solid–liquid crystal phase transition. Its DSC scan showed endothermic peaks at 236 K (ΔH = +32 kJ mol^{-1}), 351 K (ΔH = +172 kJ mol^{-1}), and 454 K (ΔH value was not given) on heating, assigned to crystal-to-mesophase, mesophase–to-mesophase and mesophase-to-isotropic liquid transitions, respectively. On cooling, there were exothermic peaks at 421 K, 334 K, and 229 K for the reversible mesophase-to-crystal transition. Its optical textures showed solid crystalline-like chestnut burr at 203 K (**Figure 2.44**).

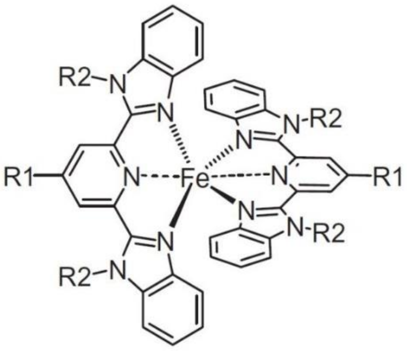

Figure 2.43 The proposed structure of $[Fe(L3)_2](BF_4)_2$ (R1 = $OC_{27}H_{55}$, R2 = $C_{27}H_{55}$) [84]

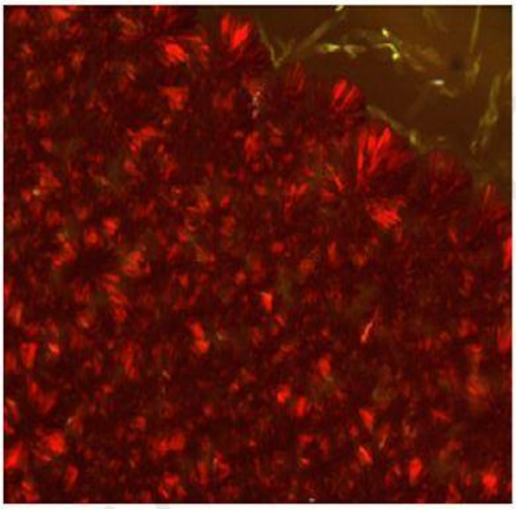

Figure 2.44 Optical textures of $[Fe(L3)_2](BF_4)_2$ at 203 K [84]

Shahbazi-Raz *et al*. [85] reported $[Fe(5,5'\text{-dmbipy})(NCS)_2(\mu\text{-}OCH_3)]_2$, where 5,5'-dmbipy = 5,5'-Dimethyl-2,2'-bipyridine (**Figure 2.45**), obtained as deep red plate crystals from the reaction of $FeCl_2.4H_2O$ with KSCN in CH_3OH, followed by 5,5'-dmbipy in CH_3CN. Its TGA curve (**Figure 2.46**) shows four thermal decomposition steps. The first step (in the range 200 ºC and 315 ºC) was assigned to loss of two methyl groups from two methoxy groups (found = 3.6%; calc. = 3.8%). In the last three steps (in the range 320 ºC and 630 ºC) were assigned to loss of four NCS anions, two oxygen atoms and two 5,5'-dmbipy molecules (found = 77.6%; calc.= 75.5%). The final residual weight was 19.1% assigned to Fe_2O_3 (calc. = 20.7%). Its DTA curve shows four exothermic peaks at 181 ºC, 340 ºC, 385 ºC and 509 ºC.

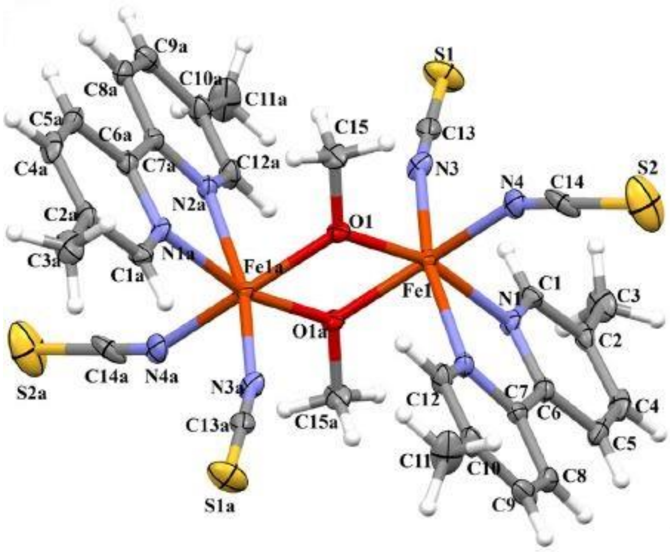

Figure 2.45 The proposed structure of $[Fe(5,5'\text{-dmbipy})(NCS)_2(\mu\text{-}OCH_3)]_2$ [85]

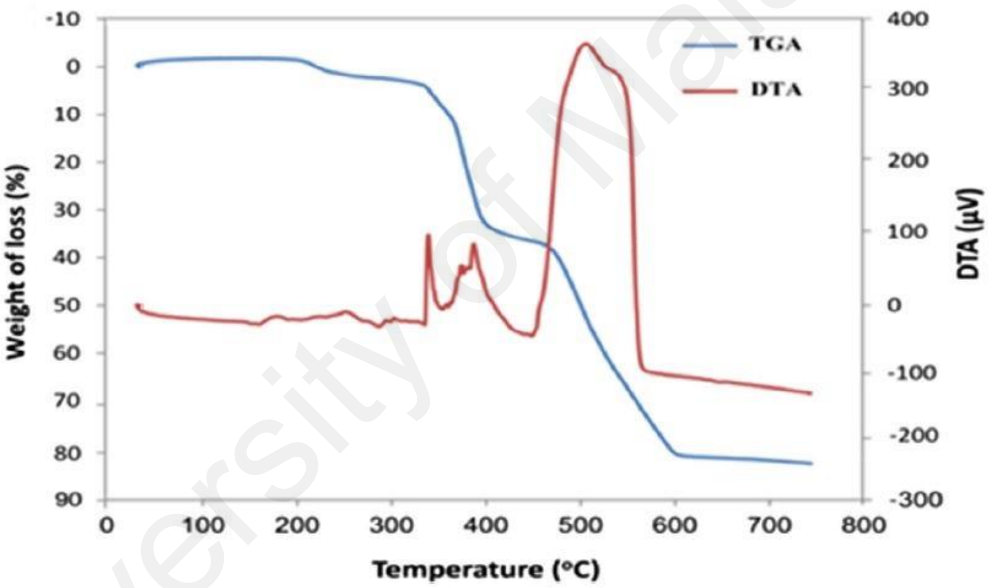

Figure 2.46 The thermal behaviour of $[Fe(5,5'\text{-dmbipy})(NCS)_2(\mu\text{-}OCH_3)]_2$ [85]

Abdullah *et al.* [8] reported $[Fe(L1)_3](BF_4)_2{\cdot}4H_2O$ (**Figure 2.47(b)**), obtained as a dark purple powder from the reaction of iron(II) tetrafluoroborate hexahydrate in the presence of ascorbic acid (as antioxidant) and L1 (**Figure 2.47(a)**) under nitrogen. Its IR spectrum showed peaks at 2917, 2849, 1670, 1594, 1266, and 1054 cm^{-1} for $\nu(CH_{2asym})$, $\nu(CH_{2sym})$, ν(vinylic C=C), ν(aromatic C=C), ν(C–O) and $\nu(BF_4^-$ ion). Its UV-vis spectrum showed peaks at 310 nm (ε_{max} = 44000 M^{-1} cm^{-1}) and 392 nm (ε_{max} = 40000 M^{-1} cm^{-1}) for intraligand bands, and at 561 nm (ε_{max} = 13000 M^{-1} cm^{-1}) for

MLCT from LS Fe(II) atom. Its $\chi_M T$ value was 1.0 cm^3 K mol^{-1}, indicating 33% HS and 67% LS Fe(II) atoms at 25 ºC. The percentage of LS Fe(II) atom was high due the presence of stronger ligand field in the complex. From thermoelectrical data, its S_e value was -0.54 ± 0.02 mV K^{-1}, and was ascribed to BF_4^- anions as dominant charge carriers due to its smaller mass and volume (higher mobility) than the larger cationic complex.

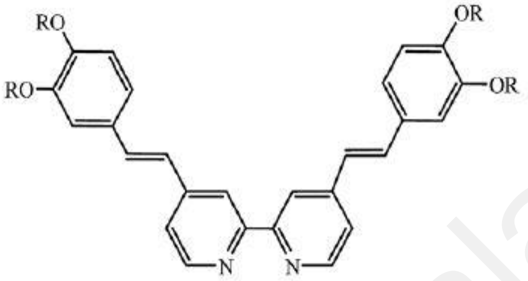

(a)

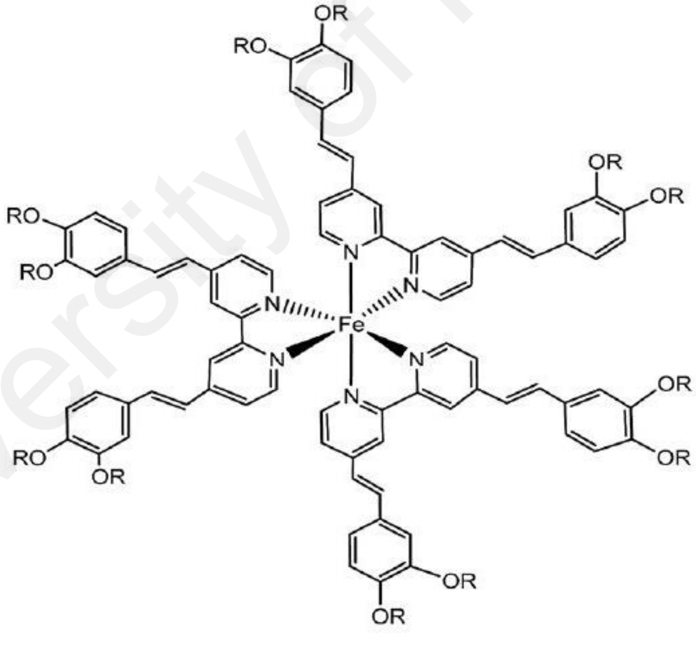

(b)

Figure 2.47 The structural formulae of (a) L1 (R = $CH_3(CH_2)_{13}$), and (b) $[Fe(L1)_3]^{2+}$ [8]

Santos *et al*. [86] reported *trans*-$[Fe(cyclam)(NCS)_2](PF_6)$, obtained as red crystals from the reaction of *trans*-$[Fe(cyclam)FeCl_2]Cl$ with KCNS and NH_4PF_6. Its structure shows a distorted octahedral complex with the thiocyanate groups *trans*-coordinated to Fe(III) atom (**Figure 2.48**).

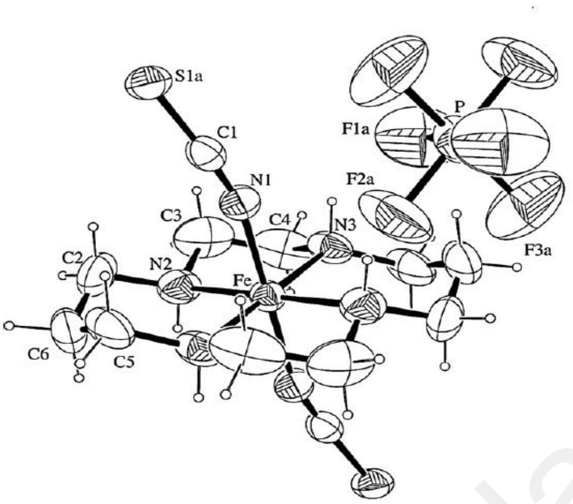

Figure 2.48 Crystal structure of *trans*-[Fe(cyclam)(NCS)$_2$](PF$_6$) [86]

Vasconcellos *et al.* [87] reported *cis*-[Fe(cyclam)(qH)](PF$_6$)$_2$ (qH = C_6H_5NO) (**Figure 2.49**), isolated as dark blue microcrystals from the reaction of equimolar amount of *cis*-[Fe(cyclam)(qH)](PF$_6$)$_2$ and 2-aminophenol in 1:1 methanol-water. The calculated percentages of C, H, and N were 29.4% C, 4.4% H and 10.7% N, while the results from elemental analyses were 29.7% C, 4.3% H and 10.5% N. Its structure showed Fe(II) atom hexacoordinated to four nitrogen atoms of cyclam, and one oxygen atom and one nitrogen atom of qH ligand.

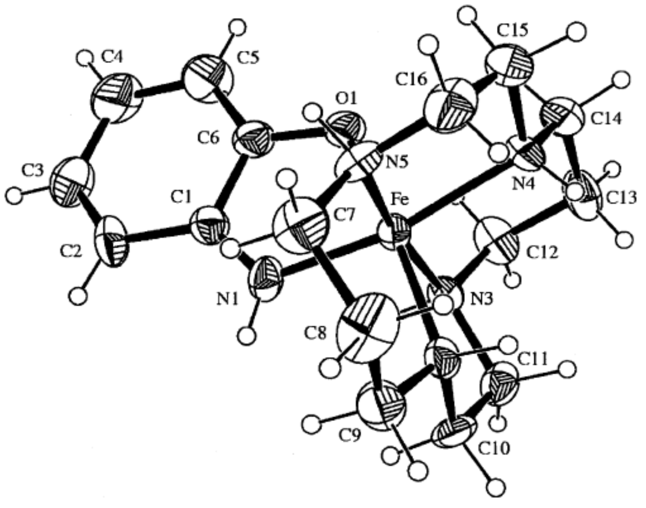

Figure 2.49 Crystal structure of *cis*-[Fe(cyclam)(qH)](PF$_6$)$_2$ [87].

To summarise, Fe(II) carboxylates usually have octahedral geometry and are easily oxidized to Fe(III) complexes. Both Fe(II) and Fe(III) complexes may exhibit SCO phenomenon, and are normally made up of a mixture of HS and LS atoms. Thermoelectrical data for these complexes gave negative S_e values, ascribed to anions as dominant charge carriers due to their smaller mass and volume (higher mobility) compared to the cationic complex.

2.6 Complexes of Manganese, Arylcarboxylate Ions and Cyclam

Manganese is a first-row transition metal with atomic number 25 (valence electron configuration $4s^2d^6$). It forms stable Mn(II) ion (valence electron configuration $3d^5$) and Mn(III) ion (valence electron configuration $3d^4$). Both HS Mn(II) ($t_{2g}^2e_g^3$) and LS Mn(II) (t_{2g}^5) complexes are paramagnetic, with five and one unpaired electrons, respectively.

Manganese carboxylates show several coordination modes for the carboxylate ligands, but the bridging ligands are widely used for designing polynuclear complexes [88].

For example, Kar *et al.* [89] reported a one-dimensional coordination polymer, $[Mn(4,4'\text{-azpy})(o\text{-}(NO_2)C_6H_4COO)_2(H_2O)_2]_n$, where 4,4’-azpy = 4,4’-azobis(pyridine), synthesized by reacting $Mn(o\text{-}(NO_2)C_6H_4COO)_2\cdot 4H_2O$ with 4,4’-azpy in methanol. The polymer was isolated as red crystals. Its IR spectrum showed peaks (in cm^{-1}) at 1526, 1375, 3405, 1594 for $\upsilon_{asym}COO$, $\upsilon_{sym}COO$, υOH, and υN≡N, respectively. Its structure (**Figure 2.50**) showed a fish-bone chain with Mn(II) atom in an octahedral geometry formed by two monodentate *o*-nitrobenzoato ligands and two water molecules in the equatorial plane, and two bridging 4,4’-azpy at the axial positions that connects Mn(II) to form a linear chain. Its $\chi_M T$ value was ca. 4.4 cm^3 K mol^{-1} per Mn(II) at room temperature (expected for an isolated S = 5/2 Mn(II) ion), indicating the coupling between the Mn(II) centres was negligible (it behaves as isolated monomers with zero-field splitting). Its TGA trace showed a two-steps decomposition process. The first weight loss

(80 ºC to 105 ºC) was assigned to loss of water molecules (found = 5.78%, calculated = 5.92%) , while the second weight loss (256 ºC to 310 ºC) was assigned to loss of 4,4'-azpy (found = 30.31%, calculated = 30.48%).

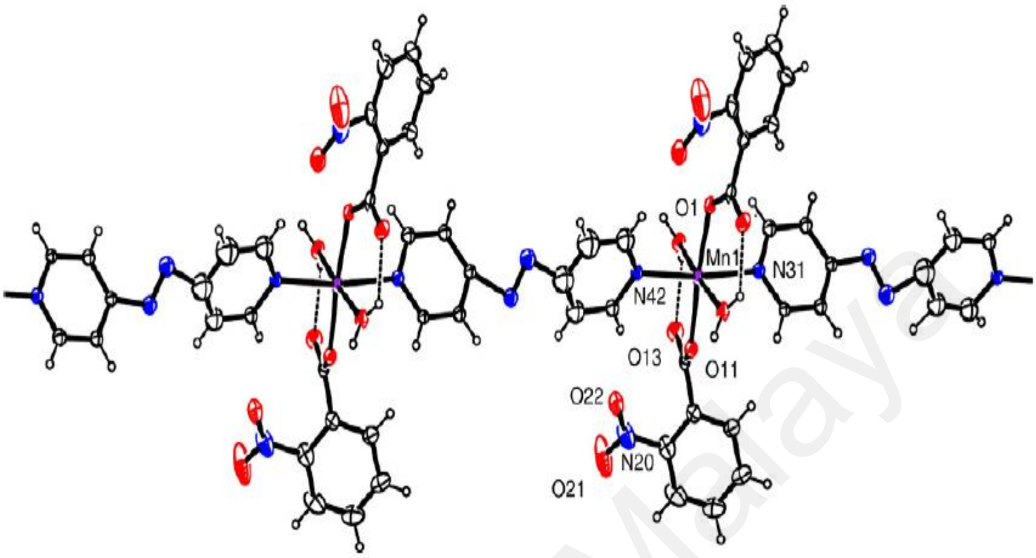

Figure 2.50 Crystal structure of $[Mn(4,4'\text{-azpy})(o\text{-}(NO_2)C_6H_4COO)_2(H_2O)_2]_n$ [89]

Paul *et al*. [90] reported $[Mn(OBz)_2(bipy)(H_2O)]$, where OBz = benzoate, and bipy = 2,2'-bipyridine (**Figure 2.51**), synthesized by reacting a methanolic solution of manganese(II) acetate tetrahydrate and 2,2'-bipyridine with an aqueous methanolic solution of benzoic acid and sodium bicarbonate. The complex was isolated as yellow crystals. The calculated percentages for C, H, and N were 61.2% C, 4.3% H and 6.0% N, while the results from the elemental analyses were 61.2% C, 4.3% H and 6.0% N. Its IR spectrum showed peaks (in cm^{-1}) at 3412, 1593, 1535, 1406, 1382, 411 for υOH, υ_{asym}COO, υ_{asym}COO, υ_{sym}COO, υ_{sym}COO and υMn-O, respectively. The values were 211 cm^{-1} and 129 cm^{-1}, indicating monodentate and bidentate carboxylate binding modes, respectively.

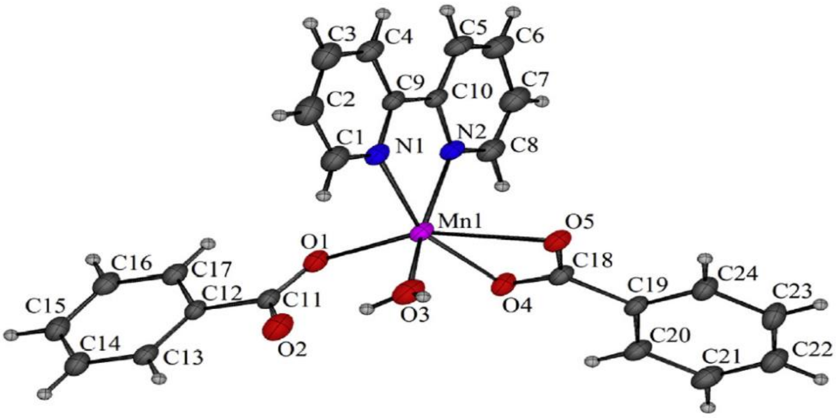

Figure 2.51 Crystal structure of [Mn(OBz)$_2$(bipy)(H$_2$O)] [90]

Chandra and Kumar [91] reported [Mn(L)$_2$Cl$_2$], obtained from reaction of MnCl$_2$ with L (**Figure 2.52**). Its μ_{eff} value was 5.82 BM, indicating five unpaired electrons (HS Mn(II) [92]. Its UV-vis spectrum showed weak absorption bands at 335 nm, 345 nm, 416 nm and 508 nm, assigned to $^6A_{1g}$ to $^4T_{1g}$, $^6A^{1g}$ to ^4E_g, $^6A_{1g}$ to $^4E_g$$^6A_{1g}$ and $^6A_{1g}$ to $^4A_{1g}$ transitions (**Figure 2.53**), respectively, for an octahedral Mn(II) complex [57].

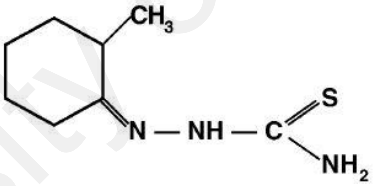

Figure 2.52 The structure of L [91]

A Mn(III) complex, [Mn^{III}(OL)$_2$]Cl·3H$_2$O (**Figure 2.54**), was formed from the reaction of MnCl$_2$·4H$_2$O with 2-(2-pyridylmethyleneamino (L) [93] as a result of air-oxidation during synthesis. Its UV-vis spectrum showed weak *d-d* bands at 550 nm (ε = 14 M^{-1} cm^{-1}) and 860 nm (ε = 12 M^{-1} cm^{-1}) for an octahedral Mn(III) complex. Its μ_{eff} value was similar to the expected value for a LS Mn(III) complex (2.8 BM) at 77 K. However on heating, the value was 4.4 BM 300 K, indicating a HS Mn(III) atom (S = 2) Hence, the complex was made up of 76% HS Mn(III) atom at 300 K, and showed gradual LS-to-HS spin transition (**Figure 2.55**).

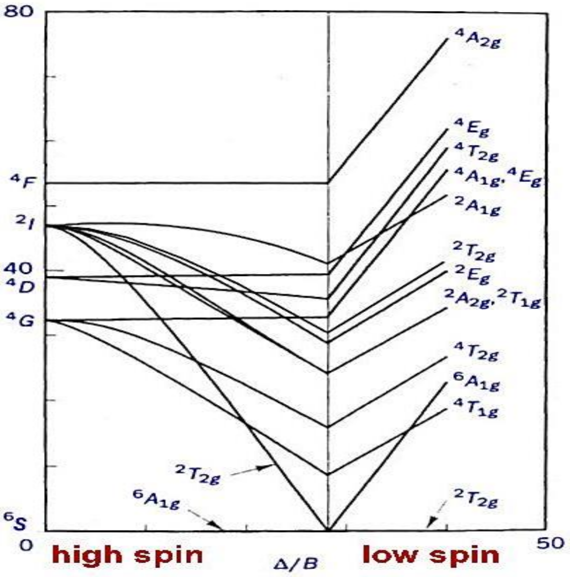

Figure 2.53 Tanabe-Sugano diagram for d^5 complexes

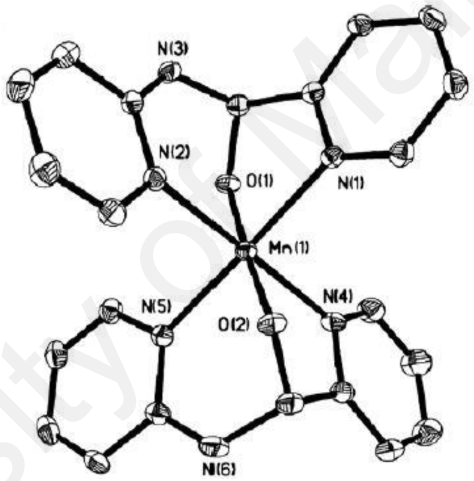

Figure 2.54 The structure of $[Mn(OL)_2]^+$ ion [93]

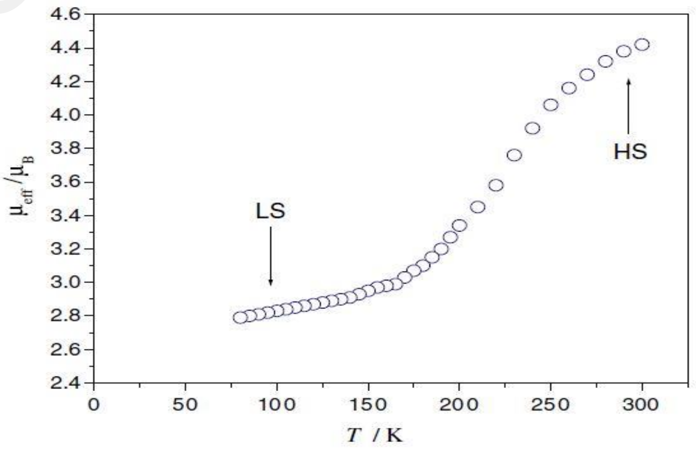

Figure 2.55 Magnetic moment (μ_{eff}) versus T for $[Mn^{III}(OL)_2]Cl{\cdot}3H_2O$ [93]

Mossin *et al*. [94] reported an ionic mononuclear *trans*-[Mn(cyclam)$(OH_2)_2$]$(CF_3SO_3)_3$•H_2O (**Figure 2.56**), synthesized by adding cyclam and CF_3SO_3H to Mn$(CF_3SO_3)_2$•$4H_2O$ in ethanol. The complex formed was then reacted with sodium perchlorate, perchloric acid, and sodium acetate to form [Mn(cyclam)(CH_3COO)(CH_3COOH)]$(ClO_4)_2$ [94], which crystallised in the space group $P2_1$ with two formula units in the asymmetric unit. Its structure showed pseudo-chain (**Figure 2.57**) due to extremely short intermolecular hydrogen bonds. Its magnetic moments were in the range 4.9 - 5.0 BM (the spin-only value was 4.9 BM for a HS d^4 electron configuration).

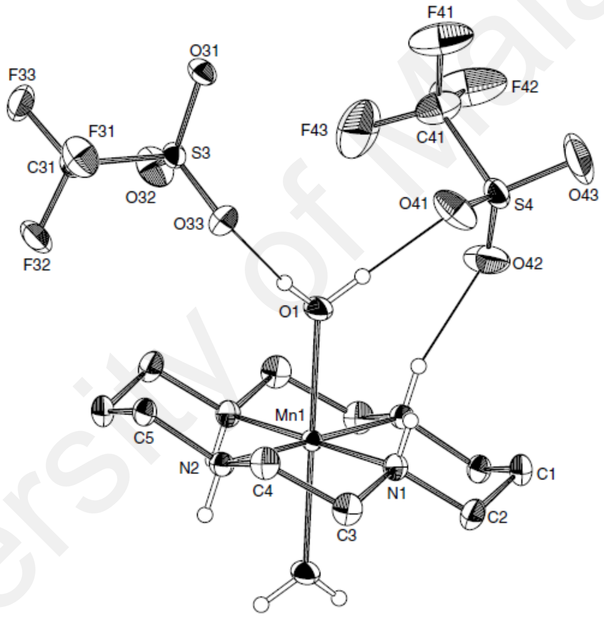

Figure 2.56 Crystal structure of *trans*-[Mn(cyclam)$(OH_2)_2$]$(CF_3SO_3)_3$•H_2O [94]

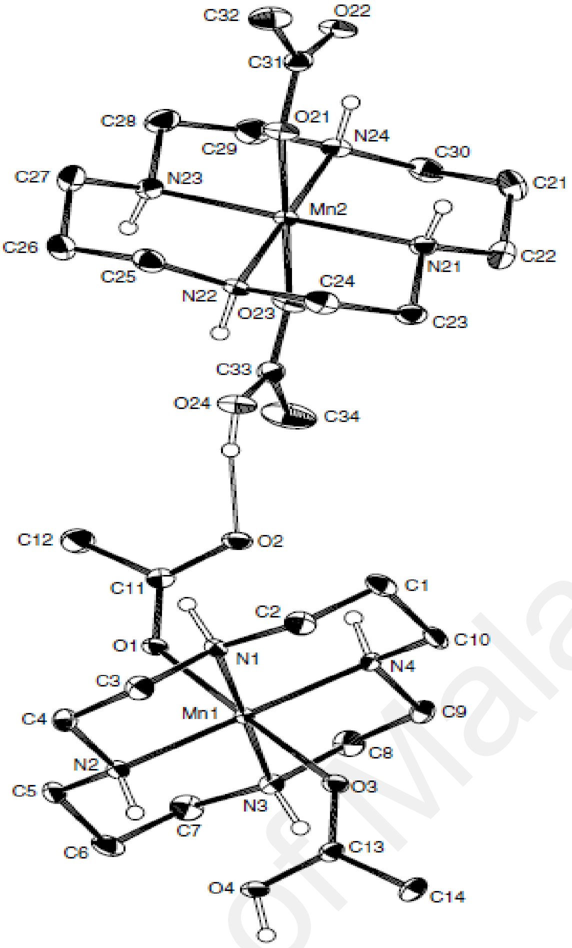

Figure 2.57 Crystal structure of $[Mn(cyclam)(CH_3COO)(CH_3COOH)](ClO_4)_2$ with hydrogen bonded chain showing two crystallographically different cations [94]

Olmstead *et al*. [95] reported a dinuclear complex, $[Mn_2O_2(cylam)_2]Cl_2{\cdot}2CH_3CN$ (**Figure 2.58**), isolated as dichroic red-green crystals from the reaction of $MnCl_2{\cdot}4H_2O$ with cyclam, NaN_3, and $NaBPh_4$. Its structure showed Mn(III)-Mn(IV) centrosymmetric disordered mixed-valence dimeric cation bridged by two oxo ligands. Each Mn atom coordinates with cyclam to form a distorted octahedral geometry. The structure at both Mn(III) and Mn(IV) was similar.

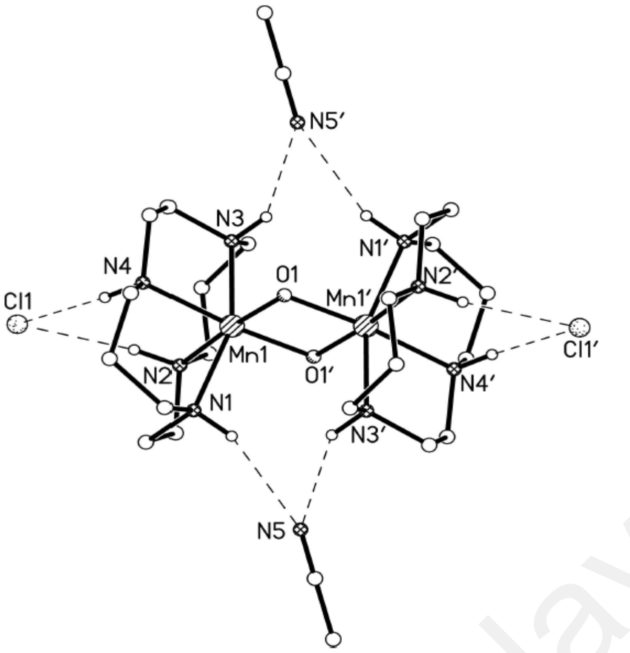

Figure 2.58 Crystal structure of $[Mn_2O_2(cylam)_2]Cl_2 \cdot 2CH_3CN$ [95]

To summarise, most manganese carboxylates involving bridging ligands were polymeric. Mn(II) complexes were easily air-oxidized to Mn(III) complexes. Both Mn(II) and Mn(III) complexes were made up of a mixture of HS and LS atoms, and may exhibit SCO phenomenon.

CHAPTER 3: EXPERIMENTAL

3.1 Introduction

This research involved syntheses and characterisation of complexes of copper(II), nickel(II), cobalt(II) and cobalt(III), iron(II) and iron(III), and manganese(II) and manganese(III), with cyclam, 4-tetradecyloxypyridine (L1) and 4-hexadecyloxypyridine (L2) as N-donor ligands, and benzoate and substituted benzoate ions as counterions.

3.2 Chemicals

The chemicals used in this research (**Table 3.1**) were AnalaR reagents obtained commercially, and were used as received. L1 [96], and crystals of [Cu(cyclam)(4-$X$$C_6H_4COO)_2$] ($X$ = H, OCH_3, CH_3) and [Cu(cyclam)(4-$HOC_6H_4COO)_2$].$2H_2O$ [97] were previously prepared and characterised.

Table 3.1 List of chemicals used in this research, arranged alphabetically

Name	Structural formula	Formula weight (g mol^{-1})	Supplier
Benzoic acid	C_6H_5COOH	122.13	HmbG
1-Bromohexadecane	$CH_3(CH_2)_{15}Br$	305.34	Merck
1-Bromotetradecane	$CH_3(CH_2)_{13}Br$	22.28	Aldrich
Cobalt(II) chloride hexahydrate	$CoCl.6H_2O$	237.93	Friendemann
Cyclam	$C_{10}H_{24}N_4$	200.32	Merck
4-Hydroxypyridine	4-HOC_5H_5N	95.10	Aldrich
Iron(II) sulphate heptahydrate	$FeSO_4.7H_2O$	170.48	R&M
Manganese(II) chloride tetrahydrate	$MnCl_2.4H_2O$	197.91	R&M
Nickel(II) chloride hexahydrate	$NiCl_2.6H_2O$	237.71	R&M

3.3 Ligand 4-($CH_3(CH_2)_{15}O)C_5H_4N$ (L2)

A mixture of 4-HOC_5H_4N (5.01 g, 52.70 mmol), K_2CO_3 (17.28 g, 125.10 mmol), and KI (0.33 g, 2.00 mmol) in DMF (200 mL) in a round-bottomed flask was stirred vigorously at room temperature. $CH_3(CH_2)_{15}Br$ (15.25 g, 50.0 mmol) was added portion wise to the magnetically-stirred solution. The reaction mixture was then refluxed for 72 hours, and left to cool at room temperature overnight. Distilled water was added into the mixture and it was left overnight. The yellow solid formed was collected by suction filtration and washed with distilled water. The product was a white powder and its yield was 12.98 g (81.27%).

3.4 Copper(II) complexes

3.4.1 $[Cu(cyclam)(L1)_2](C_6H_5COO)_2 \cdot 3H_2O$ (1)

A suspension of $[Cu(cyclam)(H_2O)_2](C_6H_5COO)_2 \cdot 2H_2O$ (0.16 g, 0.28 mmol) in CH_3OH (30 mL) was magnetically stirred at room temperature. A solution of L1 (0.16 g, 0.55 mmol) in $CHCl_3$ (20 mL) was added portion wise to the magnetically stirred suspension. The reaction mixture was further stirred for one hour, and then filtered. The product was a purple powder, and its yield was 0.30 g (94.9%).

3.4.2 $[Cu(cyclam)(L1)(H_2O)](4\text{-}CH_3C_6H_4COO)_2 \cdot 3H_2O$ (2)

The procedure was the same as described in **Section 3.4.1**, using $[Cu(cyclam)(H_2O)_2]$ $(4\text{-}CH_3C_6H_4COO)_2.H_2O$ (0.10 g, 0.17 mmol), and L1 (0.10 g, 0.34 mmol). The product was a purple powder, and its yield was 0.12 g (78.6%).

3.4.3 $[Cu(cyclam)(L1)(H_2O)](4\text{-}CH_3OC_6H_4COO)_2 \cdot 4H_2O$ (3)

The procedure was the same as described in **Section 3.4.1**, using $[Cu(cyclam)(H_2O)_2](4\text{-}CH_3OC_6H_4COO)_2 \cdot 2H_2O$ (0.06 g, 0.09 mmol), and L1 (0.06 g, 0.19 mmol). The product was a purple powder, and its yield was 0.08 g (93.8%).

3.4.4 $[Cu(4\text{-}HOC_6H_4COO)_2(cyclam)$

The procedure was the same as described in **Section 3.4.1**, using $[Cu(4\text{-}HOC_6H_4COO)_2(cyclam)] \cdot 2H_2O$ (0.15 g, 0.28 mmol), and L1 (0.16 g, 0.56 mmol).

The products were a mixture of purple and pale yellow powder. The mixture was separated using water.

3.5 C_6H_5COONa

NaOH (3.54 g, 88.48 mmol) was dissolved in H_2O (100 mL) and stirred magnetically at room temperature. C_6H_5COOH (10.81 g, 88.46 mmol) was added portion wise to the solution. The reaction was further stirred for one hour, and filtered. The product was a white powder and its yield was 12.34 g (96.87%).

3.6 Nickel(II) complexes

3.6.1 $[Ni(C_6H_5COO)_2(H_2O)_2]$

C_6H_5COONa (5.00 g, 34.70 mmol) was dissolved in H_2O (50 mL) and stirred magnetically at room temperature for one hour. $NiCl_2 \cdot 6H_2O$ (4.13 g, 17.36 mmol) was added portion wise to the aqueous suspension. The reaction mixture was further stirred for two hours, and filtered. The product was a green powder, and its yield was 4.81 g (82.2%).

3.6.2 $[Ni(C_6H_5COO)_2(cyclam)]$

A suspension of $[Ni(C_6H_5COO)_2(H_2O)_2]$ (0.38 g, 1.24 mmol) in CH_3CH_2OH (100 mL) was magnetically stirred and heated. A solution of cyclam (0.25 g, 1.25 mmol) in C_2H_5OH (50 mL) was added portion wise to the magnetically stirred hot suspension. The reaction mixture was further stirred and heated for one hour, and then filtered hot. The product was a purple crystal, and its yield was 0.58 g (93.1%).

3.6.3 $[Ni(cyclam)(L1)(H_2O)](C_6H_5COO)_2 \cdot H_2O$ (4)

A suspension of $[Ni(C_6H_5COO)_2(cyclam)]$ (0.14 g, 0.28 mmol) in CH_3CH_2OH (50 mL) was magnetically stirred. A solution of L1 (0.16 g, 0.55 mmol) in $CHCl_3$ (20 mL) was added portion wise to the magnetically stirred suspension. The reaction mixture was further stirred and heated for one hour, and filtered. The product was a dark brown semi-solid, and its yield was 0.30 g (77.4%).

3.6.4 [Ni(cyclam)(L2)$_2$](C_6H_5COO)$_2$•H_2O (5)

A suspension of [Ni(cyclam)(C_6H_5COO)$_2$] (0.39 g, 0.78 mmol) in CH_3CH_2OH (50 mL) was magnetically stirred. A solution of L2 (0.50 g, 1.56 mmol) in $CHCl_3$ (20 mL) was added portion wise to the magnetically stirred suspension. The reaction mixture was further stirred and heated for one hour, and filtered. The product was a brown powder, and its yield was 0.56 g (63.1%).

3.7 Co(II) and Co(III) complexes

3.7.1 [Co_2(μ-C_6H_5COO)$_2$(μ-H_2O)$_2$(C_6H_5COO)(H_2O)$_2$]

The procedure was the same as described in **Section 3.6.1**, using $CoCl_2$•$6H_2O$ (4.13 g, 17.36 mmol) and C_6H_5COONa (5.00 g, 34.70 mmol). The product was a purple powder, and its yield was 5.15 g (53.6%).

3.7.2 [Co(C_6H_5COO)$_2$(cyclam)](C_6H_5COO)

The procedure was the same as described in **Section 3.6.2**, using [Co_2(μ-C_6H_5COO)$_2$ (μ-H_2O)$_2$(C_6H_5COO)(H_2O)$_2$] (0.38 g, 0.69 mmol) and cyclam (0.25 g, 1.25 mmol). The product was a dark brown semi-solid, and its yield was 0.56 g (72.4%).

3.7.3 [Co(cyclam)(L1)$_2$](C_6H_5COO)$_2$•$3H_2O$ (6)

The procedure was the same as described in **Section 3.6.3**, using [Co(C_6H_5COO)$_2$(cyclam)](C_6H_5COO) (0.55 g, 0.89 mmol) and L1 (0.64 g, 2.21 mmol). The product was a dark brown semi-solid and its yield was 0.99 g (96.6%).

3.7.4 [Co(cyclam)(L2)$_2$](C_6H_5COO)$_3$•$4H_2O$ (7)

The procedure was the same as described in **Section 3.6.4**, using [Co(C_6H_5COO)$_2$(cyclam)](C_6H_5COO) (0.39 g, 0.63 mmol) and L2 (0.50 g, 1.56 mmol). The product was a dark brown semi-solid, and its yield was 0.71 g (84.4%).

3.8 Fe(II) and Fe(III) complexes

3.8.1 [Fe_2(μ-H_2O)$_2$(C_6H_5COO)$_4$]

The procedure was the same as described in **Section 3.6.1**, but was done under nitrogen, using $FeSO_4$·$7H_2O$ (2.69 g, 9.68 mmol) and C_6H_5COONa (2.79 g, 19.35 mmol). The product was a brown powder and its yield was 2.51 g (41.0%).

3.8.2 [Fe(C_6H_5COO)$_2$(cyclam)]·$2H_2O$

The procedure was the same as described in **Section 3.6.2**, using [Fe_2(μ-H_2O)$_2$(C_6H_5COO)$_4$] (0.38 g, 0.60 mmol) and cyclam (0.25 g, 1.25 mmol). The product was a dark brown powder, and its yield was 0.60 g (93.6%).

3.8.3 [Fe(cyclam)(L1)$_2$](C_6H_5COO)$_2$·$2H_2O$ (8)

The procedure was the same as described in **Section 3.5.3**, using [Fe(C_6H_5COO)$_2$(cyclam)]·$2H_2O$ (0.22 g, 0.41 mmol) and L1 (0.23 g, 0.81 mmol). The product was a dark brown semi-solid, and its yield was 0.34 g (74.2%).

3.8.4 [Fe(cyclam)(L2)$_2$](C_6H_5COO)$_3$]·$4H_2O$ (9)

The procedure was the same as described in **section 3.5.4**, using [Fe(C_6H_5COO)$_2$(cyclam)]·$2H_2O$ (0.39 g, 0.73 mmol) and L2 (0.5 g, 1.56 mmol). The product was a dark brown semi-solid, and its yield was 0.60 g (61.8%).

3.9 Mn(II) and Mn(III) complexes

3.9.1 [Mn_2(μ-H_2O)$_2$(C_6H_5COO)$_4$]·H_2O

The procedure was the same as described in **Section 3.6.1**, using $MnCl_2$·$6H_2O$ (3.44 g, 17.36 mmol) and C_6H_5COONa (5.00 g, 34.70 mmol). The product was a white powder, and its yield was 4.51 g (80.1%).

3.9.2 [Mn(C_6H_5COO)$_2$(cyclam)]$\cdot$7H_2O

The procedure was the same as described in **Section 3.6.2**, using [Mn_2(μ-H_2O)$_2$(C_6H_5COO)$_4$]$\cdot$$H_2O$ (0.37 g, 0.57 mmol) and cyclam (0.25 g, 1.25 mmol) The product was a brown semi-solid, and its yield was 0.46 g (65.1%).

3.9.3 [Mn(cyclam)(L1)$_2$](C_6H_5COO)$_2$$\cdot$4$H_2O$ (10)

The procedure was the same as described in **Section 3.6.3**, using [Mn(C_6H_5COO)$_2$(cyclam)]$\cdot$7H_2O (0.41 g, 0.66 mmol) and L1 (0.48 g, 1.65 mmol). The product was a brown semi-solid, and its yield was 0.69 g (90.5%).

3.9.4 [Mn(cyclam)(L2)(H_2O)](C_6H_5COO)$_3$$\cdot$3$H_2O$ (11)

The procedure was the same as described in **Section 3.6.4**, using [Mn(C_6H_5COO)$_2$(cyclam)]$\cdot$7H_2O (0.39 g, 0.63 mmol) and L2 (0.5 g, 1.56 mmol). The product was a brown semi-solid, and its yield was 0.61 g (95.9%).

3.10 Instrumental Analyses

The structures of crystalline complexes were deduced by single crystal X-ray crystallography, while the structural formulas of non-crystalline complexes were deduced from combined elemental analyses, Fourier transform infrared spectroscopy (FTIR), UV-vis spectroscopy, and room temperature magnetic susceptibilities by the Gouy method. In addition, the structure of L2 was ascertained using ^{1}H-NMR spectroscopy. The thermal stability was determined by thermogravimetry (TG), and the mesomorphic properties by differential scanning calorimetry (DSC) and polarising optical microscopy (POM). The spin crossover properties were determined by variable temperature UV-vis spectroscopy, while the Seebeck coefficients (S_e) were determined by thermoelectrical experiments in solutions.

3.10.1 X-ray crystallographic data and structural determination

Intensity data for single crystal X-ray diffraction were collected on a Bruker Apex II CCD fitted with graphite monochromated Mo K_α radiation (λ = 0.71073 Å). The intensities were collected using ω-2θ scan mode. All hydrogen atoms were refined isotropically in their idealized positions except for water-bound H atoms, which were located in the difference map and then fixed in their found position. The molecular structure of the crystals was drawn with 50 or 70 % displacement ellipsoids using the Mercury software.

3.10.2 ^{1}H-Nuclear magnetic resonance spectroscopy

The ^{1}H-NMR spectrum was recorded on a JEOL FT-NMR lambda 400 MHz spectrometer. A small amount of the sample was dissolved in $CDCl_3$ or CD_3OD, and placed to a height of about 4 cm in an NMR tube.

3.10.3 CHN elemental analyses

The elemental analyses (carbon, hydrogen, nitrogen) were recorded on a Perkin-Elmer PE 2400 Series II CHNS/O analyser and Thermo-Finnigan Flash EA 110. A small amount of sample (1.5 - 2.0 mg) was placed in a tin capsule with a dimension of 5 mm x 8 mm. The weighed sample was wrapped and then folded into a smaller piece before being placed into the analyser.

3.10.4 Fourier transforms infrared spectroscopy

The FTIR spectra were recorded neat from 4000 – 400 cm^{-1} at room temperature on a Perkin-Elmer Spectrum 400 FT-IR/FT-IR Spectrometer with a pike 22107 Technologies GladiATR attachment.

3.10.5 UV-vis spectroscopy

The UV-vis spectrum was recorded from 1000 nm to 300 nm on a Shimadzu UV-vis-NIR 3600 spectrophotometer. An exactly known amount of the sample (about 5 mg) was dissolved in a suitable solvent (chloroform, methanol or DMSO) in a 10-mL or 5-mL volumetric flask, and then placed into a 1-cm quartz cuvette. The spectrum was recorded against the solvent as background, with the following parameter: measuring mode = absorbance; scan speed = fast. The molar absorptivity (ε) was calculated using the Beer-Lambert law: A = *εcl*, where A is the absorbance, *c* is the molarity, and *l* is the path length (1 cm).

3.10.6 Magnetic susceptibility

The magnetic susceptibility value was measured by the Gouy method at room temperature using a Sherwood Auto Magnetic Susceptibility Balance. The finely ground sample was packed into a clean tube to a length of greater than 1.5 cm. The tube was inserted in the balance, and the length and weight of sample were keyed in. The value of mass magnetic susceptibility (χ_g) was noted from the instrumental reading. The molar susceptibility (χ_m) was calculated using the equation:

$$\chi_m = \chi_g \times \mathrm{MW}$$

The molar susceptibility (χ_m) was corrected for the diamagnetism of the constituent atom (χ_{dia}) using Pascal's constant, using the following equation:

$$\chi_m^{corr} = \chi_m - \chi_{dia}$$

Then, the effective dipole moment (μ_{eff}) was calculated using the following equation:

$$\mu_{\mathrm{eff}} = 2.83\sqrt{\mathrm{T}(\chi_{\mathrm{m}}^{\mathrm{corr}} - \mathrm{N}\alpha)}$$

where T is the absolute temperature (298 K), and Nα is the temperature-independent paramagnetism.

3.10.7 Thermogravimetry

The thermogravimetric trace was recorded on a Pyris Diamond TG/DTA Perkin-Elmer instrument. The samples were heated in an oven at about 80 ^{o}C for a few days to remove lattice water. An empty ceramic pan was placed in the holder, and then tared. The sample (about 4 mg) was loaded onto the pan and its weight was recorded. The trace was recorded in the temperature range 30 ^{o}C to 900 ^{o}C under N_2 at the flow rate of 20 ^{o}C min^{-1}.

3.10.8 Differential scanning calorimetry

The differential scanning calorimetry was performed on a METTLER TOLEDO DSC 822. The sample was weight (about 4.0 mg) in an aluminium pan by using external microbalance and then placed inside the DSC heating stage. The scans were recorded for two heating and cooling cycles in the temperature range 25 ^{o}C to 200 ^{o}C. The heating and cooling rates were 5 ^{o}C min^{-1}.

3.10.9 Polarising optical microscopy

The photomicrographs were captured on an Olympus polarizing microscope equipped with a Mettler Toledo FP90 central processor and FN82HT hot stage. The magnification was 50X. A small amount of the sample was placed between two glass slide covers, and heated on the hot stage under a polarized light at the scan rate of 10 ^{o}C min^{-1} and cooling rate of 2 ^{o}C min^{-1} for several heating and cooling cycles.

3.10.10 Thermoelectrical studies

A solution, prepared by dissolving the complex (0.01 g), KI-KI$_3$ (0.01 g) and tetra-*n*-butylammonium tetrafluoroborate (TBATFB; 0.92 g) in a suitable solvent (10 cm^3) was introduced into a cell made up of two compartments separated by a solution bridge. Each compartment contained a platinum wire electrode, which was cleaned using dilute HCl, followed by distilled water. The compartments were subjected to a temperature gradient by heating one cell (hot side) and leaving the other at room temperature (cold side) in two separate water baths. The temperature of each solution was determined using a k-thermocouple, and the potential difference was measured using an agilent 34461A Digital Multimeter.

CHAPTER 4: RESULTS AND DISCUSSION

4.1 Introduction

This research was focused on the structural, thermal, mesomorphic and thermoelectric studies of complexes formed the reactions of benzoates (4-XC_6H_4COO; X = H, CH_3, OCH_3, OH) of copper(II), nickel(II), cobalt(II), iron(II) and manganese(II) with N-donor ligands (cyclam, 4-tetradecyloxypyridine and 4-hexadecyloxypyridine).

4.2 4-Alkyloxypyridines

Two 4-alkyloxypyridines used in this research were 4-$CH_3(CH_2)_{13}OC_5H_4N$ (L1) and 4-$CH_3(CH_2)_{15}OC_5H_4N$ (L2). They were ligands used to induce the mesomorphic properties to these complexes and to form ionic compounds for thermoelectric studies. L1 was previously synthesized and characterised [96], while the synthesis and characterisation of L2 are described below.

4-Hexadecyloxypyridine (L2) was obtained as a white powder in good yield (81.3%) by refluxing 4-hydroxypyridine (4-HOC_5H_4N) with 1-bromohexadecane ($CH_3(CH_2)_{15}Br$) for 72 hours in DMF. In this reaction, K_2CO_3 was added to neutralize the HBr formed, while KI acted as a catalyst. The reaction equation is shown below:

$$\text{4-}HOC_5H_4N + CH_3(CH_2)_{15}Br \longrightarrow \text{4-}CH_3(CH_2)_{15}OC_5H_4N + HBr$$

The ligand was readily soluble in $CHCl_3$ and hexane. The results of CHN **elemental analyses** (76.0% C; 13.1% H; 3.9% N) were in good agreement with those calculated for the empirical formula, $C_{21}H_{37}NO$ (76.5% C; 12.6% H; 3.3% N; formula weight 337.52 g mol^{-1}).

Its **^{1}H-NMR** spectrum in $CDCl_3$ is shown in **Figure 4.1**, and the corresponding assignments are recorded in **Table 4.1**.

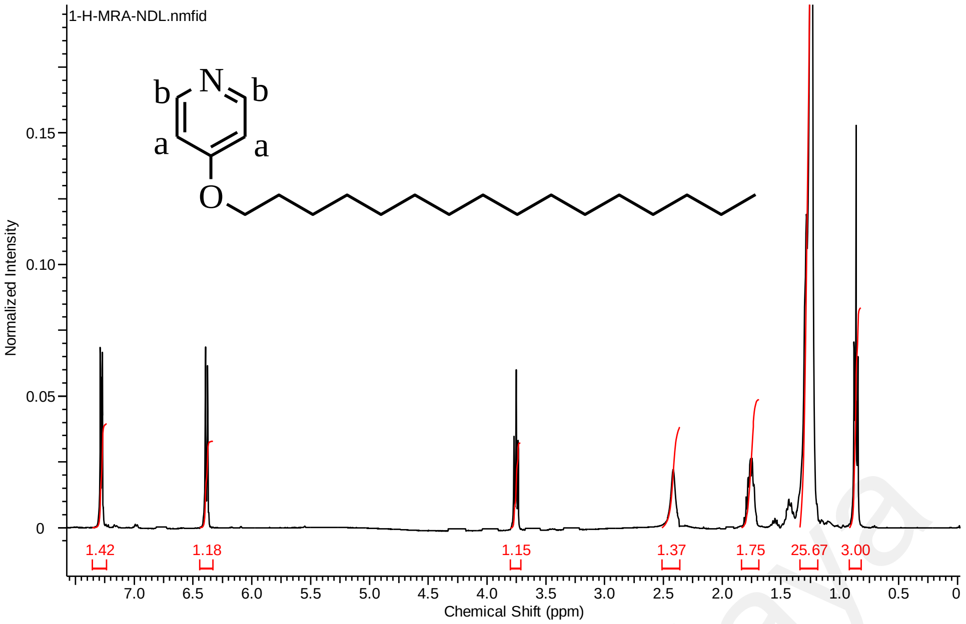

Figure 4.1 ^{1}H-NMR spectrum of **L2**

Table 4.1^{1}H-NMR data for **L2**

Chemical shift (ppm)	Integral	Multiplicity	Assignment
0.85	3.00	Triplet	3 H; C**H$_3$**
1.25	25.67	Multiplet	26 H; (C**H$_2$**)$_{13}$
1.75	1.75	Multiplet	2 H; OCH$_2$C**H**$_2$
3.75	1.15	Triplet	2 H; OC**H$_2$**
6.35	1.18	Doublet	2 H, **H**$_a$ (aromatic)
7.30	1.42	Doublet	2 H, **H**$_b$ (aromatic)

Its **FTIR** spectrum (**Figure 4.2**) shows two strong peaks at 2918 cm^{-1} and 2850 cm^{-1} for CH$_2$ asymmetric and symmetric stretching, respectively, a strong peak at 1638 cm^{-1} for aromatic C=N, a strong peak at 1596 cm^{-1} for aromatic C=C, and a strong peak at 1188 cm^{-1} for C-O-C stretching.

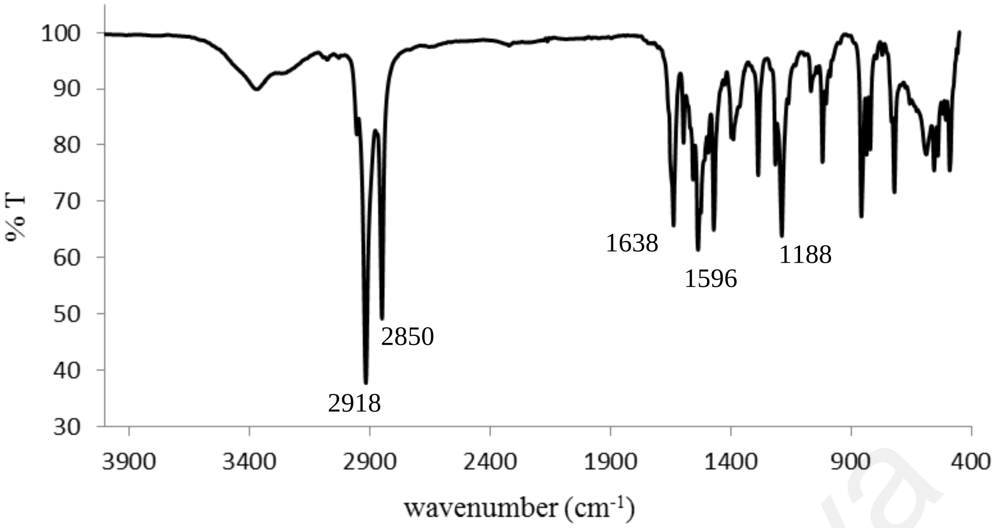

Figure 4.2 FTIR spectrum of **L2**

4.3 Complexes of Copper(II) with Cyclam and 4-Tetradecyloxypyridine (L1)

The structural formulae of the precursor complexes used in the reactions with L1 were [Cu(cyclam)(H_2O)$_2$](4-XC_6H_4COO)$_2$·2H_2O (X = H [97], CH_3 [25], OCH_3 [98]) and [Cu(cyclam)(4-HOC_6H_4COO)$_2$]·2H_2O [98]. These complexes were single crystals. They were reacted with L1 in a mole ratio 1:2 in CH_3OH-$CHCl_3$.

4.3.1 [Cu(cyclam)(L1)$_2$](C_6H_5COO)$_2$·3H_2O (1)

(a) ***Synthesis and structural deduction***

[Cu(cyclam)(H_2O)$_2$](C_6H_5COO)$_2$·2H_2O reacted with L1 to form a purple powder. Its structural formula, [Cu(cyclam)(L1)$_2$](C_6H_5COO)$_2$·3H_2O (**Figure 4.3**), is proposed based on combined instrumental data discussed below. Hence, its yield was 94.9%.

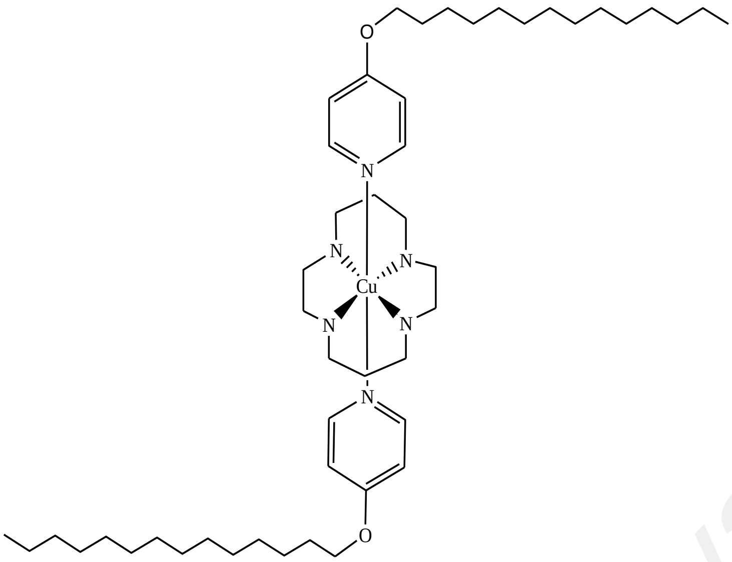

Figure 4.3 Proposed structure for 1^{2+} ($C_6H_5COO^-$ ion and lattice H_2O molecules are not shown)

The results of its **elemental analyses** (65.5% C; 9.3% H; 7.1% N) were in good agreement with those calculated for $C_{62}H_{106}CuN_6O_9$ (65.1% C; 9.4% H; 7.4% N; formula weight, 1143.1 g mol^{-1}).

Its **FTIR** spectrum **(Figure 4.4)** shows two overlapping broad peaks centred at 3372 cm^{-1} and 3225 cm^{-1} for H-bonded H_2O, two strong peaks at 2918 cm^{-1} and 2850 cm^{-1} for asymmetric and symmetric stretching of CH_2, respectively, a strong peak at 1638 cm^{-1} for aromatic C=N, a strong peak at 1596 cm^{-1} for aromatic C=C, a strong peak at 1189 cm^{-1} for C-O-C stretching, a strong peak at 1535 cm^{-1} for $\upsilon_{as,COO}$ and a strong peak at 1383 cm^{-1} for $\upsilon_{s,COO}$. The Δ_{COO} value ($\upsilon_{as,COO}$ - $\upsilon_{s,COO}$) was 152 cm^{-1}, which suggests ionic (non-coordinated) $C_6H_5COO^-$ ion [81].

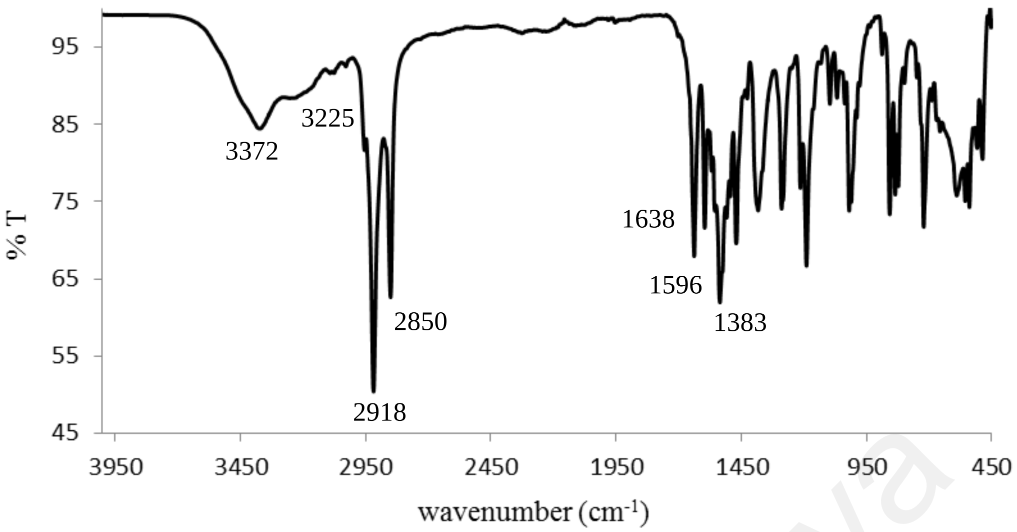

Figure 4.4 FTIR spectrum of **1**

Its **UV-vis** spectrum in CH_3OH (0.61 mmol dm^{-3}) is shown in **Figure 4.5.** It shows a *d-d* band at 531 nm (ε_{max} = 134 M^{-1} cm^{-1}), indicating a square planar geometry at Cu(II) [99]. The result implied that the octahedral geometry was not maintained in solution. This is likely due to the dissociation of the weakly coordinated L1 molecules at the axial positions, as a result of four strong Cu–N_{cyclam} equatorial bonds.

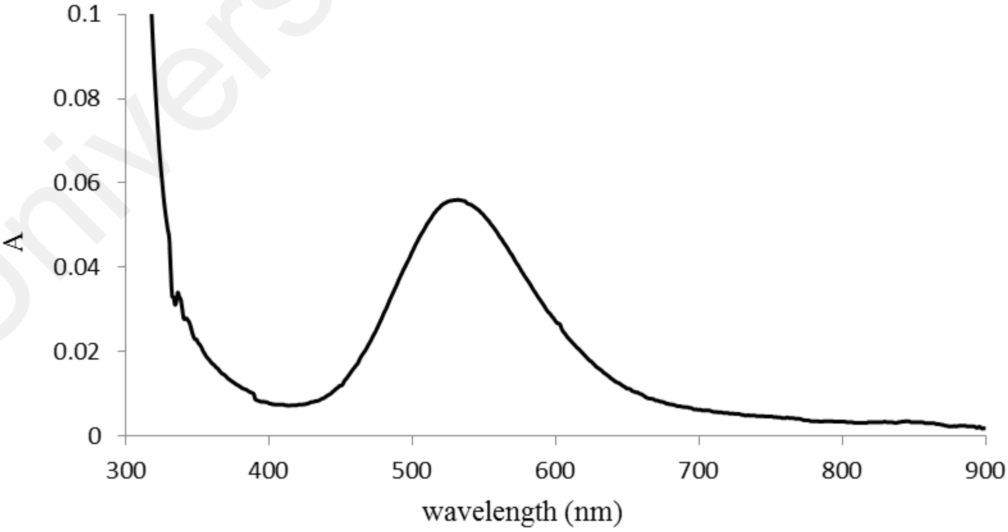

Figure 4.5 UV-vis spectrum of **1**

The value of the **effective magnetic moment** (μ_{eff}) was calculated using the following equation:

$$\mu_{eff} = 2.83[T(\chi_M^{corr} - N\alpha)]^{\frac{1}{2}}$$

where T = temperature in K, χ_M^{corr} = corrected molar susceptibility, and $N\alpha$ = temperature independent paramagnetism = 60 x 10^{-6} cm^3 mol^{-1} per Cu(II)).

For **1**, the values of FM = 1143.1 g mol^{-1}, χ_g = 5.7 x 10^{-7} cm^3 g^{-1}, χ_M = 6.52 x 10^{-4} cm^3 mol^{-1}, χ_{dia} = -5.72 x 10^{-4} cm^3 mol^{-1} (χ_{dia} = 0.5 x FM x 10^{-6} [83]), and hence χ_M^{corr} = 1.22 x 10^{-3}. Therefore, the value of μ_{eff} was 1.71 BM at 298 K. This is in good agreement with the theoretical value of 1.73 BM for an octahedral Cu(II) complex (S = ½; χ_M^{corr}T = 0.375 cm^3 K mol^{-1} [28]).

(b) ***Thermal and mesogenic properties***

The thermal property was studied by thermogravimetry (TG) and the mesogenic property by differential scanning calorimetry (DSC) and polarizing optical microscopy (POM).

The **TG** trace for **1** is shown in **Figure 4.6**. It shows an initial weight loss in the temperature range of 50 °C to about 100 ºC due to the evaporation of three lattice H_2O molecules (found = 3.8%; calculated = 4.4%). This was followed by a major weight loss from 175 °C to 589 ºC assigned to the decomposition of cyclam and L1 ligands, and $C_6H_5COO^-$ ion (found = 88.1%; calculated = 89.7%). Hence, its decomposition temperature was 175 ºC. The amount of residue at temperatures above 589 °C was 8.1% (calculated = 8.7 %, assuming pure CuO [100]). These data were in good agreement with its proposed formula, indicating high purity of the compound.

Its **DSC** scan (**Figure 4.7**) was recorded for one successive heating–cooling cycle in the temperature range 25-115 °C. On heating, there were endothermic peaks at 34.8 ºC (ΔH = +56.8 kJ mol^{-1}), assigned to its melting temperature, and 94.2 ºC (ΔH = +12.2 kJ mol^{-1}), which may be due to evaporation of lattice H_2O. However, there were no peaks on cooling.

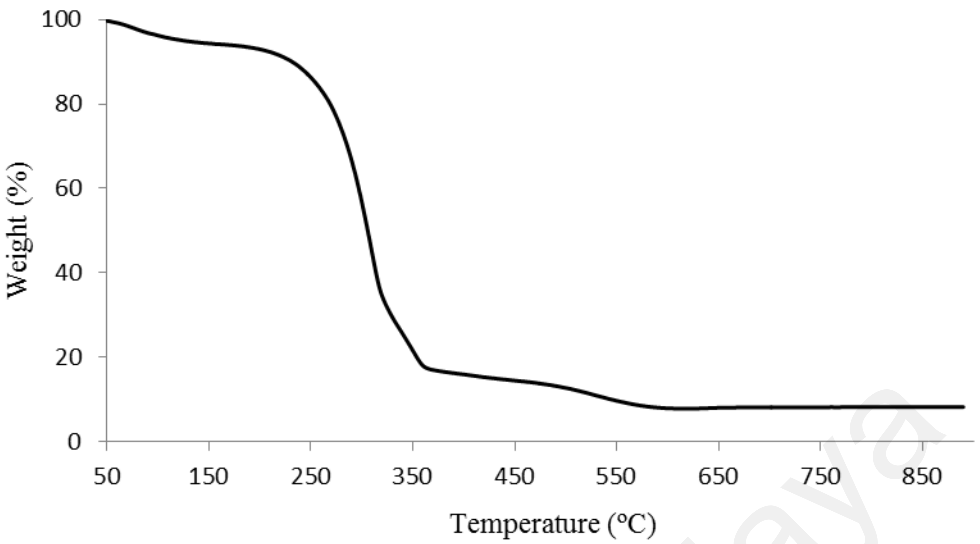

Figure 4.6 **TG trace of** 1

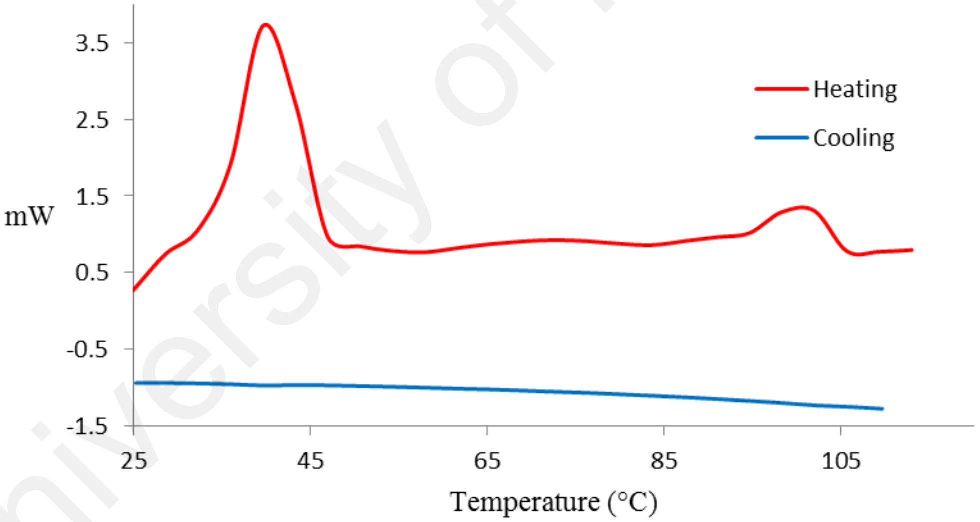

Figure 4.7 DSC scan of **1** (endothermic peaks up)

Viewed under **POM**, **1** was observed to melt at 27 °C (in agreement with DSC) and started to clear (but incomplete) at 85 °C (**Figure 4.8(a)).** On cooling from this temperature, an optical texture was observed at the clear region at 36 °C (**Figure 4.8(b)**). This texture was similar to that of L1 (**Figure 4.8(c)**). Hence, it is inferred that L1 dissociated from the complex on heating at about 85 ^{o}C. Therefore, the complex did not exhibit mesomorphism.

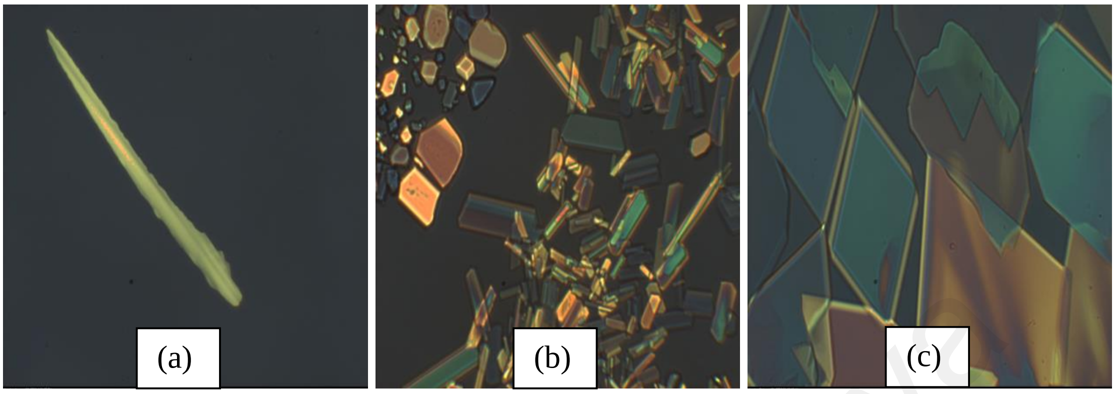

Figure 4.8 Photomicrographs of **1** on: (a) heating at 85 °C, (b) cooling at 36 °C, and (c) **L1** on cooling at 33 °C

(c) *Thermoelectrical property*

Complex **1** was an ionic complex and may be a potential thermoelectric material [49]. An important thermoelectric parameter is **Seebeck coefficient**, S_e. Based on the relationship $\Delta V = S_e \Delta T$, where ΔV is potential difference and ΔT is temperature different, the S_e value may be calculated from the slope of a linear graph of ΔV versus ΔT.

The S_e value was determined for a solution of **1** in $CHCl_3$ in the presence of KI-KI_3 as the redox couple and tetrabutylammonium tetrafluoroborate (TBATFB) as the electrolyte in the temperature range of 27 °C to 50 °C for three heating-and-cooling cycles. The graphs of ΔV versus ΔT for **1** were linear (**Figure 4.9**), indicating a good thermoelectric behaviour, and the mean S_e value was -0.45 ± 0.06 mV K^{-1}. Comparing the S_e value for **1** with the values for KI-KI_3 in $CHCl_3$ (-0.03 mV K^{-1}) [49] and a mixture of KI-KI_3 and TBATFB in $CHCl_3$ (+0.57 mV K^{-1}) [49], it is inferred that **1** was functioning as a thermoelectric material in this solvent. It is noted that its S_e value was similar to $[Cu_2(\text{2-hexyldecanoate})_4(bpy)]_x$ (S_e = -0.47 mV K^{-1} in $CHCl_3$) [49].

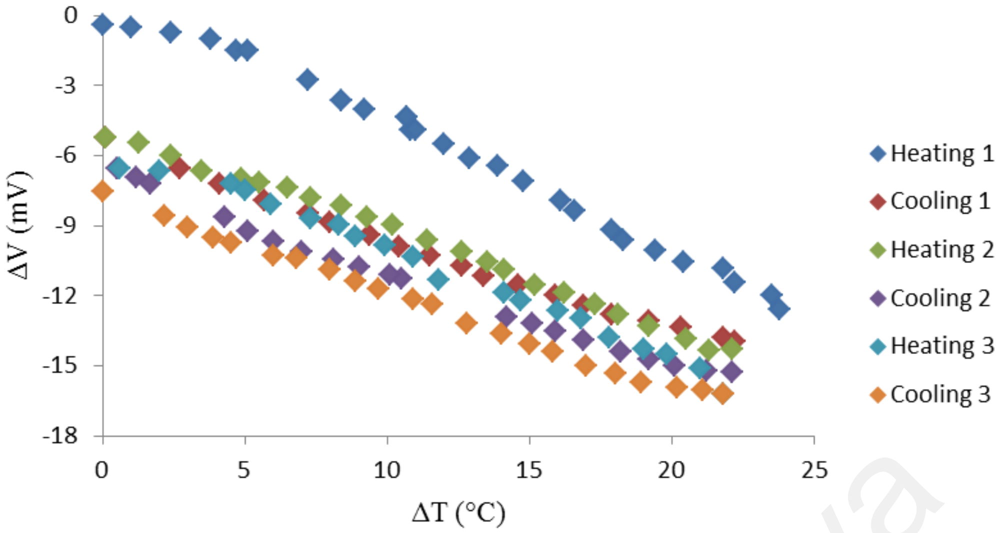

Figure 4.9 Plots of ΔV versus ΔT of **1**

The thermoelectric result for **1** may be explained as follows: in $CHCl_3$ micelle- like structures were formed due the presence of long alkyl chain of the ligands. The ions from KI-KI_3 and TBATFB were trapped inside these structures. On heating, the micelles absorbed heat and expanded sizes, allowing the trapped ion to escape. The increased entropy of the solution accounted for the Seebeck effect, and the negative S_e value arose from the oxidation of I^- ion at the hot electrode.

4.3.2 [Cu(cyclam)(L1)(H_2O)](4-$CH_3C_6H_4COO$)$_2$·3H_2O (2)

(a) ***Synthesis and structural deduction***

[Cu_2(cyclam)(H_2O)$_2$](4-$CH_3C_6H_4COO$)$_2$·H_2O reacted with L1 to form a purple powder. Its structural formula, [Cu(cyclam)(L1)(H_2O)](4-$CH_3C_6H_4COO$)$_2$·3H_2O (**Figure 4.10**), was similarly deduced as previously discussed. Hence, its structure was different from **1**. Its yield was 78.6%.

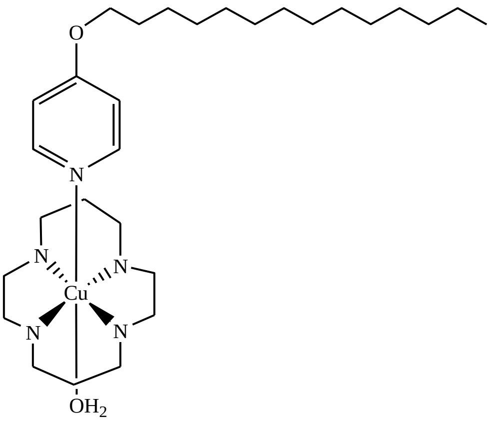

Figure 4.10 Structural formula of $\mathbf{2}^{2+}$ ($4\text{-}CH_3C_6H_4COO^-$ ion and lattice H_2O are not shown)

The results of its **elemental analyses** (60.2% C; 9.0% H; 7.8% N) were in good agreement with those calculated for $C_{45}H_{79}CuN_5O_9$ (60.2% C; 8.9% H; 7.8% N; formula weight, 897.7 g mol^{-1}).

Its **FTIR** spectrum (**Figure 4.11)** shows the presence of the expected functional groups and bonds as discussed for complex **1**. The Δ_{COO} value for $4\text{-}CH_3C_6H_4COO^-$ ion was 170 cm^{-1} ($\upsilon_{as,COO}$ = 1536 cm^{-1} and $\upsilon_{s,COO}$ = 1366 cm^{-1}). Hence as for **Complex 1**, the carboxylate ion in this complex was also not coordinated to the Cu(II) atom.

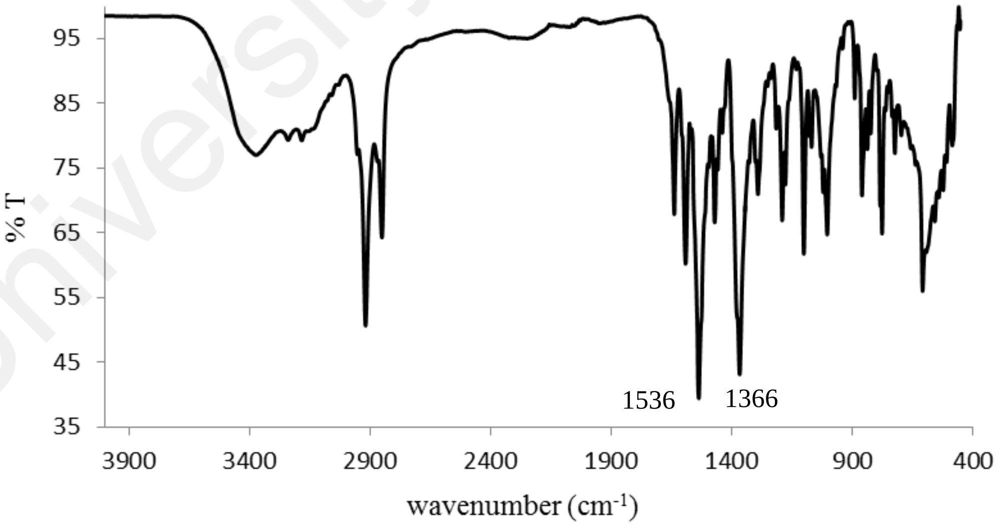

Figure 4.11 FTIR spectrum of **2**

Its **UV-vis** spectrum in CH_3OH (0.71 mmol dm^{-3}) is shown **Figure 4.12**. It shows *d-d* bands at 533 nm (ε_{max} = 67.1 M^{-1} cm^{-1}) and at about 350 nm (shoulder; ε = 33.6 M^{-1} cm^{-1}). These suggest that the geometry at Cu(II) in this complex was similar **1**, and may be similarly explained.

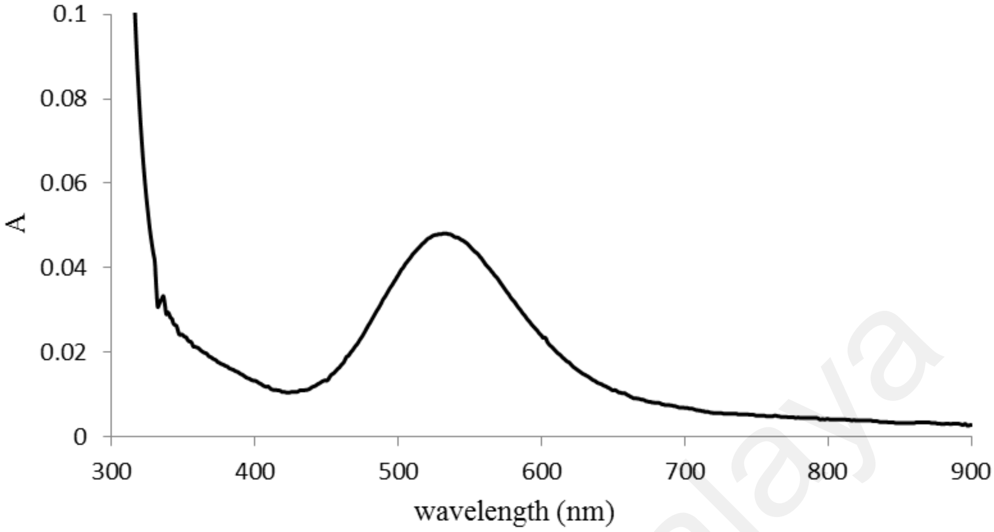

Figure 4.12 UV-vis spectrum of **2**

The value of μ_{eff}, calculated as before from the values of FM = 897.7 g mol^{-1}, χ_g = 5.7 x 10^{-7} cm^3 g^{-1}, χ_M = 5.12 x 10^{-4} cm^3 mol^{-1}, and χ_{dia} = -4.49 x 10^{-4} cm^3 mol^{-1}, was 1.47 BM at 298 K. The value was lower than the theoretical value (1.73 BM) for an octahedral Cu(II) complex, indicating a strong antiferromagnetic interaction between two neighbouring molecules through H-bonds between two axially coordinated H_2O ligands (**Figure 4.13**) [109].

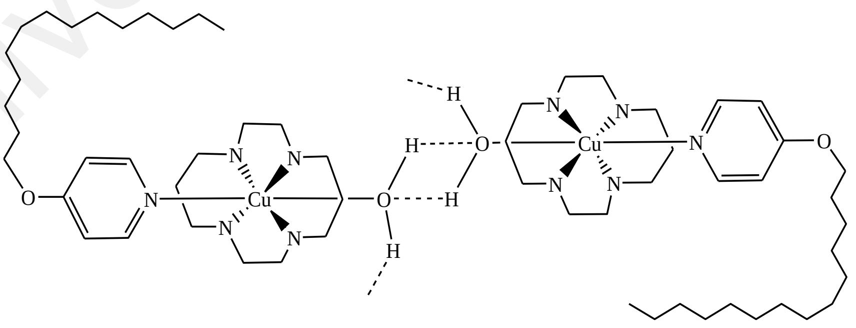

Figure 4.13 H-bond between two axially coordinated H_2O ligands in $\mathbf{2}^{2+}$

(b) ***Thermal and mesogenic properties***

Its TG trace (**Figure 4.14**) shows an initial weight loss from 80 °C to about 100 °C due to evaporation of lattice and coordinated H_2O molecules (found = 6.9 %, calculated = 6.0%) [101]. This is followed by a major weight loss from 203 °C to 580 ºC, assigned to the decomposition of cyclam and L1 ligands, and 4-$CH_3C_6H_4COO^-$ ion (found = 83.9%; calculated = 84.9%). The amount of residue at temperatures above 580 °C was 8.6%. This correlates well with the calculated value of 9.1%, assuming that it was made up of pure CuO. These data were in good agreement with its proposed formula, indicating high purity of the compound. Hence, its decomposition temperature was 203 ºC, which was higher than **1** (175 °C). This is due to the presence of an electron releasing methyl group in **2** which strengthened the 4-$CH_3C_6H_4$–COO bond [102].

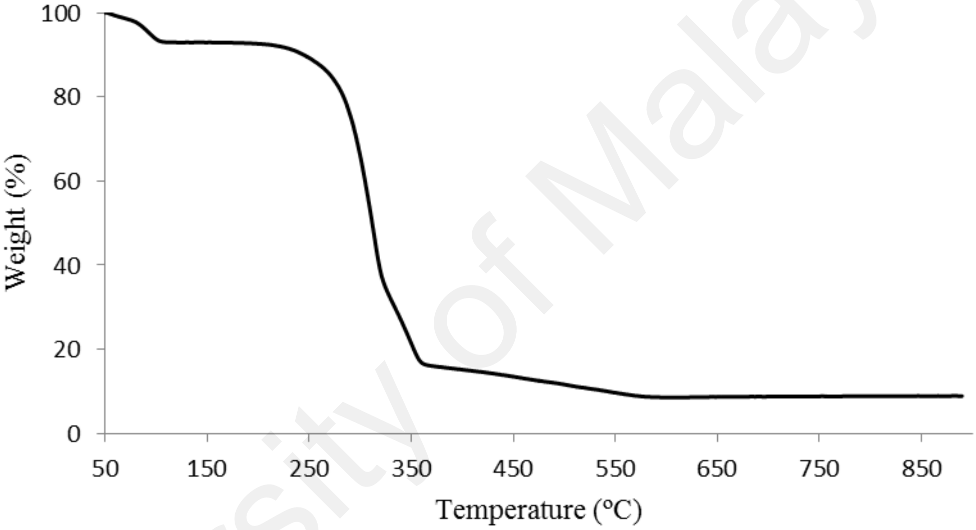

Figure 4.14 TG trace of **2**

Its **DSC** scan (**Figure 4.15**) was recorded in a heating–cooling cycles in the temperature range 25-165 °C. On heating, there was an endothermic peak at 49.5 ºC (ΔH = 40.3 kJ mol^{-1}) assigned to dissociation of L1, and overlapping endothermic peaks at 121.3 ºC ($\Delta H_{combined}$ = 33.2 kJ mol^{-1}) assigned to melting of L1. On cooling there was an exothermic peak at 77.6 ºC (ΔH = 34.7 kJ mol^{-1}) assigned to isotropic liquid (I) to mesophase (M) transition for L1.

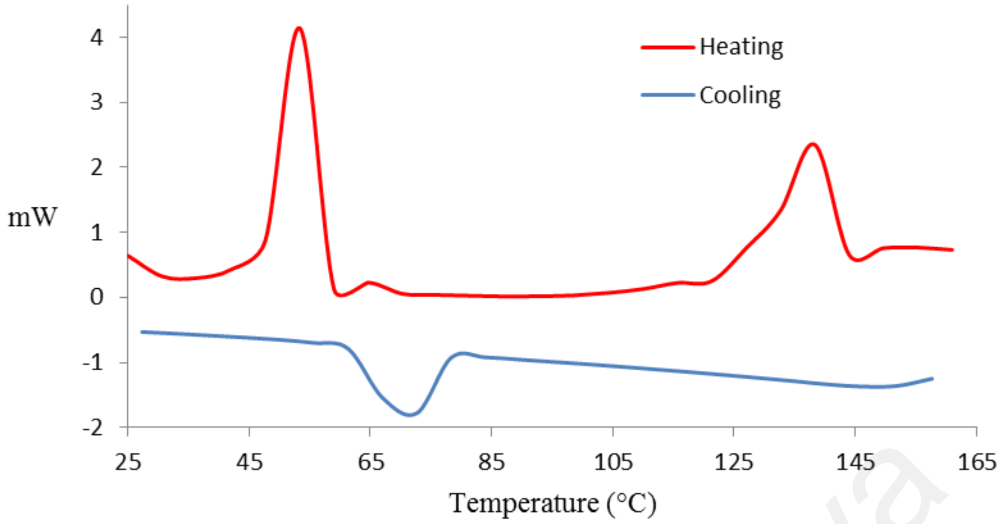

Figure 4.15 DSC scans of **2** (Endothermic peaks up)

Viewed under **POM**, **2** was fluidic at 87 °C, and then optical textures were observed on further heating at 104 °C (**Figure 4.16**). These textures were similar to L1 (**Figure 4.8(c)**), suggesting its dissociation from Cu(II) centre of the complex, as similarly suggested for **1.** Therefore, the complex was not mesomorphic.

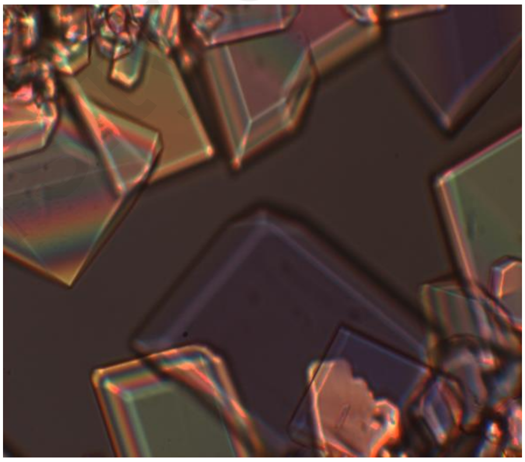

Figure 4.16 Photomicrograph of **2** on heating at 104 °C

(c) ***Thermoelectrical properties***

The **Seebeck coefficients** for **2** were similarly determined as for 1. The graphs of ΔV versus ΔT for **2** (**Figure 4.17**) were linear, and the mean S_e value was -0.51 ± 0.04 mV K^{-1}. The value was similar to **1** (-0.45 ± 0.06 mV K^{-1}), suggesting insignificant effect of the substituent on the aromatic ring of the carboxylate ion and numbers of L1.

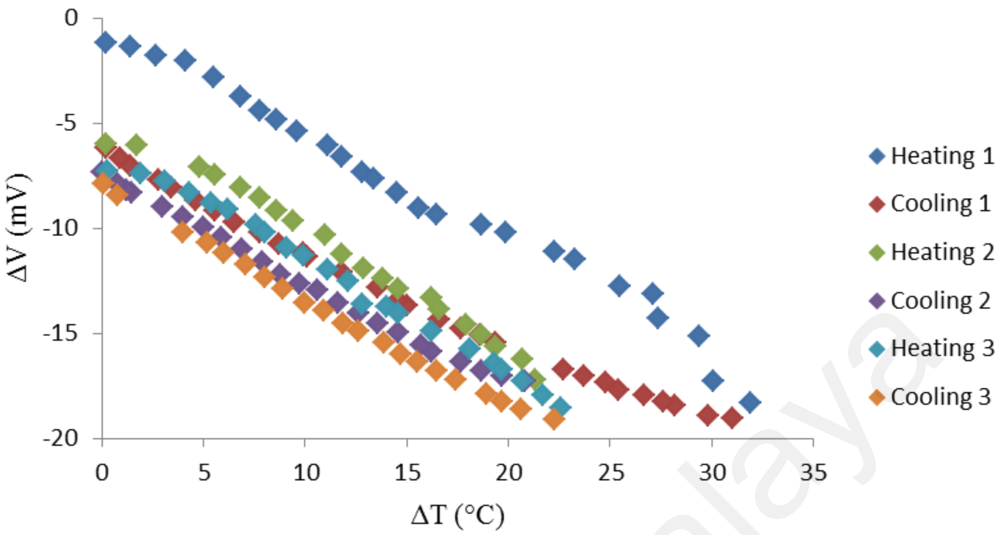

Figure 4.17 Plots of ΔV versus ΔT of **2**

4.3.3 [Cu(cyclam)(L1)(H_2O)](4-$CH_3OC_6H_4COO$)$_2$·4H_2O (3)

(a) ***Synthesis and structural deduction***

[Cu(cyclam)(H_2O)$_2$](4-$CH_3OC_6H_4COO$)$_2$·2H_2O reacted with L1 to form a purple powder. Its structural formula, [Cu(cyclam)(L1)(H_2O)](4-$CH_3OC_6H_4COO$)$_2$·4H_2O, was similarly deduced as for previously discussed complexes. Hence, it is proposed that its structure was similar to **2**, and its yield was 93.8%.

The results of its **elemental analyses** (57.0% C; 8.3% H; 8.1% N) were in good agreement with those calculated for $C_{45}H_{81}CuN_5O_{12}$ (57.0% C; 8.6% H; 7.4% N; formula weight, 947.7 g mol^{-1}).

Its **FTIR** spectrum **(Figure 4.18)** shows the expected peaks and bonds similar to the previously discussed complexes. The Δ_{COO} value for 4-$CH_3OC_6H_4COO^-$ ion was 165 cm^{-1} ($\upsilon_{as,COO}$ = 1537 cm^{-1} and $\upsilon_{s,COO}$ = 1372 cm^{-1}), which was similar to the carboxylate ions of complexes **1** **(**Δ_{COO} = 152 cm^{-1}) and **2**.(Δ_{COO} = 170 cm^{-1}).

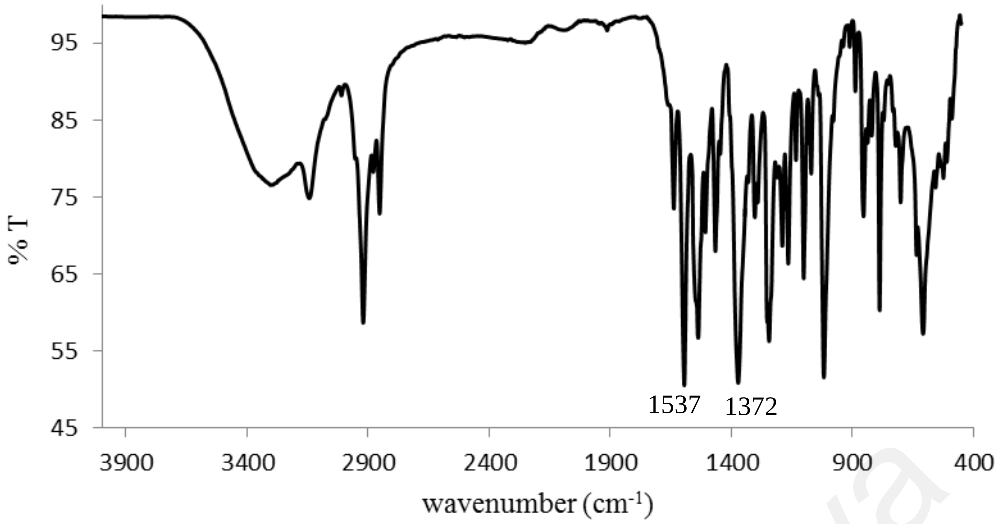

Figure 4.18 FTIR spectrum of **3**

Its **UV-vis** spectrum in CH_3OH (0.61 mmol dm^{-3}) is shown in **Figure 4.19**. It shows *d-d* bands at 531 nm (ε_{max} = 120.0 M^{-1} cm^{-1}) and at about 332 nm (ε = 76.7 M^{-1} cm^{-1}; a shoulder). These suggest that the geometry at Cu(II) in this complex in solution was similar to **1** and **2,** and may be similarly explained.

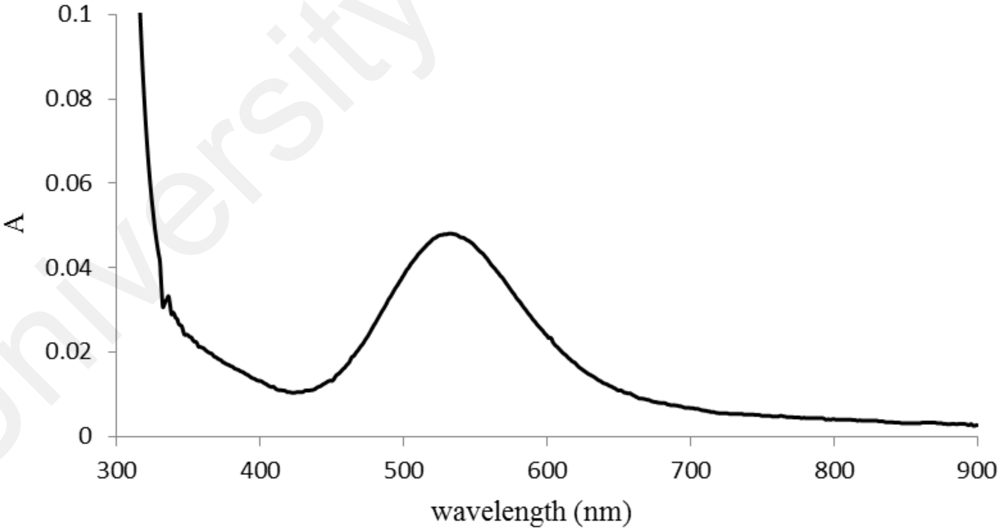

Figure 4.19 UV-vis spectrum of **3**

The value of $\boldsymbol{\mu_{eff}}$, calculated from the values of FM = 947.7 g mol^{-1}, χ_g = 6.6 x 10^{-7} cm^3 g^{-1}, χ_M = 6.25 x 10^{-4} cm^3 mol^{-1}) and χ_{dia} = -4.74 x 10^{-4} cm^3 mol^{-1}, was

1.57 BM at 298 K. there were antiferromagnetic interactions between the Cu(II) atoms in the complex, as similarly suggested for **2** (1.47 BM).

(b) ***Thermal and mesogenic properties***

Its TG trace (**Figure 4.20**) shows an initial weight loss at 82 °C to about 113 ºC due to evaporation of coordinated and lattice H_2O molecules (found = 3.5%; calculated = 4.0%). The next major weight loss from 206 °C to about 660 ºC corresponded to the decomposition of cyclam and L1 ligands, and $4\text{-}CH_3OC_6H_4COO^-$ ion (found = 87.9%; calculated = 88.9%). The amount of residue at temperature above 660 °C was 8.6%, which correlated well with the calculated value of 7.1%, assuming that it was made up of pure CuO. These data were in good agreement with its proposed formula, indicating high purity of the compound. Hence, its decomposition temperature was 206 ºC, which was higher compare **1** (175°C) and **2** (206°C). This is due to the presence of an electron releasing methoxy group in **3** which strengthened the $4\text{-}CH_3OC_6H_4\text{–}COO$ bond [102].

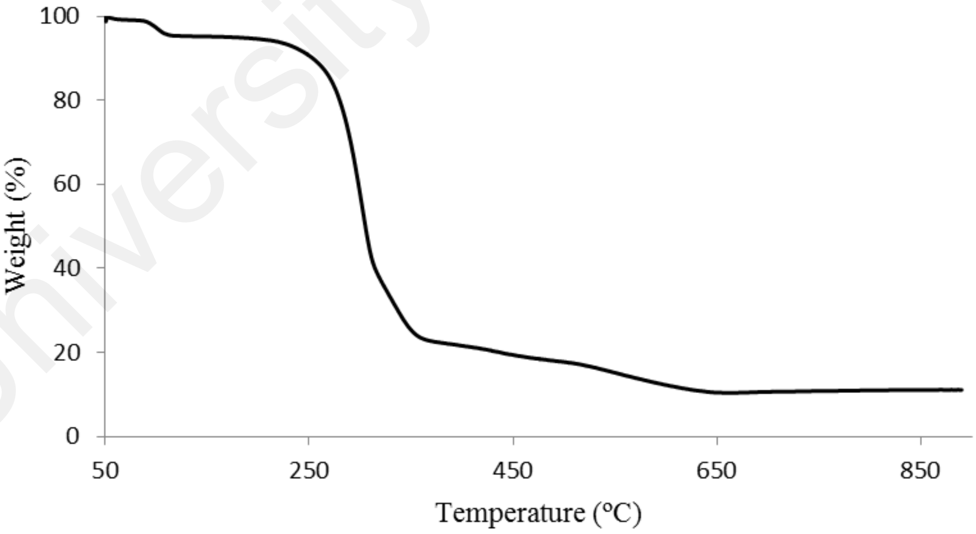

Figure 4.20 TG trace of **3**

Its **DSC** scan (**Figure 4.21**) was recorded for a heating–and-cooling cycle in the temperature range 25-165 °C. On heating, there were an endothermic peak at 46.5 ºC (ΔH = 34.6 kJ mol^{-1}) assigned as its melting temperature, and 147.8 ºC

(ΔH = 229.4 kJ mol^{-1}) assigned as its clearing and decomposition temperatures. Hence, there were no peaks on cooling.

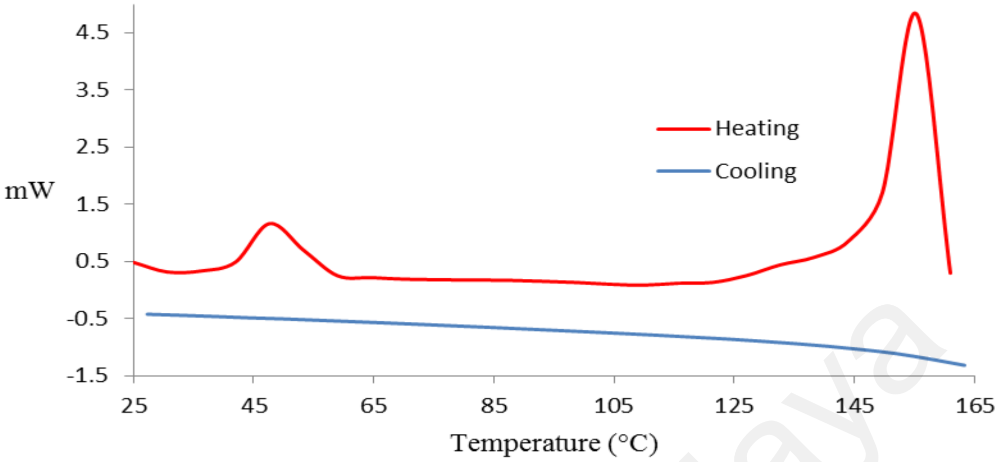

Figure 4.21 DSC of **3** (endothermic peaks up)

Viewed under **POM (Figure 4.22a)**, **3** showed an optical texture at 99 ºC **(Figure 4.22)** on cooling from 100 ºC (fluidic). Hence, the complex was mesomorphic.

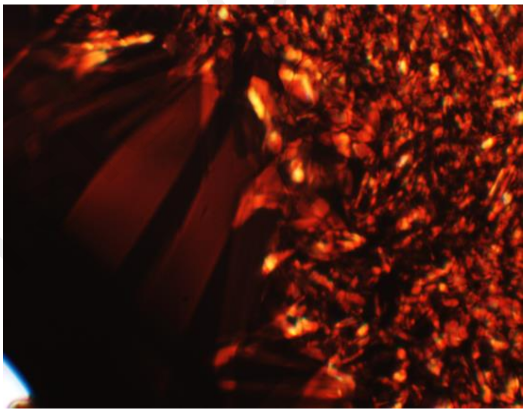

Figure 4.22 Photomicrograph of **3** on cooling at 99 °C

(c) ***Thermoelectrical properties***

The **Seebeck coefficients** for **3** were similarly determined as for the other complexes. The graph of ΔV versus ΔT (**Figure 4.23**) was linear, and the mean S_e value was -0.42 ± 0.07 mV K^{-1}. The value was similar to those of **1** (-0.45 ± 0.06 mV K^{-1}**)** and **2** **(**-0.51 ± 0.04 mV K^{-1}**)**, and may be similarly explained.

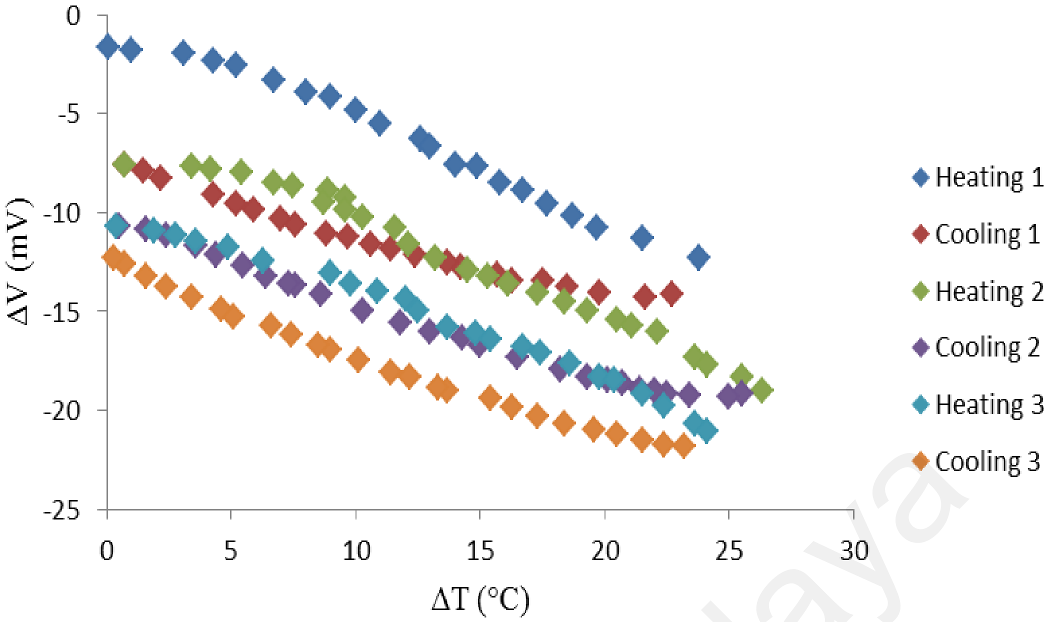

Figure 4.23 Plots of ΔV versus ΔT of **3**

4.3.4 [Cu(4-HOC$_6$H$_4$COO)$_2$(cyclam)]

(a) ***Synthesis and structural deduction***

[Cu(4-HOC$_6$H$_4$COO)$_2$(cyclam)]·2H$_2$O was found not to react with L1 as the 'products' obtained were a mixture of purple and pale yellow powders. The mixture was separated using water (L1 was insoluble), and the purple solid obtained from the solution has similar IR as the starting complex (**Figure 4.24**), and did not melt even on heating to 200 °C (observation under POM). This result may be due to the fact that in contrast to other substituted benzoato ions, 4-HOC$_6$H$_4$COO$^-$ ion was directly coordinated to Cu(II) in this complex and could not be replaced by L1 under similar experimental conditions [103].

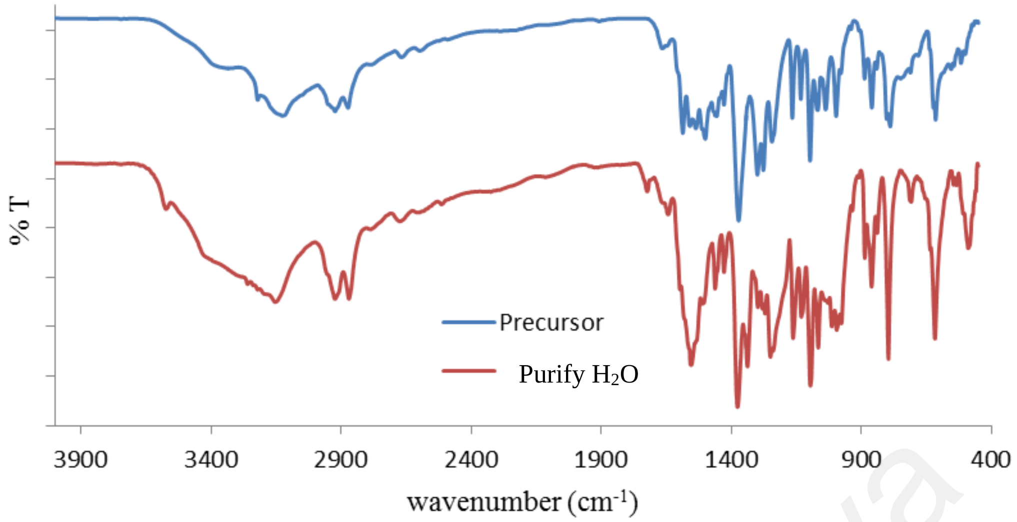

Figure 4.24 FTIR spectrum of [Cu(4-HOC_6H_4COO)$_2$(cyclam)]·2H_2O (precursor) and the purple powder obtained from its "reaction" with L (after purification with water)

4.3.5 *Summary*

The results of the analytical data for **1**, **2** and **3** are summarised in **Table 4.2**.

Table 4.2 Summary for complexes **1**, **2** and **3**

Chemical formula	Δ_{COO} (cm^{-1})	λ (nm)	μ_{eff} (BM)	T_{dec} (°C)	M	S_e (mV K^{-1})
[Cu(cyclam)(L1)$_2$](C_6H_5COO)$_2$·3H_2O (**1**)	152 (ionic)	531 (sp)	1.77	175	No	-0.45 (±0.06)
[Cu(cyclam)(L1)(H_2O)] (4-$CH_3C_6H_4$COO)$_2$·3H_2O (**2**)	170 (ionic)	533 (sp)	1.47	203	No	-0.51 (±0.04)
[Cu(cyclam)(L1)(H_2O)] (4-$CH_3OC_6H_4$COO)$_2$·4H_2O (**3**)	165 (ionic)	531 (sp)	1.57	206	Yes	-0.42 (±0.07)

sp = square planar; M = mesomorphic

Complexes **1** – **3** reacted with L1. Complex **4** did not react with L1 due to the strong coordination of 4-HOC_6H_4COO at the axial positions. The structural formulas for **2** and **3** were similar, and differed from that of **1**. All complexes were mononuclear with octahedral Cu(II) atoms and ionic. The μ_{eff} value for **1** were in good agreement with the theoretical value for a mononuclear Cu(II) complex, while the values for **2** and **3** were lower due antiferromagnetic intermolecular interactions. The thermal stability of **2** and **3** were similar, while that of **1** was significantly lower. All complexes functioned as thermoelectric materials in $CHCl_3$, but only **3** was mesomorphic.

4.4 Complexes of Nickel

4.4.1 [Ni(cyclam)(L1)(H_2O)](C_6H_5COO)$_2$•H_2O (4)

(a) ***Synthesis and structural deduction***

The steps for the synthesis of [Ni(cyclam)(L1)(H_2O)](C_6H_5COO)$_2$•H_2O (**5**) is shown in **Scheme 4.1**.

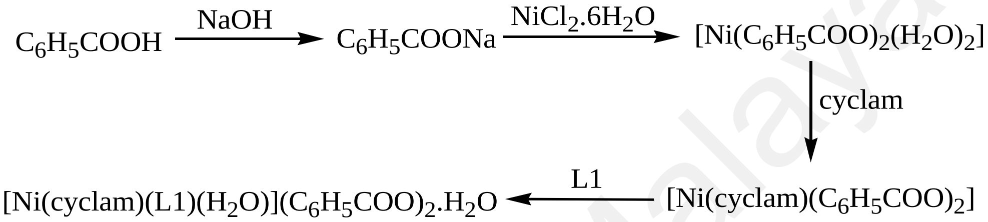

Scheme 4.1 Synthetic steps for [Ni(cyclam)(L1)(H_2O)](C_6H_5COO)$_2$•H_2O (**4**)

In the first step, C_6H_5COOH reacted with NaOH in water to form C_6H_5COONa, which then reacted with $NiCl_2$•$6H_2O$ in CH_3CH_2OH to form [Ni(C_6H_5COO)$_2$(H_2O)$_2$] (green powder). The structural formula of [Ni(C_6H_5COO)$_2$(H_2O)$_2$] (**Figure 4.25**) was proposed based on combined instrumental data discussed below.

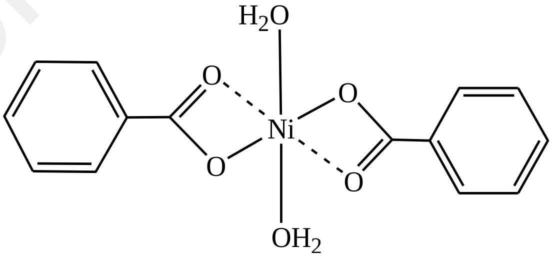

Figure 4.25 Proposed structure for [Ni(C_6H_5COO)$_2$(H_2O)$_2$]

The results of its **elemental analyses** (50.2% C; 3.6% H) were in good agreement with those calculated for the chemical formula $C_{14}H_{14}NiO_6$ (49.9% C; 4.2% H; formula weight, 337.0 g mol^{-1}).

Its FTIR spectrum (**Figure 4.26**) shows peak at 3061 cm^{-1} for H-bonded H_2O, a peak for aromatic C=C at 1690 cm^{-1}, a strong peak at 1555 cm^{-1} for $\upsilon_{as,COO}$, and a strong peak at 1368 cm^{-1} for $\upsilon_{s,COO}$. The Δ_{COO} value was 187 cm^{-1}, suggesting monodentate binding mode for $C_6H_5COO^-$ ion.

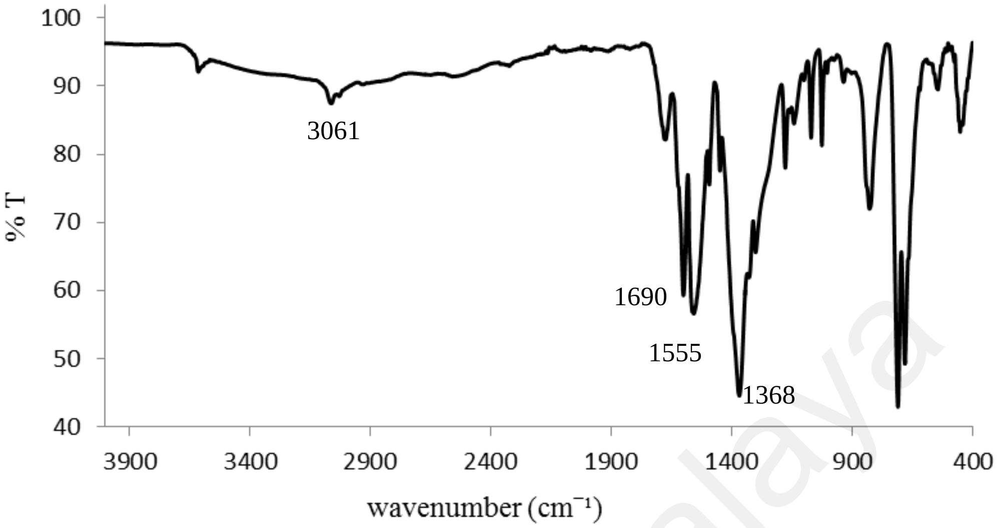

Figure 4.26 FTIR spectrum of $[Ni(C_6H_5COO)_2(H_2O)_2]$

Its **UV-vis** spectrum in CH_3OH (3.50 mmol dm^{-3}) is shown in **Figure 4.27**. It shows a *d-d* band at 411 nm (ε_{max} = 91 M^{-1} cm^{-1}) assigned to $^3A_{2g}$ to $^3T_{1g}$ (P) electronic transition. This indicates an octahedral geometry at Ni(II) in this complex [104].

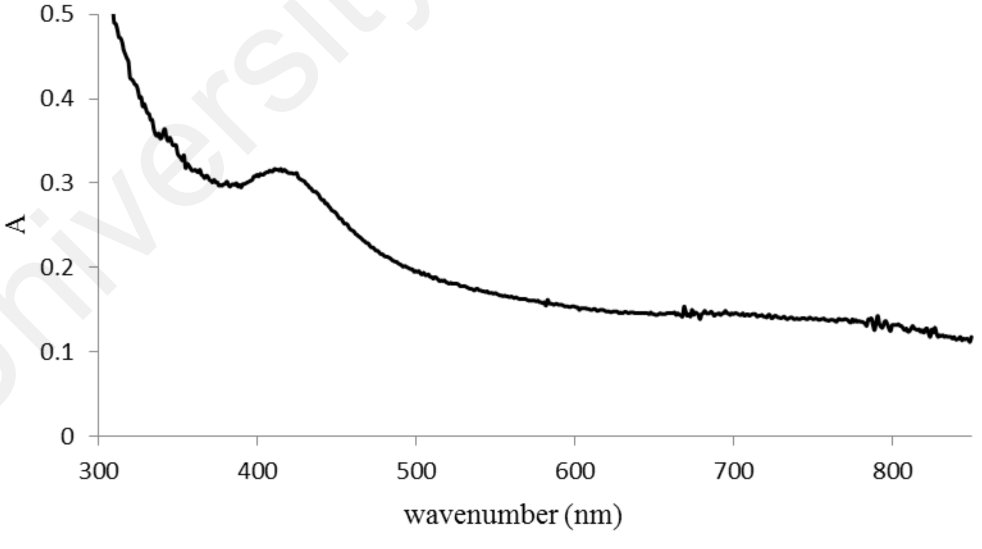

Figure 4.27 UV-vis spectrum of $[Ni(C_6H_5COO)_2(H_2O)_2]$

The value of μ_{eff}, calculated as before from the values of FM = 336.95 g mol^{-1}, χ_g = 1.47 x 10^{-5} cm^3 g^{-1}, χ_M = 4.95 x 10^{-3} cm^3 mol^{-1}, and χ_{dia} = -1.68 x 10^{-4} cm^3 mol^{-1}, and $N\alpha$ = 100 x 10^{-6} cm^3 mol^{-1} per Ni(II)) was 3.45 BM at 298 K. This is in good agreement with the theoretical spin-only value for a mononuclear Ni(II) octahedral complex (3.1 BM) [105].

In the third step, $[Ni(C_6H_5COO)_2(H_2O)_2]$ reacted with cyclam in CH_3CH_2OH to form purple crystals. Its structural formula, $[Ni(C_6H_5COO)_2(cyclam)]$ was determined by X-ray crystallography, and supported by elemental analytical data and FTIR spectroscopy.

$[Ni(C_6H_5COO)_2(cyclam)]$ crystallized in orthorhombic space group *Pbca*. Crystal data and refinement details are given in **Table 4.3** and selected bond lengths and angles are given in **Table 4.4**. Its molecular structure (**Figure 4.28**) and space group were similar to $[Ni(C_6H_5COO)_2(cyclam)]$ that reported by Lindoy *et al.* [54], but cell dimensions (a = 18.034(10) Å, b = 12.981(2) Å, c = 10.318(3) Å), number of molecules per cell unit (Z = 4) and density (D_c = 1.378 g cm^{-3}) were different. These differences due to the different of the precursor complex used: $[Ni(C_6H_5COO)_2(H_2O)_2]$ was synthesized by reaction of $NiCl_2.6H_2O$ with RCOONa in H_2O at room temperature, while Lindoy *et al.* [54] had used $[Ni(C_6H_5COO)_2]$ obtained from $NiCO_3.2Ni(OH)_2.4H_2O$ with C_6H_5COOH in hot CH_3CH_2OH [106].

The results of its **elemental analyses** (57.0% C; 6.8% H; 11.2% N) were in good agreement with those calculated for the chemical formula $C_{24}H_{34}NiN_4O_4$ (57.5% C; 6.8% H; 11.2% N; formula weight, 501.3 g mol^{-1}).

Its **FTIR** spectrum **(Figure 4.29)** shows the presence of the expected functional groups and bonds as previously discussed. The Δ_{COO} value was 226 cm^{-1} ($\upsilon_{as,COO}$ = 1602 cm^{-1} and $\upsilon_{s,COO}$ = 1376 cm^{-1}), in agreement with the monodentate binding mode for $C_6H_5COO^-$ ion as revealed from its crystal structure.

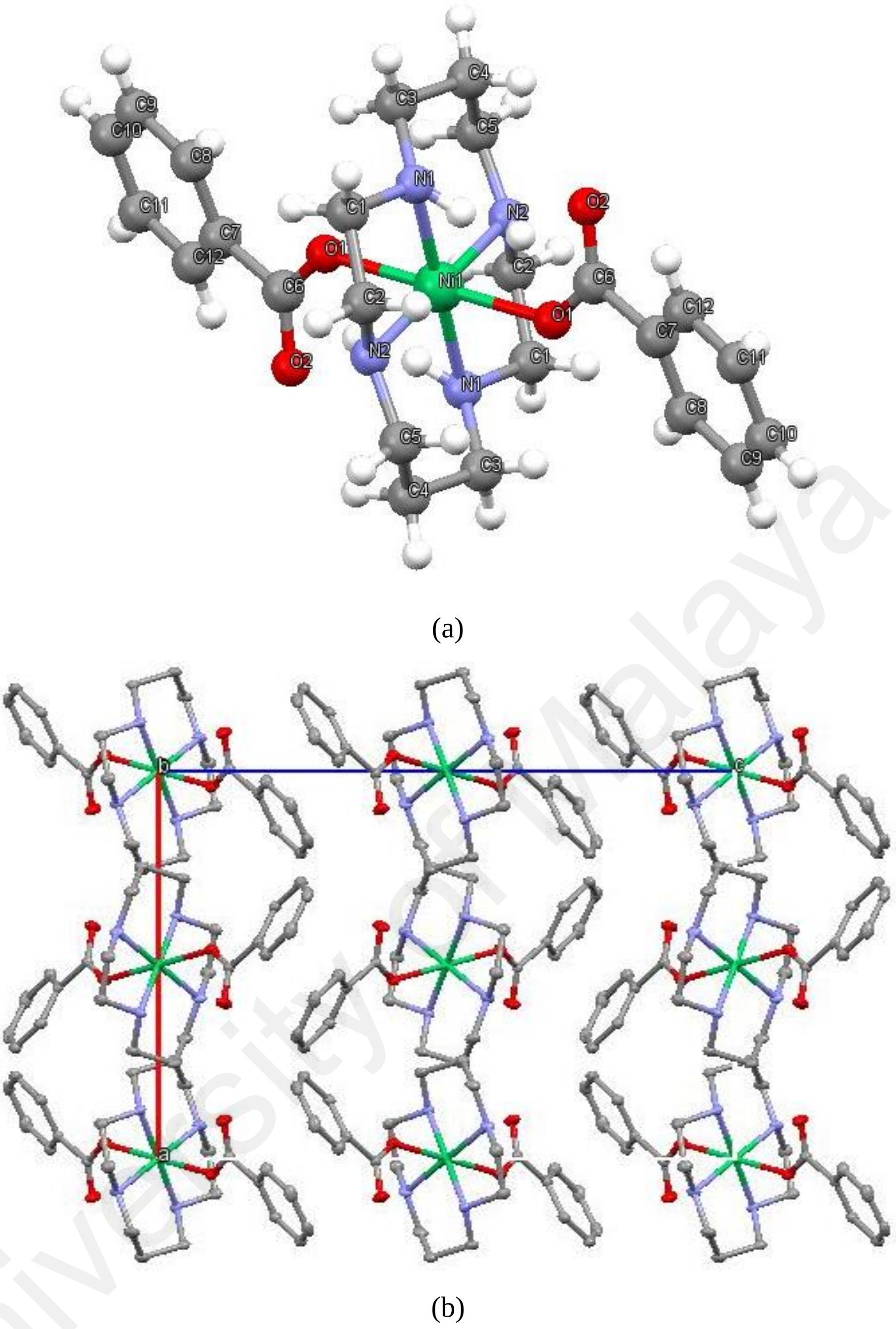

Figure 4.28 (a) Molecular structure of [Ni(C_6H_5COO)$_2$(cyclam)]; and (b) its packing (thermal ellipsoid with 50% probability) view along *b*-axis

Table 4.3 Crystal data and refinement of [Ni($C_6H_5COO)_2$(cyclam)]

Chemical formula	$C_{24}H_{34}N_4NiO_4$
Formula mass (g mol^{-1})	501.26
T(K)	293 (2)
Crystal system	Orthorhombic
Space group	*Pbca*
a (Å)	12.9299(8)
b (Å)	10.2549(5)
c (Å)	17.5942(10)
α (°)	90
β (°)	90
γ (°)	90
V (Å^3)	2332.9 (2)
Z	1
D_{calc} (g cm^{-3})	1.427
F(000)	1064
Index ranges	$-15 \leq h \leq 14$; $-8 \leq k \leq 12$; $-18 \leq l \leq 21$
Reflections collected	6774
Independent reflections (R_{int})	2287 (0.0347)
Parameters	152
Goodness-of-fit on F^2	1.036
Final R indices	$R_1 = 0.0375$
[$I \geq 2.0\sigma(I)$]	$wR_2 = 0.0982$
R indices	$R_1 = 0.0463$
	$wR_2 = 0.1055$
$\Delta\rho_{max}$ $\Delta\rho_{min}$, (e Å^{-3})	0.798, -0.703

Table 4.4. Selected bond lengths (Å) and bond angles (°) for [Ni($C_6H_5COO)_2$(cyclam)]

Bond length		Bond angle	
N(1)-Ni(1)	2.0782	N(1)-Ni-N(2)	85.27
N(2)-Ni(1)	2.0575	N(1)-Ni-O(1)	86.17
O(1)-Ni(1)	2.1114	N(2)-Ni-O(1)	89.70

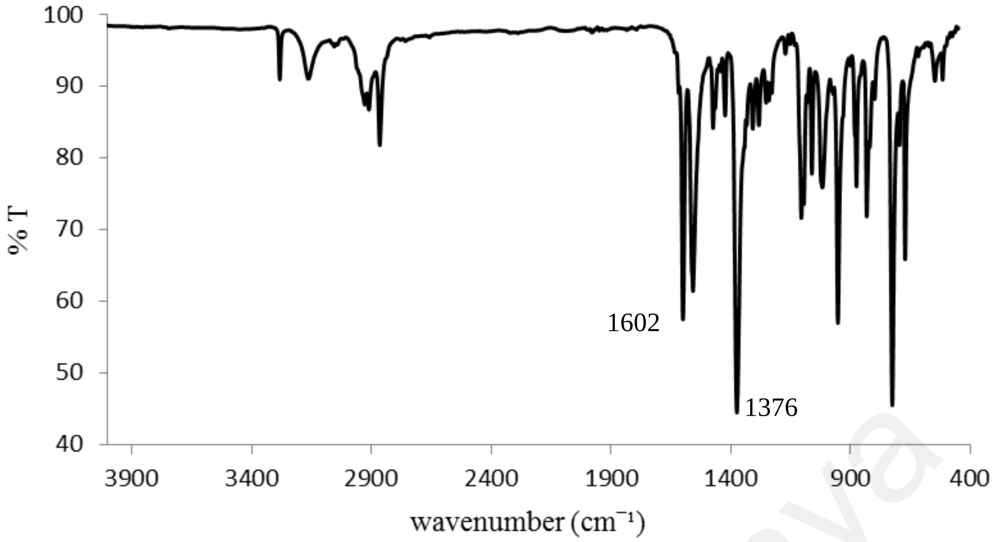

Figure 4.29 FTIR spectrum of [Ni($C_6H_5COO)_2$(cyclam)]

Its **UV-vis** spectrum in CH_3OH (2.63 mmol dm^{-3}) is shown in **Figure 4.30**. It shows a *d-d* band at 520 nm (ε_{max} = 15.0 M^{-1} cm^{-1}), indicating a t*rans*-III octahedral geometry at Ni(II) [104]. Hence, its geometrical in the solid state remained intact in solution.

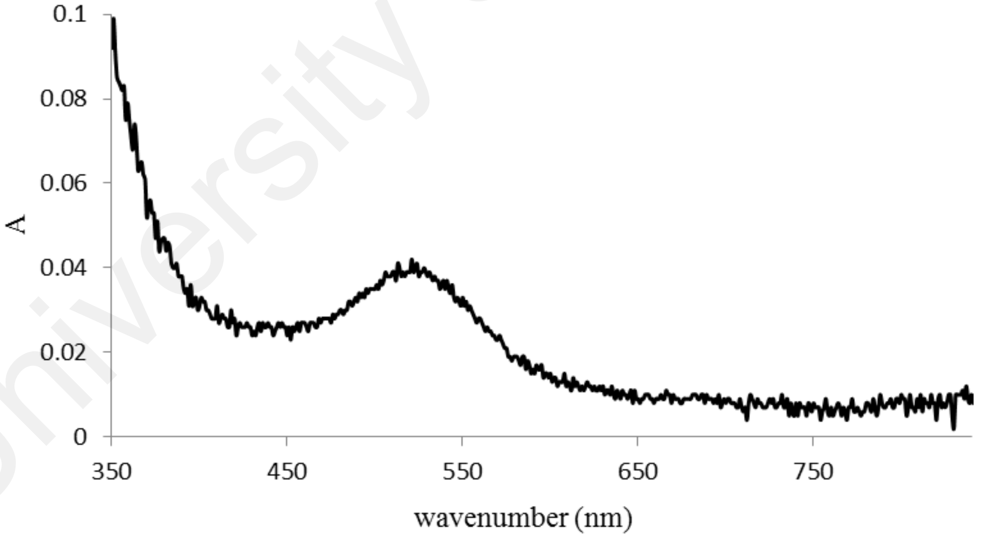

Figure 4.30 UV-vis spectrum of [Ni($C_6H_5COO)_2$(cyclam)]

The value of μ_{eff}, calculated as before from the values of FM = 501.25 g mol^{-1}, χ_g = 8.4 x 10^{-6} cm^3 g^{-1}, χ_M = 4.22 x 10^{-3} cm^3 mol^{-1}, and χ_{dia} = -2.51 x 10^{-4} cm^3 mol^{-1}, and $N\alpha$ = 100 x 10^{-6} cm^3 mol^{-1} per Ni(II)), was 3.3 BM at 298 K. This is in good agreement with the theoretical spin-only value for a mononuclear octahedral Ni(II) complex (3.1 BM) [105].

In the last step, $[Ni(C_6H_5COO)_2(cyclam)]$ reacted with L1 in a mole ratio 1:2 in CH_3CH_2OH-$CHCl_3$ to form a brown semi-solid. Its structural formula, $[Ni(cyclam)(L1)(H_2O)](C_6H_5COO)_2 \cdot H_2O$ **(4)**, was proposed based on combined instrumental data as previously done, and discussed below. Hence, its structure was similar to **2** (**Figure 4.10**), and its yield was 77.4%.

The results of its **elemental analyses** (62.3% C; 8.6% H; 7.6% N) were in good agreement with those calculated for the chemical formula $C_{43}H_{71}NiN_5O_7$ (62.3% C; 8.6% H; 8.5% N; formula weight, 828.8 g mol^{-1}).

Its **FTIR** spectrum **(Figure 4.31)** shows the presence of the expected functional groups and bonds as previously discussed. The Δ_{COO} value was 178 cm^{-1} ($\upsilon_{as,COO}$ = 1552 cm^{-1} and $\upsilon_{s,COO}$ = 1374 cm^{-1}), suggesting free (non-coordinated) $C_6H_5COO^-$ ion.

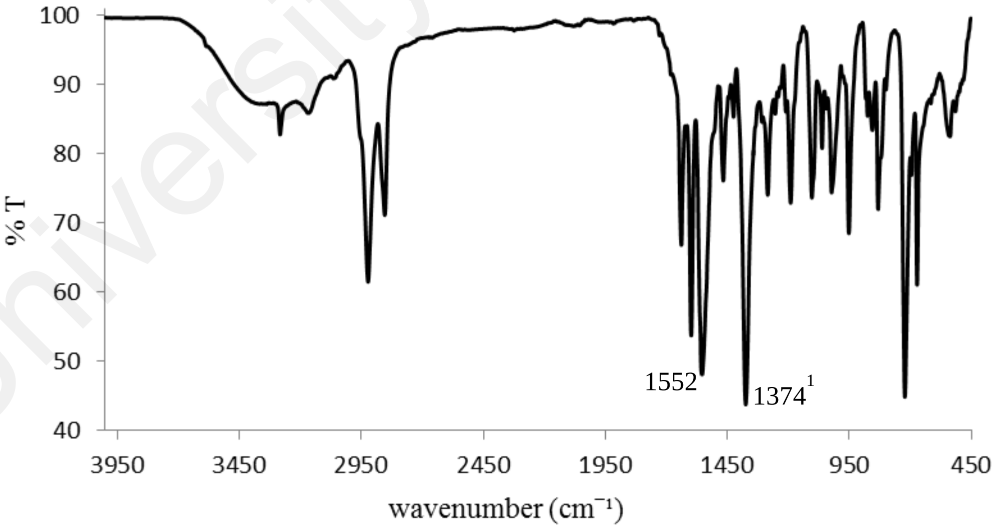

Figure 4.31 FTIR spectrum of **4**

Its **UV-vis** spectrum in $CHCl_3$ (**Figure 4.32)** shows three broad and overlapping *d-d* bands at 352 nm (ε = 420 M^{-1} cm^{-1}) and 455 nm (ε = 239 M^{-1} cm^{-1}) and 579 nm

(ε = 130 M^{-1} cm^{-1}). These bands are assigned that the electronic transitions from $^3A_{2g}$ to $^3T_{1g}$ (P), $^3T_{1g}$ (F) and $^3T_{2g}$, respectively, for an octahedral Ni(II) complexes [107].

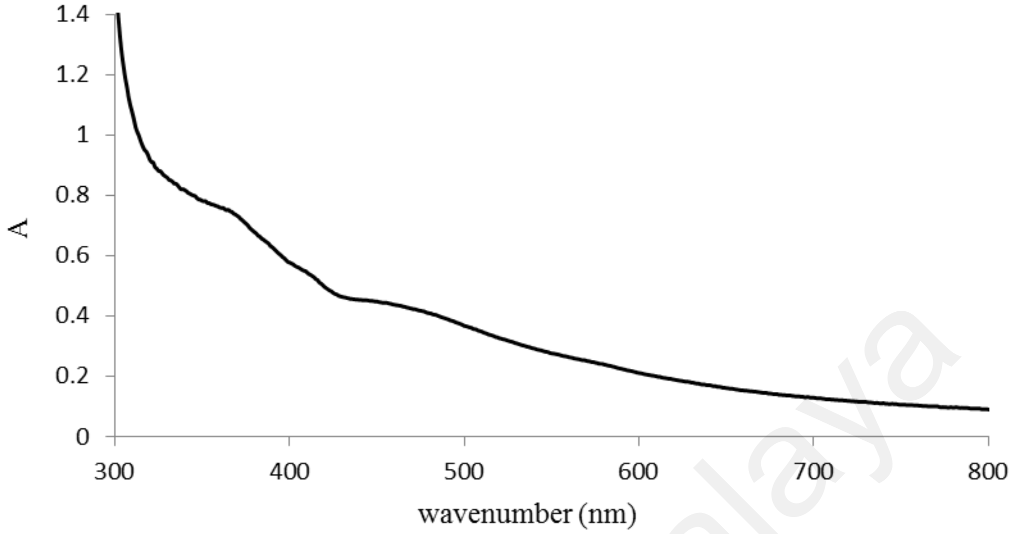

Figure 4.32 UV-vis spectrum of 4

Its μ_{eff} value could not be determined by the Gouy method as the complex was a semi-solid. However, its **^{1}H-NMR** spectrum in CD_3OD **(Figure 4.33)** shows several peaks, suggesting a diamagnetic complex. These suggest square planar diamagnetic Ni(II), indicating dissociation of axial ligands (H_2O and L1) in solution.

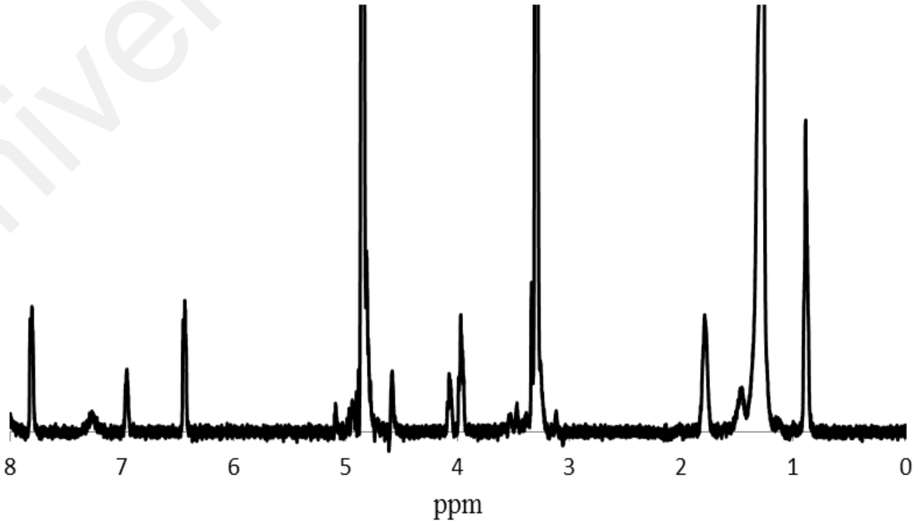

Figure 4.33 ^{1}H-NMR spectrum of **4**

(b) ***Thermal and mesogenic properties***

Its TG trace (**Figure 4.34**) shows an initial weight loss from 78 °C to about 140 °C due to the evaporation of lattice and coordinate H_2O molecules at (found = 4.7%; calculated = 4.3%). The next major weight loss from 140 °C to 660 °C was assigned to the decomposition of cyclam and L1 ligands, and $C_6H_5COO^-$ ion (found = 87.5%; calculated = 88.6%). The amount of residue at temperature above 660 °C was 7.8%, which was in good agreement with the calculated value of 9.0%, assuming that it is made up of pure NiO [108]. Hence, its decomposition temperature was 140 ^{o}C.

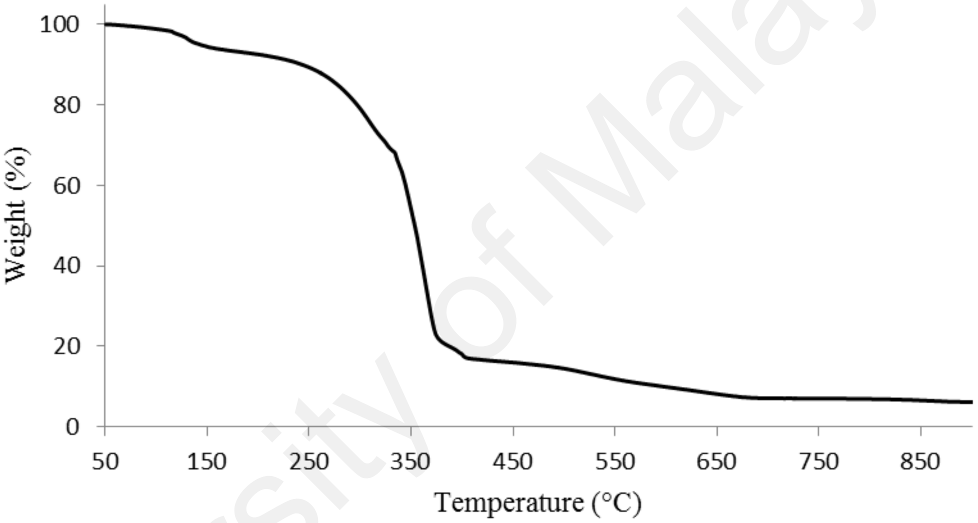

Figure 4.34 TG trace of **4**

Its **DSC** scan (**Figure 4.35**) was recorded in a successive heating–cooling cycles in the temperature range 25-130 °C. On heating, there were an endothermic peak at 25.6 ºC (ΔH = 19.8 kJ mol^{-1}) assigned as its melting temperature, and at 47.3 ºC (ΔH = 1.6 kJ mol^{-1}) assigned as its mesophase-1-to-mesophase-2 (M1-M2) transition. However, there were no peaks on cooling.

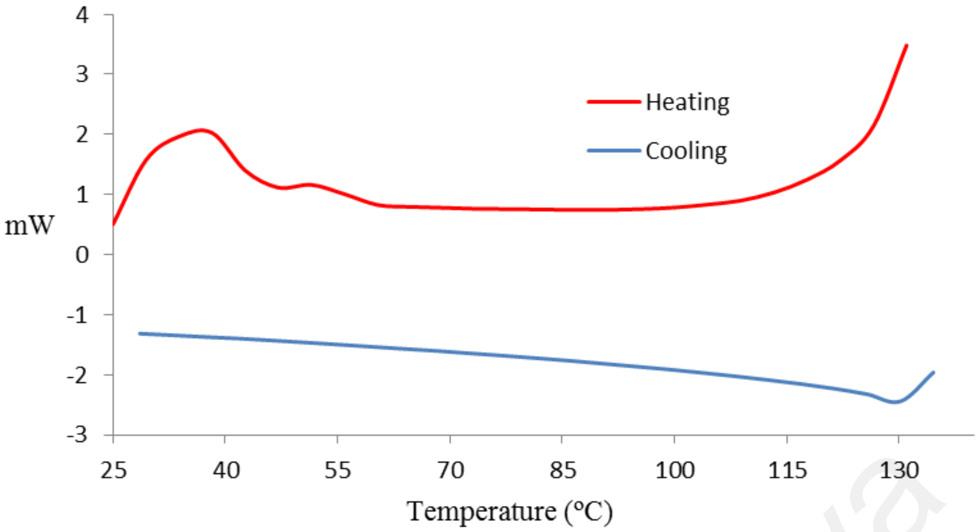

Figure 4.35 DSC of **4** (endothermic peak up)

Viewed under **POM**, **4** was observed to melt at 40 °C (**Figure 4.36**), which is in agreement with the data from DSC. On cooling, an optical texture was observed at the clear region at 70 °C (**Figure 4.43(b)**). The texture was similar to that L1 ((**Figure 4.8(c)**).

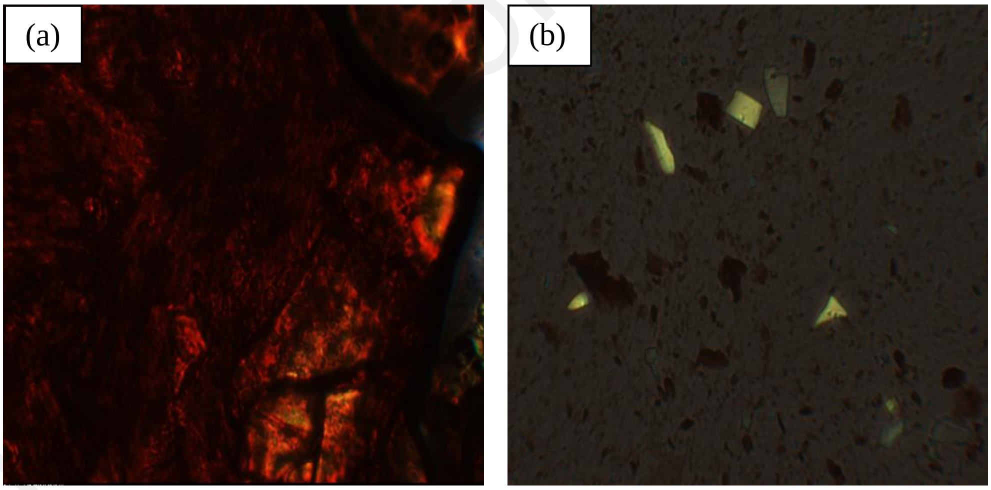

Figure 4.36 Photomicrographs of **4**: (a) on heating at 40 °C; and (b) on cooling at 70 °C

(c) ***Thermoelectrical property***

The **Seebeck coefficients** were determined for a solution of **4** in in the presence of TBATFB and KI-KI_3 for three heating-and-cooling cycles. The solvent was CH_3CH_2OH as it was insoluble in $CHCl_3$ and CH_3OH. The temperature range was 25 °C to 55 °C. The graphs of ΔV versus ΔT (**Figure 4.37**) were linear with positive slopes indicating good thermoelectric behaviour. The mean S_e value was +0.27 ± 0.01 mV K^{-1}.

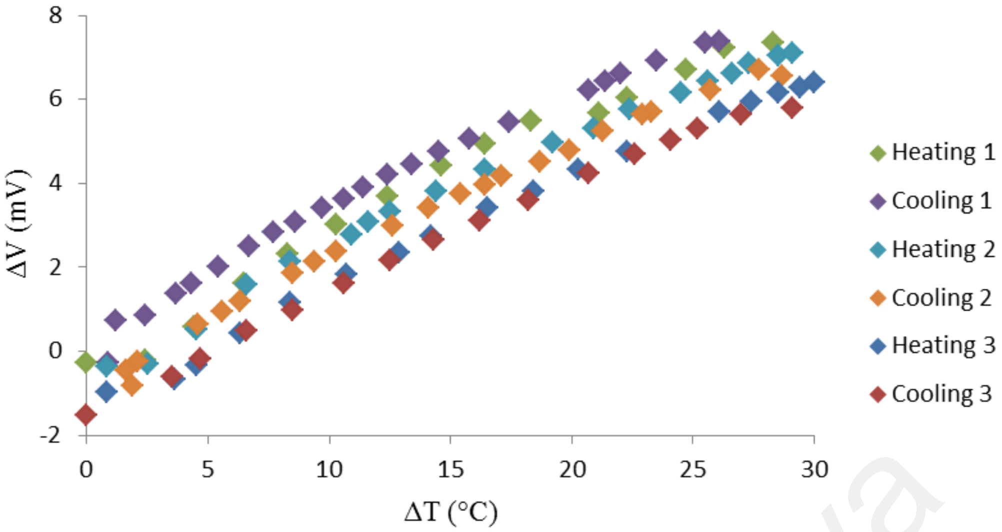

Figure 4.37 Plots of ΔV *versus* ΔT for a solution of **4** in the presence of TBATFB and KI-KI$_3$ in CH$_3$CH$_2$OH

A control experiment was also done for a solution of a mixture of KI-KI$_3$ and TBATFB in CH$_3$CH$_2$OH for one heating-and-cooling cycle. The graphs of ΔV versus ΔT (**Figure 4.38**) were also linear, and the mean S_e value was +0.35 ± 0.004 mV K^{-1}. This was higher than that of the solution of **4**. Therefore, it may be inferred that **4** was not functioning as a thermoelectric material in this solvent.

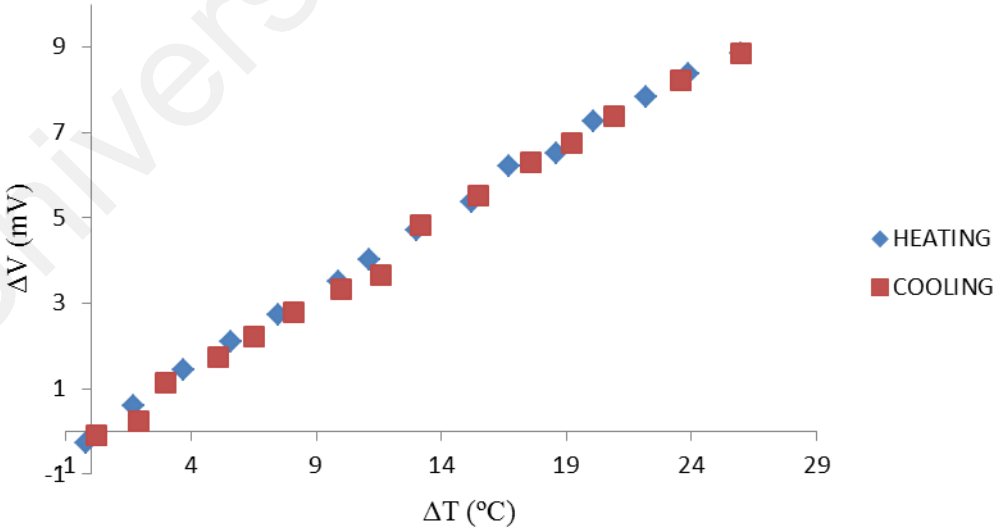

Figure 4.38 Plots of ΔV *versus* ΔT for a solution of a mixture of KI-KI$_3$ and TBATFB in CH$_3$CH$_2$OH

4.4.2 [Ni(cyclam)(L2)$_2$](C_6H_5COO)$_2$.H_2O (5)

(a) ***Synthesis and structural deduction***

[Ni(cyclam)(C_6H_5COO)$_2$] reacted with L2 in a mole ratio 1:2 in CH_3CH_2OH-$CHCl_3$ to form a brown powder. Its structural formula, [Ni(cyclam)(L2)$_2$](C_6H_5COO)$_2$.H_2O, was similarly deduced as previously done. The yield was 63.1%. Hence, its structure was similar to **1**.

The result of its elemental analyses (68.2% C; 9.9% H; 6.9% N) was in good agreement with those calculated for the chemical formula $NiC_{66}H_{110}N_6O_7$ (68.4% C; 9.6% H; 7.3% N; formula weight, 1158.3 g mol^{-1}).

Its **FTIR** spectrum (**Figure 4.39**) shows the presence of the expected functional groups and bonds as previously discussed. The Δ_{COO} value was 159 cm^{-1} ($\upsilon_{asymCOO}$ = 1536 cm^{-1} and $\upsilon_{sym,COO}$ = 1377 cm^{-1}), suggesting ionic (non-coordinated) $C_6H_5COO^-$ ion.

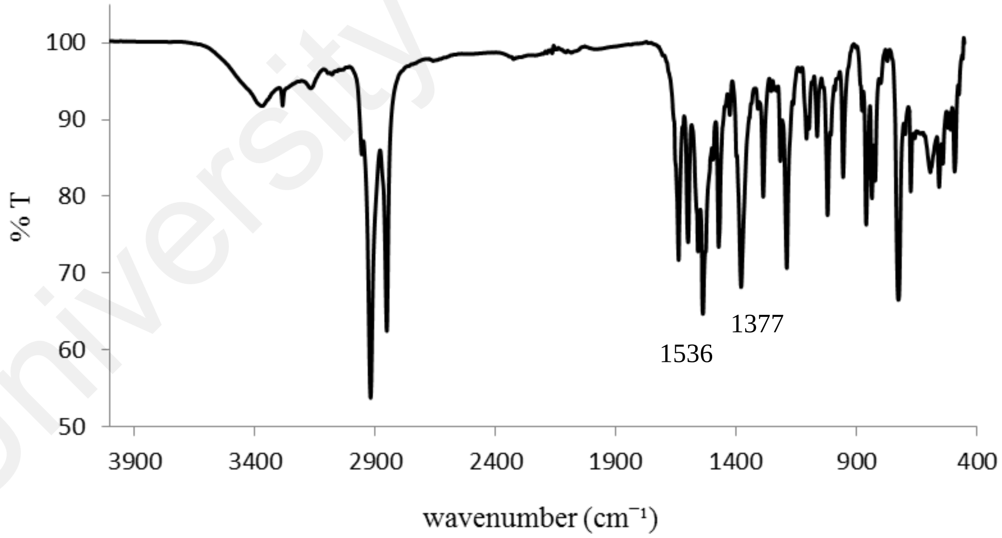

Figure 4.39 FTIR spectrum of **5**

Its **UV-vis** spectrum in $CHCl_3$ (**Figure 4.40**) shows overlapping *d-d* bands at 386 nm (ε = 141 M^{-1} cm^{-1}) and 458 nm (ε = 72 M^{-1} cm^{-1}). These bands are assigned that the electronic transitions from $^3A_{2g}$ to $^3T_{1g}$ (P) and $^3T_{1g}$ (F), respectively, for an octahedral Ni(II) complex.

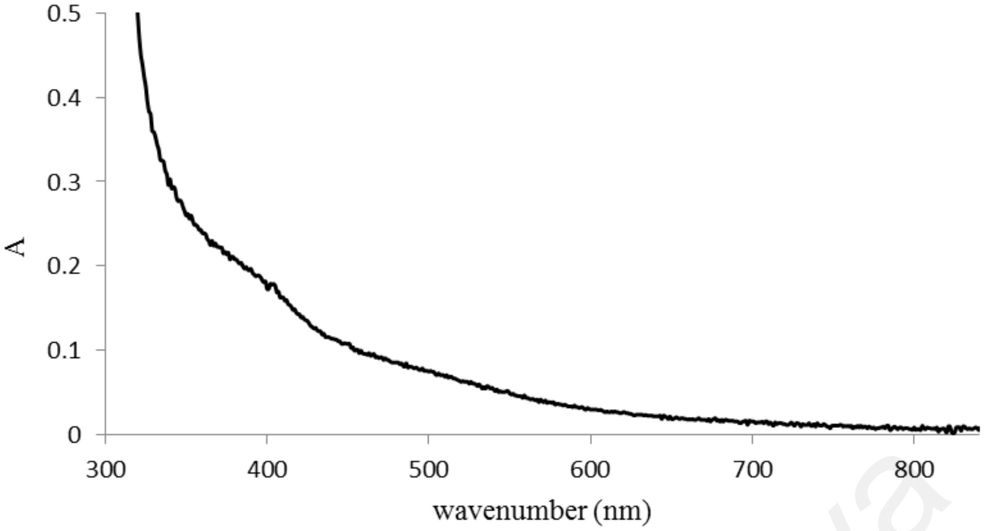

Figure 4.40 UV-Vis spectrum of **5**

The value of μ_{eff}, calculated as before from the values of FM = 1158.3 g mol^{-1}, χ_g = 8.0 x 10^{-7} cm^3 g^{-1}, χ_M = 9.3 x 10^{-4} cm^3 mol^{-1}, χ_{dia} = -5.79 x 10^{-4} cm^3 mol^{-1}, and $N\alpha$ = 100 x 10^{-6} cm^3 mol^{-1}, was 1.83 BM at 298 K. This is significantly lower than the expected value of 3.1 BM, indicating significant intermolecular antiferromagnetic interactions between the Ni(II) atoms, likely through H-bonds involving lattice H_2O [109].

(b) ***Thermal and mesogenic properties***

Its TG trace (**Figure 4.41**) shows a major weight loss from 212 °C to 550°C was due to the decomposition of cyclam and L2 ligands, and $C_6H_5COO^-$ ion (found = 94.9%; calculated = 94.8%). The amount of residue at temperature above 550 °C was 5.1% in agreement with the calculated value of 6.5%, assuming it was made up of pure NiO. Hence, its decomposition temperature was 212 °C.

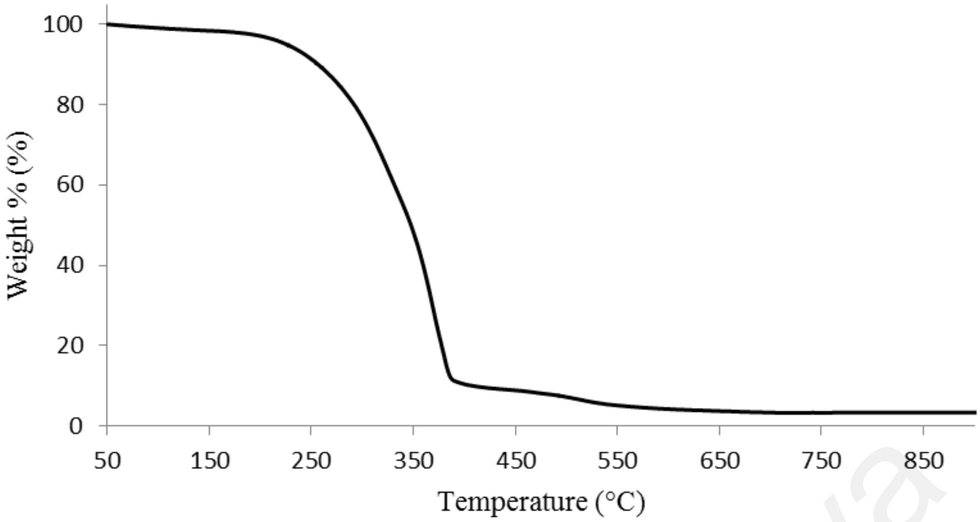

Figure 4.41 TG trace of **5**

Its DSC scan (**Figure 4.42**) was recorded in one successive heating–cooling cycle in the temperature range 25-125 °C. On heating, there were two overlapping endothermic peaks in the range 31.2 °C to 53.5 °C ($\Delta H_{combined}$ = 76.2 kJ mol^{-1}) assigned to dissociation of axially coordinated L2 and melting of L2.

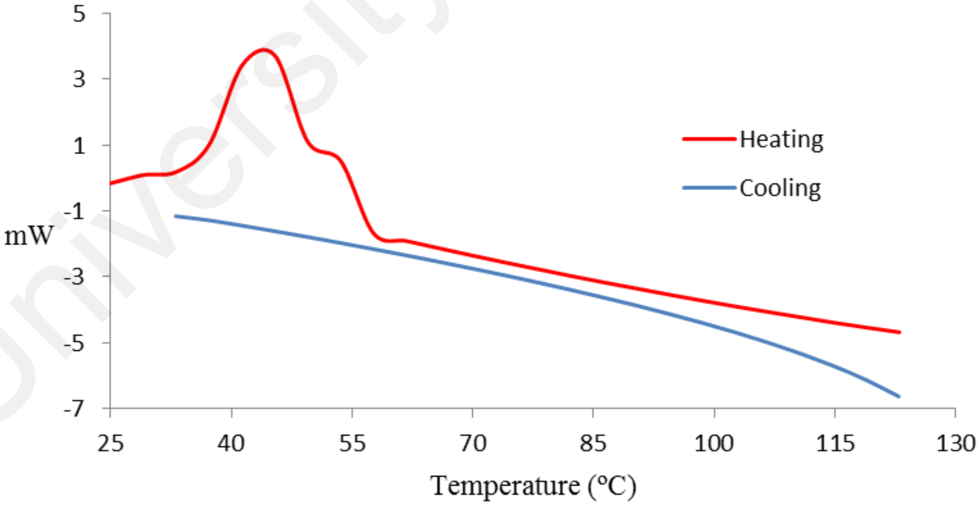

Figure 4.42 DSC of **5** (endothermic peaks up)

Viewed under **POM**, **6** was observed to melt at 45 °C, was highly fluidic at 53°C, but did not clear even at 189 °C. When a new sample was heated to 55 °C (incomplete isotropization) and then cooled, an optical texture was observed at the clear region at

53 °C (**Figure 4.43(a)**). The texture was similar to that L2 (**Figure 4.43(b)**). These suggest that L2 were weakly coordinated at the axial positions of Ni(II) of the complex. Therefore, the complex was not mesomorphic.

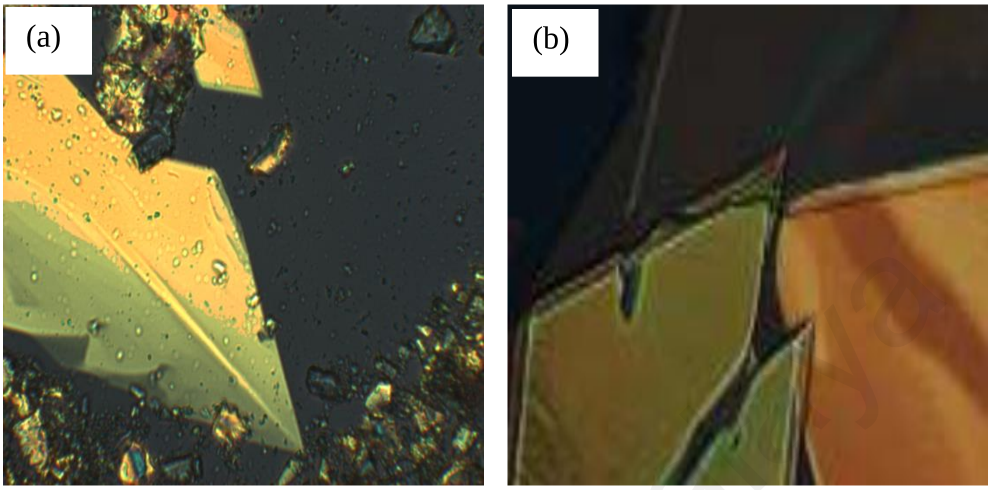

Figure 4.43 Photomicrographs of (a) **5** on cooling at 53 °C; and (b) ligand L2 at 53°C

(c) ***Thermoelectrical property***

The **Seebeck coefficient** for a solution of **5** was similarly determined as for **4**. The graphs of ΔV versus ΔT (**Figure 4.44**) was linear with positive slopes, and the mean S_e value was +0.23 ± 0.02 mV K^{-1}. Since the S_e value was lower than value for mixture of KI-KI_3 and TBATFB in CH_3CH_2OH (+0.352 ± 0.004 mV K^{-1}), the complex was not functioning as a thermoelectric material in CH_3CH_2OH.

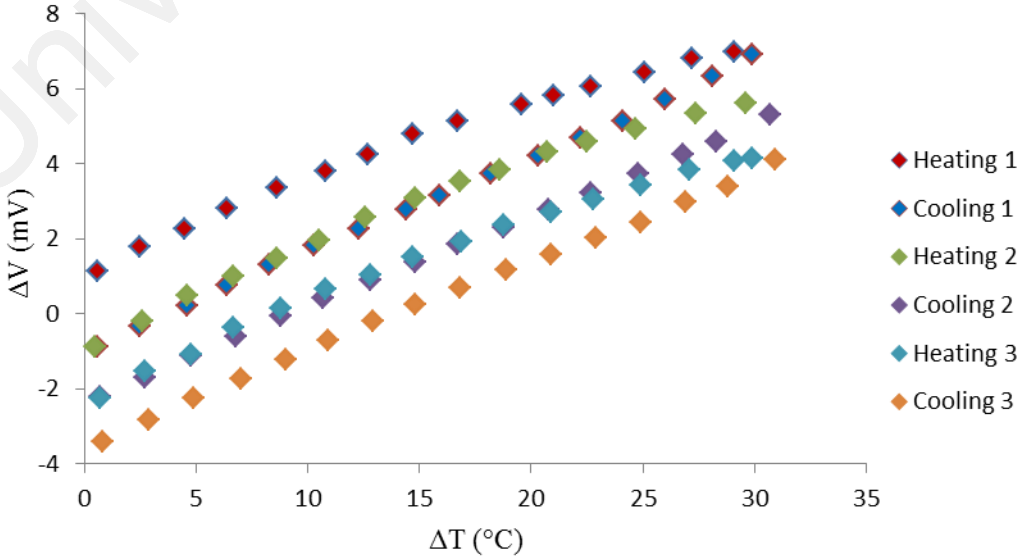

Figure 4.44 Plots of ΔV versus ΔT of **5**

4.4.3 *Summary*

The results of the analytical data for **4** and **5** are summarised in **Table 4.5**. The structural formula for **4** was different from **5**. However, both complexes were mononuclear with octahedral Ni(II) atoms and ionic. The magnetic properties of **4** in the solid state could not be determined, but **5** was paramagnetic with strong intermolecular interactions between the Ni(II) centres. The thermal stability of **4** was significantly lower than **5**. Both complexes did not function as thermoelectric materials in ethanol, and were not mesomorphic.

Table 4.5 Summary for complexes **4** and **5**

Chemical formula	Δ_{COO} (cm^{-1})	λ (nm)	μ_{eff} (BM)	T_{dec} (°C)	S_e (mV K^{-1})	M
$[Ni(cyclam)(L1)(H_2O)](R)_2{\cdot}H_2O$ (**4**)	178 (ionic)	455 (*)	-	140	0.27 ±0.01	-
$[Ni(cyclam)(L2)_2](R)_2{\cdot}H_2O$ (**5**)	159 (ionic)	386 (*)	1.83	212	0.23 (±0.02)	-

R = C_6H_5COO ; * = octahedral; M = mesomorphism

4.5 Complexes of Cobalt

4.5.1 $[Co(cyclam)(L1)_2](C_6H_5COO)_2{\cdot}3H_2O$ (6)

(a) ***Synthesis and structural deduction***

$[Co(cyclam)(L1)_2](C_6H_5COO)_2{\cdot}3H_2O$ (**6**) was prepared by the steps as shown in **Scheme 4.2**.

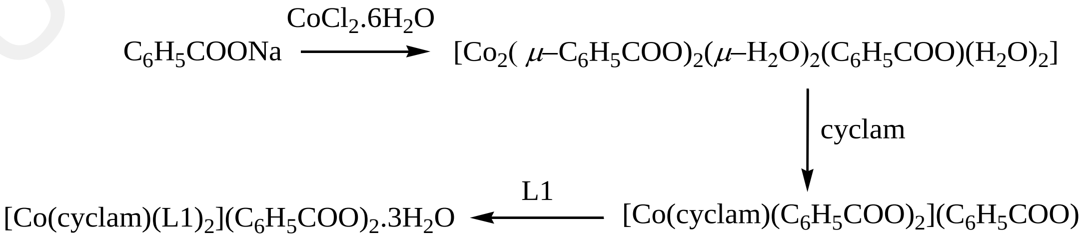

Scheme 4.2 Synthetic steps for $[Co(cyclam)(L1)_2](C_6H_5COO)_2{\cdot}3H_2O$ (**6**)

In the first step, C_6H_5COONa reacted with $CoCl_2{\cdot}6H_2O$ in CH_3CH_2OH to form $[Co_2(\mu\text{-}C_6H_5COO)_2(\mu\text{-}H_2O)_2(C_6H_5COO)(H_2O)_2]$ (purple powder). Its structural formula (**Figure 4.45**) was proposed based on combined instrumental data discussed below.

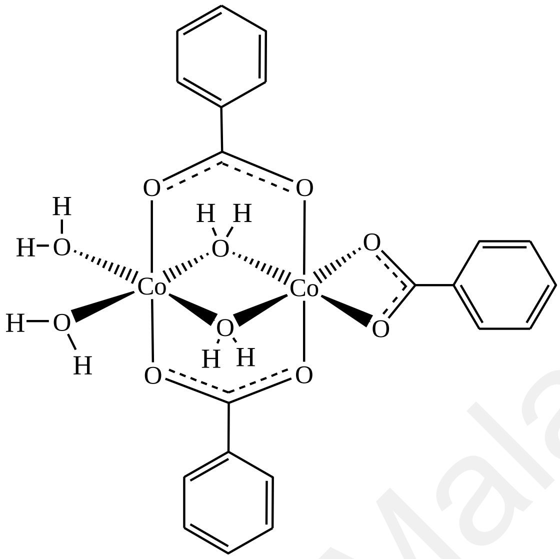

Figure 4.45 Proposed structure for $[Co_2(\mu\text{-}C_6H_5COO)_2(\mu\text{-}H_2O)_2(C_6H_5COO)(H_2O)_2]$

The results of its **elemental analyses** (46.3% C; 3.4% H) were in good agreement with those calculated for the chemical formula $C_{21}H_{23}Co_2O_{10}$ (45.6% C; 4.2% H; formula weight, 553.3 g mol^{-1}).

Its FTIR spectrum (**Figure 4.46**) shows the presence of the expected functional groups and bond. The Δ_{COO} values were 164 cm^{-1} and 146 cm^{-1} ($\upsilon_{asym,COO}$ = 1546 cm^{-1}; $\upsilon_{sym,COO}$ = 1382 cm^{-1}, 1400 cm^{-1}), suggesting bridging bidentate and chelating binding modes for $C_6H_5COO^-$ ion, respectively.

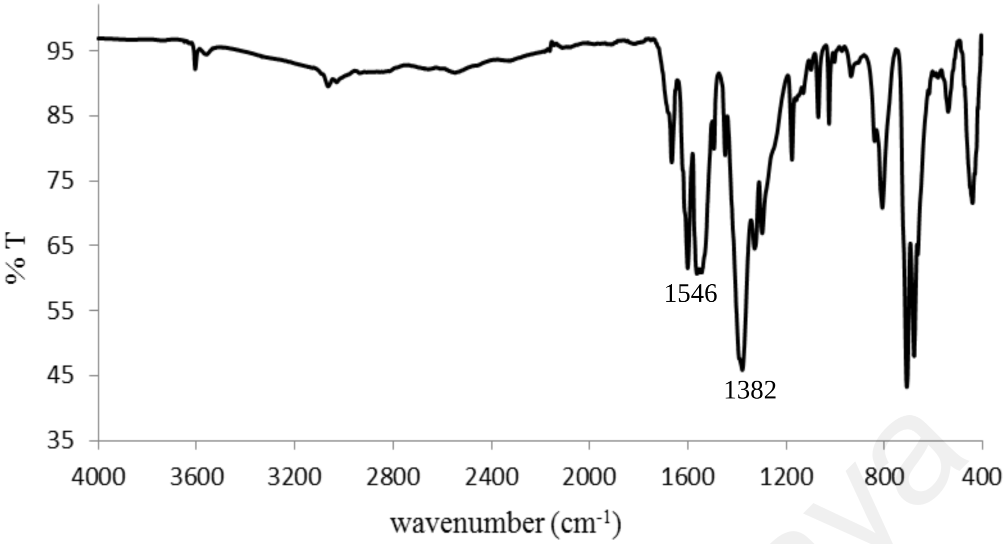

Figure 4.46 FTIR spectrum of [Co_2(μ-C_6H_5COO)$_2$(μ-H_2O)$_2$(C_6H_5COO)(H_2O)$_2$]

Its **UV-vis** spectrum in $(CH_3)_2SO$ (DMSO) (1.45 mmol dm^{-3}) is shown in **Figure 4.47**. It shows a *d-d* band with a maximum at 551 nm (ε_{max} = 185 M^{-1} cm^{-1}), assigned to the $^4T_{1g}$(F) to $^4T_{1g}$(P) electronic transition, indicating an octahedral complex with HS Co(II) atoms [110].

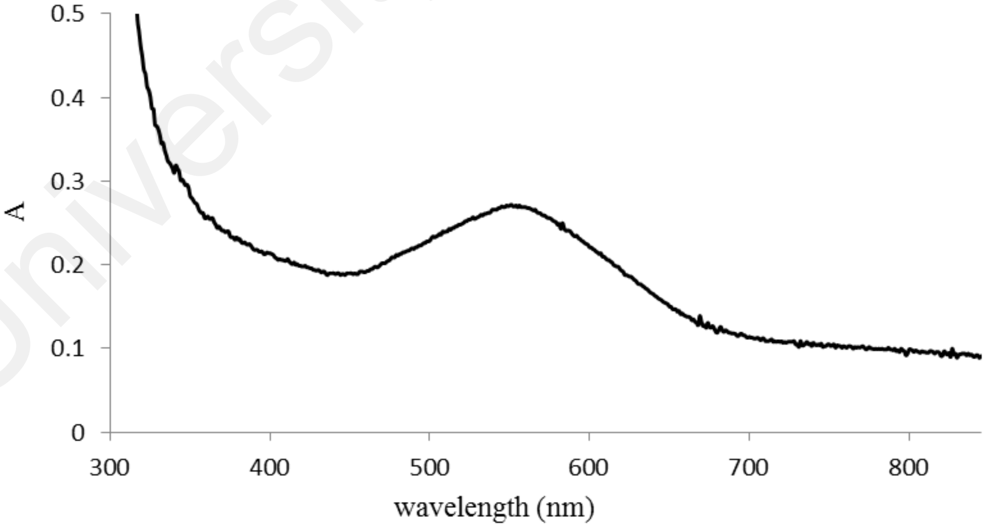

Figure 4.47 UV-vis spectrum of [Co_2(μ-C_6H_5COO)$_2$(μ-H_2O)$_2$(C_6H_5COO)(H_2O)$_2$]

The value of ***μ_{eff}***, calculated as before from the values of FM = 553.27 g mol^{-1}, χ_g = 2.61 x 10^{-5} cm^3 g^{-1}, χ_M = 1.44 x 10^{-2} cm^3 mol^{-1}, and χ_{dia} = -2.77 x 10^{-4} cm^3 mol^{-1}, and

$N\alpha$ = 100 x 10^{-6} cm^3 mol^{-1} per Co(II), was 5.90 BM at 298 K. This was slightly lower than the expected spin value for six unpaired electrons (μ_{eff} = 6.93 BM) for a dinuclear high-spin Co(II) (d^7) octahedral complex, indicating antiferromagnetic interactions between the two Co(II) centers. Similar suggestion was proposed by Anagnostopoulos for $Co[2,3\text{-}py(CO_2)(CO_2H)]_2 \cdot 2H_2O$ (μ_{eff} = 4.84 BM) [108].

In the second step, $[Co_2(\mu\text{-}C_6H_5COO)_2(\mu\text{-}H_2O)_2(C_6H_5COO)(H_2O)_2]$ reacted with cyclam in CH_3CH_2OH to form a brown semi-solid. It was crystallized to formed brown crystals in CH_3OH. Its structural formula, $[Co(C_6H_5COO)_2(cyclam)](C_6H_5COO)$, was determined by X-ray crystallography, and supported by elemental analytical data and FTIR spectroscopy. Hence, the Co(II) in the reactant was oxidised to Co(III) during this reaction.

$[Co(C_6H_5COO)_2(cyclam)](C_6H_5COO)$ crystallized in monoclinic space group $P2_1/c$. Crystal data and refinement details are given in **Table 4.6** and selected bond lengths and angles are given in **Table 4.7.** Its molecular structure is shown in **Figure 4.48(a)** and packing diagram in **Figure 4.48(b).** The crystal structure shows the Co(III) atom adopts a *trans*-octahedral geometry by two of C_6H_5COO bound to the metal at axial positions and one uncoordinated (ionic) benzoate around the complex. The C_6H_5COO ligands bind to the Co(III) in monodentate mode.

The results of its **elemental analyses** (58.6% C; 6.7% H; 11.9% N) were in good agreement with those calculated for the chemical formula $C_{31}H_{39}CoN_4O_6$ (59.8% C; 6.3% H; 9.0% N; formula weight, 622.60 g mol^{-1}).

Its FTIR spectrum (**Figure 4.49**) shows the presence of the expected functional groups and bonds. The Δ_{COO} value was 202 cm^{-1} ($\upsilon_{as,COO}$ = 1555 cm^{-1}, $\upsilon_{s,COO}$ = 1353 cm^{-1}), suggesting a monodentate binding mode for $C_6H_5COO^-$ ion.

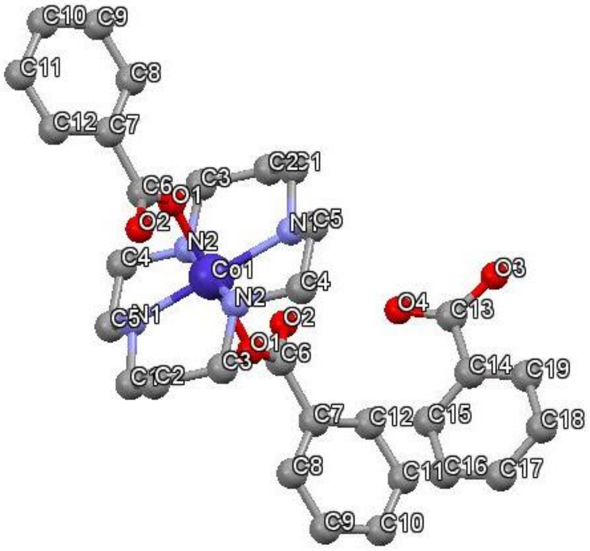

(a)

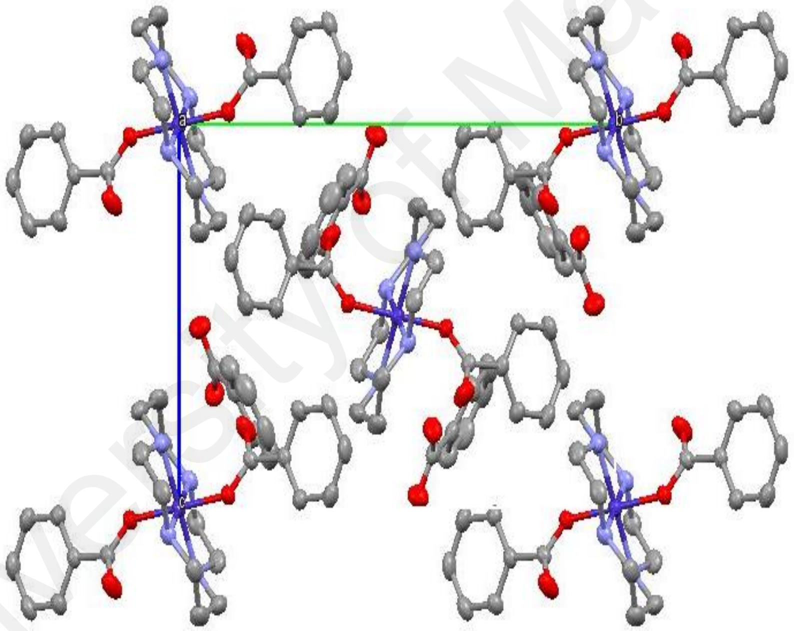

(b)

Figure 4.48 (a) Molecular structure of [Co($C_6H_5COO)_2$(cyclam)](C_6H_5COO) (thermal ellipsoid with 50% probability); and (b) its packing diagram view along *a*-axis.

Table 4.6 Crystal data and refinement of [Co($C_6H_5COO)_2$(cyclam)](C_6H_5COO)

Chemical formula	$C_{31}H_{39}CoN_4O_6$
Formula mass (g mol^{-1})	622.60
T (K)	302(2)
Crystal system	Monoclinic
Space group	$P\ 2_1/c$
a (Å)	10.8995(4)
b (Å)	15.8743(7)
c (Å)	11.6496(6)
α (°)	90
β (°)	117.770(2)
γ (°)	90
V (Å^3)	1783.48(14)
Z	2
D_{calc} (g cm^{-3})	1.385
F(000)	782
Index ranges	$-14 \leq h \leq 14; -20 \leq k \leq 21; -14 \leq l \leq 15$
Reflections collected	17837
Independent reflections (R_{int})	4444 (0.0393)
Parameters	241
Goodness-of-fit on F^2	1.102
Final R indices	$R_1 = 0.0476$
[$I \geq 2.0\sigma(I)$]	$wR_2 = 0.0955$
R indices	$R_1 = 0.0749$
	$wR_2 = 0.1149$
$\Delta\rho_{max}$ $\Delta\rho_{min}$, (e Å^{-3})	0.543, -0.376

Table 4.7 Selected bond lengths (Å) and bond angles (°) for [Co($C_6H_5COO)_2$(cyclam)](C_6H_5COO)

Bond length		Bond angle	
Co(1)-N(1)	1.976(2)	N(1)-Co(1)-N(2)	93.69(9)
Co(1)-N(2)	1.977(2)	O(1)-Co(1)-N(1)	91.55(8)
Co(1)-O(1)	1.9214(15)	O(1)-Co(1)-N(2)	93.38(8)

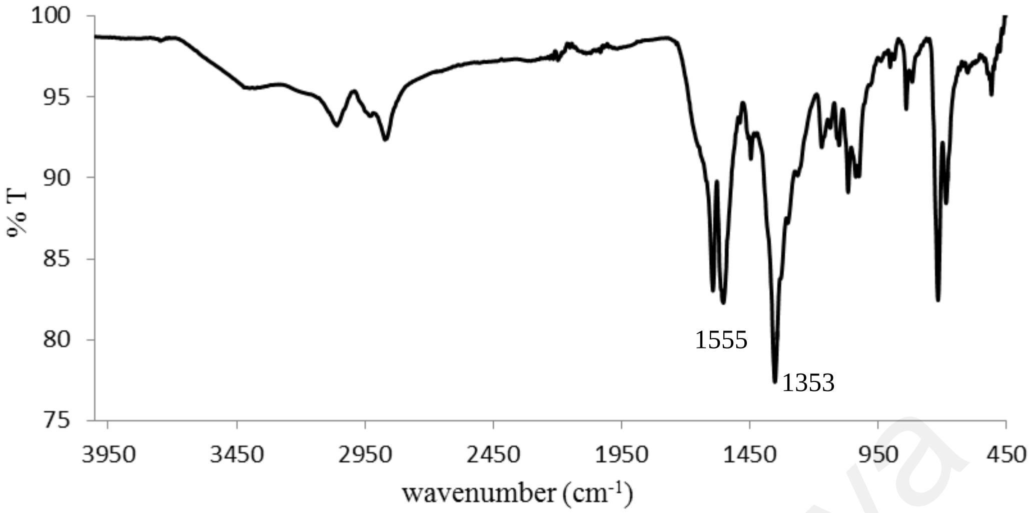

Figure 4.49 FTIR spectrum of [Co(C_6H_5COO)$_2$(cyclam)](C_6H_5COO)

In the final step, [Co(C_6H_5COO)$_2$(cyclam)](C_6H_5COO) reacted with L1 (mole ratio 1:2) in CH_3CH_2OH-$CHCl_3$ to form [Co(cyclam)(L1)$_2$](C_6H_5COO)$_2$.$3H_2O$ (**6**). It was obtained as a brown semi-solid, and its yield was 96.6%. Based on combined analytical data discussed below, its proposed structure is similar to **1 (Figure 4.3)**.

The results of its elemental analyses (65.7% C; 9.3% H; 6.9% N) were in good agreement with those calculated for chemical formula $C_{62}H_{106}CoN_6O_9$ (65.4% C; 9.4% H; 7.4% N; formula weight, 1152.49 g mol^{-1}).

Its **FTIR** spectrum (**Figure 4.50)** shows the presence of the expected functional groups and bonds. The Δ_{COO} value was 207 cm^{-1} ($\upsilon_{asym,COO}$ = 1560 cm^{-1}; $\upsilon_{sym,COO}$ = 1353 cm^{-1}), suggesting monodentate binding mode for $C_6H_5COO^-$ ion.

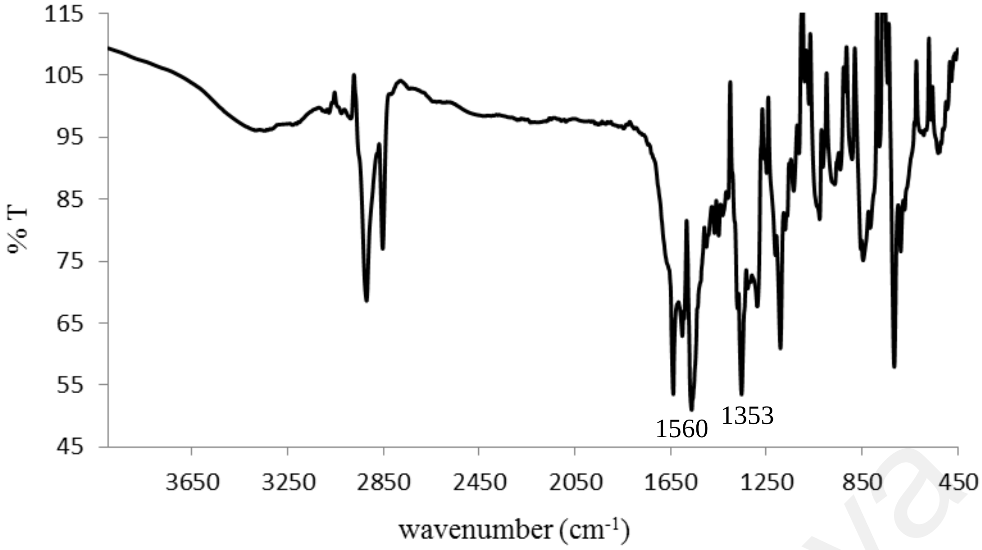

Figure 4.50 FTIR spectrum of **6**

Its **UV-vis** spectrum in $CHCl_3$ (0.21 mmol dm^{-3}) is shown in **Figure 4.51**. Its shows a continuously increasing absorbance from about 800 nm to a shoulder on a strong MLCT band at 399 nm (ε = 55.7 x 10^2 M^{-1} cm^{-1}) [71].

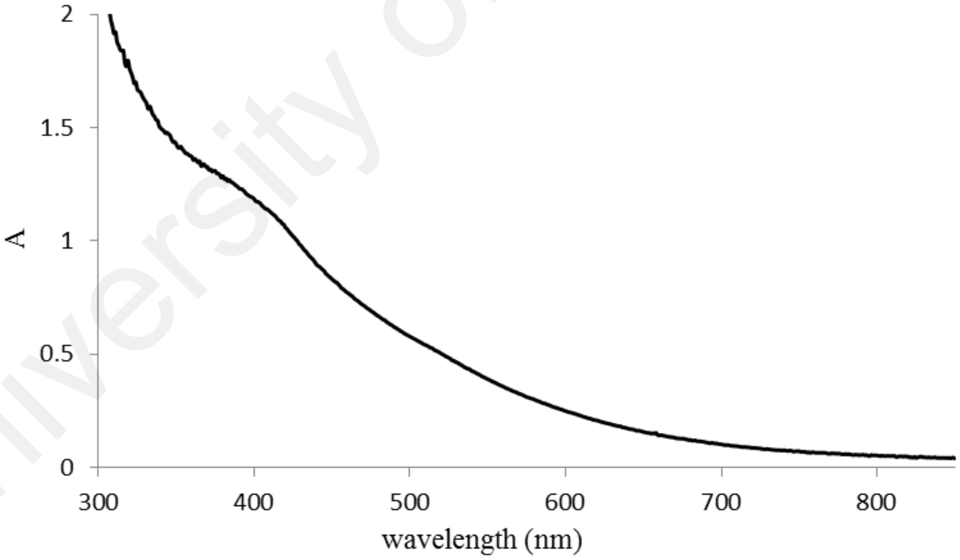

Figure 4.51 UV-Vis spectrum of **6**

Its ***μ*****eff** value could not be determined by the Gouy method as the complex was a semi-solid. However, its **^{1}H-NMR** spectrum in CD_3OD **(Figure 4.52)** does not show all peaks for the organic ligands, suggesting a paramagnetic complex. Hence, the metal ion in the complex was Co(II) (either LS or HS), and not Co(III) atom which is expected to be LS and diamagnetic (*d*^{6}).

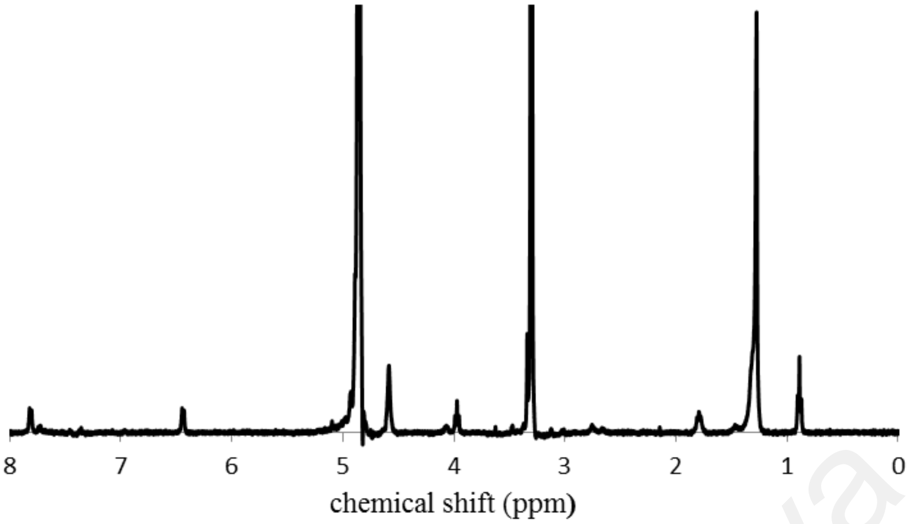

Figure 4.52 ^{1}H-NMR spectrum of **6**

(b) ***Spin-crossover behaviour***

Its temperature-dependence ε was measured for a solution in DMSO at 438 nm (ε = 620 M^{-1} cm^{-1}), which corresponds to LS Co(II), in the temperature range of 20 °C to 70 °C on two successive heating-cooling cycles. The results (**Figure 4.53**) show that on heating, the ε values remained almost unchange at about 620 M^{-1} cm^{-1} from 25 °C to 60 °C, and then increased abruptly to 881 M^{-1} cm^{-1} at 70 °C. Upon cooling from this temperature, the values increased abruptly to 1005 M^{-1} cm^{-1} at 65 °C, and then decreased to 561 M^{-1} cm^{-1} below this temperature and remained unchange on further cooling to 15 °C. On reheating, the values decreased to 458 M^{-1} cm^{-1} at 25°C, increased to about 567 M^{-1} cm^{-1} at 35 °C, and remained unchange from this temperature to 65 °C, and then increased abruptly to 727 M^{-1} cm^{-1} at 70 °C. During the second cooling, the ε value increased abruptly to 822 M^{-1} cm^{-1} at 65 °C, then decreased to 560 M^{-1} cm^{-1} at 55 ^{o}C and remained unchanged on further cooling to 15 °C. From these results, it may be inferred that the complex showed reversed SCO behaviour (HS-LS on heating) in solution in the temperature range of 60 ^{o}C to 65 ^{o}C, and this behaviour was reversible.

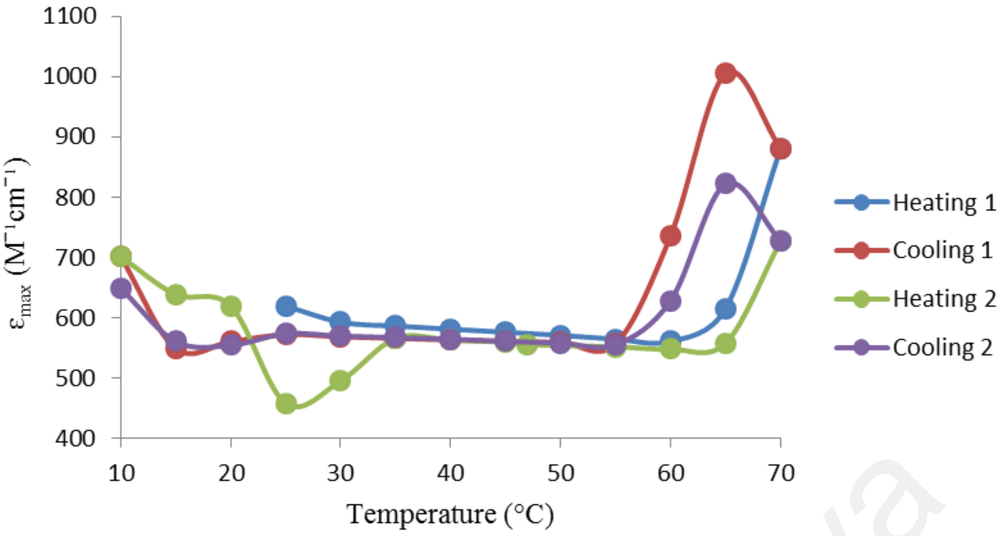

Figure 4.53 Temperature-dependent ε_{max} values for **6** at 438 nm

Similar reversed SCO behaviour was reported by Hayami for $[Co(C_n\text{-terpy})_2](BF_4)_2$ (n = 16, 14 and 12) in the solid state [76]. This was ascribed it to the 'hook' effect of the long alkyl chain. It was postulated that this effect pulled out the ligand from the metal centre, resulting in longer bonds (HS). On heating, the van der Waals forces between the alkyl chain were broken, allowing for a closer approach of the ligand to the metal centre (shorter bonds), hence LS.

(c) *Thermal and mesogenic properties*

Its TG trace (**Figure 4.54**) shows an initial weight loss from 70 °C to about 156 °C due to evaporation of lattice H_2O molecules (found = 5.0%; calculated = 4.7%). The next weight loss from 156 °C to about 282 °C was due to the decomposition of cyclam (found = 18.3%; calculated = 17.6%). This is followed by another weight loss from 282 °C to 438 °C due to the decomposition of L1 (found = 50.7%; calculated = 51.2%) and from 438 °C to 694 °C due to the decomposition $C_6H_5COO^-$ ion (found = 20.0%; calculated = 21.3%). The amount of residue at temperatures above 694 °C was 5.9%. This correlates well with the calculated value of 6.5%, assuming that it is made up of pure CoO [111].

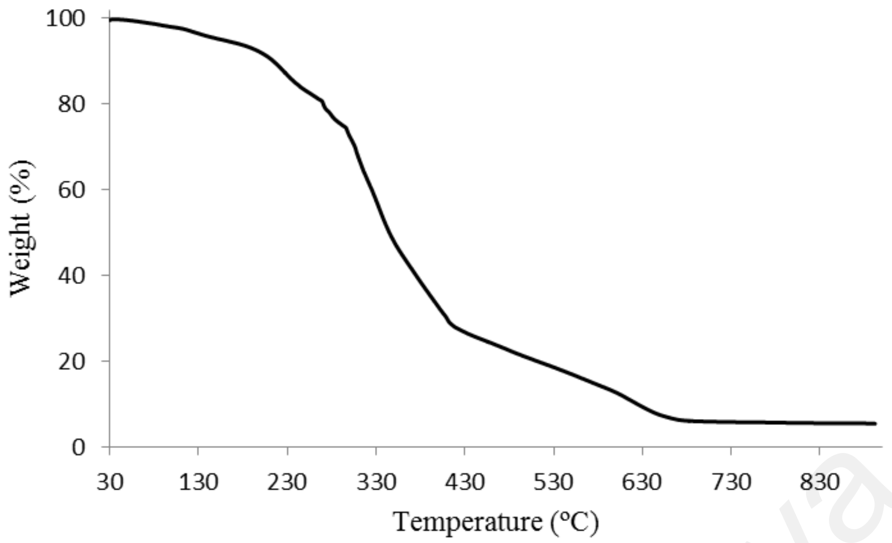

Figure 4.54 TG trace of **6**

Its **DSC** scan (**Figure 4.55**) was recorded in a heating–cooling cycle in the temperature range of 25-125 °C. On heating, there were weak endothermic peaks at 107.9 °C (ΔH = +3.2 kJ mol^{-1}), 113.4 °C (ΔH = +0.8 kJ mol^{-1}) and 118.6 °C (ΔH = +0.7 kJ mol^{-1}), suggesting breaking of weak intermolecular forces. However, there were no peaks on cooling from this temperature.

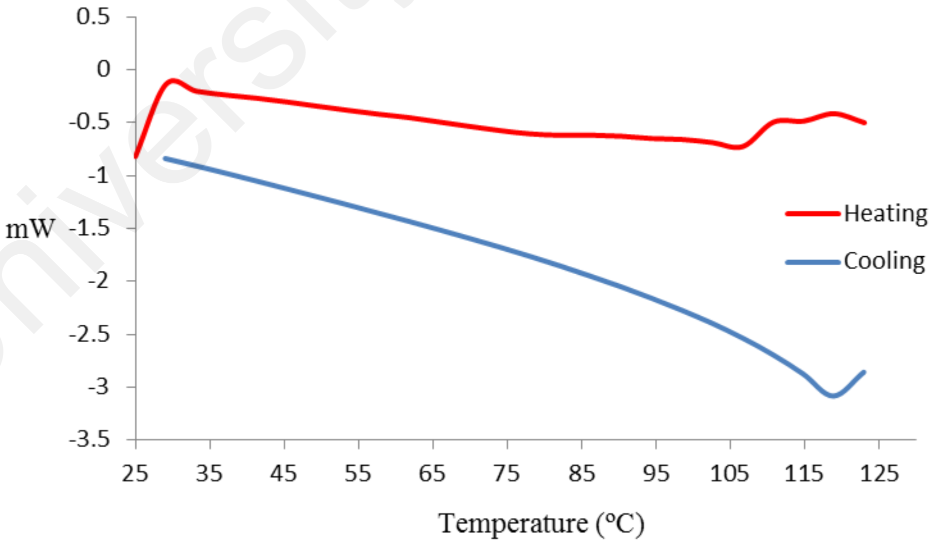

Figure 4.55 DSC scan of **6** (endothermic peaks up)

Viewed under **POM**, **6** started to clear at 115 °C, but there were no optical textures on cooling. Hence, the complex was not mesomorphic.

(d) ***Thermoelectrical property***

The S_e value was determined for a solution of **6** in DMSO in the presence of KI-KI$_3$ as the redox couple and TBATFB as the electrolyte in the temperature range of 25 °C to 70 °C for three heating-and-cooling cycles. The graphs of ΔV versus ΔT (**Figure 4.56**) was linear with positive slope from ΔT = 0 K to ΔT ~ 40 K. The mean S_e value was +0.24 ± 0.06 mV K^{-1} in this range. It is interesting to note that at higher ΔT values, the gradient was negative on heating, while on cooling the gradient was higher. The change in the gradients may be due to the change in the spin state of the complex, from HS below ΔT ~ 40 K, and LS above this ΔT (reversed SCO). Hence, the results from the thermoelectric study are in agreement with the reversed SCO behaviour observed from the variable temperature UV-vis spectroscopic study above [106].

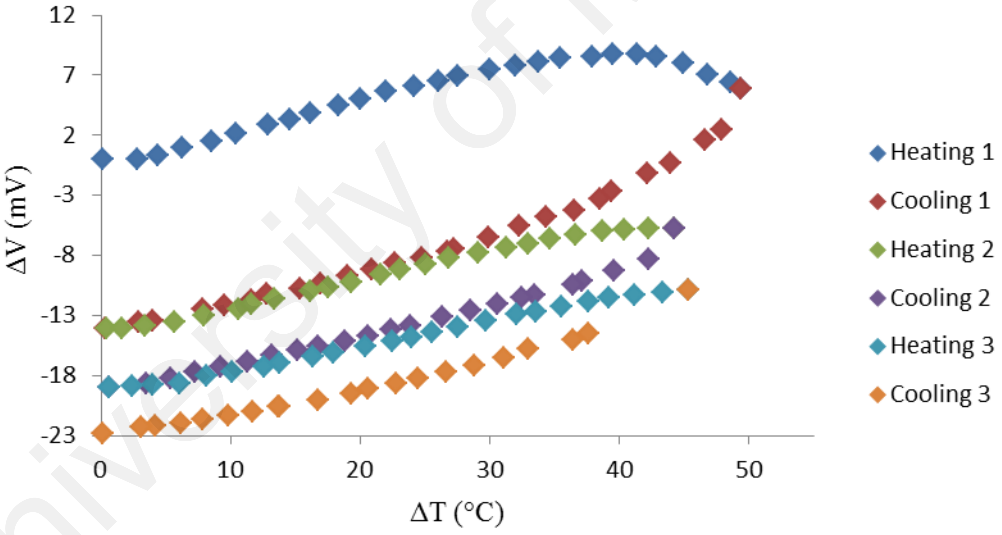

Figure 4.56 Plots of ΔV *versus* ΔT of **6**

A control experiment was similarly done for a solution of a mixture of KI-KI$_3$ and TBATFB in DMSO. The graphs of ΔV versus ΔT (**Figure 4.57**) were linear, and the value of S_e was +0.44 ± 0.02 mV K^{-1}. The value was higher than that of **6**, indicating the complex was not functioning as a thermoelectric material in DMSO.

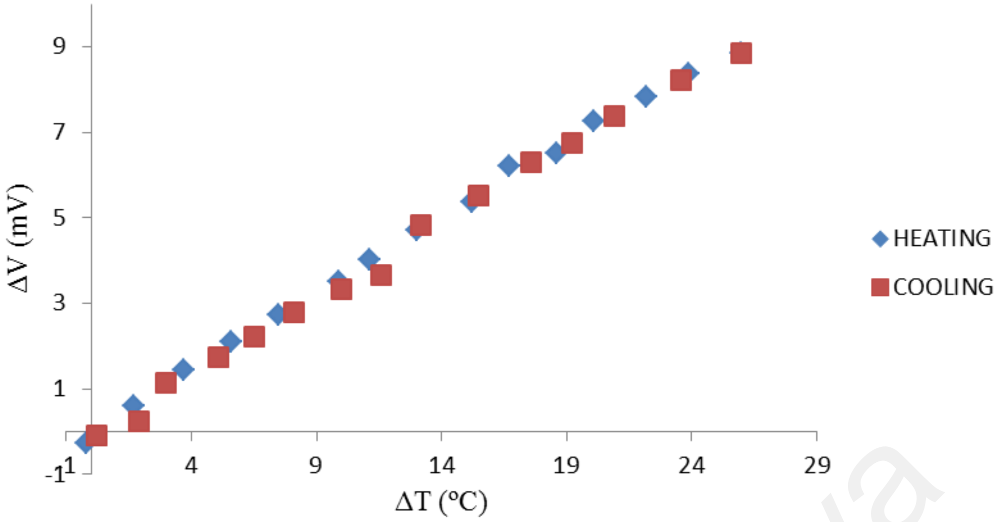

Figure 4.57 Plots of ΔV *versus* ΔT for KI-KI$_3$ and TBATFB in DMSO

4.5.2 [Co(cyclam)(L2)$_2$](C$_6$H$_5$COO)$_3$·4H$_2$O (7)

(a) ***Synthesis and structural deduction***

[Co(cyclam)(L2)$_2$](C$_6$H$_5$COO)$_3$·4H$_2$O **(7)** was obtained as a brown semi-solid from the reaction of [Co(C$_6$H$_5$COO)$_2$(cyclam)](C$_6$H$_5$COO) with L2 in a mole ratio 1:2 in CH$_3$CH$_2$OH-CHCl$_3$. The yield was 84.4%. Based on combined analytical data discussed below, the structure of **Complex 7** is proposed to be similar to **1** (**Figure 4.3**).

Its chemical formula, based on the results of elemental analyses (65.7% C; 9.5% H; 6.0% N), was in good agreement with those calculated for chemical formula $CoC_{73}H_{121}N_6O_{12}$ (65.7% C; 9.1% H; 6.3% N; formula weight, 1333.71 g mol^{-1}).

Its **FTIR** spectrum **(Figure 4.58)** shows the presence of the expected functional groups and bonds. The Δ_{COO} value was 206 cm^{-1} ($\upsilon_{asym,COO}$ = 1560 cm^{-1}; $\upsilon_{sym,COO}$ = 1354 cm^{-1}), which was similar to **Complex 7**.

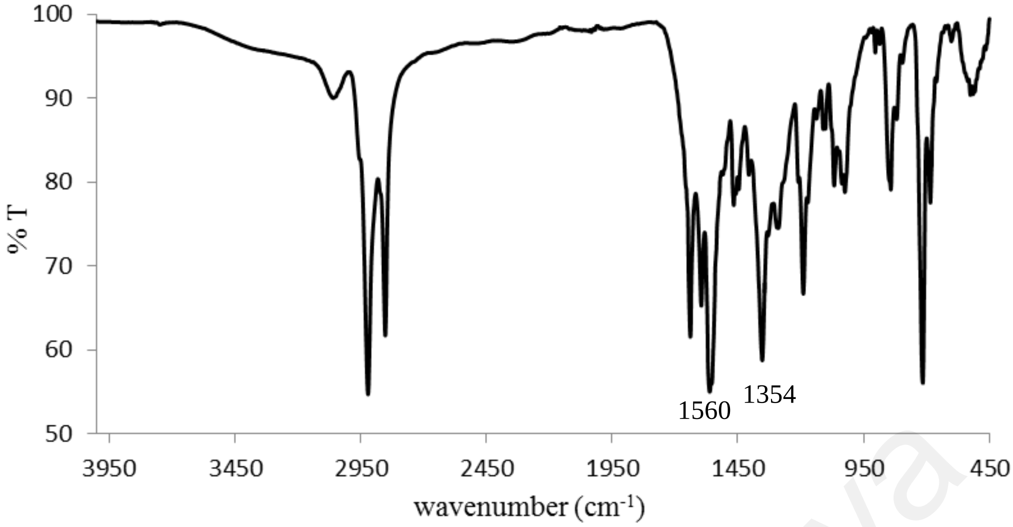

Figure 4.58 FTIR spectrum of **7**

Its **UV-vis** spectrum in CH_3OH (1.29 mmol dm^{-3}) is shown in **Figure 4.59**. It shows a continously increasing absorbance from 800 nm to a shoulder of a *d-d* band at about 550 nm (ε = 387 M^{-1} cm^{-1}) of a CT band at about 375 nm (ε = 1.6 x 10^{3} M^{-1} cm^{-1}). The *d-d* band is assigned due to the electronic transition from $^1A_{1g}$ to $^1T_{1g}$ for a LS octahedral Co(III) complex [112].

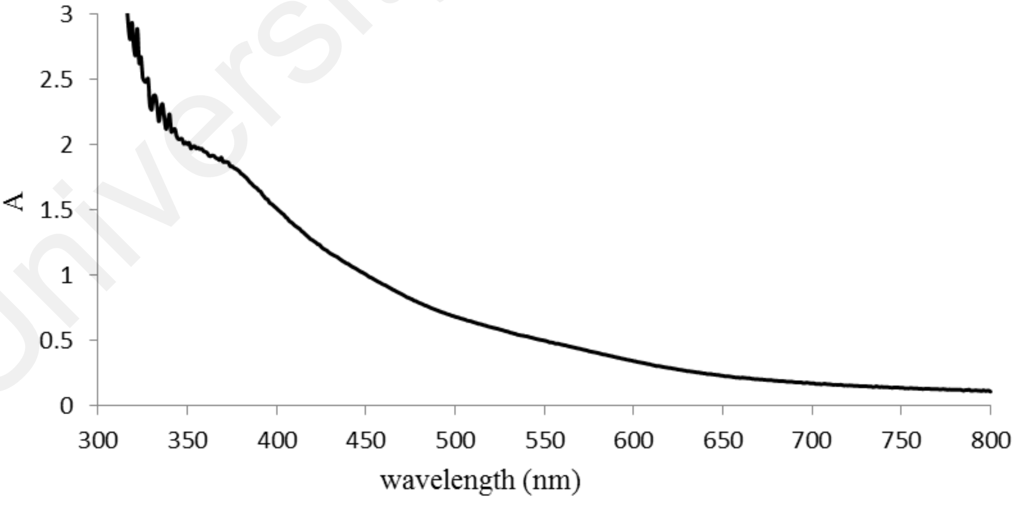

Figure 4.59 UV-Vis spectrum of **7**

Its μ_{eff} value could not be determined by the Gouy method as the complex was a semi-solid. However, its ^{1}H-NMR spectrum in CD_3OD **(Figure 4.60)** shows peaks for the organic ligands, suggesting a diamagnetic complex (3d^6; LS).

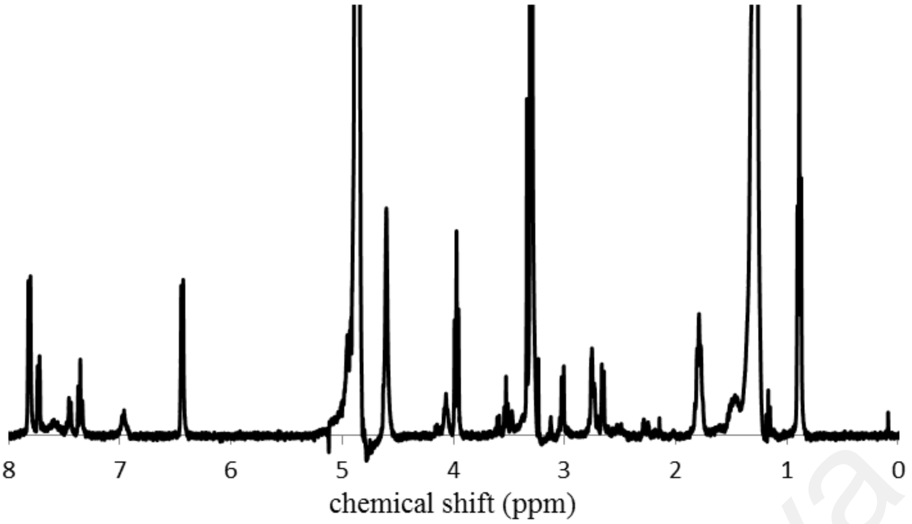

Figure 4.60^{1}H-NMR spectrum of **7**

(b) ***Spin-crossover behaviour***

The **temperature-dependence ε** was measured for a solution of **7** in DMSO at 448 nm (ε = 863 M^{-1} cm^{-1} at 25 °C, which corresponds to LS Co(III), in the temperature range of 20 °C to 70 °C (since the freezing point of DMSO is 19 ^{o}C), on two successive heating-cooling cycles. The results (**Figure 4.61)** show that on heating, the ε values remained unchanged at about 863 M^{-1} cm^{-1} from 25 °C to 30 °C, and then decreased to 645 M^{-1} cm^{-1} at about 45 ^{o}C and remained unchanged on further heating to 70 °C. Upon cooling from this temperature to 20 ^{o}C and reheating back 70 °C, the values remained almost unchanged at about 700 M^{-1} cm^{-1}. Hence, the complex showed a normal SCO behaviour in solution (LS-HS) at 30 ^{o}C on initial heating only. This is likely due to loss of H-bonded lattice H_2O, which were reported to favour a LS complex in the solid state [113].

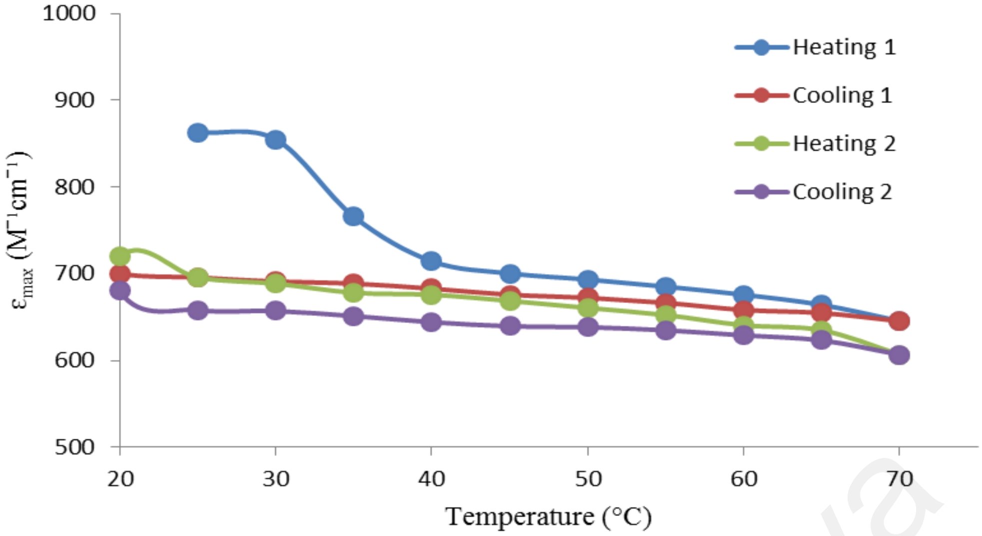

Figure 4.61 Temperature-dependent ε values for **7** at 448 nm

(c) ***Thermal and mesogenic properties***

The TG trace for **7** (**Figure 4.62**) shows an initial weight loss from 147 °C to 279 °C due to the decomposition of cyclam (found = 16.0%; calculated = 15.9%). This is followed by a major weight loss from 279 °C to 637 °C due to the decomposition of L2 and $C_6H_5COO^-$ ion (found = 77.1%; calculated = 79.5%). The amount of residue at temperatures above 637 °C was 6.9%. This correlates well with the calculated value of 6.2%, assuming pure CoO. Hence, its decomposition temperature was 147 ^{o}C.

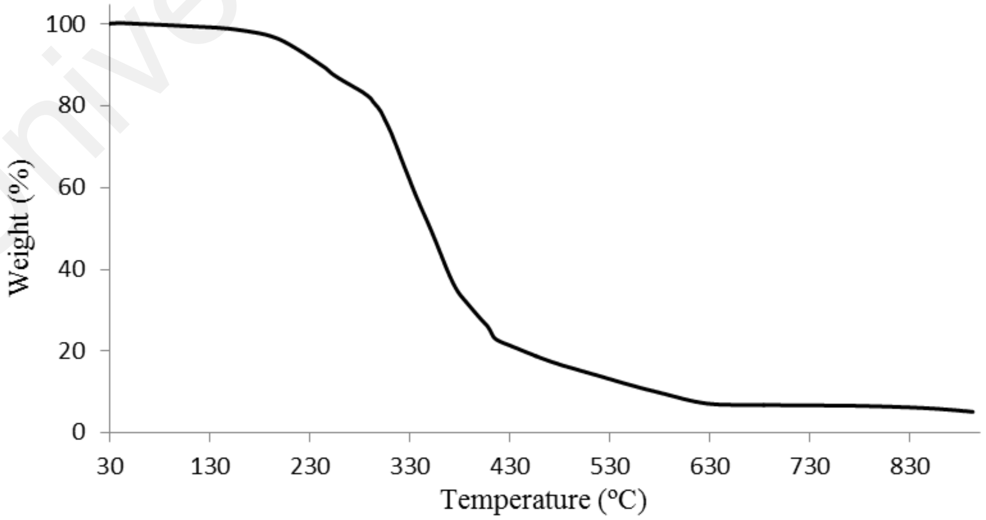

Figure 4.62 TG trace of **7**

Its DSC scans **(Figure 4.63)** were recorded for a heating–cooling cycle in the temperature range 25-120 °C. On heating, there was a strong and broad endothermic peak at 50 ^{o}C (ΔH = 93.1 kJ mol^{-1}) assigned to breaking of strong bonds, leading to initial decomposition of the complex (T$_{dec}$ = 147 ^{o}C from TGA). Hence there were no peaks from 120 ^{o}C to about 35 ^{o}C on cooling.

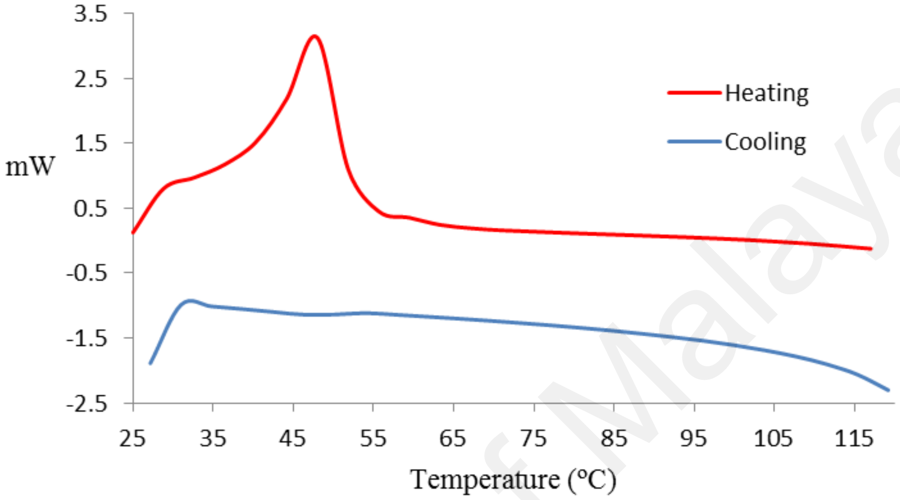

Figure 4.63 DSC of **7** (endothermic peak up)

Viewed under **POM**, **7** was observed to start clearing at 131 °C (incomplete isotropization) (**Figure 4.64(a)**), and on cooling from this temperature, an optical texture was observed at the clear region at 47 °C (**Figure 4.64(b)**), which was the same as ligand L2. Hence, the complex was not a metallomesogen.

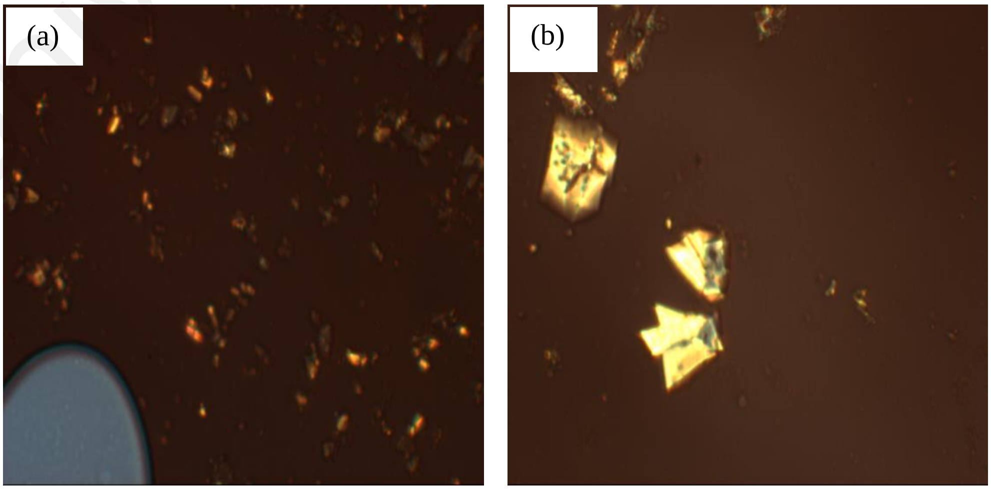

Figure 4.64 Photomicrographs of **7** on (a) heating at 131° C; and (b) cooling at 47 °C

(d) ***Thermoelectrical property***

The **Seebeck coefficients** for **7** were similarly determined as for **6**. The graphs of ΔV versus ΔT for **7** (**Figure 4.65**) was linear, and the mean S_e value was +0.33 ± 0.05 mV K^{-1}. The value was lower than that for a mixture of KI-KI_3 and TBATFB in DMSO (+0.44 ± 0.02 mV K^{-1}). Therefore, the complex was not functioning as a thermoelectric material in this solvent.

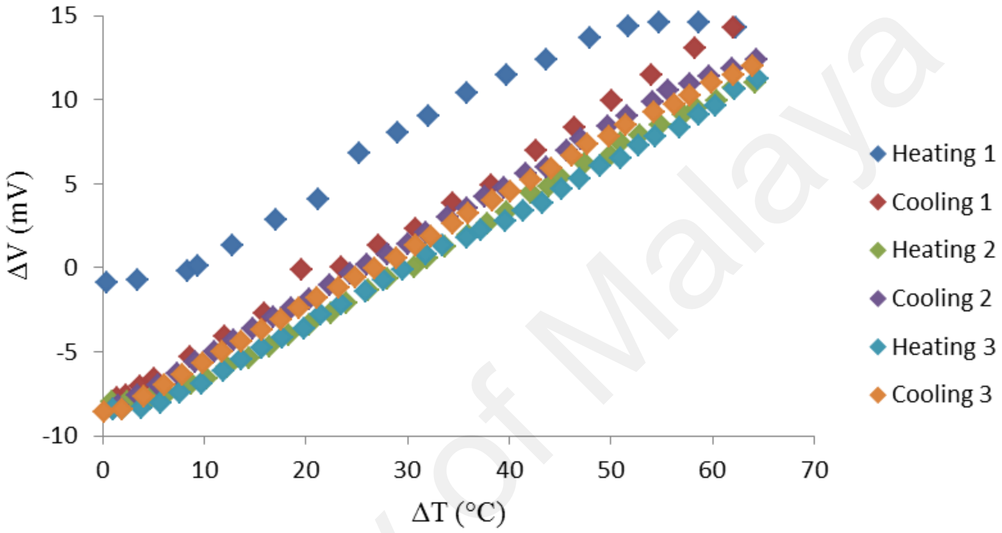

Figure 4.65 Plots of ΔV versus ΔT of **7**

4.5.3 *Summary*

The results of the analytical data for **6** and **7** are summarised in **Table 4.8**.

Table 4.8 Summary for complexes **6** and **7**

Chemical formula	Δ_{COO} (cm^{-1})	λ (nm)	Magnetism	T_{dec} (°C)	M	S_e (mV K^{-1})
[Co(cyclam)(L1)$_2$](R)$_2$·3H_2O (**6**)	207 (ionic)	654 (*)	Paramagnetic	156	No	0.24 ±0.06
[Co(cyclam)(L2)$_2$](R)$_3$·4H_2O (**7**)	206 (ionic)	555 (*)	Diamagnetic (LS)	147	No	0.33 (±0.05)

R = C_6H_5COO ; * = octahedral; M = mesomorphic

Both complexes were mononuclear with octahedral Co(II) atoms, ionic and have similar structural formulae. However, **6** was a paramagnetic Co(II) complex, while **7** was a diamagnetic LS Co(III) complex. Both complexes have similar thermal stability, were not mesomorphic, and did not function as thermoelectric materials in DMSO.

4.6 Complexes of Iron

4.6.1 [Fe(cyclam)(L1)$_2$](C$_6$H$_5$COO)$_2$$\cdot$2H$_2$O (8)

(a) *Synthesis and structural deduction*

[Fe(cyclam)(L1)$_2$](C$_6$H$_5$COO)$_2$.2H$_2$O (**8**) was prepared by the steps as shown in **Scheme 4.3**.

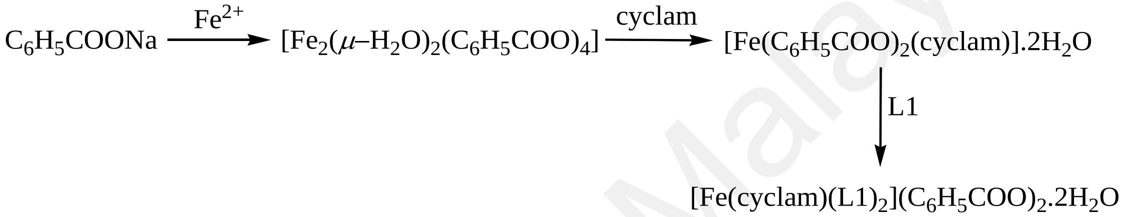

$$\begin{array}{r} C_6H_5COONa \xrightarrow{Fe^{2+}} [Fe_2(\mu\text{–}H_2O)_2(C_6H_5COO)_4] \xrightarrow{\text{cyclam}} [Fe(C_6H_5COO)_2(\text{cyclam})].2H_2O \\ \downarrow \text{L1} \quad\quad\quad\quad \\ [Fe(\text{cyclam})(L1)_2](C_6H_5COO)_2.2H_2O \end{array}$$

Scheme 4.3 Synthetic steps for [Fe(cyclam)(L1)$_2$](C$_6$H$_5$COO)$_2$$\cdot$2H$_2$O (**8**)

In the first step, C$_6$H$_5$COONa reacted with FeSO$_4$$\cdot$7H$_2$O in CH$_3CH_2$OH to form [Fe$_2$($\mu$-H$_2$O)$_2$(C$_6H_5$COO)$_4$] (brown powder). Its structural formula (**Figure 4.66**) was proposed based on combined instrumental data discussed below.

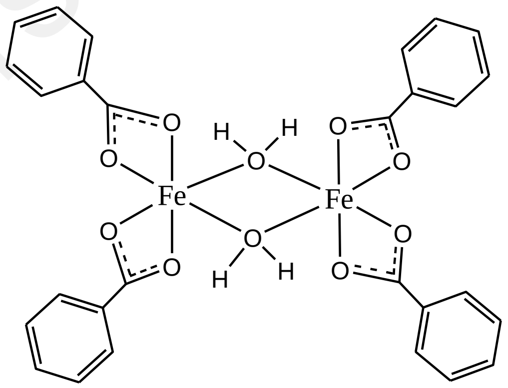

Figure 4.66 Proposed structure for [Fe$_2$(μ-H$_2$O)$_2$(C$_6$H$_5$COO)$_4$]

The results of its **elemental analyses** (52.6% C; 3.5% H) were in good agreement with those calculated for the chemical formula C$_{28}$H$_{24}$Fe$_2$O$_{10}$ (53.2% C; 3.8% H; formula weight, 632.2 g mol^{-1}). From its FTIR spectrum (**Figure 4.67**), the Δ_{COO}

value was 117 cm^{-1} ($\upsilon_{as,COO}$ = 1517 cm^{-1}; $\upsilon_{s,COO}$ = 1399 cm^{-1}), suggesting chelating binding mode for $C_6H_5COO^-$ ion.

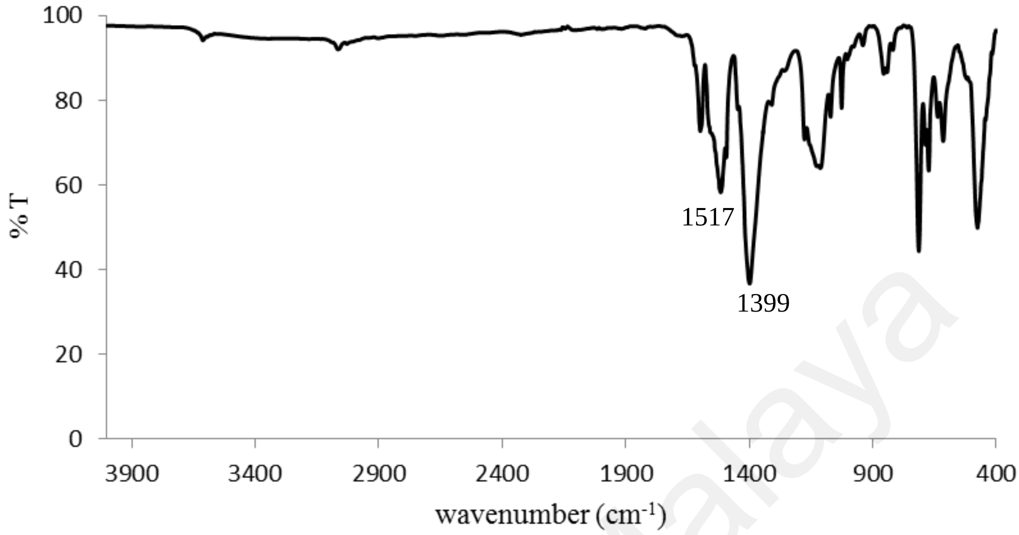

Figure 4.67 FTIR spectrum of $[Fe_2(\mu\text{-}H_2O)_2(C_6H_5COO)_4]$

Its **UV-vis** spectrum in DMSO (11.39 mmol dm^{-3}) is shown in **Figure 4.68**. It shows a *d-d* band appearing as a weak shoulder at 341 nm (ε = 140 M^{-1} cm^{-1}).

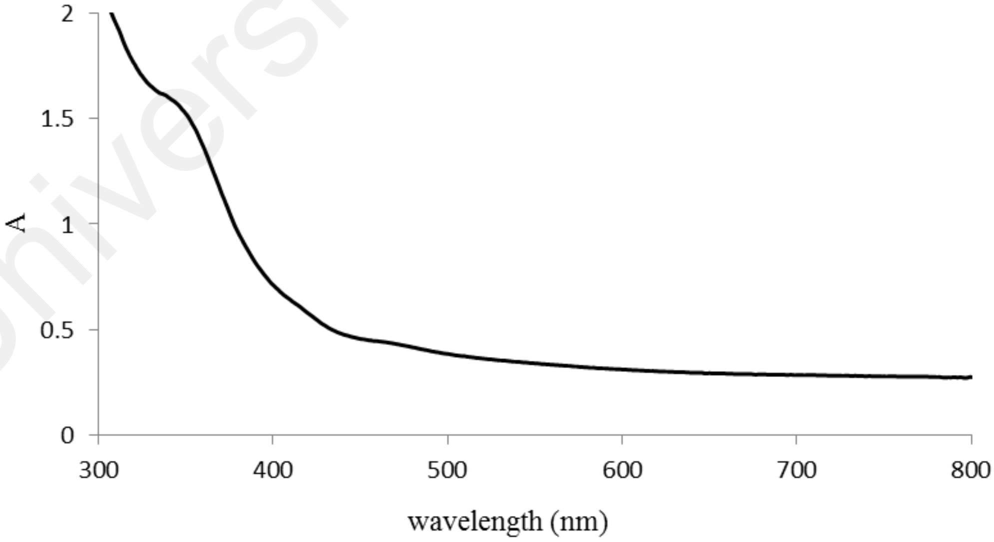

Figure 4.68 UV-vis spectrum of $[Fe_2(\mu\text{-}H_2O)_2(C_6H_5COO)_4]$

The value of μ_{eff}, calculated as before from the values of FM = 632.2 g mol^{-1}, χ_g = 2.38 x 10^{-5} cm^3 g^{-1}, χ_M = 1.51 x 10^{-2} cm^3 mol^{-1}, and χ_{dia} = -3.16 x 10^{-4} cm^3 mol^{-1}, was

6.1 BM at 298 K. The value was as expected for a dinuclear octahedral complex with HS Fe(II) atoms (6.9 BM).

$[Fe_2(\mu\text{-}H_2O)_2(C_6H_5COO)_4]$ reacted with cyclam in CH_3CH_2OH to form a brown semi-solid, $[Fe(C_6H_5COO)_2(cyclam)]\cdot 2H_2O$. Its structure is proposed to be similar to $[Ni(C_6H_5COO)_2(cyclam)]$ (**Figure 4.28**).

The results of its **elemental analyses** (53.3% C; 6.9% H; 9.8% N) were in good agreement with those calculated for the chemical formula $C_{24}H_{38}FeN_4O_6$ (53.9% C; 7.2% H; 10.5% N; formula weight, 534.4 g mol^{-1}). From its FTIR spectrum (**Figure 4.70**), the Δ_{COO} value was 184 cm^{-1} ($\upsilon_{asym,COO}$ = 1547 cm^{-1}; $\upsilon_{sym,COO}$ = 1363 cm^{-1}), suggesting monodentate binding mode for $C_6H_5COO^-$ ion.

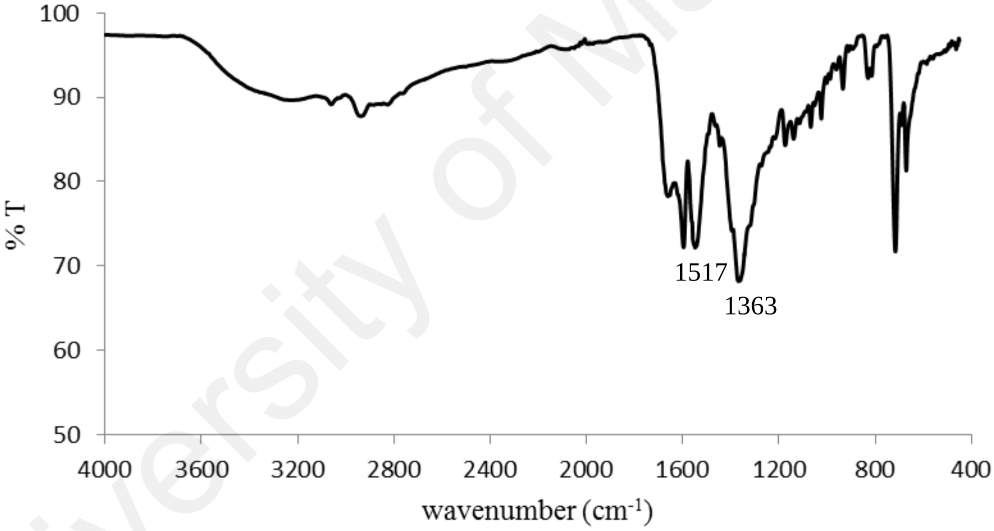

Figure 4.69 FTIR spectrum of $[Fe(C_6H_5COO)_2(cyclam)]\cdot 2H_2O$

$[Fe(C_6H_5COO)_2(cyclam)]\cdot 2H_2O$ reacted with L1 (mole ratio 1:2) in CH_3CH_2OH-$CHCl_3$ to form $[Fe(cyclam)(L1)_2](C_6H_5COO)_2\cdot 2H_2O$ (**8**), obtained as a brown semi-solid and the yield was 74.2%. Based on combined analytical data discussed below, it is proposed that its structure was similar to **1** (**Figure 4.3**).

The results of elemental analyses (66.2% C; 9.8% H; 7.0% N) were in good agreement with those calculated for the chemical formula $C_{62}H_{104}FeN_6O_8$ (66.6% C; 9.4% H; 7.5% N; formula weight, 1117.4 g mol^{-1}).

Its FTIR spectrum **(Figure 4.70)** shows the presence of the expected functional groups and bonds as previously discussed. The Δ_{COO} value was 179 cm^{-1} ($\upsilon_{asym,COO}$ = 1551 cm^{-1}; $\upsilon_{sym,COO}$ = 1372 cm^{-1}), indicating free $C_6H_5COO^-$ ion.

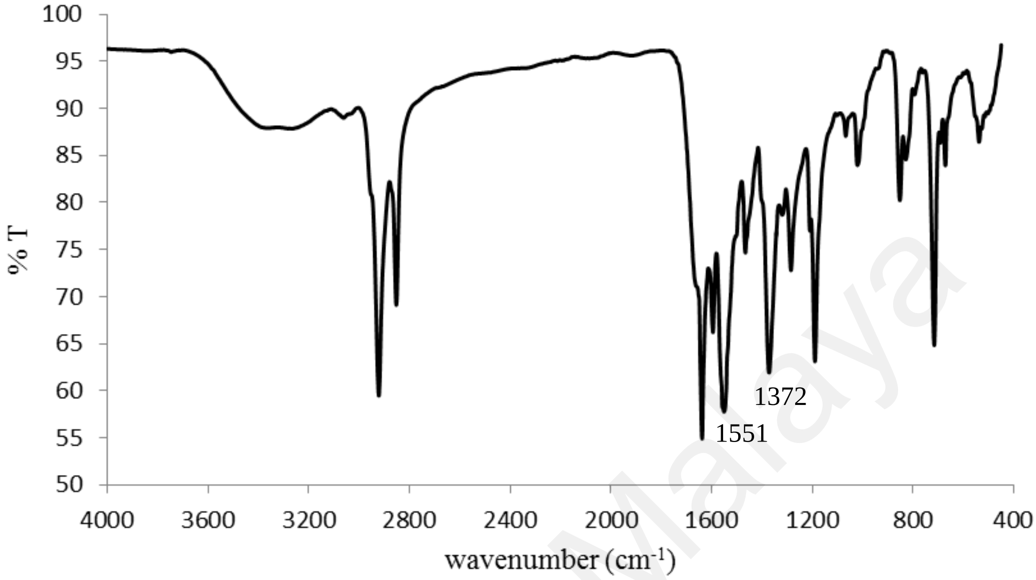

Figure 4.70 FTIR spectrum of **8**

Its **UV-vis** spectrum in CH_3OH (0.89 mmol dm^{-3}) is shown in **Figure 4.71**. It shows a continuously increasing absorbance from about 700 nm to a shoulder at 454 nm (ε = 479.4 M^{-1} cm^{-1}). These *d-d* bands are assigned to overlapping electronic transitions from $^1A_{1g}$ to $^1T_{1g}$ and $^1T_{2g}$ for an octahedral complex with LS Fe(II) atom.

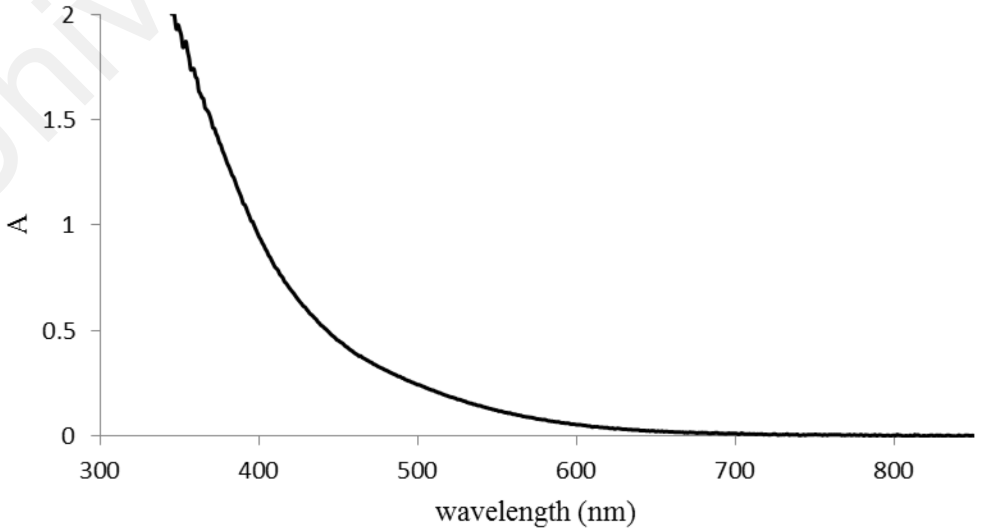

Figure 4.71 UV-vis spectrum of **8**

μ_{eff} value could not be determined by the Gouy method as the complex was a semi-solid. However, its ^{1}H-NMR spectrum in CD_3OD **(Figure 4.72)** shows peaks for the organic ligands, suggesting a diamagnetic Fe(II) complex (3d^6; LS)).

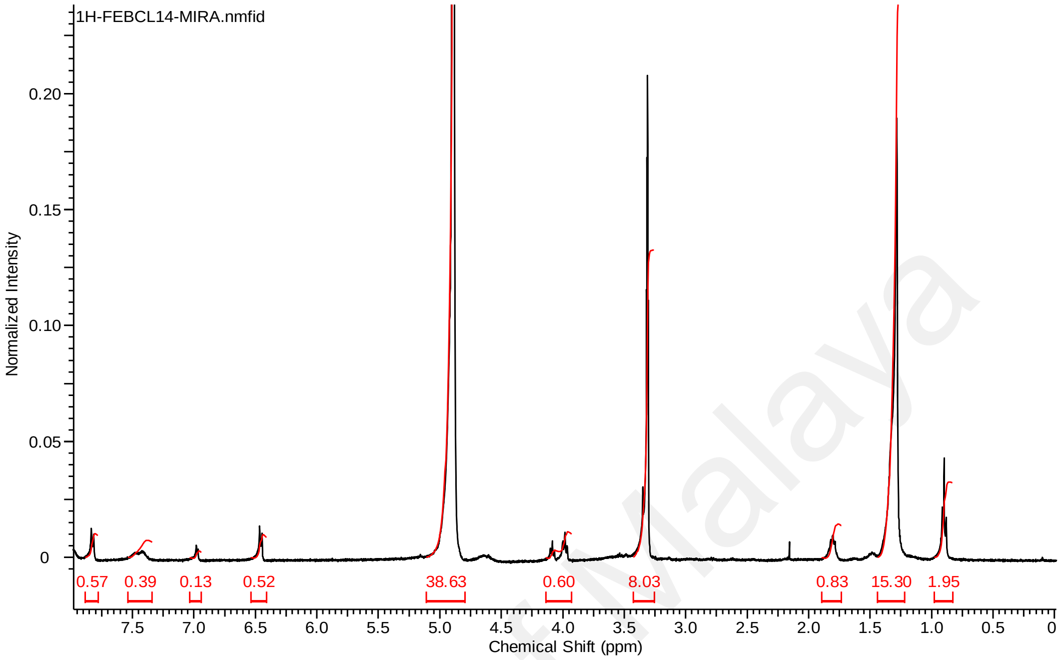

Figure 4.72 ^{1}H-NMR spectrum of **8**

(b) ***Spin-crossover behaviour***

The temperature dependence ε for **8** was measured for a solution in DMSO at 504 nm (ε = 595 M^{-1} cm^{-1}), which corresponds to LS Fe(II), in the temperature range of 20 °C to 70 °C on two successive heating-cooling cycles. The results are shown in **Figure 4.73**. On initial heating, the ε values gradually decreased to about 565 M^{-1} cm^{-1} at 70 °C. On cooling from this temperature to 20 °C, the values remained unchanged at about 568 M^{-1} cm^{-1}. On reheating, the value decreased abruptly to 540 M^{-1} cm^{-1} at 25 °C, then increased abruptly to about 568 M^{-1} cm^{-1} at 30 °C, and then decreased gradually to about 555 M^{-1} cm^{-1} at 70 °C. On cooling again from this temperature, the values gradually increased to about 573 M^{-1} cm^{-1} at 20 °C. From these results, it may be inferred that the complex showed normal SCO behaviour (LS-HS transition on heating) in solution in the first heating-cooling cycle, and re-entrant behaviour (LS-HS-LS transition) at 30 °C on reheating.

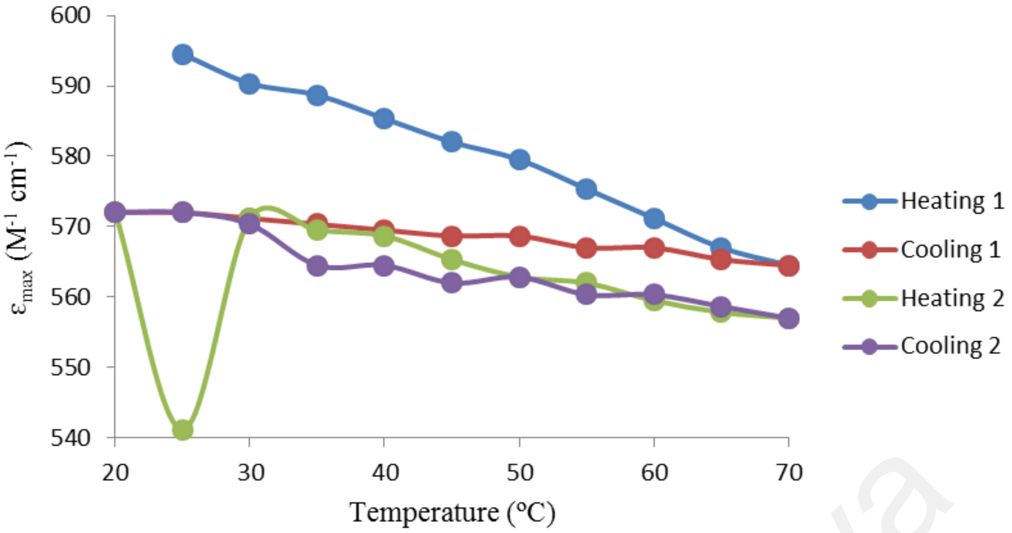

Figure 4.73 Temperature-dependent ε values for **8** at 504 nm

(c) ***Thermal and mesogenic properties***

Its **TG** trace (**Figure 4.74**) shows an initial weight loss from 56 °C to 150 °C due to evaporation of lattice H_2O molecules at (found = 4.0%; calculated = 3.2%). The next weight loss from 150 °C to 472 °C was due to the decomposition of L1 and $C_6H_5COO^-$ ion (found = 74.4%; calculated = 73.9%). Finally, the weight loss from 472 °C to 693 °C was due to the decomposition of cyclam (found = 18.0%; calculated = 17.9%). The amount of residue at temperatures above 693 °C was 3.6%. This correlates well with the calculated value of 5.0%, assuming that it is made up of pure Fe. Hence, its decomposition temperature was 150 °C.

Its **DSC** scans **(Figure 4.75)** were recorded in a heating–cooling cycle within the temperature range -50 – 110 °C. It shows broad and overlapping endothermic peaks at onset -33.3 °C (ΔH ~ +12 kJ mol^{-1}) and another endothermic peak at 29.1 °C (ΔH = +31.2 kJ mol^{-1}) on heating assigned to crystal-to-crystal transition and its melting temperature, respectively. On cooling, there were two exothermic peaks at -1.4 °C (ΔH ~ -0.9 kJ mol^{-1}) and -13.2 °C (ΔH = -7.4 kJ mol^{-1}), indicating formation of weak intermolecular forces.

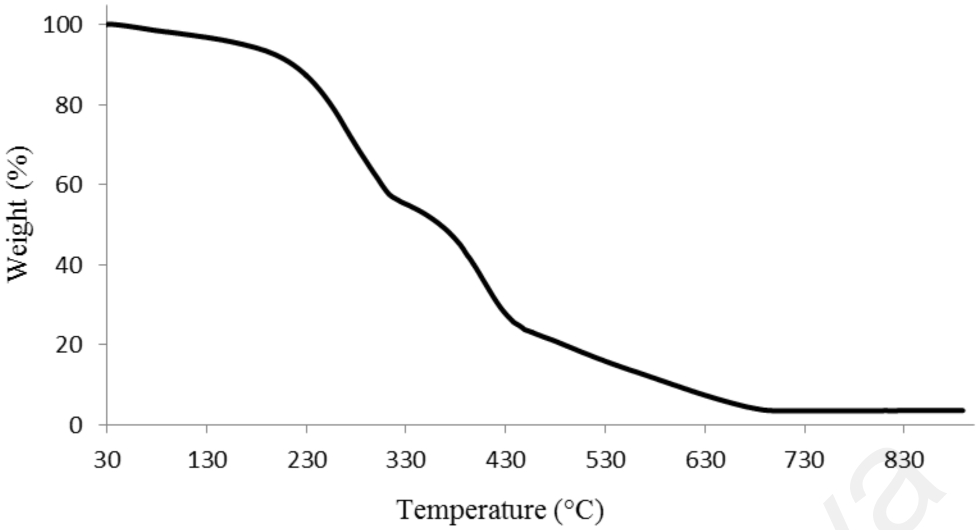

Figure 4.74 TG trace of **8**

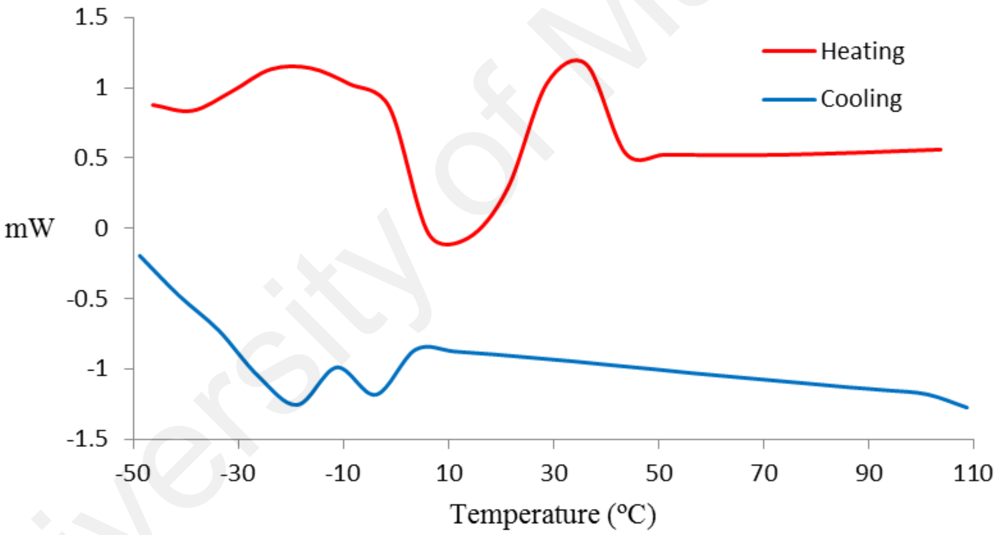

Figure 4.75 DSC of **8** (endothermic peaks up)

Viewed under **POM**, the complex was fluidic at room temperature with no optical texture (**Figure 4.76(a)**). However, its colour darkens on heating to 68 °C (**Figure 4.76(b))** indicating a change in the spin state of Fe(II) from HS to LS [8]. On cooling from this temperature, there was no an optical texture. Hence, the complex was not mesomorphic.

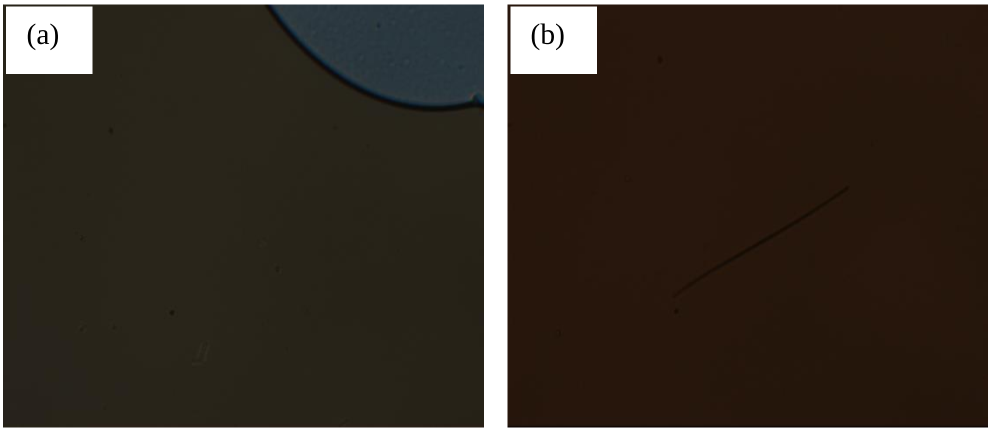

Figure 4.76 Photomicrographs of **8** on (a) room temperature, (b) heating at 68 °C

(d) *Thermoelectrical property*

The **Seebeck coefficients** were determined for a solution of **8** in methoxypropanonitrile (MPN) in the temperature range of 25 °C to 90 °C for two heating-cooling cycles. The graphs of ΔV versus ΔT (**Figure 4.77**) were linear with positive slopes, and the mean S_e value was +0.33 ± 0.03 mV K^{-1}.

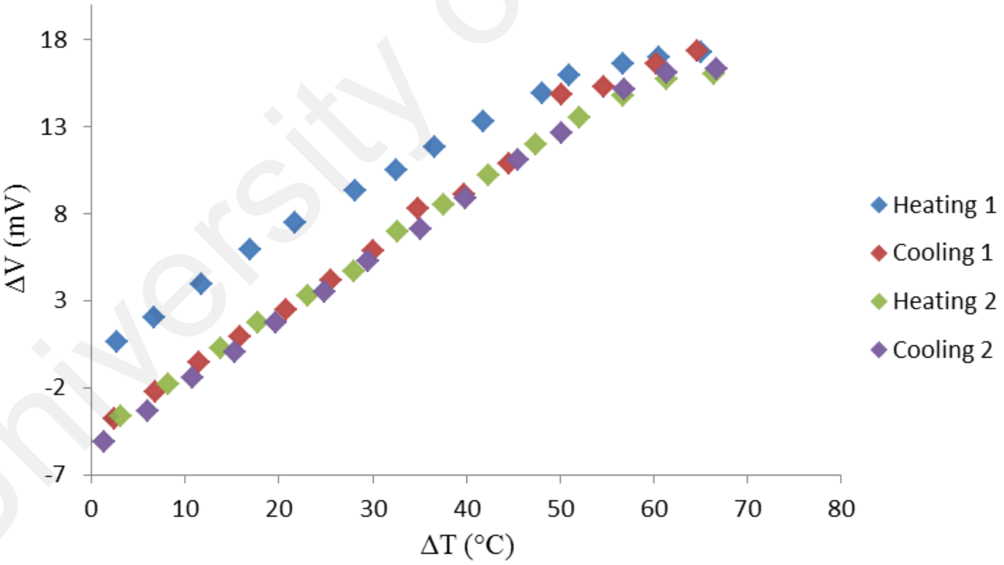

Figure 4.77 Plots of ΔV *versus* ΔT of **8**

A control Seebeck experiment was performed a solution of a mixture of KI-KI_3 and TBATFB in methoxypropionitrile (MPN). The graphs of ΔV *versus* ΔT are shown in **Figure 4.78**. The mean S_e value was +0.25 ± 0.04 mV K^{-1}, which was lower than that for **8**. Therefore, **8** was functioning as a thermoelectric material in MPN.

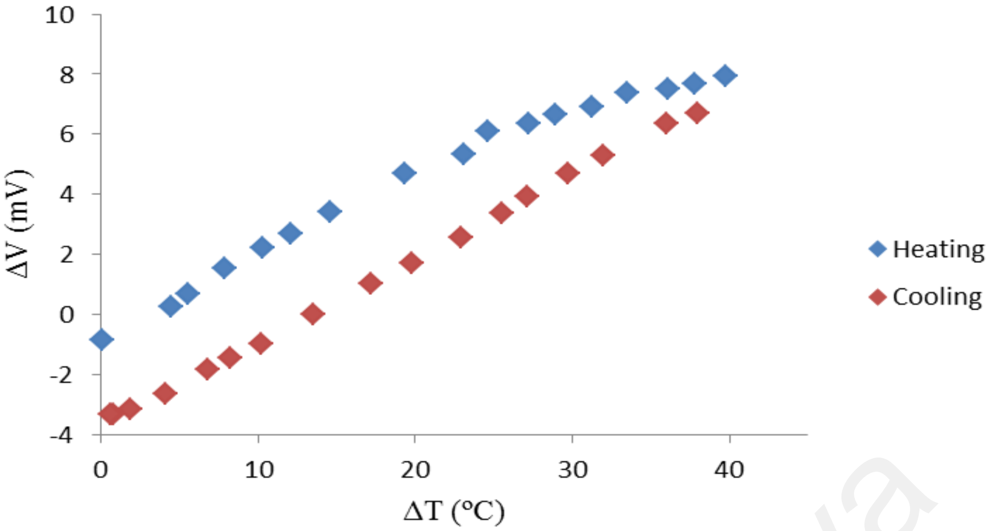

Figure 4.78 Plots of ΔV *versus* ΔT for a solution of a mixture of KI-KI_3 and TBATFB in MPN

4.6.2 [Fe(cyclam)(L2)$_2$](C_6H_5COO)$_3$]·4H_2O (9)

(a) ***Synthesis and structural deduction***

[Fe(cyclam)(C_6H_5COO)$_2$].2H_2O reacted with L2 in a mole ratio 1:2 in CH_3CH_2OH-$CHCl_3$ to form a brown semi-solid. Its structural formula, similarly deduced as previously done, and discussed below, was [Fe(cyclam)(L2)$_2$](C_6H_5COO)$_3$]·4H_2O (**9**), and its yield was 61.7%. Hence, its structure was similar to **1** (**Figure 4.3**).

The results of its **elemental analyses** (65.3% C; 10.0% H; 6.0% N) were in good agreement with those calculated for $C_{73}H_{121}FeN_6O_{12}$ (65.9% C; 9.2% H; 6.3% N; formula weight, 1330.6 g mol^{-1}).

Its **FTIR** spectrum **(Figure 4.79)** shows the presence of the expected functional groups and bonds as previously discussed. The Δ_{COO} value was 147 cm^{-1} ($\upsilon_{asym,COO}$ = 1536 cm^{-1}; $\upsilon_{sym,COO}$ = 1389 cm^{-1}), suggesting ionic (non-coordinated) $C_6H_5COO^-$ ion.

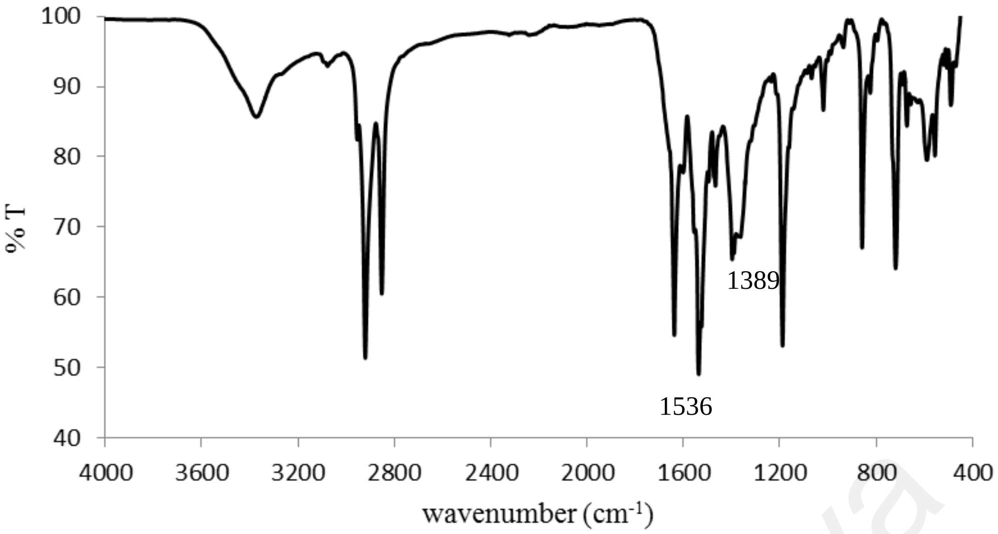

Figure 4.79 FTIR spectrum of **9**

Its **UV-vis** spectrum in MPN (0.59 mmol dm^{-3}) is shown in **Figure 4.80**. It shows a continuously increasing absorbance from about 700 nm to a shoulder at 447 nm (ε = 764 M^{-1} cm^{-1}). These suggest overlapping electronic transitions from $^2T_{2g}$ to $^2A_{2g}$, $^2T_{1g}$, and ^2E_g for an octahedral LS Fe(III) complex.

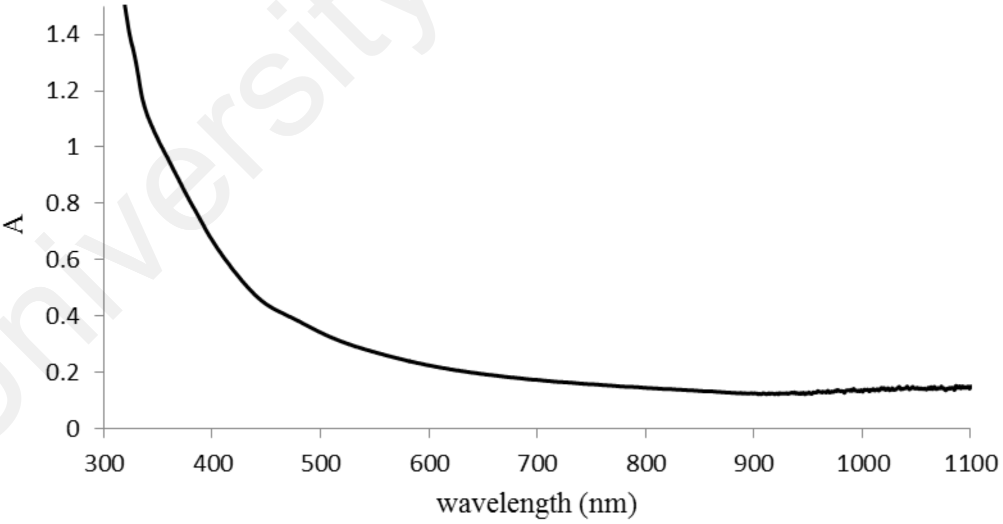

Figure 4.80 UV-Vis spectrum of **9**

Its μ_{eff} value could not be determined by the Gouy method as the complex was a semi-solid. However, its **^{1}H-NMR** spectrum in CD_3OD **(Figure 4.81)** shows several broad peaks, indicating a paramagnetic complex.

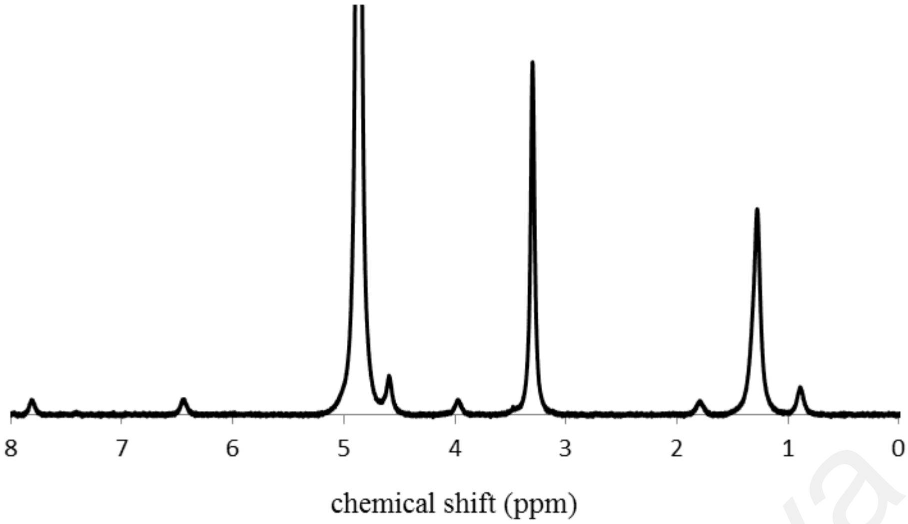

Figure 4.81^{1}H-NMR spectrum of **9**

(b) *Spin-crossover behaviour*

Its **temperature-dependence ε_{max}** was measured for a solution of **9** in MPN at 447 nm (ε = 764 M^{-1} cm^{-1}), which corresponds to LS Fe(III), in the temperature range of 15 °C to 70 °C for two successive heating-cooling cycles (**Figure 4.82**). On heating, the ε values gradually decreased to 528 M^{-1} cm^{-1} at 70 °C. On cooling from this temperature, the values gradually decreased to 471 M^{-1} cm^{-1} at 25 °C, and then remained constant at about 486 M^{-1} cm^{-1} from 20 °C to 15 °C. On reheating from this temperature, the value abruptly increased to 840 M^{-1} cm^{-1} at 20 °C, then decreased abruptly to 459 M^{-1} cm^{-1} at 25 °C, and then the values gradually decreased to 388 M^{-1} cm^{-1} at 70 °C. On cooling from this temperature, the ε values remained unchanged. It may be inferred that **9** exhibits normal SCO behaviour (LS-HS) on heating, reverse SCO (LS-HS) on cooling in solution and re-entrant behaviour (HS-LS-HS transition) at 25 ^{o}C on reheating.

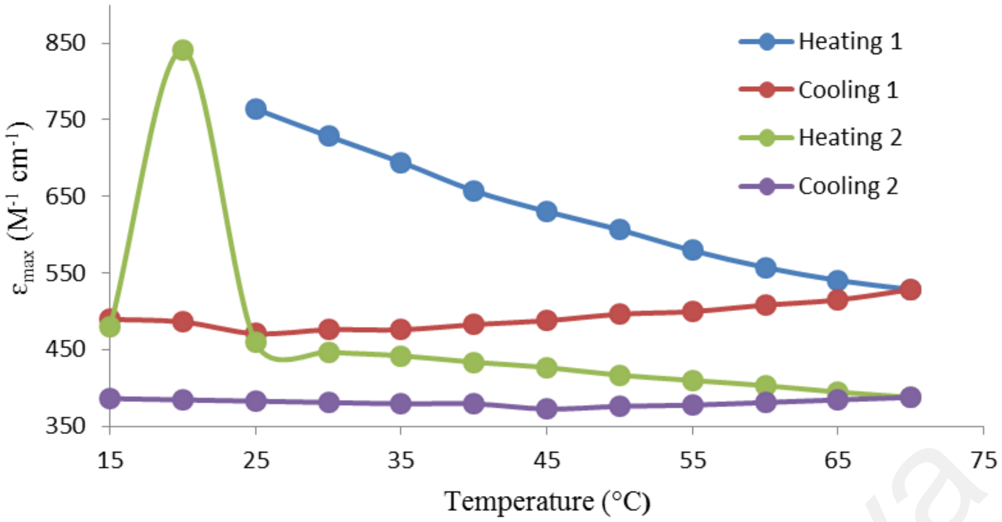

Figure 4.82 Temperature-dependentce ε values for **9** at 447 nm

(c) ***Thermal and mesogenic properties***

Its **TG** trace (**Figure 4.83**) shows an initial weight loss from 52 °C to about 144 °C due to evaporation of four lattice H_2O molecules at (found = 3.7%; calculated = 4.1%). The next weight loss from 144 °C to about 607 °C due to the decomposition of cyclam, L2, and $C_6H_5COO^-$ ion (found = 89.8%; calculated = 90.0%). The amount of residue at temperature above 607 °C was 6.5%, which was in agreement with the calculated value of 6.0%, assuming pure FeO_2.

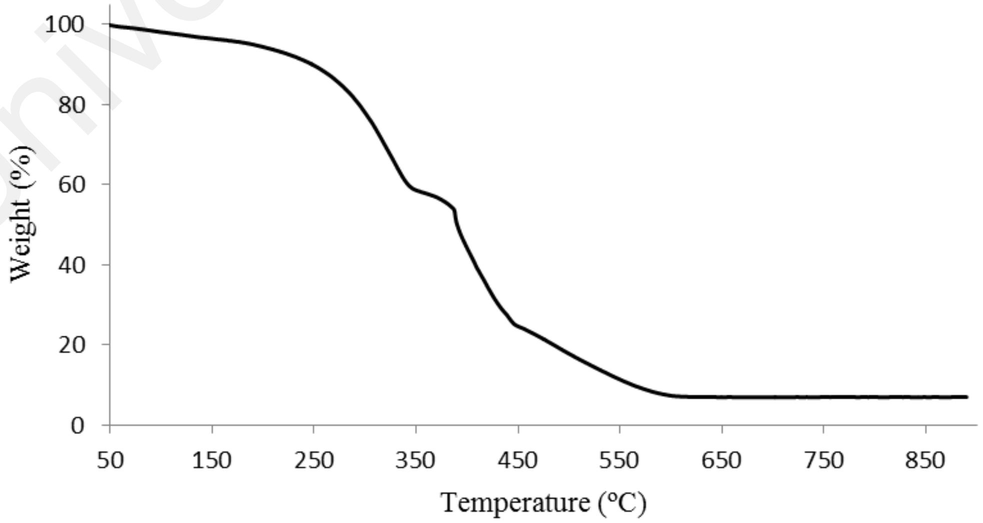

Figure 4.83 TG trace of **9**

Its **DSC** scan **(Figure 4.84)** was recorded in a heating–cooling cycle in the temperature range 25-125 °C. On heating, there was a strong endothermic peak at 44.5 ^{o}C (ΔH = +112.6 kJ mol^{-1}) assigned to its melting temperature. On cooling, there was a weak exothermic peak at 55.0 ^{o}C (ΔH = -2.0 kJ mol^{-1}) assigned to the isotropic-to-mesophase transition.

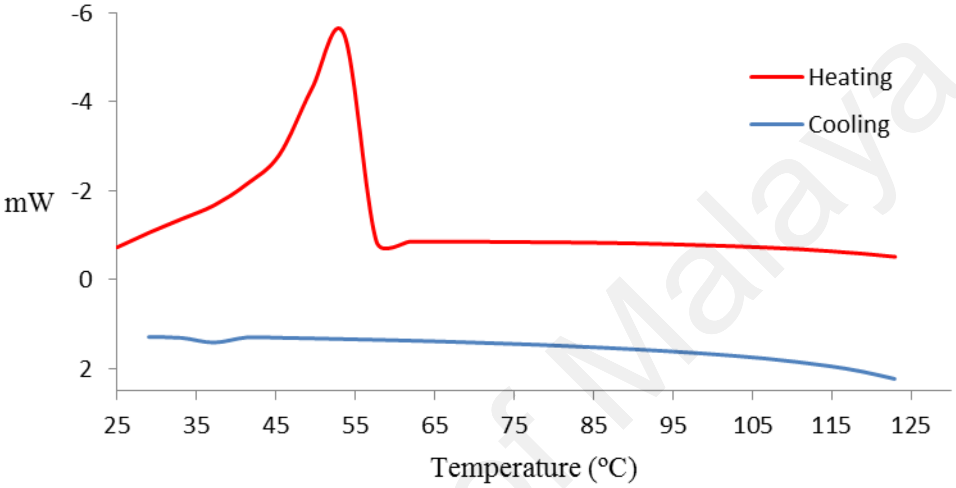

Figure 4.84 DSC of **9** (endothermic peak up)

Viewed under **POM**, **9** was fluidic at 54 °C (**Figure 4.85(a)**), and cleared at 70 ^{o}C. On cooling from this temperature, optical textures were observed at 30 ^{o}C (**Figure 4.85**(**b**)). Hence, the complex was mesomorphic.

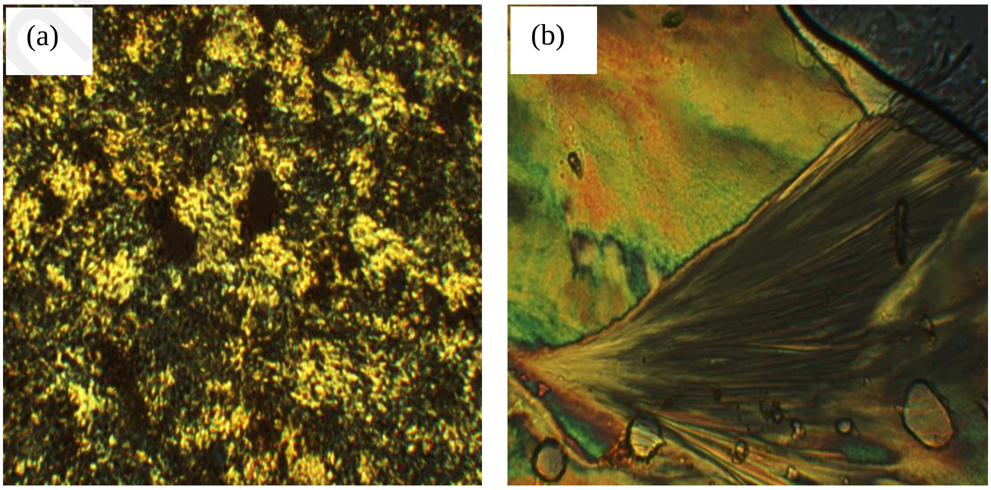

Figure 4.85 Photomicrographs of **9** on: (a) heating at 54 °C, and cooling at 30 °C

(d) ***Thermoelectrical property***

The S_e value was determined for a solution of **9** in MPN in the temperature range of 25 °C to 90 °C on a heating-cooling cycle. The graph of ΔV versus ΔT (**Figure 4.86**) was linear in the ΔT range of 15 °C to 45 °C with negative slopes. The mean S_e value was -0.8 ± 0.3 mV K^{-1}. Comparing this value with that of a mixture of KI-KI_3 and TBATFB in MPN (+0.25 ± 0.04 mV K^{-1}), it may inferred that the complex was functioning as a thermoelectric material in this solvent.

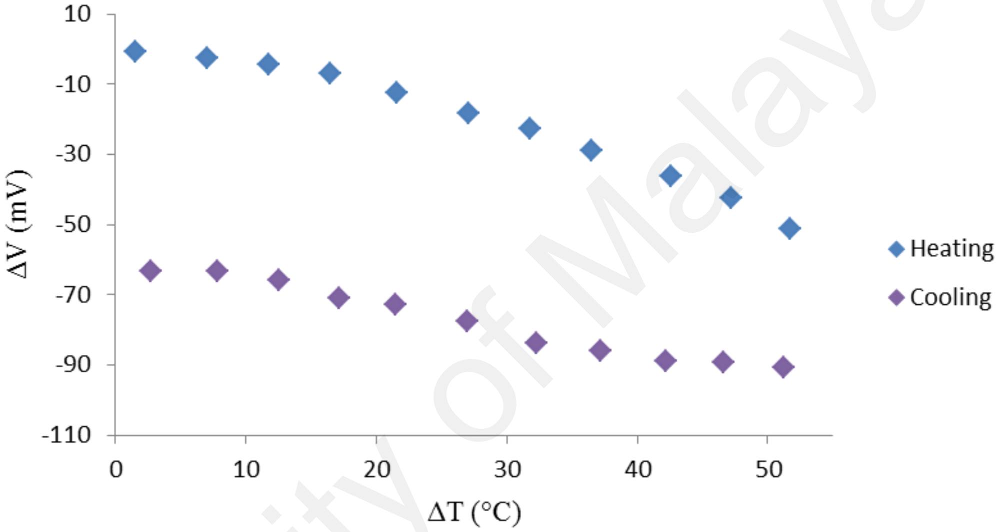

Figure 4.86. Plots of ΔV versus ΔT of **10**

4.6.3 *Summary*

The results of the analytical data for **8** and **9** are summarised in **Table 4.9**.

Table 4.9 Summary for complexes **8** and **9**

Chemical formula	Δ_{COO} (cm^{-1})	λ (nm)	Magnetism	T_{dec} (°C)	M	S_e ($mV\ K^{-1}$)
$[Fe(cyclam)(L1)_2](R)_2 \cdot 2H_2O$ (**8**)	179 (ionic)	454 (*)	Diamagnetic (LS)	150	No	0.33±0.03
$[Fe(cyclam)(L2)_2](R)_3 \cdot 4H_2O$ (**9**)	146 (ionic)	447 (*)	Paramagnetic (LS)	144	Yes	-0.8±0.3

R = C_6H_5COO; * = octahedral; M = mesomorphic

Both complexes were mononuclear, ionic and have similar structural formulae. However, **8** was a diamagnetic Fe(II) octahedral complex, while **9** was a paramagnetic LS Fe(III) octahedral complex. Both complexes have similar thermal stability, and were functioning as thermoelectric materials in MPN, but only **9** was mesomorphic.

4.7 Complexes of Manganese

4.7.1 [Mn(cyclam)(L1)$_2$]($C_6H_5COO)_2\cdot 4H_2O$ (11)

(a) *Synthesis and structural deduction*

[Mn(cyclam)(L1)$_2$]($C_6H_5COO)_2\cdot 4H_2O$ (**10**) was prepared by the steps as shown in **Scheme 4.4**.

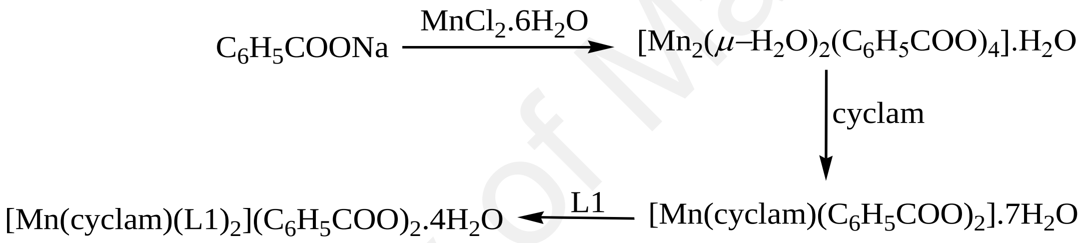

Scheme 4.4 Synthetic steps for [Mn(cyclam)(L1)$_2$]($C_6H_5COO)_2\cdot 4H_2O$ (**10**)

In the first step, C_6H_5COONa reacted with $MnCl_2\cdot 6H_2O$ in CH_3CH_2OH to form $[Mn_2(\mu\text{-}H_2O)_2(C_6H_5COO)_4]\cdot H_2O$ (white powder). Its structural formula (**Figure 4.87**) was proposed based on combined instrumental data discussed below.

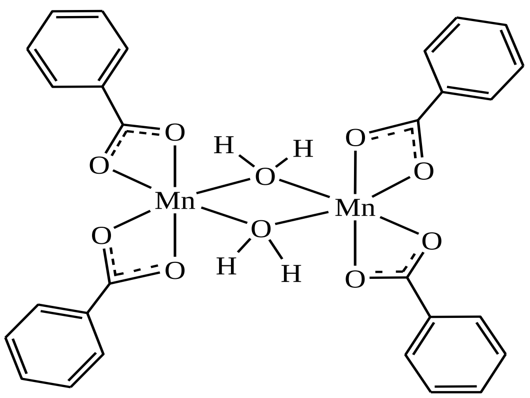

Figure 4.87 Proposed structure for $[Mn_2(\mu\text{-}H_2O)_2(C_6H_5COO)_4]\cdot H_2O$

The results of its **elemental analyses** (51.9% C; 4.5% H) were in good agreement with those calculated for the chemical formula $C_{28}H_{26}Mn_2O_{11}$ (51.8% C; 4.0% H; formula weight, 648.4 g mol^{-1}).

Its FTIR spectrum (**Figure 4.88**) shows the presence of the expected functional groups and bonds. The Δ_{COO} value were 146 cm^{-1} ($\upsilon_{asym,COO}$ = 1530 cm^{-1}; $\upsilon_{sym,COO}$ = 1385 cm^{-1}), suggesting chelating binding mode for $C_6H_5COO^-$ ion.

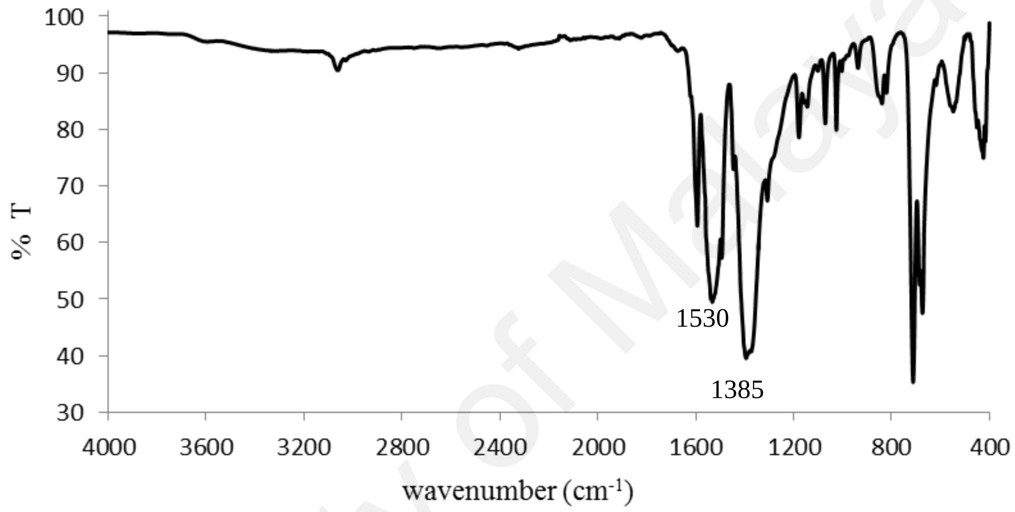

Figure 4.88 FTIR spectrum of $[Mn_2(\mu\text{-}H_2O)_2(C_6H_5COO)_4]{\cdot}H_2O$

Its **UV-vis** spectrum in DMSO (1.63 mmol dm^{-3}) is shown in **Figure 4.89**. It shows a *d-d* band at 387 nm (ε = 10 M^{-1} cm^{-1}), assigned to the $^6A_{1g}$ to $^6A_{1g}$ electronic configurations, and indicating an octahedral complex with HS Mn(II) atoms. The band was weak due to the spin-forbidden transition.

The value of $\chi_M T$, calculated from the values of FM = 648.56 g mol^{-1}, χ_g = 3.93 x 10^{-5} cm^3 g^{-1}, χ_M = 2.55 x 10^{-2} cm^3 mol^{-1}, and χ_{dia} = -3.24 x 10^{-4} cm^3 mol^{-1}, was 7.6 cm^3 K mol^{-1} at 298 K. The theoretical $\chi_M T$ value for a LS dinuclear Mn(II) octahedral complex is 0.75 cm^3 K mol^{-1}, while that for a HS Mn(II) is 8.7 cm^3 K mol^{-1}. Hence, it may be inferred that this complex was made up of 14.4% LS Mn(II) and 85.6% HS Mn(II) atoms at this temperature in the solid state (**Appendix 4**).

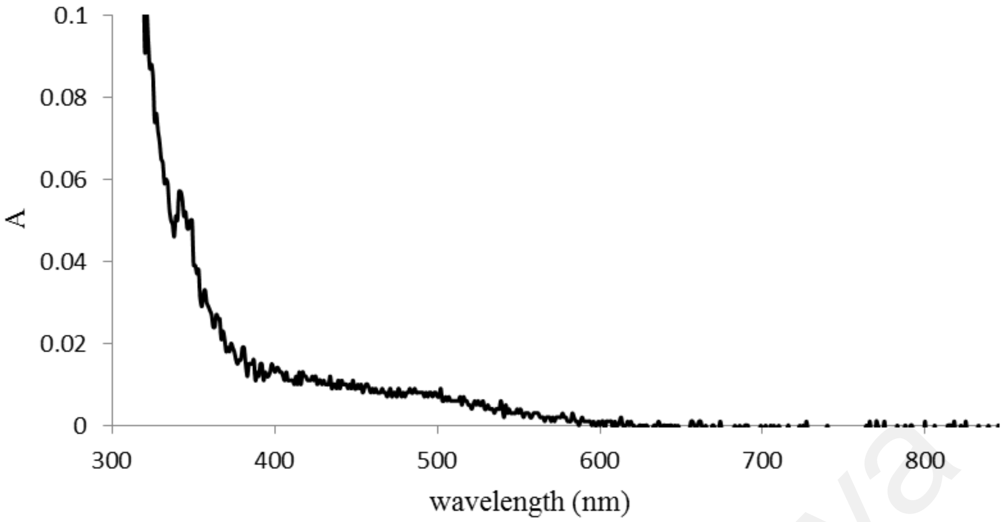

Figure 4.89 UV-vis spectrum of $[Mn_2(\mu\text{-}H_2O)_2(C_6H_5COO)_4]{\cdot}H_2O$

In the second step, $[Mn_2(\mu\text{-}H_2O)_2(C_6H_5COO)_4]{\cdot}H_2O$ reacted with cyclam in CH_3CH_2OH to form a brown semi-solid. Its structural formula $[Mn(C_6H_5COO)_2(cyclam)]{\cdot}7H_2O$ was proposed based on elemental analytical data and FTIR spectroscopy, discussed below. Hence, its structure was similar to $[Ni(cyclam)(C_6H_5COO)_2]$ (**Figure 4.28**), and its yield was 65.1%.

The results of its **elemental analyses** (46.7% C; 7.1% H; 9.2% N) were in good agreement with those calculated for the chemical formula $C_{24}H_{44}MnN_4O_{11}$ (46.5% C; 7.2% H; 9.0% N; formula weight, 619.6 g mol^{-1}).

Its **FTIR** spectrum **(Figure 4.90)** shows the presence of the expected functional groups and bonds as previously discussed. The Δ_{COO} value was 166 cm^{-1} ($\upsilon_{as,COO}$ = 1554 cm^{-1} and $\upsilon_{s,COO}$ = 1388 cm^{-1}), suggesting monodentate binding mode for $C_6H_5COO^-$ ion.

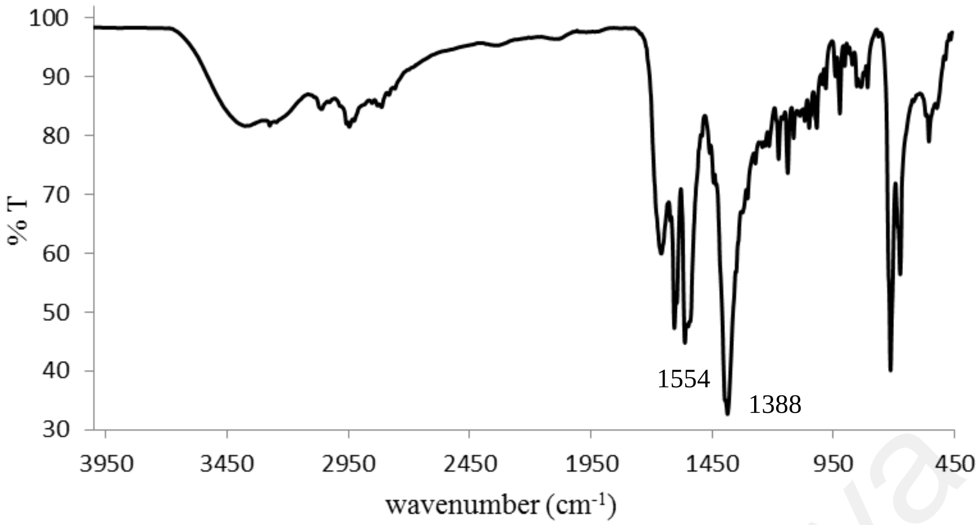

Figure 4.90 FTIR spectrum of [Mn(C_6H_5COO)$_2$(cyclam)]$\cdot$7H_2O

In the last step, [Mn(C_6H_5COO)$_2$(cyclam)].7H_2O reacted with L1 in a mole ratio of 1:2 in CH_3CH_2OH-$CHCl_3$ to form a brown semi-solid. Its structural formula, [Mn(cyclam)(L1)$_2$](C_6H_5COO)$_2$$\cdot$4$H_2O$, was proposed based on combined instrumental data as previously done. Hence, its structure was similar to **1** (**Figure 4.3**), and its yield was 90.5%.

The results of its **elemental analyses** (64.9% C; 9.5% H; 6.8% N) were in good agreement with those calculated for the chemical formula $C_{62}H_{108}MnN_6O_{10}$ (64.6% C; 9.5% H; 7.3% N; formula weight, 1152.5 g mol^{-1}).

Its FTIR spectrum **(Figure 4.91)** shows the presence of the expected functional groups and bonds as previously discussed. The Δ_{COO} value was 183 cm^{-1} ($\upsilon_{as,COO}$ = 1555 cm^{-1} and $\upsilon_{s,COO}$ = 1372 cm^{-1}), suggesting free (non-coordinated) $C_6H_5COO^-$ ion.

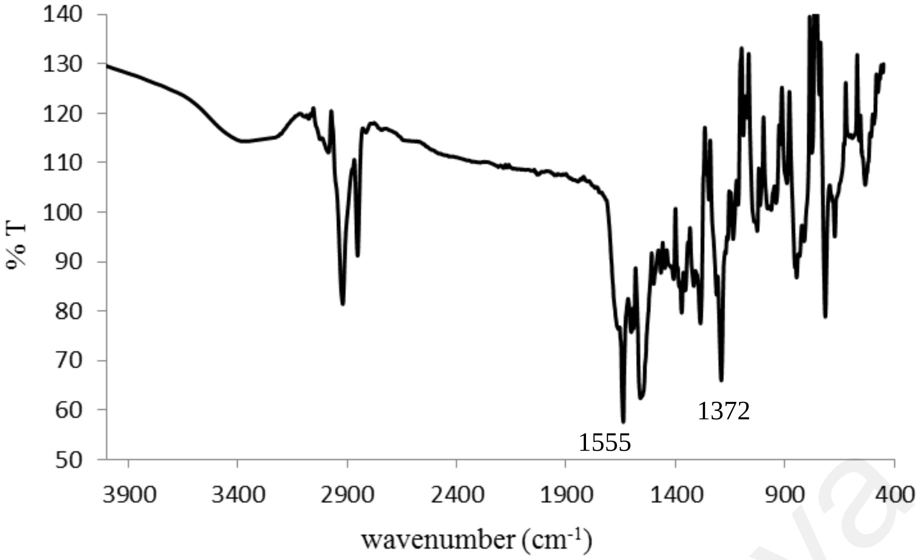

Figure 4.91 FTIR spectrum of **10**

Its **UV-vis** spectrum in $CHCl_3$ (0.50 mmol dm^{-3}) is shown in **Figure 4.92**. It shows a *d*-*d* band at 674 nm (ε_{max} = 439 M^{-1} cm^{-1}) and a MLCT band at about 340 nm (ε_{max} = 1146 M^{-1} cm^{-1}). These *d*-*d* bands assigned that the electronic configurations from $^2T_{2g}$ to $^2A_{2g}$. $^2T_{1g}$ for an octahedral LS Mn(II) complex.

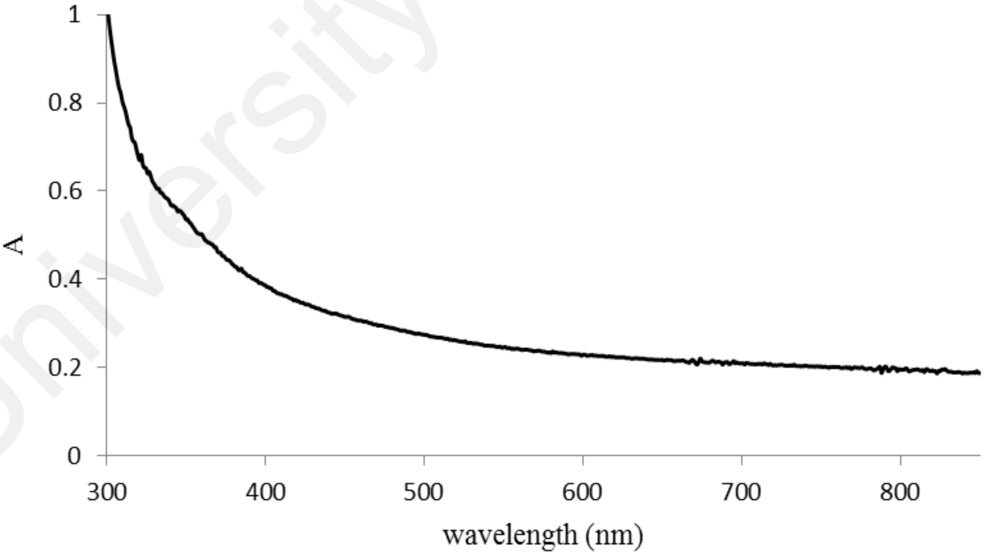

Figure 4.92 UV-vis spectrum of **11**

Its μ_{eff} value could not be determined by the Gouy method as the complex was a semi-solid. However, its ^{1}H-NMR spectrum in CD_3OD **(Figure 4.93)** shows several broad peaks for the organic ligands, suggesting a paramagnetic complex.

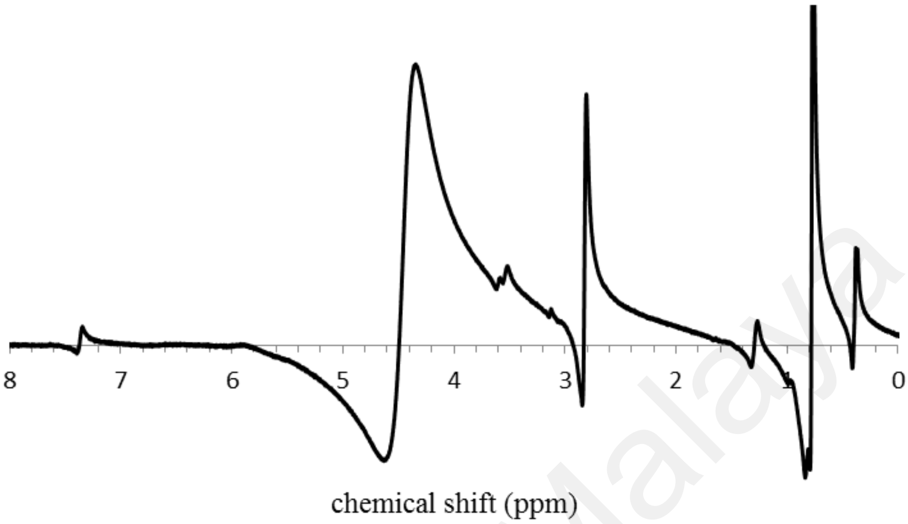

Figure 4.93 ^{1}H-NMR spectrum of **10**

(b) ***Spin-crossover behaviour***

Its temperature dependence ε was measured for a solution in DMSO at 360 nm (ε = 775 M^{-1} cm^{-1}), which corresponds to LS Mn(II), in the temperature range of 10 °C to 70 °C on two successive heating-cooling cycles. The result (**Figure 4.94**) shows that on heating, the ε values gradually decreased to 699 M^{-1} cm^{-1} at 70 °C. Upon cooling from this temperature the values increased gradually to about 739 M^{-1} cm^{-1} at 30 ^{o}C, and then decreased abruptly to about 710 M^{-1} cm^{-1} at 20 °C. On reheating, the values increased to about 730 M^{-1} cm^{-1} from 20 °C to 30 °C, and then decreased gradually to about 690 M^{-1} cm^{-1} from 30 °C to 70 °C. On cooling from this temperature, the value increased gradually to about 739 M^{-1} cm^{-1} at 20 °C. From these results, it may be inferred that the complex showed normal SCO behaviour (LS-HS on heating) in solution.

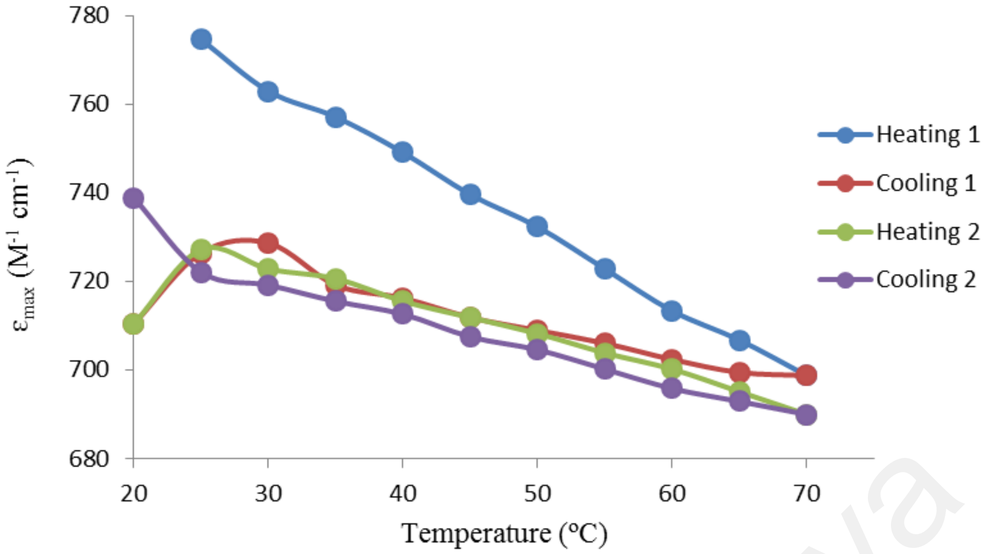

Figure 4.94 Temperature-dependent ε_{max} values for **10** at 360 nm

(c) ***Thermal and mesogenic properties***

Its TG trace (**Figure 4.95**) shows an initial weight loss from 80 °C to 129 °C due to evaporation of lattice H_2O molecules at (found = 2.9%; calculated = 3.2%). The next major weight loss from 129 °C to 680 °C was due to the decomposition of cylam and L1 ligands, and $C_6H_5COO^-$ ion (found = 89.7%; calculated = 90.4%). The amount of residue at temperature above 680 °C was 7.4%. This correlates well with the calculated value of 6.4%, assuming that it is made up of pure MnO [115]. These data further support the proposed chemical formula.

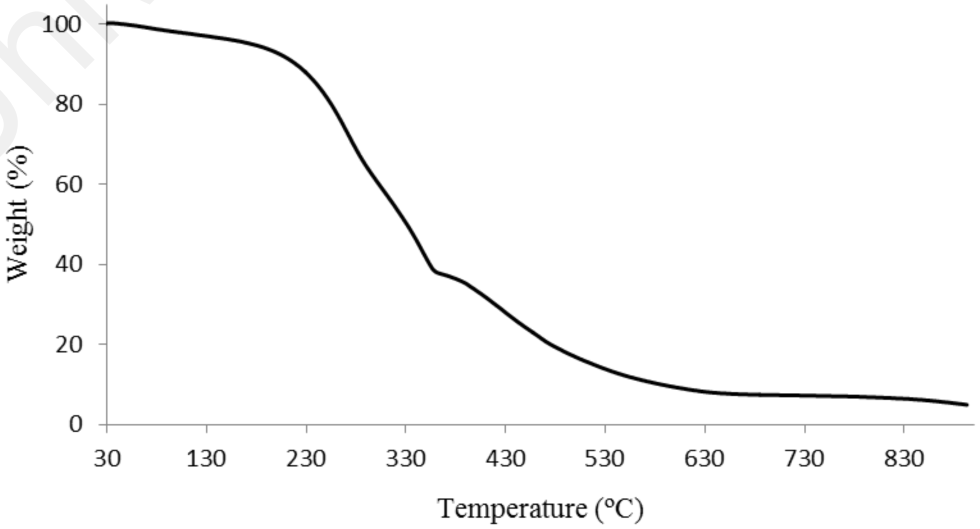

Figure 4.95 TG trace of **10**

Its DSC scan **(Figure 4.96)** was recorded in a heating–cooling cycles within the temperature range 25-125°C. It shows two endothermic peaks at onset 50.0 °C (ΔH = +4.8 kJ mol^{-1}) and 113.3°C (ΔH = +2.1 kJ mol^{-1}) on heating assigned to crystal-to-mesophase transition and mesophase-to-isotropic transition respectively. On cooling, it shows one exothermic peaks at 41.6°C (ΔH = +0.6 kJ mol^{-1}) assigned to isotropic-to-mesophase transition.

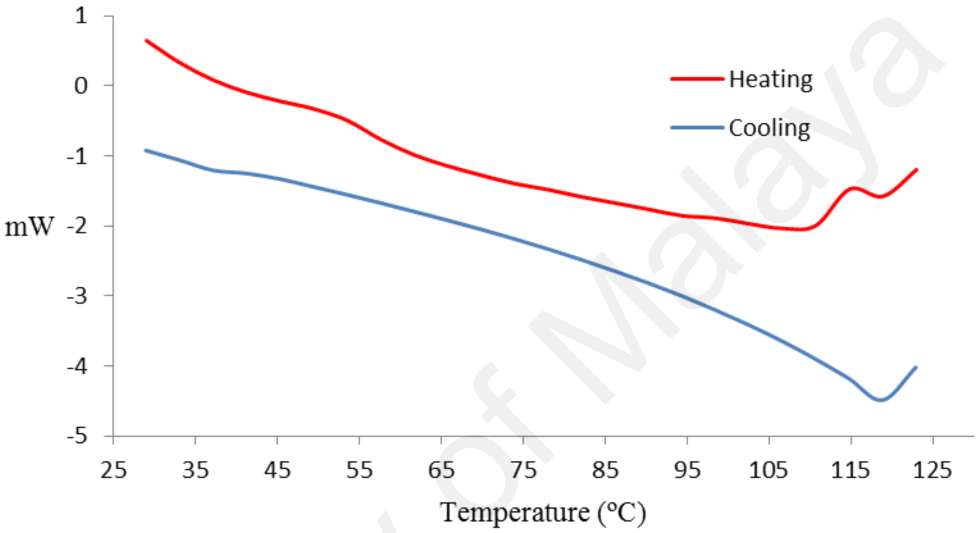

Figure 4.96 DSC scan of **10** (endothermic peak up)

Viewed under **POM**, **10** melted at 28 °C (**Figure 4.97(a)**), and started to clear (but incomplete) at 60 °C (**Figure 4.97(b)**). On cooling, an optical texture was observed at the clear region at 43 °C (**Figure 4.97(c)**). This texture was similar to that of L1 (**Figure 4.8(c)**). Hence, it is inferred that L1 dissociated from the complex on heating. Therefore, the complex did not exhibit mesomorphism.

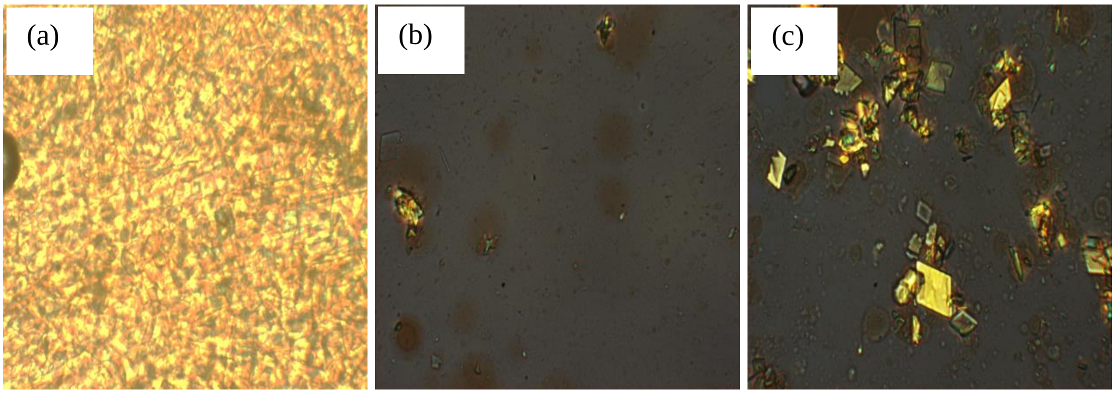

Figure 4.97 Photomicrographs of **10** on: (a) heating at 28 °C; (b) heating at 60 °C; and (c) cooling at 43 °C

(d) ***Thermoelectrical property***

The **Seebeck coefficient** for a solution of **10** in DMSO was similarly determined as for **6**. The graphs of ΔV versus ΔT (**Figure 4.98**) were linear from ΔT = 0 K to ΔT ~ 40 K with positive slopes, and the mean S_e value was +0.22 ± 0.08 mV K^{-1}. Since the S_e value was lower than value for mixture of $KI\text{-}KI_3$ and TBATFB in DMSO (S_e = +0.44 ± 0.02 mV K^{-1}), the complex was not functioning as a thermoelectric material in this solvent.

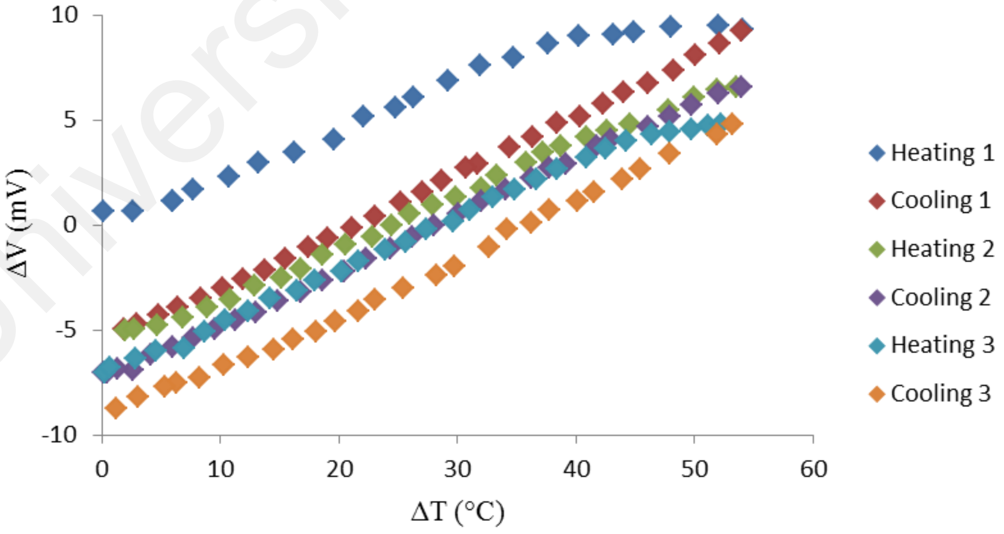

Figure 4.98 Plots of ΔV versus ΔT of **10**

It is noted that similar to the corresponding Co(II) complex (**7**), there was a reduction in the gradients of the slopes in the heating cycles at about ΔT ~ 40 K, signalling a change in the spin state of Mn(II) from LS to HS.

4.7.2 [Mn(cyclam)(L2)(H_2O)](C_6H_5COO)$_3$·3H_2O (11)

(a) ***Synthesis and structural deduction***

[Mn(cyclam)(L2)(H_2O)](C_6H_5COO)$_3$]·3H_2O (**11**) was obtained as a brown semi-solid from the reaction of [Mn(C_6H_5COO)$_2$(cyclam)]·7H_2O with L2 in a mole ratio 1:2 in CH_3CH_2OH-$CHCl_3$. The yield was 95.9%. Hence, Mn(II) in the reactant was oxidised to Mn(III) during this reaction. Based on combined analytical data discussed below, the structure of **Complex 11** is proposed to be similar to **2** (**Figure 4.10**).

The result of its elemental analyses (61.2% C; 8.8% H; 6.4% N) was in good agreement with those calculated for the chemical formula $C_{52}H_{84}MnN_5O_{11}$ (61.8% C; 8.4% H; 6.9% N; formula weight, 1010.2 g mol^{-1})

Its FTIR spectrum **(Figure 4.99)** shows the presence of the expected functional groups and bonds. The Δ_{COO} value was 165 cm^{-1} ($\upsilon_{as,COO}$ = 1550 cm^{-1}; $\upsilon_{s,COO}$ = 1385 cm^{-1}), suggesting ionic (non-coordinated) $C_6H_5COO^-$ ion.

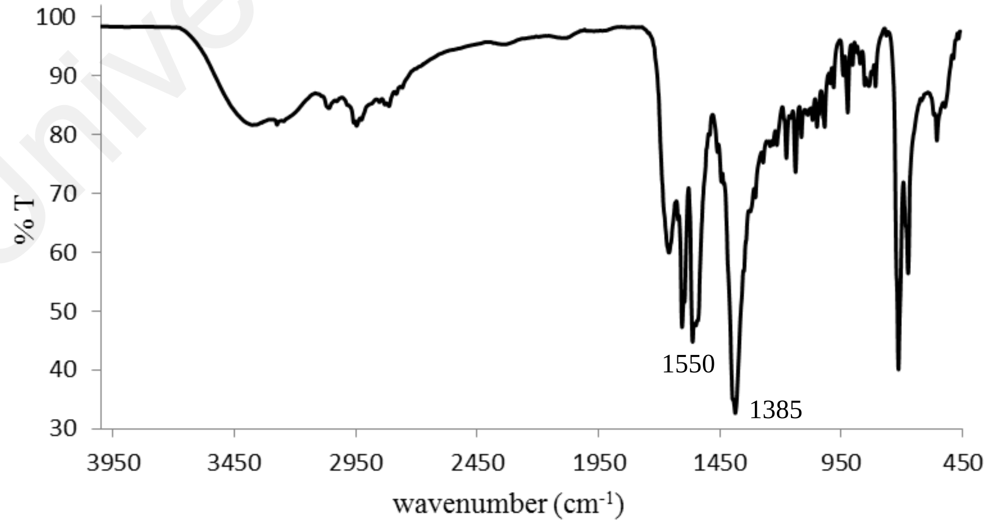

Figure 4.99 FTIR spectrum of **11**

Its **UV-vis** spectrum in CH_3OH (3.11 mmol dm^{-3}) is shown in **Figure 4.100**. It shows a continuously increasing absorbance from about 850 nm to about 475 nm.

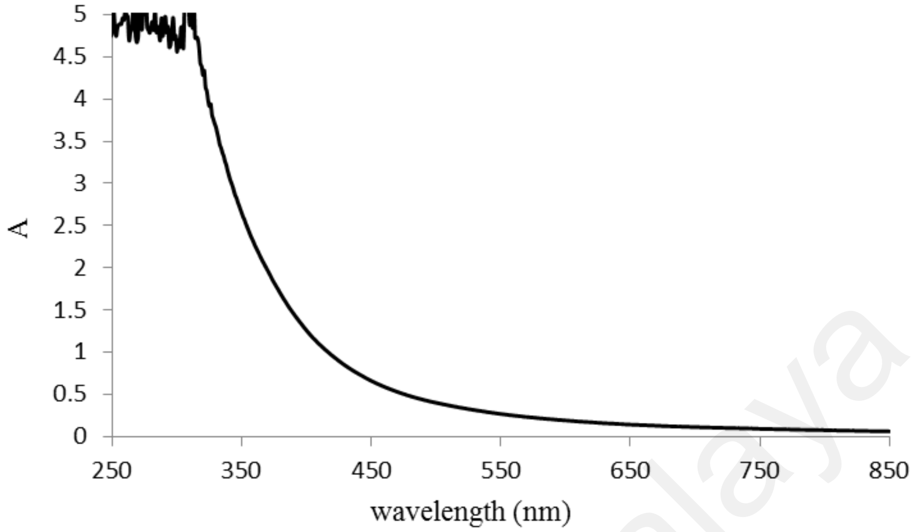

Figure 4.100 UV-vis spectrum of **11**

Its μ_{eff} value could not be determined by the Gouy method as the complex was a semi-solid. However, its ^1H-NMR spectrum in CD_3OD **(Figure 4.101)** shows a very broad peaks for the organic ligands, suggesting a paramagnetic complex.

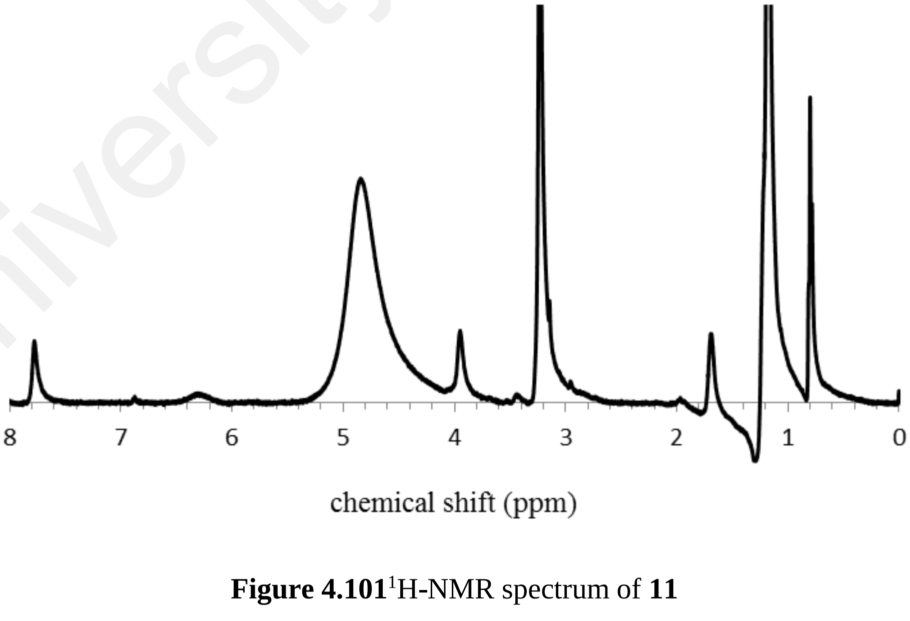

Figure 4.101^1H-NMR spectrum of **11**

(b) ***Spin-crossover behaviour***

Its **temperature-dependence ε** was measured for a solution in DMSO at 357 nm (ε = 745 M^{-1} cm^{-1} at 25 °C), which corresponds to LS Mn(III), in the temperature range of 20 °C to 70 °C on two successive heating-cooling cycles. The result (**Figure 4.102**) shows that on heating, the ε values gradually decreased to 705 M^{-1} cm^{-1} at 70 °C. Upon cooling from this temperature, the values gradually increased to 745 M^{-1} cm^{-1} at 25 °C, and then abruptly decreased to about 715 M^{-1} cm^{-1} at 20 °C. On reheating, the values abruptly decreased to about 676 M^{-1} cm^{-1} at 25 °C, then abruptly increased to 725 M^{-1} cm^{-1} at 30 °C, and then gradually decreased to 705 M^{-1} cm^{-1} at 70 °C. On cooling from this temperature, the values gradually increased to 740 M^{-1} cm^{-1} at 20 °C. Hence, the complex showed "re-entrant SCO" [76] at the first cooling mode between 30 °C to 20 °C (HS-LS-HS) and upon second heating between 20 °C to 30 °C (LS-HS-LS). It may be inferred that **11** exhibits spin crossover (SCO) behaviour in solution.

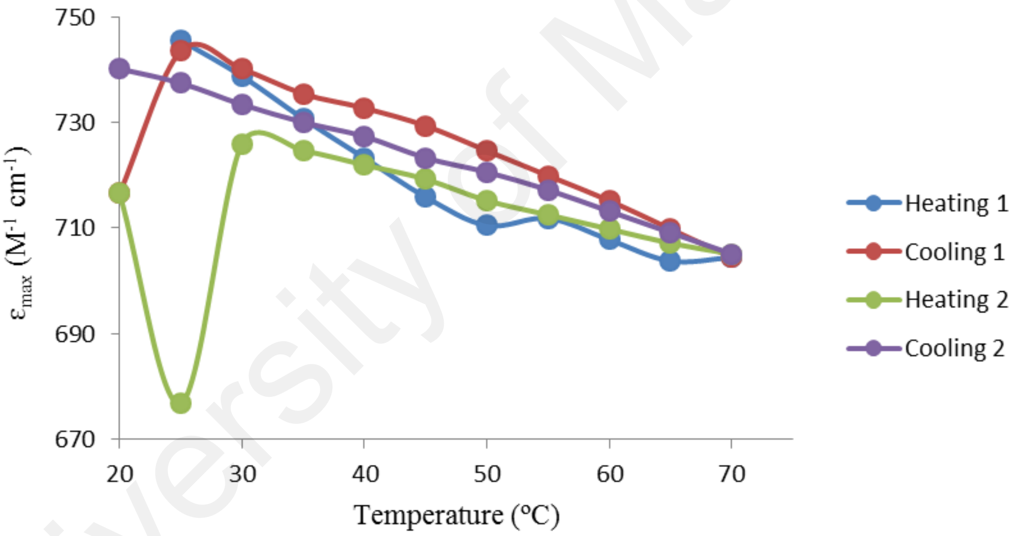

Figure 4.102 Temperature-dependent ε_{max} values for **11** at 357 nm

(c) *Thermal and mesogenic properties*

Its TGA trace (**Figure 4.103**) shows an initial weight losses from 140 °C to 189 °C due to loss of coordinate H_2O molecules (found = 2.0%; calculated = 1.9%). The next major weight loss from 189 °C to 704 °C was due to the decomposition of cyclam, L2 ligands, and $C_6H_5COO^-$ ion (found = 90.5%; calculated = 92.4%). The amount of residue at temperatures above 704 °C was 7.0% which was in good agreement with the expected amount of 7.0% (assuming pure MnO). It is noted that there was no weight loss corresponding to lattice H_2O molecules as shown in its chemical formula, suggesting that the molecules have evaporated off on storage.

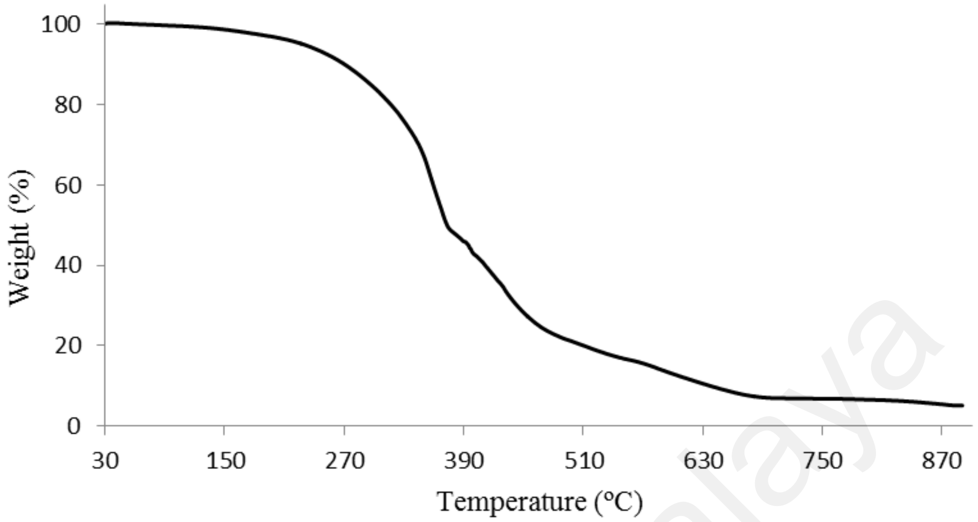

Figure 4.103 TG trace of **11**

Its DSC scan (**Figure 4.104**) was recorded in one successive heating–cooling cycle within the temperature range 25-125°C. It shows three endothermic peaks at onset 25.0 °C (ΔH = +13.6 kJ mol^{-1}), 43.6 °C (ΔH = +1.0 kJ mol^{-1}) and 68.1 °C (ΔH = +1.1 kJ mol^{-1}) assigned to crystal-to-mesophase 1 transition, mesophase 1-to-mesophase 2 transition, and mesophase 2-to-isotropic liquid transition [116]. On cooling, only one exothermic peaks at 47.6 °C (ΔH = +1.1 kJ mol^{-1}), assigned to isotropic liquid-to-mesophase 2 transition.

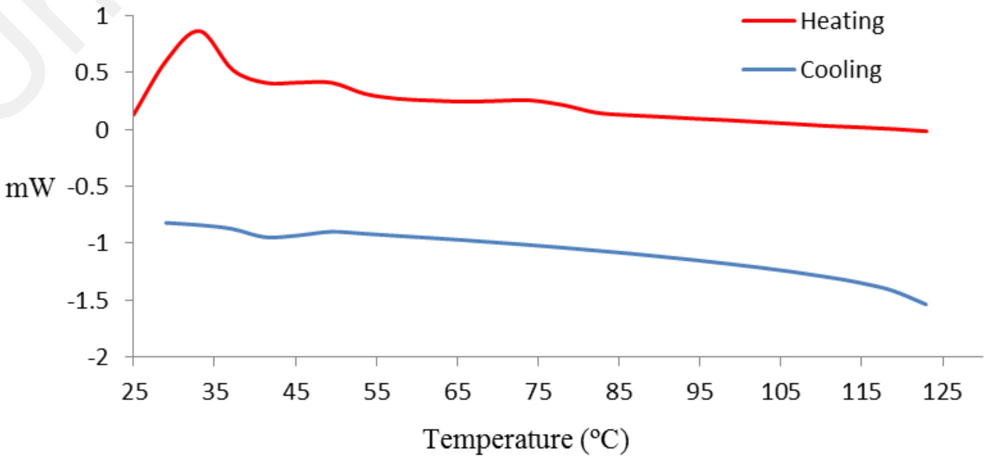

Figure 4.104 DSC scan of **11** (endothermic peaks up)

Under **POM**, **11** was heated to about 100 ^{o}C (incomplete isotropization), and showed optical textures in the clear region at 58 ^{o}C on cooling (**Figure 4.105**). The texture was different from that of L2. Hence, this ligand did not dissociate from the complex. Accordingly, the complex was mesomorphic.

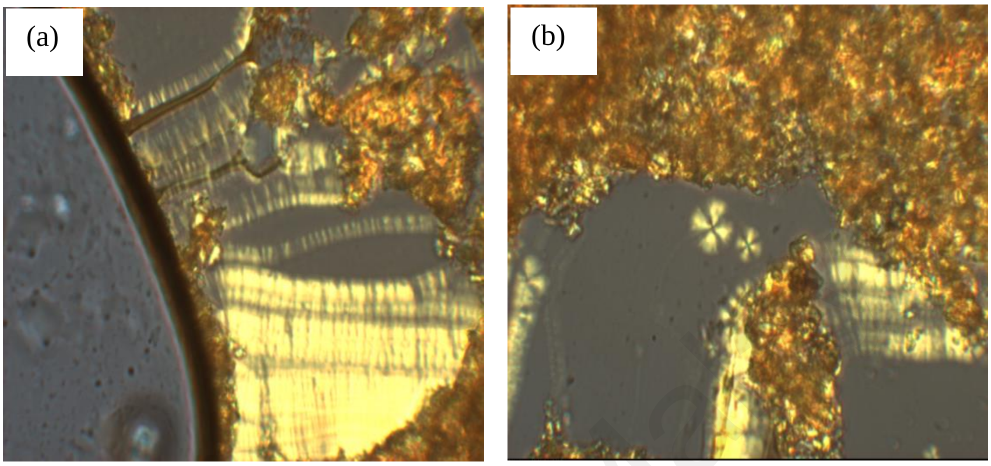

Figure 4.105 Photomicrographs of **11** on cooling at 58 ^{o}C at different sites

(d) ***Thermoelectrical property***

The **Seebeck coefficient** for a solution of **11** was similarly determined in CH_3CH_2OH as for **4**. The graphs of ΔV versus ΔT (**Figure 4.106**) were linear from ΔT = 0 K to ΔT ~ 25 K with positive slopes, and the mean S_e value was +0.24 ± 0.03 mV K^{-1}. Since the value was lower than that for mixture of KI-KI_3 and TBATFB in CH_3CH_2OH (+0.352 ± 0.004 mV K^{-1}), the complex was not functioning as a thermoelectric material in this solvent.

It is noted that similar to complex **10**, there was a reduction in the gradients of the slopes in the heating cycles at about ΔT ~ 25 K, signalling a change in the spin state of Mn(III) from LS to HS.

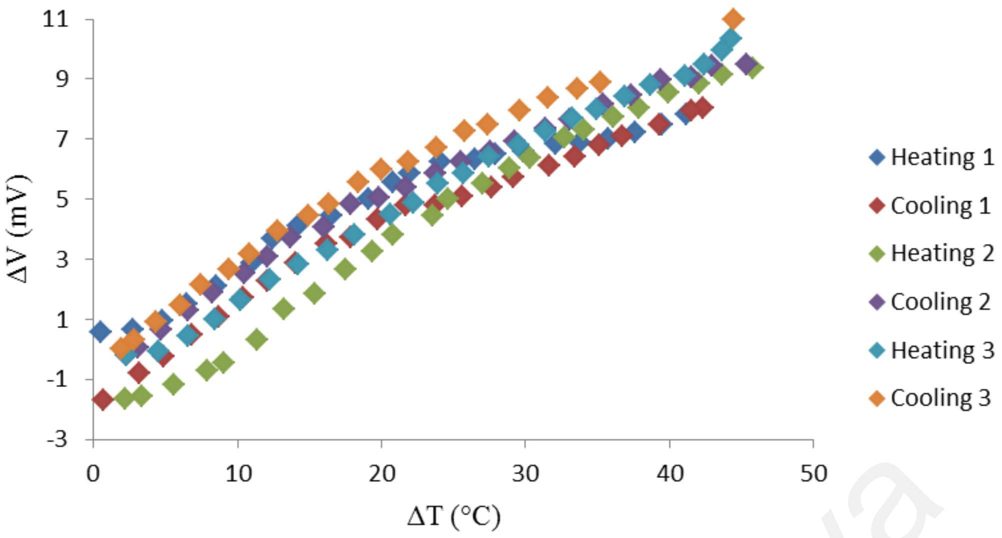

Figure 4.106 Plots of ΔV versus ΔT of **11**

4.7.3 *Summary*

The results of the analytical data for **10** and **11** are summarised in **Table 4.10**.

Table 4.10 Summary for complexes **10** and **11**

Chemical formula	Δ_{COO} (cm^{-1})	λ (nm)	Magnetism	T_{dec} (°C)	M	S_e ($mV\ K^{-1}$)
$[Mn(cyclam)(L1)_2](R)_2\cdot 4H_2O$ (**11**)	146 (ionic)	674 (*)	Paramagneti	129	No	+0.22±0.08
$[Mn(cyclam)(L2)(H_2O)](R)_3\cdot 3H_2O$ (**12**)	165 (ionic)	675 (*)	Paramagneti	189	Yes	+0.24±0.03

R = C_6H_5COO * = octahedral; M = mesomorphism

Both complexes were mononuclear, octahedral, ionic, and paramagnetic, but they have different structural formulae. In addition, **10** was a Mn(II) complex, while **11** was a Mn(III) complex. The thermal stability of **10** was significantly lower than **11**. Complex **10** was not mesomorphic, while **11** was mesomorphic. Finally, both complexes did not function as thermoelectric materials.

CHAPTER 5: CONCLUSIONS AND SUGGESTIONS FOR FUTURE WORKS

5.1 Conclusions

$[Cu(cyclam)(H_2O)_2](4\text{-}XC_6H_4COO)_2$, where X = H, CH_3, OCH_3, reacted with $4\text{-}CH_3(CH_2)_{13}OC_5H_4N$ (L1), while $[Cu(4\text{-}HOC_6H_4COO)_2(cyclam)]\cdot 2H_2O$ did not react with this ligand. In addition, complexes of Ni(II), Co(II), Co(III), Fe(II), Fe(III), Mn(II) and Mn(III) with cyclam, $C_6H_5COO^-$ ion, L1 or $4\text{-}CH_3(CH_2)_{15}OC_5H_4N$ (L2) were successfully synthesized. These complexes were obtained in good yields (61-97%), and their structural formulae (**Table 5.1**) were deduced by elemental analyses, FTIR spectroscopy, UV-vis spectroscopy, and magnetic susceptibility by the Gouy method or ^{1}H-NMR spectroscopy (for semi-solid complexes).

Table 5.1 Structural formulae of complexes

Complex	**Stuctural Formula**
1	$[Cu(cyclam)(L1)_2](C_6H_5COO)_2\cdot 3H_2O$
2	$[Cu(cyclam)(L1)(H_2O)](4\text{-}CH_3C_6H_4COO)_2\cdot 3H_2O$
3	$[Cu(cyclam)(L1)(H_2O)](4\text{-}CH_3OC_6H_4COO)_2\cdot 4H_2O$
4	$[Ni(cyclam)(L1)(H_2O)](C_6H_5COO)_2\cdot H_2O$
5	$[Ni(cyclam)(L2)_2](C_6H_5COO)_2\cdot H_2O$
6	$[Co(cyclam)(L1)_2](C_6H_5COO)_2\cdot 3H_2O$
7	$[Co(cyclam)(L2)_2](C_6H_5COO)_3\cdot 4H_2O$
8	$[Fe(cyclam)(L1)_2](C_6H_5COO)_2\cdot 2H_2O$
9	$[Fe(cyclam)(L2)_2](C_6H_5COO)_3]\cdot 4H_2O$
10	$[Mn(cyclam)(L1)_2](C_6H_5COO)_2\cdot 4H_2O$
11	$[Mn(cyclam)(L2)(H_2O)](C_6H_5COO)_3\cdot 3H_2O$

All complexes were octahedral, mononuclear, ionic and thermally stable (T_{dec} > 130 °C). These features were independent of the substituents at the aromatic ring, different alkyloxy chain length in the pyridinyl ligands, and metal ions. All complexes with L1 have metal(II) atoms, while all complexes with L2 have metal(III) atoms, except for $[Ni(cyclam)(L2)_2](C_6H_5COO)_2\cdot H_2O$ (**5**) which has a Ni(II) atom.

$[Co(cyclam)(L2)_2](C_6H_5COO)_3\cdot 4H_2O$ **(7**) and $[Fe(cyclam)(L1)_2](C_6H_5COO)_2\cdot 2H_2O$ **(8**) were diamagnetic, while all other complexes were paramagnetic. The cobalt and iron complexes were mainly LS at the room temperature. $[Co(cyclam)(L1)_2](C_6H_5COO)_2\cdot 3H_2O$ (**6**) showed reverse SCO while $[Fe(cyclam)(L2)_2](C_6H_5COO)_3]\cdot 4H_2O$ (**9**) showed normal SCO on heating but reverse SCO on cooling. All other complexes showed normal SCO behaviour in solutions.

Complexes $[Cu(cyclam)(L1)(H_2O)](4\text{-}CH_3OC_6H_4COO)_2\cdot 4H_2O$ **(3**), $[Fe(cyclam)(L2)_2](C_6H_5COO)_3]\cdot 4H_2O$ **(9)** and $[Mn(cyclam)(L2)(H_2O)](C_6H_5COO)_3\cdot 3H_2O$ (**11**) were mesogenic. Other complexes were not mesogenic due to the dissociation of L1 or L2 on heating.

Finally, only Cu(II), Fe(II) and Fe(III) complexes were functioning as thermoelectric materials in solutions. The mean S_e values for all Cu(II) complexes (**1 – 3**) in $CHCl_3$ were negative with almost similar magnitude (~ -0.45 mV K^{-1}), while the values for $[Fe(cyclam)(L1)_2](C_6H_5COO)_2\cdot 2H_2O$ (**8**) and $[Fe(cyclam)(L2)_2](C_6H_5COO)_3]\cdot 4H_2O$ (**9**) were positive, +0.33 mV K^{-1} and -0.80 mV K^{-1}, respectively.

5.2 Suggestions for Future Work

The structures of complexes studied in this work need to be ascertained by either X-ray crystallography of single crystals or molecular modeling. Their SCO properties should be studied in the solid state at low temperatures by SQUID magnetometry, or by other techniques, such as vibrational spectroscopy, heat capacity, X-ray structural studies, synchrotron radiation studies, and magnetic resonance studies. In this research, the SCO properties were induced by temperature, and it would be fascinating to study the effect of other stimuli, such as pressure, light induced excited spin state trapping (LIESST), and magnetic field [117]. Also, their mesomorphisms may be determined by small-and-wide angle X-ray scattering (SWAXS) experiment at different temperatures.

Similar studies may be extended to complexes with odd number of carbon atoms (to observe the odd-even effect on mesomorphisms) and branched alkyloxy chains (to lower the melting temperatures and hence prevent their dissociation on heating, and increase solubility in solvents such as $CHCl_3$ for thermoelectric studies) in the pyridinyl ligands, and other arylcarboxylate ions ($XC_6H_4COO^-$, X = F, Cl, Br, I, NH_2, NO_2), alkylcarboxylates, alkyloxybenzoates, and inorganic anions such as BF_4^- and SCN^- ions.

The thermoelectric properties may be studied in less polar and higher boiling points solvents, such as toluene, in the solid or gel state, or for mixed-valence complexes. Other thermoelectric properties of interest include power, current, and resistance.

Other potential applications of these complexes may be pursued. Examples are as dye-sensitized solar cell (DSSC) materials [118], and especially for the Ni(II) complexes, as anti-cancer drugs [119].

REFERENCES

[1] Fischer, M., Hoffmann, F., Fröba, M. (2010). Molecular simulation of hydrogen adsorption in metal-organic frameworks. *Colloids and Surfaces A: Physicochemical and Engineering Aspects*, **357**, 35–42.

[2] Gaspar, A. B., Seredyuk, M. (2014). Spin Crossover in Soft Matter. *Coordination Chemistry Reviews*, **268**, 41–58.

[3] Chandrasekhar, S., Sadashiva, B. K., Ramesha, S., Srikanta, B. S. (1986). Paramagnetic nematic liquid crystals. *Pramana*, **27**, L713–L715.

[4] Gaspar, A. B., Seredyuk, M., Gütlich, P. (2009). Spin crossover in metallomesogens. *Coordination Chemistry Reviews*, **253**, 2399–2413.

[5] Decurtins, S., Gütlich, P., Köhler, C. P., Spiering, H., Hauser, A. (1984). Light-induced excited spin state trapping in a transition-metal complex: The hexa-1-propyltetrazole-iron(II) tetrafluoroborate spin-crossover system. *Chemical Physics Letters*, **105**, 1–4.

[6] Létard, J.-F. (2006). Photomagnetism of iron(II) spin crossover complexes - the T(LIESST) approach. *Journal of Materials Chemistry*, **16**, 2550-2559.

[7] Tritt, T. M., Subramanian, M. a. (2006). Thermoelectric Materials, Phenomena, and Applications: A Bird’s Eye View. *MRS Bulletin*, **31**, 188–198.

[8] Abdullah, N., Elsheikh, M. H., Nik Ibrahim, N. M. J., Mohd Said, S., Mohd Sabri, M. F., Haji Hassan, M., Marlina, A. (2015). Magnetic, thermal, mesomorphic and thermoelectric properties of mononuclear, dimeric and polymeric iron(II) complexes with conjugated ligands. *RSC Advances*, **5**, 50999–51007.

[9] Subramanian, P. S., Suresh, E., Shukla, R. S. (2005). Cu(II) complexes with labile apical coordination: Synthesis, crystal structure, ^{1}H-NMR investigation, and oxidation properties of mononuclear [Cu^{II}(dien)(2-PhIm)(ClO4)]$^+$ (1), [Cu^{II}(dien)(2-MeBzIm)]$^{2+}$ (2), complexes. *Inorganica Chimica Acta*, **358**, 2651–2660.

[10] Kato, M., Muto, Y. (1988). Factors affecting the magnetic properties of dimeric copper(II) complexes. *Coordination Chemistry Reviews*, **92**, 45–83.

[11] Yamanaka, M., Uekusa, H., Ohba, S., Saito, Y., Iwata, S., Kato, M., Steward, O. W. (1991). Correlation of electron density and spin-exchange interaction in dimeric copper(II) formates, acetates and silanecarboxylates. *Acta Crytallographica, Section B*, **47**, 344–355.

[12] Zeleňák, V., Vargová, Z., & Györyová, K. (2007). Correlation of infrared spectra of zinc(II) carboxylates with their structures. *Spectrochimica Acta*, **66**(2), 262–272.

[13] Nakamoto, K. (1986). *Infrared and Raman Spectra of Inorganic and Coordination Compounds*. Wiley Online Library.

[14] Iqbal, M., Ahmad, I., Ali, S., Muhammad, N., Ahmed, S., Sohail, M. (2013). Dimeric "paddle-wheel" carboxylates of copper(II): Synthesis, crystal structure and electrochemical studies. *Polyhedron*, **50**, 524–531.

[15] Stephan, H., Geipel, G., Appelhans, D., Bernhard, G., Tabuani, D., Komber, H., Voit, B. (2005). Pegylation of 1,4,8,11-tetraazacyclotetradecane (cyclam) and its Cu(II) complexation. *Tetrahedron Letters*, **46**, 3209–3212.

[16] Lindoy, L. F. (1989). *The Chemistry of Macrocyclic Ligand Complexes*. Cambridge: Cambridge University Press.

[17] Achmatowicz, M., Szumna, A., Zieliński, T., Jurczak, J. (2005). Structure-driven design and synthesis of chiral dioxocyclam derivatives. *Tetrahedron*, **61**, 9031–9041.

[18] Ito, T., Kato, M., Yamashita, M., Ito, H. (1986). Utilization of chemical and structural characteristics of tetraazacycloalkane complexes. *Journal of Coordination Chemistry*, **15**, 29–52.

[19] Bhattacharya, S., Mukherjee, R., Chakravorty, A. (1986). A nickel(III) complex with a NiO_6 coordination sphere. *Inorganic Chemistry*, **25**, 3448–3452.

[20] Melson, G. A., Ed. (1979). *Coordination Chemistry of Macrocyclic Compounds*. Boston, MA: Springer US.

[21] Wagler, T. R., Fang, Y., Burrows, C. J. (1989). Optically active difunctionalized dioxocyclam macrocycles: ligands for nickel-catalyzed oxidation of alkenes. *Journal of Organic Chemistry*, **54**, 1584–1589.

[22] Kinneary, J. F., Wagler, T. R., Burrows, C. J. (1988). Alkene Epoxidation Using Ni(II) Complexes of Chiral Cyclams. *Tetrahedron Letters*, **29**, 877–880.

[23] Nam, W., Ho, R., Valentine, J. S. (1991). Iron-cyclam complexes as catalysts for the epoxidation of olefins by 30% aqueous hydrogen peroxide in acetonitrile and methanol. *Journal of the American Chemical Society*, **113**, 7052–7054.

[24] Ahmad Tajidi, N. S., Abdullah, N., Arifin, Z. (2011). Diaqua(1,4,8,11-tetraazacyclotetradecane-κ4(N1,N4,N8, N11)copper(II) didodecanoate dihydrate. *Acta Crytallographica Section E*, **67**, m588–m589.

[25] Ahmad Tajidi, N. S., Abdullah, N., Arifin, Z., Tan, K. W., Ng, S. W. (2010). Diaqua(1,4,8,11-tetraazacyclotetradecane-κ4(N1, N4, N8, N11)copper(II) bis(4-methylbenzoate) monohydrate. *Acta Crytallographica Section E*, **66**, m890–m890.

[26] Ahmad Tajidi, N. S., Abdullah, N., Arifin, Z., Tan, K. W., Ng, S. W. (2010). Diaqua(1,4,8,11-tetraazacyclotetradecane-κ_4(N1,N4,N8,N11)copper(II) bis(pentafluorobenzoate) dihydrate, *Acta Crytallographica Section E*, **66**, m889–m889.

[27] Czakis-Sulikowska, D., Czylkowska, A. (2003). Complexes of Mn(II), Co(II), Ni(II) and Cu(II) with 4,4’-bipyridine and dichloroacetates. *Journal of Thermal Analysis and Calorimetry*, **71**, 395–405.

[28] Kato, M., Jonassen, H. B., Fanning, J. C. (1964). Copper(II) Complexes with Subnormal Magnetic Moments. *Chemical Reviews*, **64**, 99–128.

[29] Rodríguez-Martín, Y., Sanchiz, J., Ruiz-Pérez, C., Lloret, F., Julve, M. (2001). Synthesis, crystal structure and magnetic properties of

$[Cu(bpym)(mal)(H_2O)]\cdot 6H_2O$ and $[Cu_2(bpym)(mal)_2(H_2O)_2]\cdot 4H_2O$ (bpym = 2,2′-bipyrimidine, H_2mal =malonic acid). *Inorganica Chimica Acta*, **326**, 20–26.

[30] Bencini, A., Gatteschi, D., Zanchini, C. (1985). Anisotropic exchange in transition-metal dinuclear complexes. *Inorganic Chemistry*, **24**, 704–708.

[31] Abdullah, N., Al-Hakem, Y., Abdullah, N. (2014). Room-temperature magnetic liquid complexes of 2-hexyldecanoato ligand with Cu(II), Ni(II) and Co(II) ions. *Asian Journal of Chemistry*, **26**, 987–990.

[32] Selvakumar, P. M., Suresh, E., Subramanian, P. S. (2007). Synthesis, spectral characterization and structural investigation on some 4-aminoantipyrine containing Schiff base Cu(II) complexes and their molecular association. *Polyhedron*, **26**, 749–756.

[33] Ahuja, S., Jespersen, N. (2006). *Modern Instrumental Analysis*. *Elsevier* (47). Cambridge University Press.

[34] Earnshaw, A. (1968). *Introduction to Magneto Chemistry*. Academic Press INC.

[35] Creaven, B. S., Duff, B., Egan, D. A., Kavanagh, K., Rosair, G., Thangella, V. R., Walsh, M. (2010). Anticancer and antifungal activity of copper(II) complexes of quinolin-2(1H)-one-derived Schiff bases. *Inorganica Chimica Acta*, **363**, 4048–4058.

[36] Mandal, P. K., Nag, K., Manoharan, P. T. (1995). A Comprehensive Study of Exchange Coupling in a Macrocyclic Binuclear Copper(II) Complex in the Solid and Solution States. *Inorganic Chemistry*, **34**, 270–277.

[37] Holz, R. C., Brink, J. M. (1994). Proton NMR Spectroscopy as a Probe of Dinuclear Copper(II) Centers. *Inorganic Chemistry*, **33**, 4609–4610.

[38] G.N. Law Mar, W. Horrocks, R. H. H. (1973). *NMR of Paramagnetic Molecules*. New York: Academic Press.

[39] Bertini, I., & Luchinat, C. (1986). *NMR of paramagnetic molecules in biological systems*. *Physical Bioinorganic Chemistry Series* (Vol. 3). Retrieved from http://library.wur.nl/WebQuery/clc/529338

[40] Banci, L., Bertini, I., Luchinat, C. (1991). *Nuclear and electron relaxation: the magnetic nucleus-unpaired electron coupling in solution*. Wiley-VCH.

[41] Caglar, S., Adıgüzel, E., Caglar, B., Saykal, T., Sahin, E., Büyükgüngör, O. (2013). Synthesis, crystal structure, spectroscopic, thermal, catechol oxidase and catalase-like studies: New copper(II) complexes of 2-benzoylbenzoate and 2-pyridilpropanol ligands. *Inorganica Chimica Acta*, **397**, 101–109.

[42] Tschierske, C. (2012). *Liquid crystals: Materials design and self-assembly*. Springer Science.

[43] Bhattacharjee, C. R., Das, G., Mondal, P. (2011). Novel non-discoid chiral copper(II)-salen type [N_2O_2] donor Schiff base complexes with a cyclohexane diamine spacer: synthesis, electrochemistry, columnar mesomorphism and DFT study. *Liquid Crystals*, **38**, 441–449.

[44] Wen, C., Wang, Y.-J., Wang, H., Sheu, H., Lee, G., Lai, C. K. (2005). Columnar Metallomesogens Derived from 1,3,4-Oxadiazoles and X-ray Crystal Structure of Dichlorobis[2,5-bis(3,4,5-trimethoxyphenyl)-1,3,4-oxadiazole]palladium(II). *Chemistry of Materials*, **17**, 1646–1654.

[45] Abdullah, N., Sharmin, N., Ozair, L. N., Nordin, A. R., Mohd. Nasir, W. S. N., Mohamadin, M. I. (2015). Structures and mesomorphism of complexes of tetrakis(4-chlorobenzoate-μ-O,O′)bis(ethanol)dicopper(II) with different N-donor ligands. *Journal of Coordination Chemistry*, **68**, 1347–1360.

[46] Mishra, A., Bhattacharjee, S., Anwar, S. (2015). Simple apparatus to measure Seebeck coefficient up to 900 K. *Measurement*, **68**, 295–301.

[47] Abraham, T. J., MacFarlane, D. R., Pringle, J. M. (2013). High Seebeck coefficient redox ionic liquid electrolytes for thermal energy harvesting. *Energy & Environmental Science*, **6**, 2639-2645.

[48] Abraham, T. J., MacFarlane, D. R., & Pringle, J. M. (2011). Seebeck coefficients in ionic liquids–prospects for thermo-electrochemical cells. *Chemical Communications*, **47**(22), 6260.

[49] Abdullah, N., Hashim, R., Ozair, L. N., Al-Hakem, Y., Samsudin, H., Marlina, A., Nordin, A. R. (2015). Structural, mesomorphic, photoluminescence and thermoelectric studies of mononuclear and polymeric complexes of copper(II) with 2-hexyldecanoato and 4,4′-bipyridine ligands. *Journal of Materials Chemistry C*, **3**, 11036–11045.

[50] Karmakar, A., Deka, K., Sarma, R. J., Baruah, J. B. (2006). Benzoic acid inclusion in a dimeric nickel complex and its catalytic activity. *Inorganic Chemistry Communications*, **9**, 836–838.

[51] Kuppusamy, K., Govindarajan, S. (1996). Benzoate Complexes of Dipositive First Row Transition Metal Ions with Hydrazine. *Synthesis and Reactivity in Inorganic and Metal-Organic Chemistry*, **26**, 225–243.

[52] Karmakar, A., Sarma, R. J., Baruah, J. B. (2006). Mechanochemical Control of Synthesis and Structures of Aqua-Bridged Binuclear Nickel(II) Benzoate Complexes. *European Journal of Inorganic Chemistry*, **2006**, 4673–4678.

[53] Deka, K., Barooah, N., Sarma, R. J., Baruah, J. B. (2007). Self-assembled carboxylate complexes of zinc, nickel and copper. *Journal of Molecular Structure*, 827, 44–49.

[54] Lindoy, L. F., Mahinay, M. S., Skelton, B. W., White, A. H. (2003). Ligand assembly and metal ion complexation: syntheses and X-ray structures of Ni(II) and Cu(II) benzoate and 4- tert -butylbenzoate complexes of cyclam. *Journal of Coordination Chemistry*, **56**, 1203–1213.

[55] Glidewell, C., Ferguson, G., Gregson, R. M., Lough, A. J. (2000). Bis(4-hydroxybenzoato-O)(1,4,8,11-tetraazacyclotetradecane-κ4N)nickel(II): a three-dimensional framework built from O—H.O and N—H.O hydrogen bonds. *Acta Crystallographica Section C*, **56**, 174–176.

[56] Trávníček, Z., Pastorek, R., Slovák, V. (2008). Novel octahedral nickel(II) dithiocarbamates with bi- or tetradentate N-donor ligands: X-ray structures of [Ni(Bzppzdtc)(phen)$_2$]ClO$_4$·CHCl$_3$ and [Ni(Bz$_2$dtc)$_2$(cyclam)]. *Polyhedron*, **27**, 411–419.

[57] Lever, A. B. P. (1984). *Inorganic Electronic Spectroscopy* (2nd ed.). Elsevier.

[58] Vulfson S. G. (1998). Molecular Magnetochemistry. Gordon and Breach Science Publishers.

[59] Allen, F. H. (2002). The Cambridge Structural Database: A quarter of a million crystal structures and rising. *Acta Crytallographica Section B*, **58**, 380–388.

[60] Hudák, J., Boča, R., Moncol, J., Titiš, J. (2013). Magnetism of dinuclear benzoato cobalt(II) complexes modeled by a general bilinear exchange. *Inorganica Chimica Acta*, **394**, 401–409.

[61] Hudák, J., Boča, R., Dlháň, Ľ., Kožíšek, J., & Moncoľ, J. (2011). Structure and magnetism of mono-, di-, and trinuclear benzoato cobalt(II) complexes. *Polyhedron*, **30**, 1367–1373.

[62] Catterick, J., Hursthouse, M. B., Thornton, P., Welch, A. J. (1977). Crystal and molecular structure of tetra-μ-benzoato-bisquinolinedicobalt(II), a binuclear cobalt(II) carboxylate. *Journal of the Chemical Society, Dalton Transaction*, **3**, 223–226.

[63] Karmakar, A., Sarma, R. J., Baruah, J. B. (2007). Synthesis and characterisation of dinuclear and mononuclear cobalt(II) benzoate complexes. *Polyhedron*, **26**, 1347–1355.

[64] Gavrilenko, K. S., Gal, Y. Le, Cador, O., Golhen, S., Ouahab, L. (2007). First trinuclear paramagnetic transition metal complexes with redox active ligands derived from TTF: $Co_2M(PhCOO)_6(TTF\text{-}CH{=}CH\text{-}py)_2\cdot 2CH_3CN$, M = Co^{II}, Mn^{II}. *Chemical Communications*, **6**, 280–282.

[65] Caneschi, A., Dei, A., Gatteschi, D., Tangoulis, V. (2002). Antiferromagnetic Coupling in a Six-Coordinate High Spin Cobalt(II)−Semiquinonato Complex. *Inorganic Chemistry*, **41**, 3508–3512.

[66] Ivaniková, R., Svoboda, I., Fuess, H., Mašlejová, A. (2006). *trans*-Dichloro(1,4,8,11-tetraazacyclotetradecane)cobalt(III) chloride. *Acta Crystallographica Section E*, **62**, m1553–m1554.

[67] Simon, E., L’Haridon, P., Pichon, R., L’Her, M. (1998). Electrochemical, spectrochemical characterization and crystal structure of (1,4,8,11-

tetrazacyclotetradecane)(acetylcetonate) cobalt(III) complexes. *Inorganica Chimica Acta*, **282**, 173–179.

[68] Hung, Y., Martin, L. Y., Jackels, S. C., Tait, A. M., Busch, D. H. (1977). Ring size effects among metal complexes with macrocyclic ligands: synthesis, stereochemistry, spectrochemistry, and electrochemistry of cobalt(III) complexes with unsubstituted, saturated tetraaza macrocycles. *Journal of the American Chemical Society*, **99**, 4029–4039.

[69] Kim, B. J., Hambley, T. W., Bryce, N. S. (2011). Visualising the hypoxia selectivity of cobalt(III) prodrugs. *Chemical Science*, **2**, 2135.

[70] Cambi, L., Szego, L. (1931). Use the magnetic susceptibility of the complex compounds. *Journal of America Chemistry Society*, (A and B Series) , **64** (10), 2591-2598.

[71] Enachescu, C., Krivokapic, I., Zerara, M., Real, J. A., Amstutz, N., Hauser, A. (2007). Optical investigation of spin-crossover in cobalt(II) bis-terpy complexes. *Inorganica Chimica Acta*, **360**, 3945–3950.

[72] Judge, J. S., Baker, W. A. (1967). On the spin equilibrium in bis(2,2′,2″-terpyridine) cobalt(II) salts. *Inorganica Chimica Acta*, **1**, 68–72.

[73] Evans, D. F. (1959). The determination of the paramagnetic susceptibility of substances in solution by nuclear magnetic resonance. *Journal of the Chemical Society*, 2003–2005.

[74] Henke, W., Kremer, S. (1982). *The crystal structure of high-spin low-spin bis(2.2':6'2" -terpyridyl)Co(II) perchlorate*. *Inorganica Chimica Acta,* **65**, L115–L117.

[75] Hogg, R., Wilkins, R. C. (1962). Exchange studies of certain chelate compounds of the transition metals. VIII. 2,2’,2"-Terpyridine complexes. *Journal of the Chemical Society*, 341–350.

[76] Hayami, S., Komatsu, Y., Shimizu, T., Kamihata, H., Lee, Y. H. (2011). Spin-crossover in cobalt(II) compounds containing terpyridine and its derivatives. *Coordination Chemistry Reviews*, **255**, 1981–1990.

[77] Hayami, S., Nakaya, M., Ohmagari, H., Alao, A. S., Nakamura, M., Ohtani, R., Clegg, J. K. (2015). Spin-crossover behaviors in solvated cobalt(II) compounds. *Journal of the Chemical Society*. *Dalton Transaction*, **44**, 9345–9348.

[78] Abdullah, N., Noor, N. L. M., Nordin, A. R., Halcrow, M., MacFarlane, D. R., Lazar, M., Heinrich, B. (2015). Spin-crossover, mesomorphic and thermoelectrical properties of cobalt(II) complexes with alkylated N_3-Schiff bases. *Journal of Materials Chemistry C*, **3**, 2491–2499.

[79] Zhou, W., Zhu, Y., Jiao, C., Sun, Z.-G., Shi, S., Dai, L., Luo, H. (2014). Syntheses, crystal structures, surface photovoltage, luminescence and molecular recognition properties of zinc(ii) and iron(ii) carboxyphosphonates with 2D and 3D supramolecular structures. *Crystal Engineering Communication*, **16**, 1174

[80] Abdullah, N., Mohd Said, S., Marlina, A., Roslan, M. F., Azil, A., Nordin, A. R. (2015). Photophysical and Electrochemical Studies of Multinuclear Complexes of Iron(II) with Acetate and Extended Conjugated N-Donor Ligands. *The Scientific World Journal*, 1–8.

[81] Reviews, C., Deacon, G. B. (1980). Relationships Between the Carbon-Oxygen Strecthing Frequencies of Carboxylato Complexes and The Type of Carboxylate Coordination. *Coordination Chemistry Reviews*, **33**, 227–250.

[82] Ferrere, S. (2002). New photosensitizers based upon $[Fe^{II}(L)_2(CN)_2]$ and $[Fe^{II}L_3]$, where L is substituted 2,2′-bipyridine. *Inorganica Chimica Acta*, **329**, 79–92.

[83] Kahn, O. (1993). *Molecular Magnetism*. *Journal of Chemical Education*, VCH Publisher.

[84] Lee, Y. H., Ohta, A., Yamamoto, Y., Komatsu, Y., Kato, K., Shimizu, T., Hayami, S. (2011). Iron(II) spin crossover complexes with branched long alkyl chain. *Polyhedron*, **30**, 3001–3005.

[85] Shahbazi-Raz, F., Amani, V., Noruzi, E. B., Safari, N., Boča, R., Titiš, J., Notash, B. (2015). Synthesis, characterization, electrochemical and magnetic study of mixed ligand mono iron and O-methoxy bridged diiron complexes. *Inorganica Chimica Acta*, **435**, 262–273.

[86] Santos, V. N., Mendonça, G. L. F., Freire, V. N., Holanda, A. K. M., Sousa, J. R., Lopes, L. G. F., De Lima-Neto, P. (2013). Electrochemical and Monte Carlo studies of self-assembled *trans*-[Fe(cyclam)(NCS)$_2$]$^+$ complex ion on gold surface as electrochemical sensor for nitric oxide. *Electrochimica Acta*, **91**, 1–10.

[87] Vasconcellos, L. C. ., Oliveira, C. P., Castellano, E. E., Ellena, J., Moreira, Í. S. (2001). Structure and properties of iron–cyclam complex of 2-aminophenol. *Polyhedron*, **20**, 493–499.

[88] Kar, P., Biswas, R., Ida, Y., Ishida, T., Ghosh, A. (2011). A Unique Example of Structural Diversity Tuned by Apparently Innocent *o*-, *m*-, and *p*- Nitro Substituents of Benzoate in Their Complexes of Mn(II) with 4,4′-Bipyridine: 1D Ladder, 2D Sheet, and 3D Framework. *Crystal Growth & Design*, **11**, 5305–5315.

[89] Kar, P., Drew, M. G. B., Gómez-García, C. J., Ghosh, A. (2013). Synthesis and characterization of four novel manganese(II) chains formed by 4,4′-azobis(pyridine) and benzoate or nitrobenzoates: Stabilization of unusual ladder structures. *Polyhedron*, **50**, 229–239.

[90] Paul, P., Roy, S., Sarkar, S., Chowdhury, S., Purkayastha, R. N. D., Raghavaiah, P. Devi, S. I. (2015). Synthesis, structure and some properties of a manganese(II) benzoate containing diimine. *Journal of Molecular Structure*, **1102**, 153–160.

[91] Chandra, S., Kumar, U. (2005). Spectral and magnetic studies on manganese(II), cobalt(II) and nickel(II) complexes with Schiff bases. *Spectrochimica Acta Part A*, **61**, 219–224.

[92] Sankhla, D.S., Misra, S. (1980). Spectral and magnetic studies of manganes(II) complexes. *Journal of the Indian Chemical Society*, **57**, 300–303.

[93] Liu, Z., Liang, S., Di, X., Zhang, J. (2008). A manganese(III) complex that exhibits spin crossover behavior. *Inorganic Chemistry Communications*, **11**, 783–786.

[94] Mossin, S., Sørensen, H. O., Weihe, H., Glerup, J., Søtofte, I. (2005). Manganese(III) cyclam complexes with aqua, iodo, nitrito, perchlorato and acetic acid/acetato axial ligands. *Inorganica Chimica Acta*, **358**, 1096–1106.

[95] Olmstead, M. M., Boyce, D. W., Bria, L. E. (2011). Di-μ-oxido-bis-[(1,4,8,11-tetraaza-cyclotetradecane-κN,N’,N",N"')dimanganese(III,IV)] bis-(tetraphenylborate) chloride acetonitrile disolvate. *Acta Crytallographica Section E,* **67**, m824–825.

[96] Nordin, N. B. (2014). *The Effect of Alkyloxy Chain Length On The Thermal Properties of* $[Cu_2(C_6H_5COO)_4]$*,* MSc thesis, Faculty of Science, University of Malaya.

[97] Tajidi, N. S. A. (2013). *The Copper(II) Carboxylate-Cyclam Complexes As Thermally Stable Magnetic Materials*, MSc thesis. Faculty of Science, University of Malaya.

[98] Abdullah, N., Arifin, Z., Tiekink, E. R. T., Sharmin, N., Ahmad Tajidi, N. S., Mat Hussin, S. A. (2016). Covalent and ionic Cu(II) complexes with cyclam and substituted benzoato ligands: structural, thermal, redox and mesomorphic properties. *Journal of Coordination Chemistry*, **69**, 862–878.

[99] Hayami, S., Motokawa, N., Shuto, A., Moriyama, R., Masuhara, N., Inoue, K., Maeda, Y. (2007). Spin-crossover iron(II) compounds with liquid-crystal properties. *Polyhedron*, **26**, 2375–2380.

[100] Petrič, M., Leban, I., Šegedin, P. (1995). Preparation and characterization of copper(II) coordination compounds with linear chain fatty acids with 7–12 carbon atoms and pyridine. Crystal structure of $Cu(O_2CC_8H_{17})_2(py)_2(H_2O)$. *Polyhedron*, **14**, 983–989.

[101] Magini, M. (1982). Coordination of copper(II). Evidence of the Jahn-Teller effect in aqueous perchlorate solutions. *Inorganic Chemistry*, **21**(4), 1535–1538.

[102] Mohamadin, M. I., Abdullah, N. (2010). Thermal stability and electrochemical behaviour of tetrakis-μ-benzoatodicopper(II). *Central European Journal of Chemistry*, **8**, 1090–1096.

[103] Abdullah, N., Arifin, Z., Tiekink, E. R. T., Sharmin, N., Ahmad Tajidi, N. S., & Mat Hussin, S. A. (2016). Covalent and ionic Cu(II) complexes with cyclam and substituted benzoato ligands: structural, thermal, redox and mesomorphic properties. *Journal of Coordination Chemistry*, **69**(5), 862–878.

[104] Choi, K.-Y., Kim, K.-J. (2008). Self-assembly of metal(II) tetraazamacrocyclic complexes with cyclobutane-1-carboxylic acid-1-carboxylate ligand linked by hydrogen bond. *Structural Chemistry*, **19**, 741–747.

[105] Dojer, B., Golobič, A., Jagličić, Z., Kristl, M., Drofenik, M. (2012). Two new nickel(II) carboxylates with 3- and 4-aminopyridine: Syntheses, structures, and magnetic properties. *Monatshefte für Chemie-Chemical Monthly*, **143**, 73–78.

[106] Abdullah, N., Mohd Said, S., Halid, Y. Y., Megat Muhammad Ikhsan, M. H., Sharmin, N., Mat Hussin, S. A., Anuar, N. S. (2015). Complexes of nickel(II) carboxylates with pyridine and cyclam: crystal structures, mesomorphisms and thermoelectrical properties. *Journal of Coordination Chemistry*, **69**(19), 2954-2971.

[107] Gudasi, K. B., Patil, S. A., Vadavi, R. S., Shenoy, R. V., Patil, M. S. (2006). Synthesis and spectral studies of Cu(II), Ni(II), Co(II), Mn(II), Zn(II) and Cd(II) complexes of a new macroacyclic ligand N,N'-bis(2-benzothiazolyl)-2,6-pyridinedicarboxamide. *Journal-Serbian Chemical Society*, **71**, 529–542.

[108] Anagnostopoulos, A., Matthews, R. W., Walton, R. A. (1972). Studies on Metal Carboxylates. Part II. Cobalt(II) and Nickel(II) Complexes of Certain Pyridine Carboxylic Acids and Pyridine-3-Sulfonic Acid: Magnetic and Spectral Studies. *Canadian Journal of Chemistry*, **50**, 1307–1314.

[109] Choi, K. Y., Ryu, H., Lee, K. C., Lee, H. H., Hong, C. P., Kim, J. H., Sung, N. Do. (2003). One-Dimensional Hydrogen-Bonded Infinite Chains Composed of a Nickel(II) Macrocyclic Complex and Organic Ligands. *Bulletin of the Korean Chemical Society*, **24**, 1150–1154.

[110] Angelusiu, M. V., Barbuceanu, S.-F., Draghici, C., Almajan, G. L. (2010). New Cu(II), Co(II), Ni(II) complexes with aroyl-hydrazone based ligand. Synthesis, spectroscopic characterization and in vitro antibacterial evaluation. *European Journal of Medicinal Chemistry*, **45**, 2055–2062.

[111] Xia, C.-K., Lu, C.-Z., Yuan, D.-Q., Zhang, Q.-Z., Wu, X.-Y., Zhang, J.-J., Wu, D.-M. (2007). Syntheses, structures and magnetic properties of Co(II) complexes

based on H4BTEC and 2-(n-pyridyl)benzimidazole (n = 2, 3, and 4). *Journal of Molecular Structure*, **831**, 195–202.

[112] Wicklund, P., Brown, D. G. (1976). Synthesis and characterization of some cobalt(III) catechol complexes. *Inorganic Chemistry*, **15**, 396–400.

[113] Garcia, Y., Koningsbruggen, P. J. van, Lapouyade, R., Fournès, L., Rabardel, L., Kahn, O., … Gütlich, P. (1998). Influences of Temperature, Pressure, and Lattice Solvents on the Spin Transition Regime of the Polymeric Compound [Fe(hyetrz)3]A2·3H2O (hyetrz = 4-(2'-hydroxyethyl)-1,2,4-triazole and A- = 3-nitrophenylsulfonate). *Chemistry of Materials*, **10**(9), 2426–2433.

[114] Desplanches, C., Ruiz, E., Rodríguez-Fortea, A., & Alvarez, S. (2002). Exchange coupling of transition-metal ions through hydrogen bonding: A theoretical investigation. *Journal of the American Chemical Society*, **124**(18), 5197–5205.

[115] Shi, G., Shi, B., Wang, Q., & Li, G. (2015). Syntheses, structures and thermal properties of four manganese coordination polymers from imidazole-based multi-carboxylates. *Polyhedron*, **92**, 137–146.

[116] Prasad, V., Roy, A., Nagaveni, N. G., & Gayathri, K. (2011). Anthraquinone-based discotic liquid crystals: new monomers and dimers. *Liquid Crystals*, **38**(10), 1301–1314.

[117] Gütlich, P., & Goodwin, H. A. (2004). Spin Crossover—An Overall Perspective. In Spin Crossover in Transition Metal Compounds I, 1–47. Springer Berlin Heidelberg.

[118] Yella, A., Lee, H.-W., Tsao, H. N., Yi, C., Chandiran, A. K., Nazeeruddin, M. K., Grätzel, M. (2011). Porphyrin-sensitized solar cells with cobalt (II/III)-based redox electrolyte exceed 12 percent efficiency. *Science (New York, N.Y.)*, **334**(6056), 629–34.

[119] Samie, N., Haerian, B. S., Muniandy, S., Marlina, A., Kanthimathi, M. S., Abdullah, N. B., Aziddin, R. E. R. (2016). Mechanism of Action of the Novel Nickel(II) Complex in Simultaneous Reactivation of the Apoptotic Signaling Networks Against Human Colon Cancer Cells. *Frontiers in Pharmacology*, **6**, 1–13.

APPENDICES

PUBLICATIONS/ ABSTRACTS

CERTIFICATES OF PARTICIPATION IN NATIONAL SEMINARS

CALCULATION OF MAGNETIC SPIN STATES

APPENDIX 1

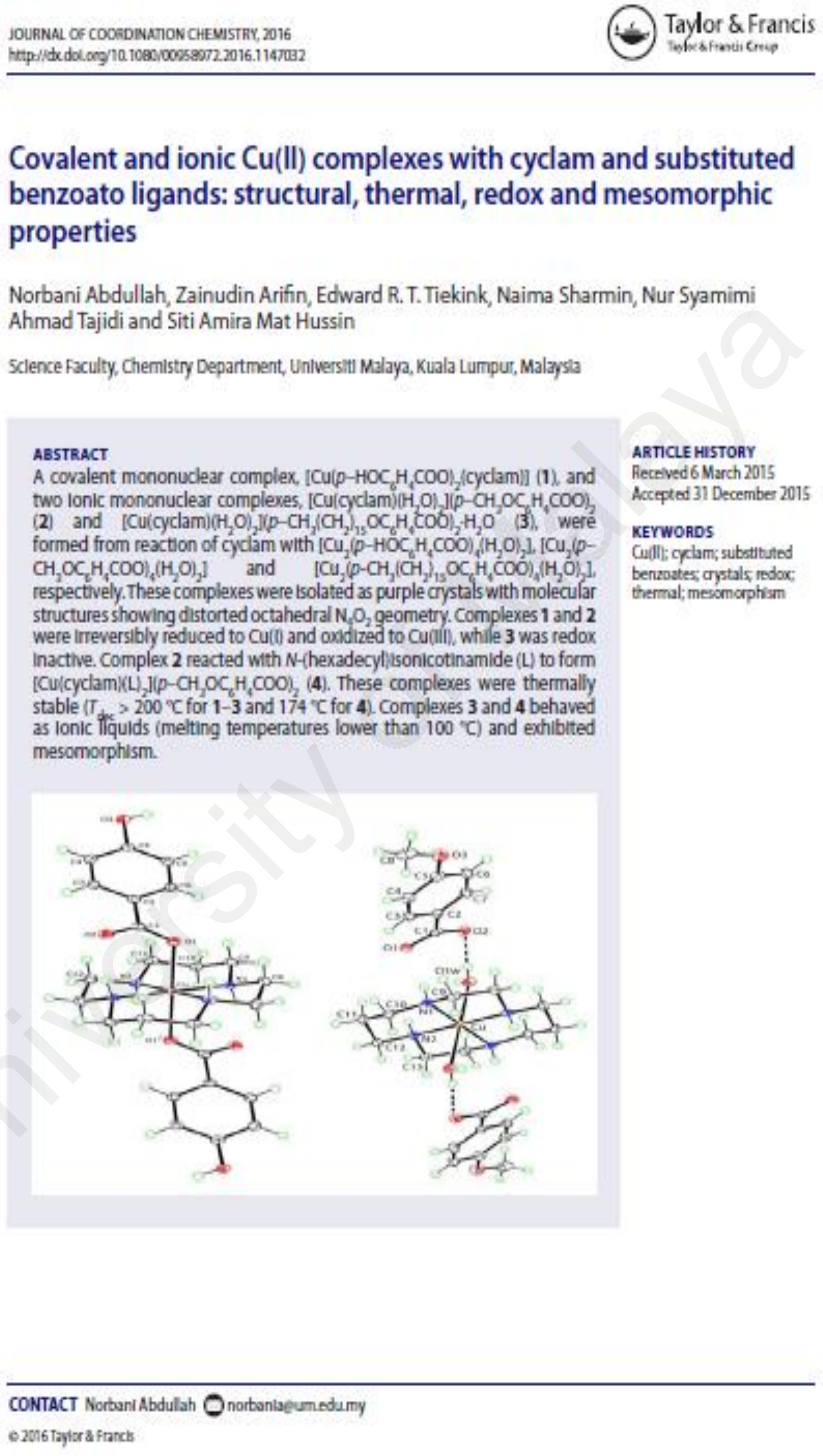

JOURNAL OF COORDINATION CHEMISTRY, 2016
http://dx.doi.org/10.1080/00958972.2016.1147032

Taylor & Francis
Taylor & Francis Group

Covalent and ionic Cu(II) complexes with cyclam and substituted benzoato ligands: structural, thermal, redox and mesomorphic properties

Norbani Abdullah, Zainudin Arifin, Edward R. T. Tiekink, Naima Sharmin, Nur Syamimi Ahmad Tajidi and Siti Amira Mat Hussin

Science Faculty, Chemistry Department, Universiti Malaya, Kuala Lumpur, Malaysia

ABSTRACT

A covalent mononuclear complex, $[Cu(p\text{–}HOC_6H_4COO)_2(cyclam)]$ (**1**), and two ionic mononuclear complexes, $[Cu(cyclam)(H_2O)_2](p\text{–}CH_3OC_6H_4COO)_2$ (**2**) and $[Cu(cyclam)(H_2O)_2](p\text{–}CH_3(CH_2)_{15}OC_6H_4COO)_2{\cdot}H_2O$ (**3**), were formed from reaction of cyclam with $[Cu_2(p\text{–}HOC_6H_4COO)_4(H_2O)_2]$, $[Cu_2(p\text{–}CH_3OC_6H_4COO)_4(H_2O)_2]$ and $[Cu_2(p\text{-}CH_3(CH_2)_{15}OC_6H_4COO)_4(H_2O)_2]$, respectively. These complexes were isolated as purple crystals with molecular structures showing distorted octahedral N_4O_2 geometry. Complexes **1** and **2** were irreversibly reduced to Cu(I) and oxidized to Cu(III), while **3** was redox inactive. Complex **2** reacted with *N*-(hexadecyl)isonicotinamide (L) to form $[Cu(cyclam)(L)_2](p\text{–}CH_3OC_6H_4COO)_2$ (**4**). These complexes were thermally stable (T_{dec} > 200 °C for **1**–**3** and 174 °C for **4**). Complexes **3** and **4** behaved as ionic liquids (melting temperatures lower than 100 °C) and exhibited mesomorphism.

ARTICLE HISTORY
Received 6 March 2015
Accepted 31 December 2015

KEYWORDS
Cu(II); cyclam; substituted benzoates; crystals; redox; thermal; mesomorphism

CONTACT Norbani Abdullah norbania@um.edu.my

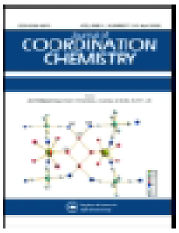

Journal of Coordination Chemistry

Taylor & Francis

ISSN: 0095-8972 (Print) 1029-0389 (Online) Journal homepage: http://www.tandfonline.com/loi/gcoo20

Complexes of nickel(II) carboxylates with pyridine and cyclam: Crystal structures, mesomorphisms and thermoelectrical properties

Norbani Abdullah, Suhana Mohd Said, Yanti Yana Halid, Megat Muhammad Ikhsan Megat Hasnan, Naima Sharmin, Siti Amira Mat Hussin, Nik Muhd Jazli Nik Ibrahim, Abdul Rahman Nordin, Nurul Atikah Safiin & Nurul Shafinaz Anuar

To cite this article: Norbani Abdullah, Suhana Mohd Said, Yanti Yana Halid, Megat Muhammad Ikhsan Megat Hasnan, Naima Sharmin, Siti Amira Mat Hussin, Nik Muhd Jazli Nik Ibrahim, Abdul Rahman Nordin, Nurul Atikah Safiin & Nurul Shafinaz Anuar (2016): Complexes of nickel(II) carboxylates with pyridine and cyclam: Crystal structures, mesomorphisms and thermoelectrical properties, Journal of Coordination Chemistry, DOI: 10.1080/00958972.2016.1221504

To link to this article: http://dx.doi.org/10.1080/00958972.2016.1221504

APPENDIX 3

UPM
UNIVERSITI PUTRA MALAYSIA

ANALIS
Persatuan Sains Analisis Malaysia

Certificate of Participation

This is to certify that

SITI AMIRA MAT HUSSIN

has participated as an

ORAL PRESENTER

at the

28TH REGIONAL SYMPOSIUM OF MALAYSIAN ANALYTICAL SCIENCES

SKAm 28

17th–20th August 2015
WEIL Hotel, Ipoh
Perak Darul Ridzuan

ANALYSIS • ASPIRE • AGRICHEMISTRY

PROF. DR. MOHD BASYARUDDIN BIN ABDUL RAHMAN
SKAM28 Chairperson

ASSOC. PROF. DR. ZAINI BIN HAMZAH
ANALIS President

Calculation of magnetic spin states

Theoretical

$\chi_M T_{(HS)}$ = 4.38 cm^3 K mol^{-1} per HS Mn(II)

$\chi_M T_{(LS)}$ = 0.38 cm^3 K mol^{-1} per LS Mn(II)

Calculation for $[Mn_2(\mu\text{-}H_2O)_2(C_6H_5COO)_4]\cdot H_2O$

Let y% LS Mn(II) atom and (100-y)% HS Mn(II) atom

χ_MT(found) = [$\chi_M T_{(LS)}$ x (y/100)] + [$\chi_M T_{(HS)}$ x (100-y/100)]

Since there are two Mn(II) in complex:

$\chi_M T_{(HS)}$ = 8.75 cm^3 K mol^{-1} for HS Mn(II)

$\chi_M T_{(LS)}$ = 0.75 cm^3 K mol^{-1} for LS Mn(II)

7.60 = [0.75y/100] + [8.75(100-y)/100]

y = 14.4%

Therefore, 14.4% LS and 85.6% HS Mn(II) atoms